THE UNIVERSITY of ADELAIDE

Characterising Ankyrin Repeat Proteins as Substrates of the Asparaginyl Hydroxylase FIH

Sarah Elizabeth Wilkins

B.Sc. Biomedical Science (Hons)

A thesis submitted in fulfilment of the requirements for the degree of Doctor of Philosophy

Discipline of Biochemistry

School of Molecular and Biomedical Science

The University of Adelaide, Australia

April 2012

Table of Contents

Thesis Summary

FIH (Factor Inhibiting HIF) is an oxygen-dependent asparaginyl hydroxylase that plays an important role in the maintenance of cellular oxygen homeostasis. It functions as an oxygen sensor, and regulates the activity of a family of transcription factors known as the Hypoxia-Inducible Factors (HIFs). The HIFs are essential mediators of the chronic response to hypoxia, and until recently, were the only published substrates of FIH. The identification of ankyrin repeat domain (ARD) proteins as an alternative class of substrate has highlighted the possibility that FIH has yet uncharacterised roles in a number of different pathways. Due to the large number of ARD proteins expressed in a cell at any given time, as well as the commonality of ARD hydroxylation, the issue of how FIH achieves specificity is key, and is a major focus of this PhD thesis.

The first section of this work identifies key differences in the binding affinity, hydroxylation efficiency and oxygen sensitivity of FIH with respect to HIF and ARD substrates. These data indicate that ARD proteins are likely to be the preferred substrate for FIH in a cellular context. Interestingly, FIH can bind to ARD proteins that are not substrates, suggesting a possible role for FIH that is mediated by binding as opposed to hydroxylation. In support of this, the robust nature of the FIH-ARD interaction enables ARD proteins to sequester FIH, and regulate hydroxylation of HIF substrates through competitive inhibition. The sensitivity of this interaction to the hydroxylation status of the ARD pool adds an additional level of complexity to this novel mechanism of HIF regulation.

The second part of this thesis presents a detailed biophysical characterisation of the molecular determinants of FIH substrate specificity. These data indicate that substrate hydroxylation is substantially influenced by the identity of amino acids directly adjacent to the target asparagine. Secondary and tertiary structure are also important determinants of both binding affinity and hydroxylation efficiency, providing an explanation for observed differences in hydroxylation of ARD proteins compared with the HIF CAD. Overall, this work reveals distinct molecular features in HIF and ARD substrates that likely enable FIH to discriminate between these two classes of substrate in a cellular context.

The final section of this thesis characterises the hydroxylation of a family of ARD proteins encoded by the poxvirus Orf. This work provides the first evidence for FIH-catalysed hydroxylation of proteins encoded by an intracellular pathogen, and reveals a novel mechanism of FIH-dependent cross-talk between viral ARD proteins and the HIF pathway, which may have important consequences for virus infection.

Overall, the work presented in this thesis explores several novel aspects of ARD hydroxylation, and contributes important insights into the role of FIH as an oxygen sensor, and its importance in normal physiology and disease.

Candidate's Declaration

This work contains no material which has been accepted for the award of any other degree or diploma in any university or other tertiary institution to Sarah Wilkins and, to the best of my knowledge and belief, contains no material previously published or written by another person, except where due reference has been made in the text. I give consent to this copy of my thesis when deposited in the University Library, being made available for loan and photocopying, subject to the provisions of the Copyright Act 1968.

The author acknowledges that copyright of published works contained within this thesis (as listed below) resides with the copyright holder(s) of those works. I also give permission for the digital version of my thesis to be made available on the web, via the University's digital research repository, the Library catalogue, the Australasian Digital Theses Program (ADTP) and also through web search engines, unless permission has been granted by the University to restrict access for a period of time.

Sarah Wilkins

26th February 2012

1 **Wilkins SE**, Karttunen S, Hampton-Smith RJ, Murchland I, Chapman-Smith A, Peet DJ. Factor inhibiting HIF (FIH) recognises distinct molecular features within hypoxia inducible factor (HIF)-α versus ankyrin repeat substrates. *J Biol Chem.* 2012 Jan. [*Accepted Paper*]

2 **Wilkins SE**, Hyvärinen J, Chicher J, Gorman JJ, Peet DJ, Bilton RL, Koivunen P. Differences in hydroxylation and binding of Notch and HIF-1alpha demonstrate substrate selectivity for factor inhibiting HIF-1 (FIH-1). *Int J Biochem Cell Biol.* 2009 Jul; 41(7):1563-71.

3 Zheng X, Linke S, Dias JM, Zheng X, Gradin K, Wallis TP, Hamilton BR, Gustafsson M, Ruas JL, **Wilkins S**, Bilton RL, Brismar K, Whitelaw ML, Pereira T, Gorman JJ, Ericson J, Peet DJ, Lendahl U, Poellinger L. Interaction with factor inhibiting HIF-1 defines an additional mode of cross-coupling between the Notch and hypoxia signaling pathways. *Proc Natl Acad Sci USA.* 2008 Mar 4; 105(9):3368-73.

Acknowledgements

Firstly, to my PhD supervisor Dan Peet, thank you for your wisdom, your patience, and above all your excellent sense of humour! You have been a great supervisor and an excellent mentor, and I am sincerely grateful for the opportunity to have worked and studied in your laboratory. To my co-supervisors Murray Whitelaw, Rebecca Bilton and Briony Forbes, I have learned a great deal from each of you and I am thankful for your input into my project, and for your contribution to my scientific development. I would also like to make special mention to Anne Chapman-Smith, for whom I have a great deal of respect; your expertise and advice have been invaluable in shaping my research.

I am grateful for contributions from collaborating researchers: Peppi Karppinen and Jaana Hyvarinen from the University of Oulu in Finland, Jeffrey Gorman and Johana Chicher from the Queensland Institute of Medical Research, Andrew Mercer and Ellena Whelan from the University of Otago in New Zealand, and Jonathan Gleadle from Flinders University in South Australia. I would also like to thank Iain Murchland, Emma Parkinson-Lawrence, and the staff at the Sansom Institute Biophysical Facility.

To past and present members of the Peet lab, in particular Sarah, Karolina, Rachel, Sam, Teresa, Natalia and Jay - thank you for making the Peet lab such an enjoyable and unique place to work. I will miss the music, laughter and conversation, and above all the friendship. Thanks must also go to my friends and colleagues in the Whitelaw laboratory, to Lynn and Tony, and all the other members of the Biochemistry Department; I feel privileged to have worked with such an outstanding group of scientists.

Last, but by no means least, I would like to thank my friends and family for their love and support, especially Sam, who has shared most of the ups and downs of my thesis, and has been a constant source of encouragement and inspiration. You challenge me to become a better scientist and a better person, and I would not be where I am today without you.

Chapter 1

Introduction

1.1 Hypoxia, HIFs and Hydroxylation

1.1.1 Oxygen Homeostasis and Hypoxia

In higher organisms, oxygen is an absolute requirement for life, but too much can lead to oxidative stress and major damage. Thus oxygen homeostasis, the balance between supply and demand, must be carefully controlled; cells must be able to sense changes in oxygen concentration, and respond accordingly. The ability to do so is critical for survival, both of individual cells, and the organism as a whole. Hypoxia is a term used to describe a state of oxygen deficiency, in which the supply of oxygen to a cell is insufficient to meet its metabolic needs. Due to the fundamental requirement for oxygen in oxidative phosphorylation, and the comparative inefficiency of anaerobic metabolism, sustained oxygen deprivation can lead to ATP depletion, cell dysfunction and, if sufficiently profound, cell death [1]. Consequently, hypoxia contributes to the pathogenesis of major human diseases such as heart attack and stroke. However, hypoxia is also involved in a number of normal physiological processes (reviewed in [2]), including adaptation to high altitude, maintenance of pluripotent cell populations, and formation of new blood vessels (angiogenesis) during wound healing and embryonic development. In these instances, major physiological and metabolic changes are required to compensate for the oxygen deficiency, and enable continued cell function and survival.

1.1.2 The Cellular Response to Hypoxia

Higher organisms have evolved complex cellular mechanisms that facilitate adaptation to hypoxia. At the pinnacle of this system are oxygen sensors, which detect the oxygen deficiency and signal to downstream effector molecules to implement a response. A key pathway that effects the cellular response to hypoxia in mammals involves a transcriptional regulator known as the hypoxia inducible factor (HIF, [3]). HIF is activated in low oxygen conditions and works in conjunction with coactivators to induce the transcription of a diverse range of hypoxia response genes (reviewed in [4, 5]). The protein products of HIF target genes are involved in physiological and metabolic processes such as angiogenesis (vascular endothelial growth factor, angiopoietin), erythropoiesis (erythropoietin), glucose uptake (glucose transporter 1) and glycolysis

(lactate dehydrogenase A, phosphoglycerate kinase 1). Collectively, these proteins work to increase the delivery of oxygenated blood to tissues, and alter metabolism to produce ATP from anaerobic glycolysis rather than oxidative phosphorylation, thus decreasing the cellular demand for oxygen. In this way, HIF coordinates a broad range of responses to hypoxia, and regulates oxygen homeostasis at both a cellular and systemic level.

Despite its fundamental role as a master regulator of the hypoxic response, HIF cannot detect hypoxia directly, and instead relies on signals from upstream oxygen sensors [6]. In particular, HIF is subject to post-translational regulation by a group of oxygen-dependent hydroxylases (discussed further in Section 1.1.4). These enzymes provide a critical link between oxygen availability and HIF, which ultimately coordinates the cellular response. Therefore, characterisation of these oxygen sensors, and their role in regulating key effectors such as HIF, is essential to fully comprehend the cellular response to hypoxia and its role in development and disease.

1.1.3 Molecular details of the Hypoxia Inducible Factor (HIF)

HIF is heterodimeric transcription factor made up of α and β subunits, both of which are members of the bHLH/PAS (basic-Helix-Loop-Helix/Per-ARNT-Sim homology) protein family [7, 8]. The HIF-α subunit is regulated by oxygen availability and is potently induced in hypoxia [9, 10]. In contrast, the HIF-β subunit, commonly known as the aryl hydrocarbon receptor nuclear translocator (ARNT), is constitutively expressed and localised to the nucleus [10], where it functions as a general dimerisation partner for members of the bHLH/PAS family (reviewed in [11]). Thus, HIF dimer formation, which is required for DNA-binding and transcriptional activity [12, 13], is regulated by the availability of the HIF-α subunit.

In hypoxia, HIF-α translocates to the nucleus [14], and following heterodimerisation with ARNT, binds to specific DNA sequences termed ‘hypoxia response elements’ (HREs) in regulatory regions of target genes [15]. N-terminal and C-terminal transactivation domains in HIF-α (NAD and CAD, respectively) recruit coactivators to form active transcriptional complexes on DNA [16-18]. In particular, the coactivator proteins CREB binding protein (CBP) and/or p300 are required for transcriptional activation of HIF target

genes [19, 20]. Regulation of coactivator recruitment is one of the ways in which HIF activity is controlled by oxygen availability (discussed further in Section 1.1.4).

There are three mammalian paralogues of the HIF-α subunit, HIF-1α [8], HIF-2α [21-24] and HIF-3α [25]. HIF-1α and HIF-2α exhibit a high degree of sequence identity, analogous domain structure and similar mechanisms of hypoxic regulation [17, 26, 27]. Both isoforms dimerise with ARNT and recognise the same core DNA sequence [22, 24]. Even so, they do exhibit some differences in target gene specificity [28, 29], and are functionally non-redundant, with distinct and essential physiological roles [30-35]. HIF-3α is less closely related [36], and its function in hypoxia is complex and poorly understood. Multiple splice variants have been identified, several of which function to suppress HIF-mediated transcription [37-39]. As such, HIF-3α may contribute to fine-tuning hypoxic gene expression, although studies indicate that the transcriptional response to hypoxia in specific cell types in culture is predominantly mediated by HIF-1α and HIF-2α [40, 41].

1.1.4 Regulation of HIF-α by hydroxylation

Both HIF-1α and HIF-2α (herein referred to as HIF-α) are tightly regulated by oxygen availability to ensure a rapid transcriptional response in hypoxic conditions and to prevent aberrant upregulation of hypoxia response genes in normal oxygen conditions (normoxia). This regulation of HIF-α is two-fold and occurs at the level of protein turnover, as well as the transcriptional activity of the CAD, and in both cases is mediated by oxygen-dependent post-translational hydroxylation.

Although HIF-α subunits are constitutively transcribed and translated in all mammalian cells, HIF-α proteins are essentially undetectable in normoxia due to rapid proteasomal degradation, but are stabilised in hypoxia [10, 42]. In contrast, the level of ARNT protein remains constant, regardless of oxygen tension [10, 14]. The rapid normoxic turnover of HIF-α is mediated by a central oxygen-dependent degradation (ODD) domain [43]. Hydroxylation of two conserved proline residues within the ODD domain of HIF-α enables an interaction with the Von Hippel Lindau protein (pVHL [44-46]) which functions as the recognition component of an E3 ubiquitin ligase complex and promotes ubiquitin-dependent proteolysis of HIF-α in normoxia [47-51]. HIF prolyl hydroxylation is catalysed by three homologous prolyl hydroxylase domain enzymes (PHD1-3, [52, 53]). These

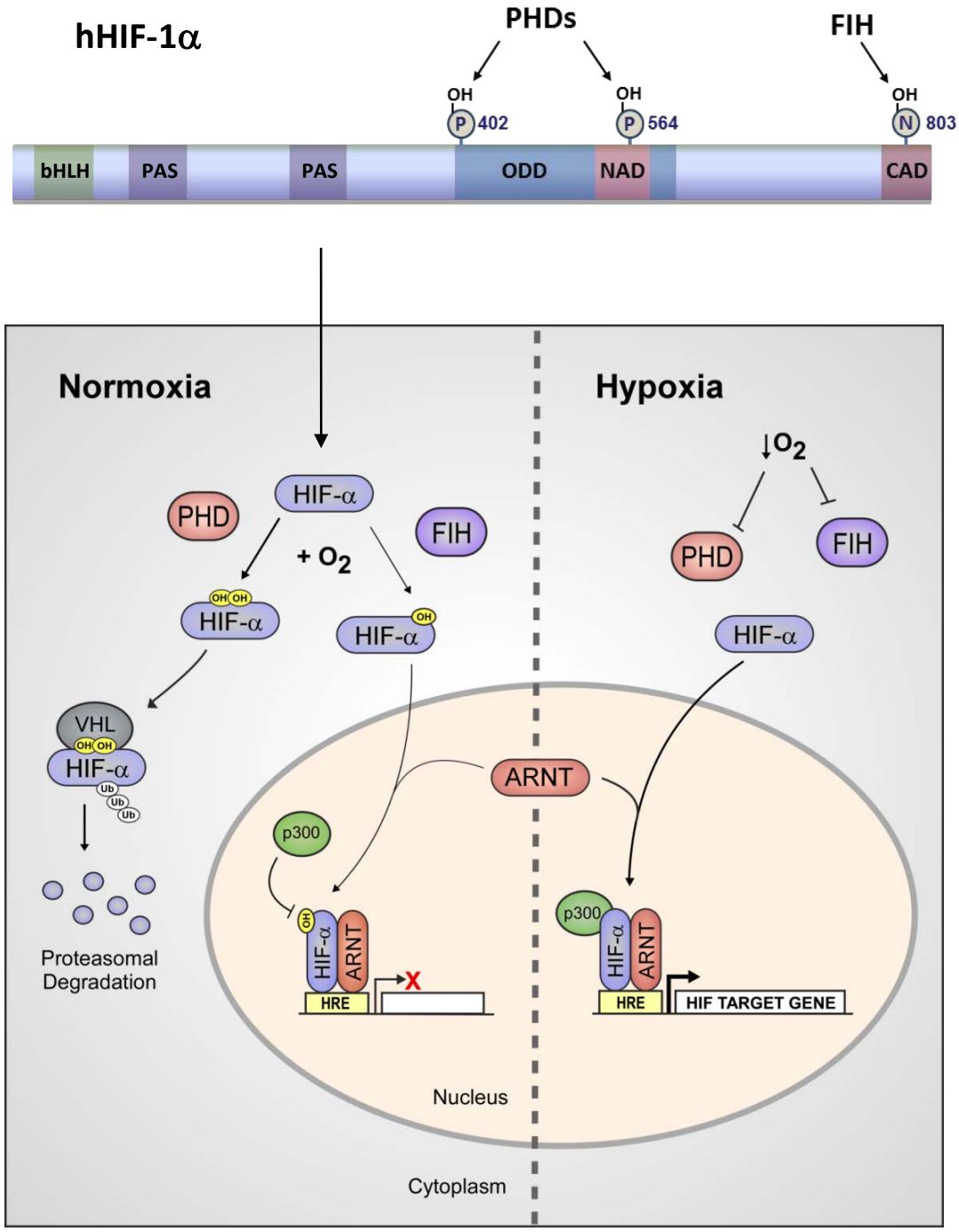

Figure 1.1 Regulation of HIF by hydroxylation

In normoxia, the PHDs hydroxylate two proline residues (Pro402 and Pro564) within the oxygen-dependent degradation (ODD) domain of HIF-α. Prolyl hydroxylation promotes an interaction with the von Hippel Lindau ubiquitin ligase complex (VHL), resulting in polyubiquitylation and subsequent degradation of HIF-α by the proteasome. Any HIF-α protein that escapes degradation is transcriptionally repressed by FIH via hydroxylation an asparagine residue in the HIF-α CAD (Asn803 in hHIF-1α), which prevents the CAD from interacting with requisite coactivators (p300). In hypoxia, oxygen is limiting and the activity of the HIF hydroxylases is inhibited. This leads to stabilisation of HIF-α, dimerisation with its partner protein ARNT, association with coactivators and transcription of target genes.

enzymes have a direct requirement for oxygen, such that their hydroxylase activity is inhibited in hypoxia, enabling newly synthesised HIF-α protein to escape pVHL-mediated degradation (Figure 1.1). Furthermore, as two of the PHDs (PHD2 and PHD3) are direct HIF targets, these enzymes provide a feed-back mechanism that ensures efficient degradation of HIF-α in response to reoxygenation [54, 55].

A separate oxygen-dependent hydroxylation event regulates the transcriptional activity of the HIF-α CAD [56]. In normoxia, an asparaginyl hydroxylase, known as Factor Inhibiting HIF (FIH), hydroxylates a conserved Asn residue within the HIF-α CAD (Figure 1.1, [57, 58]). This modification prevents the recruitment of CBP/p300 coactivators, which, as discussed previously, is required for HIF target gene expression [19, 56]. Thus, any HIF that escapes proteasomal degradation in normoxia is subject to transcriptional repression by FIH. FIH-mediated hydroxylation occurs at the β-carbon of the Asn residue [59], and generates a steric clash that directly prevents the CAD from binding to CBP/p300 [60, 61]. Like the PHDs, the hydroxylase activity of FIH is dependent on the availability of oxygen. Therefore, hypoxia triggers both the accumulation and activation of HIF, leading to a robust transcriptional response (Figure1.1).

1.1.5 The HIF hydroxylases:

Both the PHDs and FIH belong to a large superfamily of Fe(II) and 2-oxoglutarate (2OG)-dependent oxygenases. These enzymes catalyse a range of oxidative reactions [reviewed in [62]], but employ a common mechanism of catalysis, in which the oxidation of a prime substrate is coupled to the oxidative decarboxylation of 2OG [63]. Oxygen is also required as a direct co-substrate, and in the hydroxylation reactions catalysed by FIH and the PHDs, one of the atoms from dioxygen is transferred to the target Asn/Pro residue. In this way, the HIF hydroxylases provide a direct link between oxygen availability and HIF regulation, and are considered to function as oxygen sensors for the HIF-mediated hypoxic response.

1.1.6 FIH and the PHDs as oxygen sensors

Efficient oxygen sensing requires a K_m for O_2 that is above the physiological oxygen tension (pO_2), so that the rate of hydroxylation is limited by oxygen availability. In human tissues, pO_2 values range between 100 mmHg (130 μM) in the alveoli of the lungs to less

than 40 mmHg (50 μM) in most other tissues [64]. Reported apparent K_m (O_2) values for FIH range between 90-240 μM, depending on the length of the HIF peptide substrate utilised [65, 66], and comparable values (85-250 μM) have been reported for the PHDs [65, 67]. These values are well above the cellular pO_2 under physiological conditions, and provided these values are consistent with *in vivo* oxygen affinities, indicate that even a slight decrease in oxygen tension should influence the activity of these enzymes. Thus, the level of HIF activation will be determined by the severity of the oxygen deficiency, making the HIF hydroxylases well-suited to their role as cellular oxygen sensors.

Whilst it is generally accepted that the HIF hydroxylases function as physiological oxygen sensors and are directly regulated by cellular pO_2, a number of studies promote a role for the mitochondria as primary oxygen sensors that function upstream of the HIF hydroxylases to regulate their activity [68-71]. This is primarily thought to occur through the increased production of reactive oxygen species (ROS) in hypoxia [68, 72, 73]. There is, in fact, some contention as to whether the level of ROS is increased or decreased by hypoxia [74, 75]. Nevertheless, there is strong evidence to suggest that ROS can inhibit the activity of both FIH and the PHDs, leading to activation of the HIF pathway [76-79]. The mechanism has not been clearly defined, but is thought to involve a change in Fenton chemistry to favour the ferric (Fe^{3+}) form of iron, as opposed to the ferrous (Fe^{2+}) form that is required for hydroxylase activity [76, 77]. Importantly, a recent study has shown that both FIH and the PHDs display differential sensitivity to cellular hypoxia and ROS [76], suggesting that whilst an increase in ROS may contribute to inactivation of the HIF hydroxylases, it is unlikely to be their primary mechanism of regulation in hypoxia.

1.1.7 FIH regulates the expression of specific subset of HIF target genes

As described in section 1.1.3, the transcriptional activity of HIF is mediated by two transactivation domains (NAD and CAD) in HIF-α [26, 80-82]. Whilst the NAD is constitutively active, the CAD is functionally repressed in normoxia due to hydroxylation by FIH. This distinct mechanism of CAD regulation has important consequences for HIF target gene expression, as it enables the NAD and CAD to function independently of one another and contribute to the differential expression of individual target genes [83]. Some genes are driven almost exclusively by the NAD, and are therefore insensitive to

FIH. Thus, unlike the PHDs, which have a global influence on HIF target gene expression through their control of HIF-α stability, FIH activity serves to modify the expression of a particular subset of HIF targets, comprising genes that are predominantly driven by the transactivation function of the CAD [83].

1.1.8 FIH activity is non-redundant and biologically significant

Although prolyl hydroxylation is the predominant mechanism by which HIF is regulated, the role of FIH in fine-tuning the HIF response is nonetheless important. Depletion of endogenous FIH by siRNA treatment in normoxia abolishes hydroxylation of the HIF-α CAD and leads to the induction of several HIF target genes, including *Vascular Endothelial Growth Factor* (*VEGF*), *Glucose Transporter-1* (*GLUT1*) *and Carbonic Anhydrase 9* (*CA9*) [83, 84]. Interestingly, the low basal expression of these genes in normoxia can be further repressed by FIH overexpression, indicating that the activity of FIH with respect to HIF is limiting under normal oxygen conditions [84]. As such, alterations in the amount or activity of FIH will have consequences for the expression of particular HIF target genes.

1.1.9 The physiological role of FIH: insights from genetic studies in mice

In order to gain a better understanding of the function of FIH in animal development and physiology, Zhang et al (2010) generated mice with a null mutation in the *HIF1AN* gene, which encodes FIH [85]. Consistent with previous results from siRNA knockdown studies, loss of FIH completely eliminates hydroxylation of the HIF-1α CAD, and leads to a modest induction of some HIF target genes, including *Vegf* and *Ca9*. However, rather than displaying any of the typical *in vivo* effects of HIF activation, such as increased erythropoiesis or angiogenesis, FIH null mice have a largely metabolic phenotype.
Loss of FIH in mice leads to an elevated metabolic rate, hyperventilation, increased insulin sensitivity and improved glucose tolerance. $FIH^{-/-}$ mice have a reduced body mass compared to wildtype littermates, and are resistant to high-fat diet-induced weight gain. Unexpectedly, this hyper-metabolic phenotype is not accompanied by an increase in glycolysis, nor any of the other metabolic effects typically associated with increased HIF activity. Therefore, whilst FIH is clearly essential for the negative regulation of HIF CAD activity in normoxia, the extent to which the phenotype of the FIH knockout mouse is caused by changes in HIF regulation remains unclear.

Alternative substrates for FIH have recently been described (see section 1.2 below), however, the functional significance of their hydroxylation by FIH remains to be determined. Identification of the full-array of substrates and an intricate understanding of their recognition and modification by FIH will be essential to fully interpret the knockout phenotype and to elucidate the precise physiological roles that FIH is playing.

1.2 Alternative Substrates for FIH

1.2.1 Identification of ankyrin repeat domain (ARD) proteins as substrates for FIH

The first reported non-HIF substrates for FIH were p105 and IκBα, members of the NFκB signalling pathway [86]. Following the identification of p105 in a yeast two-hybrid screen for FIH-interacting proteins, both p105 and IκBα were found to interact with endogenous FIH in mammalian cells. Hydroxylation was initially inferred by *in vitro* 2OG decarboxylation assays, and later confirmed by mass spectrometry. In total, three novel hydroxylation sites were identified (one in p105 and two in IκBα), and in each case, the target asparagine residue was pinpointed to a region of the protein containing ankyrin repeats.

Ankyrin repeats are a common protein-protein interaction motif. Tandem arrays of the 33-amino acid ankyrin repeat sequence, referred to as ankyrin repeat domains (ARDs), are found in more than 6% of eukaryotic proteins [87]. As many as 34 consecutive repeats can be found in a single protein, although most ARDs contain fewer than 6 [88]. Adjacent repeats fold cooperatively into well-defined secondary and tertiary structures, which are conserved in all ARDs despite considerable sequence variation [88, 89]. As shown in Figure 1.2A, individual ankyrin repeats exhibit a helix-turn-helix conformation, with a long β-hairpin-like loop that connects one repeat to the next. The linear arrangement of repeats within an ARD results in an elongated structure that provides multiple surfaces for mediating specific protein-protein interactions, making the ARD a highly versatile framework for molecular recognition [90].

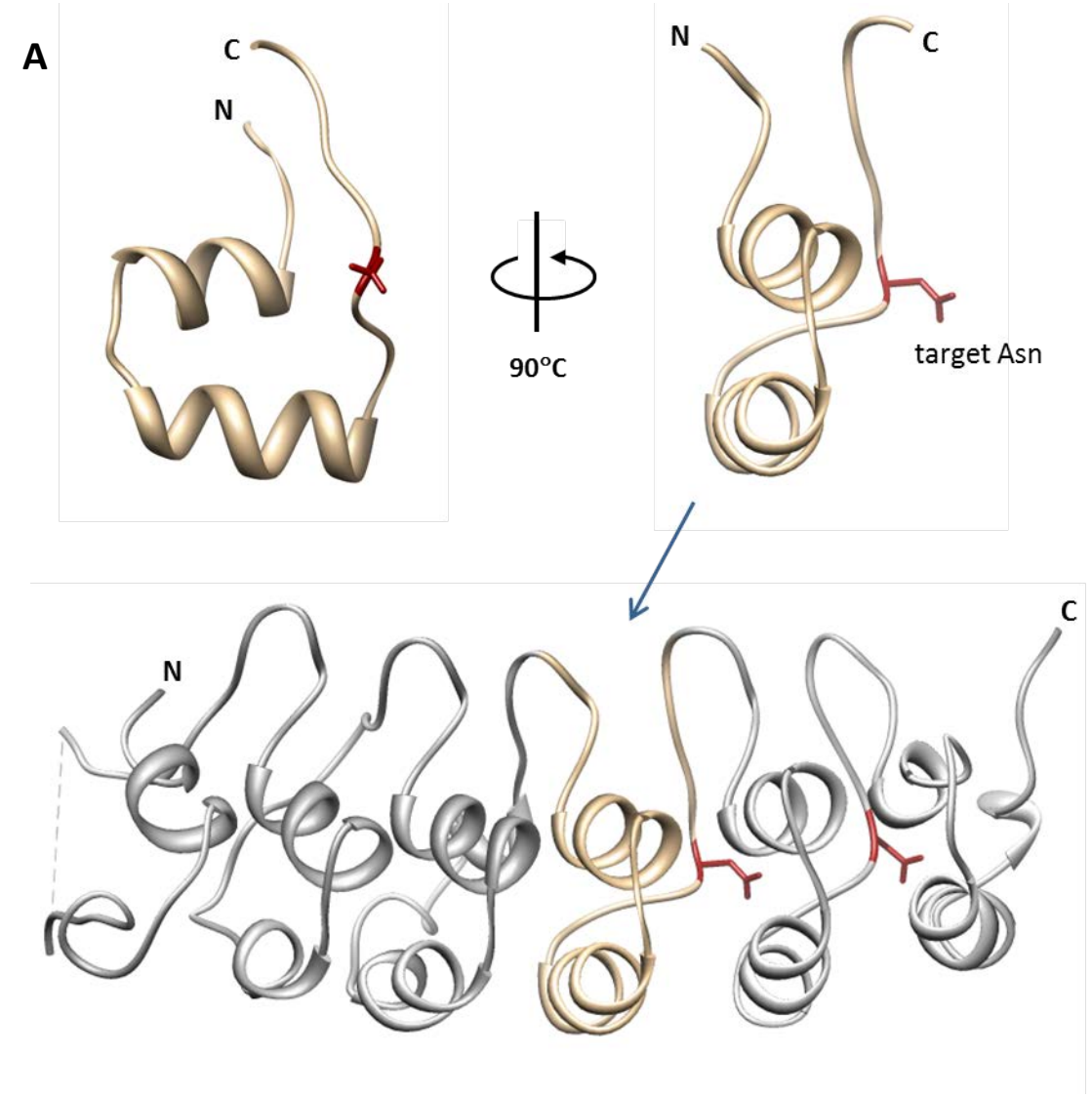

Figure 1.2 Structure of the ankyrin repeat domain

A. Two different views of a single ankyrin repeat highlight the typical helix-turn-helix-β-hairpin loop conformation exhibited by each repeat in the context of an ARD. Asn residues targeted for hydroxylation by FIH (shown in red) occur at analogous positions within the β-hairpin turns of ankyrin repeats. Images generated from a crystal structure of human IκBα [visible residues 76-281, PDB ID: 1IKN [91]] using UCSF Chimera software [92]. B. Consensus sequence for the ankyrin repeat [93] highlighting the degree of conservation of individual residues (darker font corresponds to more highly conserved residues). The secondary structural elements of the repeat are shown above the sequence. The Asn residue targeted by FIH (indicated by *) is semi-conserved.

1.2.2 FIH-mediated ARD hydroxylation is common

As highlighted in the crystal structure of IκBα (Figure 1.2), the asparagine residues targeted by FIH occur at a specific position within the ankyrin repeat sequence, just prior to the apex of the β-hairpin turn. This position is occupied by an asparagine residue in the majority of eukaryotic ankyrin repeat sequences, as indicated by its conservation within the consensus sequence [Figure 1.2B, [88]]. Given the possibility that FIH may hydroxylate other ARD proteins with Asn residues at analogous positions to those identified in IκBα and p105, Cockman et al. (2006) analysed peptide fragments from the β-hairpin loops of 9 different ARD proteins, all of which were confirmed as *in vitro* substrates for FIH [86]. These data gave the first indication that FIH-mediated hydroxylation of ARD proteins may be widespread.

FIH has since been found to hydroxylate ankyrin repeats from more than 25 different proteins *in vitro*, at least 9 of which have been shown to interact with FIH *in vivo* or have been confirmed as endogenous substrates (Table 1.1). Together, these data identify ARD proteins as a novel and extensive class of substrate for FIH, which may encompass many, if not most, of the ~260 ARD proteins encoded by the human genome.

Notch is an ARD substrate for FIH

Thus, a growing body of research now indicates that ARD proteins are common targets for hydroxylation by FIH. However, in early 2007 when the research for this thesis commenced, p105 and IκBα were the only reported ARD substrates for FIH. Our laboratory, in collaboration with the Lendahl and Poellinger groups at the Karolinska Institutet in Stockholm, had identified several members of the Notch receptor family as novel substrates for FIH. These findings were later published [94], and independently confirmed by another research group [95].

Notch receptors (Notch1-4 in mammals) are the central mediators of an intercellular signalling pathway that controls numerous cell-fate decisions in metazoan development [reviewed in [96]]. As shown in Figure 1.3, each receptor consists of an extracellular ligand-binding domain and an intracellular domain (ICD) that is responsible for signal transduction [97]. In the canonical Notch signalling pathway, ligand activation initiates a

Table 1.1 ARD proteins targeted for asparaginyl hydroxylation by FIH

Protein	Function	No. of Repeats	Asn-OH Sites	Interaction with FIH	Ref
IκBα	NFκB signalling	6	2	CoIP	[86, 98] RHS
P105	NFκB signalling	7	1	CoIP	[86]
ASB4	Ubiquitin-proteasome pathway	9	1	CoIP	[99]
Notch1	Notch signalling	7	2	CoIP	[94, 95]
Notch2	Notch signalling	7	2	CoIP	[94, 95, 100]
Notch3	Notch signalling	7	2	CoIP	[94, 95, 100]
Rabankyrin-5	Endocytosis, macropinocytosis	21	4	CoIP	[101]
RNaseL	Viral-induced apoptosis	9	1	CoIP	[101]
Tankyrase-1	Telomere regulation, vesicle trafficking	24	4	CoIP	[86, 102]
Tankyrase-2	Telomere regulation, vesicle trafficking	20	≥5	CoIP	[101]
MYPT1	Cytoskeletal organisation	7	3	CoIP	[103]
AnkyrinR	Membrane skeleton assembly	24	≥4	CoIP	[104]
AnkyrinB	Membrane skeleton assembly	24	≥3	ND	[104]
FGIF	Transactivation of γ-globin gene expression	4	≥1	CoIP	[86, 105]
ANKRD44	unknown	28	≥1	CoIP	RHS
Synthetic ARD	Artificial, consensus derived ARD	3	1	CoIP	[106]
Gankyrin	Cell-cycle regulation and oncogenesis	7	1	PD	[86], RHS
TRPV3	Thermosensitive cation channel	4	1	PD	SL, LW

Protein	Function	No. of Repeats	Asn-OH Sites	Interaction with FIH	Ref
*P19-INK4d	Cell cycle regulation	5	1*	ND	[86]
*GABP-β	Transcriptional regulation	5	1*	ND	[86]
*Myotrophin	Ubiquitin-proteasome pathway	4	1*	ND	[86]
*ILK-1	Integrin signal transduction	4	1*	ND	[86]
*FEM-1β	Ubiquitin-mediated proteolysis, apoptosis	7	1*	ND	[86]
*AnkyrinG	Membrane skeleton assembly	24	5*	ND	[104]

Asparaginyl hydroxylation by FIH was demonstrated for full-length ARDs or peptide fragments (*) of individual ankyrin repeats. An interaction with FIH was demonstrated by *in vitro* affinity pull-downs with recombinant protein (PD) or co-immunoprecipitation of proteins from cultured cells (CoIP). ND: not determined, RHS: Rachel Hampton-Smith, SL: Sarah Linke, LW: Lauren Watkins.

series of proteolytic cleavage events, which liberate the Notch ICD from the plasma membrane. Subsequent translocation to the nucleus enables it to interact with DNA-binding proteins and co-activators, leading to upregulation of downstream target genes (see [107] for review). The ICD is thus an essential component of the Notch signalling pathway. Of particular importance to this thesis, however, is that the ICD of all four Notch receptor proteins contains seven ankyrin repeats, two of which are hydroxylated by FIH in Notch 1-3 [94, 95].

The investigation of Notch as a potential substrate for FIH arose from a previous study exploring cross-talk between hypoxia and Notch signalling in the maintenance of precursor cell populations [108]. Gustafsson et al. (2005) showed that hypoxia inhibits the differentiation of neural and myogenic precursor cells in a Notch-dependent manner. Interestingly, overexpression of FIH led to a significant reduction in Notch transcriptional activity in reporter gene assays performed under both normoxic and hypoxic conditions. GST-pulldown assays demonstrated that FIH is able to interact with the Notch1 ICD, and suggested that FIH may play a direct role in regulation of Notch signalling [108]. Following on from these findings, and in collaboration with the authors of the paper, our laboratory investigated Notch as a potential substrate for FIH.

Analysis of the mouse Notch1 ARD by mass spectrometry revealed that FIH hydroxylates two asparagine residues, Asn1945 and Asn2012, located within the β-hairpin loops connecting ankyrin repeats 2/3 and 4/5, respectively (Figure 1.3). Data from my Honours research indicated that Notch2 and Notch3 were also likely substrates for FIH, although the target Asn residues remained to be identified. Notably, Notch4 is not a substrate for FIH *in vitro*, despite the presence of an Asn residue in an analogous position to Asn1945 in Notch1. This lack of hydroxylation is of particular interest, as it indicates that FIH-catalysed ARD hydroxylation, whilst common, is certainly not ubiquitous. Furthermore, subtle differences between Notch4 and the other homologues may provide insight into the specificity of recognition by FIH, as well as the requirements for hydroxylation.

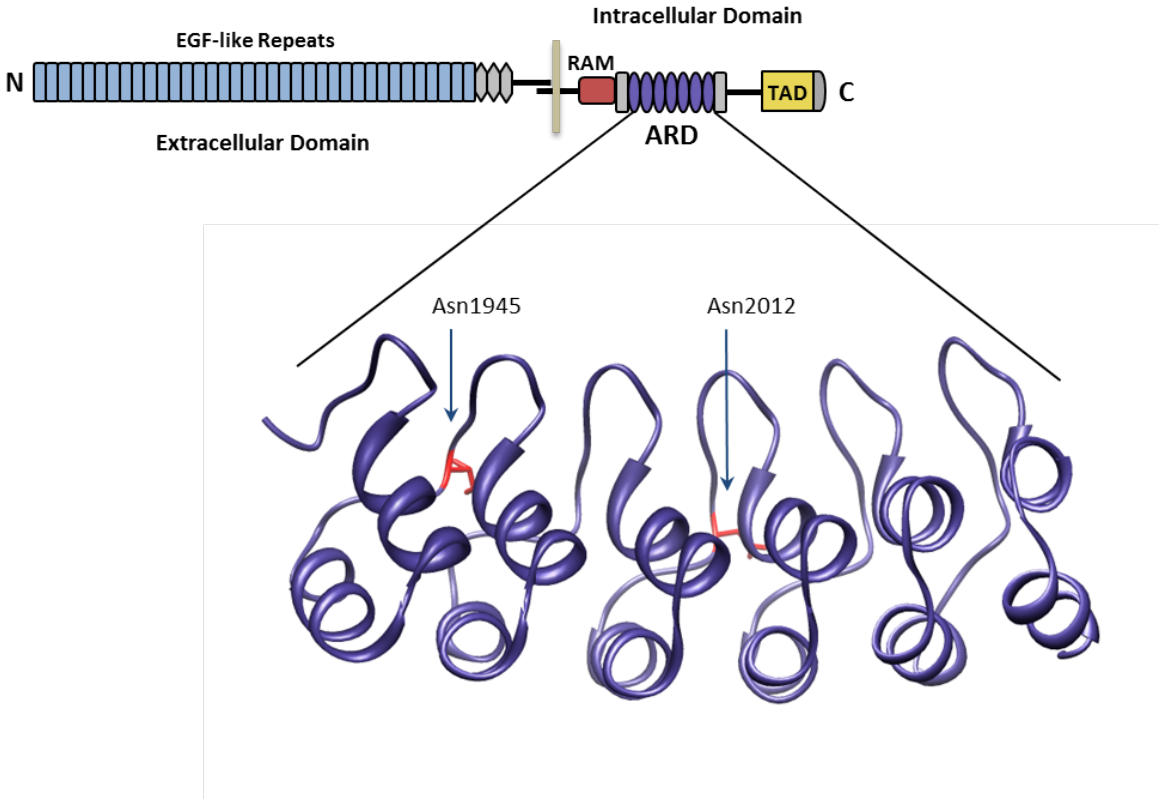

Figure 1.3 Notch1 is an ARD substrate for FIH

Domain arrangement of the mouse Notch1 receptor. The extracellular domain contains EGF-like repeats responsible for ligand binding. The intracellular domain, which is responsible for signal transduction, contains a C-terminal transactivation domain (TAD). Interactions with DNA binding proteins and coactivators are mediated by the C-terminal transactivation domain (TAD), RBPjκ-associated molecule (RAM) domain and the ankyrin repeat domain (ARD). A crystal structure of the mouse Notch1 ARD is shown [PDB ID: 2QC9 [95]]. It contains two Asn residues (Asn1945 and Asn 2012) that are hydroxylated by FIH (indicated in red).

1.2.3 Function of Notch hydroxylation

At this stage, the downstream consequences of Notch hydroxylation are unclear. The target asparagine residues in Notch1 are clearly important for its activity, as alanine substitution of one or both of these residues substantially reduces the transactivation capacity of the Notch1 ICD, and compromises its ability to repress neuronal and myogenic differentiation [94]. However, overexpression of either wildtype FIH or a catalytically inactive mutant leads to repression of Notch activity, suggesting that FIH can inhibit Notch signalling via a mechanism that is independent of catalysis [94, 95].

The effects of endogenous FIH on Notch signalling are currently unresolved due to conflicting reports from different groups, but do not appear to be major. Our collaborators observe a subtle increase in Notch activity following depletion of FIH by siRNA under normoxic, but not hypoxic, conditions [94]. In contrast, an independent study showed that siRNA-mediated knockdown of FIH has no significant effect on Notch activity in multiple cell lines [95]. Given the essential role of Notch signalling in regulating numerous aspects of development [109-112], and the lack of any apparent developmental abnormalities in the FIH knockout mice [85], it is clear that FIH does not have a major role in Notch regulation during normal mouse development. However, the precise role of FIH in regulating Notch signalling remains to be determined, as does the extent to which it is dependent on ARD hydroxylation.

1.2.4 A general function for ARD hydroxylation?

Despite the large number of ARD proteins subject to post-translational hydroxylation by FIH, extensive analyses of multiple ARD substrates have yielded few clues as to the functional significance of this modification. Given that ARDs function exclusively to mediate protein-protein interactions, it is tempting to speculate that hydroxylation might influence the binding affinity or specificity for particular protein targets by altering the structure or stability of the domain, as occurs with HIF hydroxylation [44, 45, 56]. Whilst hydroxylation appears to have little influence on ankyrin repeat structure [95], it has been shown to enhance the thermodynamic stability of certain ARDs [104, 106, 113]. This effect has been attributed to the formation of a hydrogen bond between the newly introduced hydroxyl group and the side-chain of an aspartyl residue located 2 positions N-

terminal to the Asn. However, the functional significance of this change in stability is unclear, and the effect is likely to be restricted to particular ARD substrates, as not all ARD proteins are stabilised by hydroxylation [114].

The ability of multiple ARD proteins, including Notch, to compete with HIF-α for hydroxylation by FIH both *in vitro* and in transfected cells has led to the hypothesis that ARD proteins act in concert to regulate the activity of the HIF CAD through competition for FIH [95]. In this scenario, recognition of each substrate and their relative affinity for FIH will be important determinants of FIH sequestration and consequently HIF regulation.

An important issue, therefore, is how FIH achieves specificity. We predict that key differences in the primary sequence and/or structure of ARD proteins compared with HIF-α enables FIH to distinguish between these two classes of substrate within a cellular context. This thesis will address this hypothesis by providing a detailed biochemical characterisation of the molecular determinants of substrate recognition and hydroxylation by FIH, with particular emphasis on differences between HIF and ARD substrates. The following section presents a review of the research that was published prior to the commencement of this work, detailing what was known at the time regarding the substrate requirements of FIH.

1.3 Molecular details of recognition and hydroxylation by FIH

1.3.1 Crystal Structures of FIH

Three independent groups have solved structures for FIH using X-ray crystallography; all are highly similar and provide structural insights into various aspects of substrate recognition and catalysis [115-117]. The structures reveal a homodimeric form of FIH, with each monomer adopting a double-stranded β-helix (DSBH) core fold that is characteristic of Fe(II) and 2OG-dependent dioxygenases. The DSBH, highlighted in Figure 1.4, is a barrel-like structure made up of eight β-strands that form two four-stranded β-sheets. The major sheet (shown in red) is flanked by an additional four β-strands, which

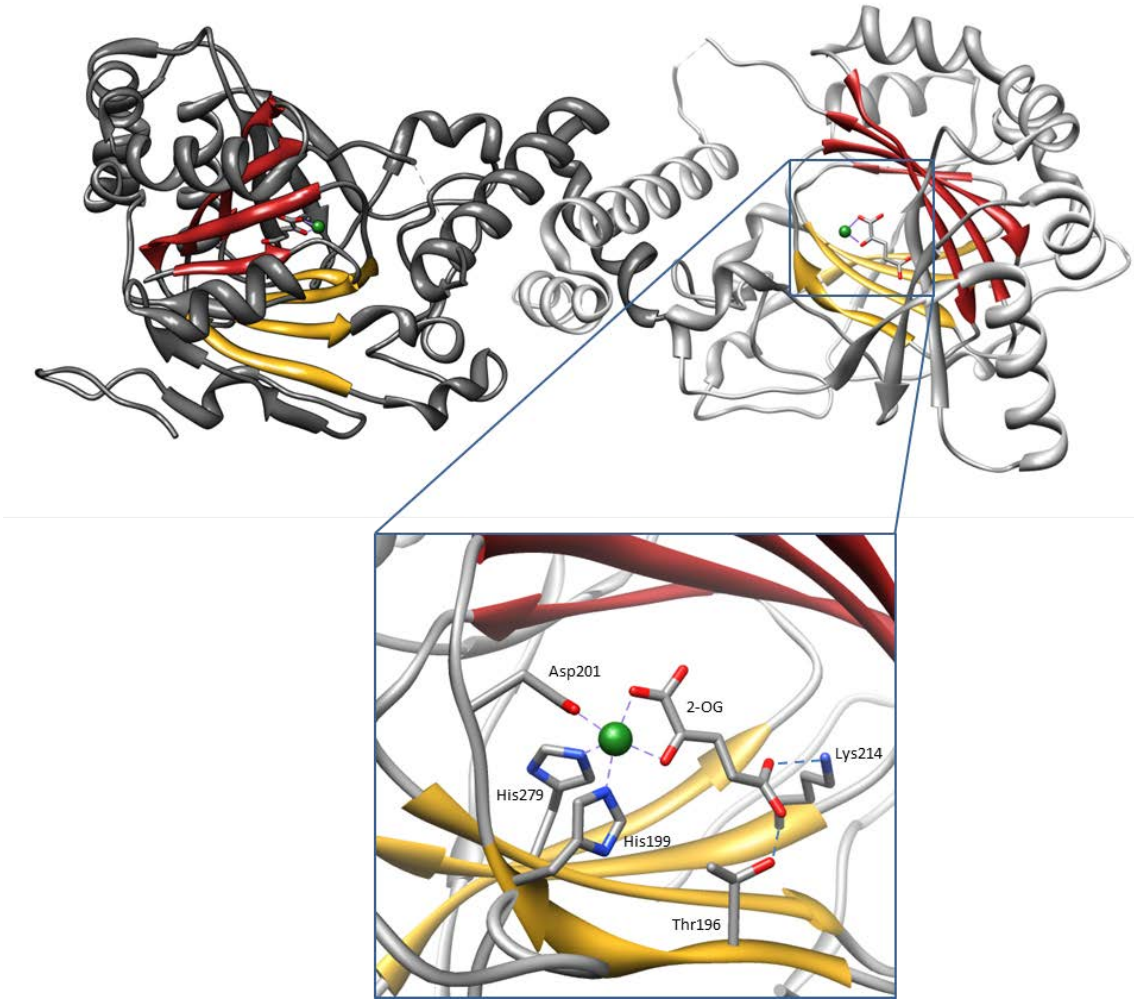

Figure 1.4 The structure of FIH

Crystal structure of FIH highlighting the major (red) and minor (yellow) β-sheets that make up the double-stranded beta helix (DSBH) of each monomer. Two molecules of FIH are shown (in light grey and dark grey) and are arranged as a homodimer in accordance with the dimer structure published by Elkins et al. (2003). The active site of one monomer is enlarged, and indicates key residues in FIH responsible for binding the iron (green) and 2-OG. Images were generated from a crystal structure of human FIH (PDB ID: 1H2L [116]) using UCSF Chimera software [92].

extend the sheet away from the DSBH. Seven α-helices from the N-terminus pack around the outside of the DSBH and stabilise the core fold, whilst two helices from the C-terminus mediate dimerisation [115]. Mutation or deletion of these C-terminal helices leads to a largely monomeric form of FIH that is structurally analogous to wildtype FIH but is catalytically inactive on HIF substrates, although the precise reason for this is unclear [115, 118].

The active site of each monomer is located at the more open end of the DSBH, and is lined with residues involved in binding Fe(II) and 2OG. As shown in Figure 1.4, the Fe(II) is coordinated by the side-chains of His199, Asp201 and His273 from strands 2 and 7 of the DSBH. These residues constitute a highly conserved 2-His-1-carboxylate (HXD/E…H) motif that is found in nearly all 2OG-dependent oxygenases [119]. The 2OG binds to the Fe(II) via its 2-oxo and 1-carboxylate groups, while its 5-carboxylate is stabilised by Thr196 and Lys214 from FIH (Figure 1.4). This method of binding 2OG is distinct from that employed by the PHDs, and unique to members of the Jumonji C (JmjC) subfamily of 2OG-dependent dioxygenases, to which FIH belongs [120, 121].

1.3.2 Catalytic mechanism of hydroxylation by FIH

The configuration of Fe(II) and 2OG within the active site, together with the order in which they bind FIH, suggest that its catalytic mechanism is analogous to that employed by most other Fe(II) and 2-OG-dependent dioxygenases (reviewed in [122]). The reaction mechanism, detailed in Figure 1.5, involves a strict order of substrate/co-substrate binding, in which the Fe(II) cofactor binds first to the active site, followed by 2OG, then substrate and finally dioxygen. The binding of substrate prior to oxygen is of particular importance, as it prevents the formation of reactive oxidising species in the absence of substrate, thus reducing the likelihood of oxidative damage to FIH or oxidation of the Fe(II) to its inactive ferric form [123, 124]. Furthermore, it has important implications for the oxygen sensing properties of FIH. Since binding of the protein substrate actually primes the active site for binding to oxygen, subtle variations in the binding of different substrates has the potential to alter the affinity of FIH for oxygen, thus enabling each substrate to govern the oxygen sensitivity of its own hydroxylation. This may explain the range of K_m [O_2] values reported for FIH with HIF peptide substrates of various lengths

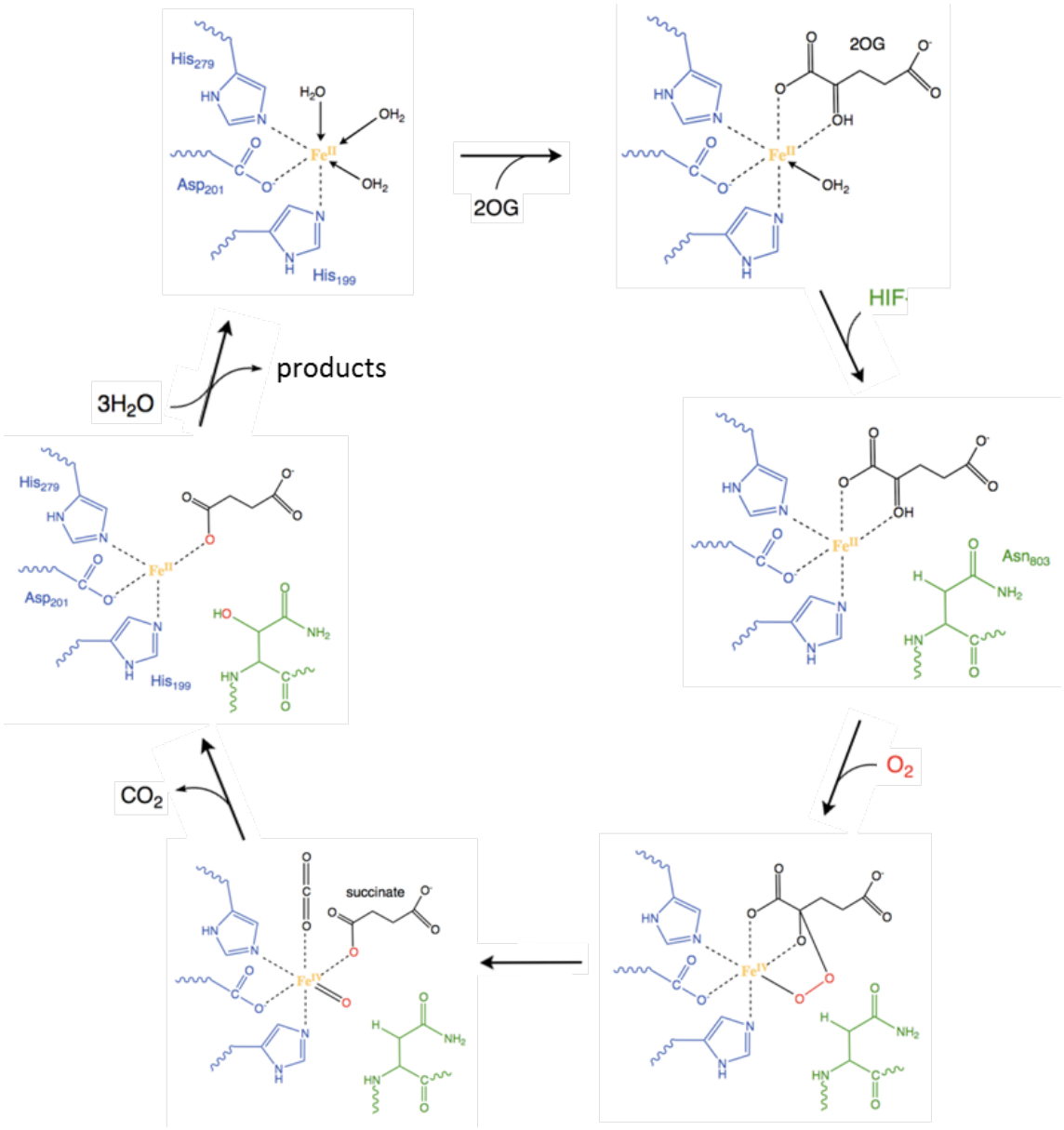

Figure 1.5 Catalytic Mechanism of Hydroxylation by FIH

Proposed mechanism of catalysis employed by FIH and other 2OG-dependent dioxygenases [122]. Within the active site of FIH, the Fe(II) is bound in an octahedral manner by the His^{199}-Asp^{201}-His^{279} facial triad. The remaining 3 coordination sites are initially occupied by water molecules, two of which are displaced upon binding of 2OG. Proximal binding of the prime substrate (HIF) leads to displacement of the final water molecule, creating an open coordination site that primes the active site for binding to dioxygen. Decarboxylation of the 2OG generates succinate and CO_2, and results in the production of a highly reactive ferryl-oxidising intermediate [Fe^{IV}=O], which is responsible for hydroxylation of the prime substrate. One of the oxygen atoms from dioxygen is incorporated into the hydroxylated product, whilst the other is incorporated into succinate. Figure generated using ChemDraw software (Cambridgesoft), and adapted from Ozer *et al*., 2007 [125].

(refer to Section 1.1.6). It will therefore be important to determine the $K_m[O_2]$ values for FIH with similar ARD peptide substrates, as these will indicate whether ARD hydroxylation is likely to be regulated by oxygen availability in a similar manner to the HIF CAD.

1.3.3 Substrate Recognition by FIH

Crystal structures of FIH in complex with peptide fragments of the hHIF-1α CAD provided the first real insight into the structural basis for substrate recognition by FIH [116]. Like most 2OG-dependent dioxygenases, substrate binding is largely mediated by residues from the first, second and eighth strands of the DSBH, which lie at the mouth of the active site. A long insertion between the 4th and 5th strands also makes important contributions, as do several of the helices that surround the DSBH core. Although FIH and HIF undergo an induced-fit interaction, the overall structure of FIH is not altered considerably upon binding. Subtle conformational changes within the active site enable FIH to accommodate the HIF peptide, and position the target Asn for hydroxylation at its β-carbon. In contrast, the HIF CAD is disordered in the absence of interacting proteins, but upon binding FIH adopts elements of secondary structure, as detailed below.

The crystal structure of the FIH-HIF complex reveals two distinct contact regions in the hHIF-1α CAD (Figure 1.6). The first of these contains the target asparagine (Asn803) and involves CAD residues 795-806, whilst additional contacts are made with a more C-terminal region comprising CAD residues 813-822. This extensive interaction interface buries a surface area of more than 2600 Å^2 and is stabilised by twelve hydrogen bonds, most of which are formed between FIH and the backbone of CAD residues at the N-terminal contact site. These CAD residues adopt an elongated conformation and bind in an extended groove in FIH. In contrast, CAD residues 816-823 form an induced α-helix that makes predominantly hydrophobic contacts with residues on the surface of FIH. HIF peptides lacking this C-terminal helix are still hydroxylated by FIH, indicating that this region is not essential for substrate recognition. Even so, kinetic analyses indicate that both the N-terminal and C-terminal contact sites are required for efficient hydroxylation [66, 116].

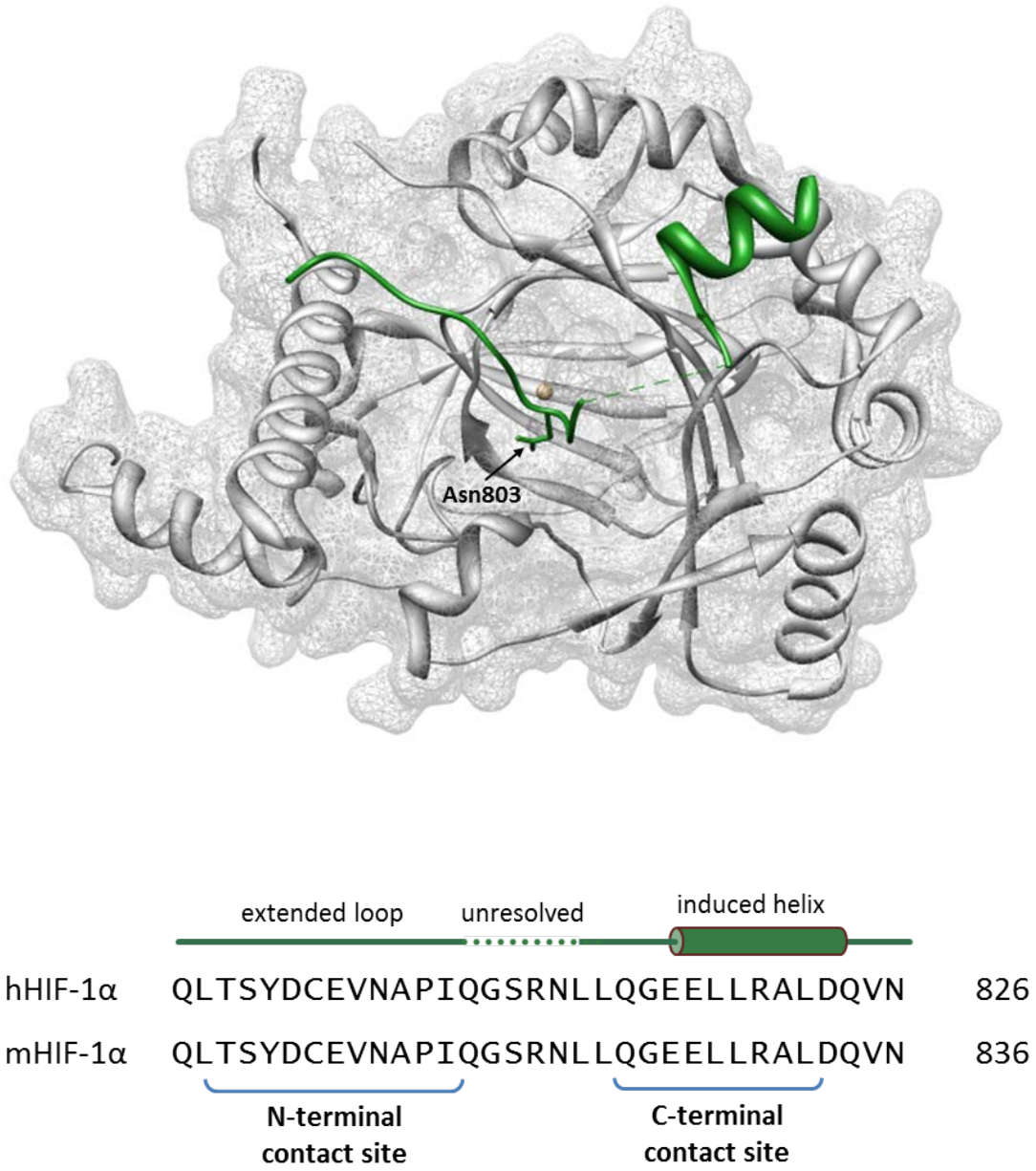

Figure 1.6 Structure of the HIF CAD in complex with FIH

A. Structure of FIH (grey ribbons and mesh surface) bound to a peptide fragment of the HIF CAD (green, visible residues 795-822). CAD residues 816-823 form an α-helix upon binding FIH. Residues 807-811, which are unresolved in the crystal structure, presumably do not interact with FIH. Image was generated from the crystal structure of the FIH-HIF complex (PDB ID: 1H2L [116]) using UCSF Chimera software [92]. B. Alignment of the hydroxylation sites in human and mouse HIF-1α. Brackets indicate the amino acids that comprise the N-terminal and C-terminal regions that contact FIH.

Precise orientation of the target Asn within the active site of FIH is required for hydroxylation. This is achieved, in part, by a backbone hydrogen bond between the residues at the -1 (Val802) and +1 (Ala804) positions relative to Asn803 in hHIF-1α [116]. This interaction generates a tight turn in the peptide backbone that projects Asn803 toward the Fe(II) centre. Even conservative substitution of these residues (V802A or A804V) leads to a significant reduction in the efficiency of hydroxylation by FIH [126, 127]. Likewise, FIH residues Arg238 and Gln239 make important contributions to the orientation of Asn803 within the active site [116, 128]. As shown in Figure 1.7, the side chains of these amino acids form hydrogen bonds with the primary amide of the Asn. These interactions are not only essential for hydroxylation, but may also account for the preference FIH displays for asparagine over aspartic acid residues [57, 104, 128]. Aside from these, FIH engages in very few specific side chain interactions with the HIF-1α CAD. Accordingly, substitution of individual CAD residues (with the exception of Val802 and Ala804) has little influence on hydroxylation [127].

The extensive size and plasticity of the substrate-binding interface also enable FIH to interact with ARD substrates, which exhibit considerable sequence variation and are structurally distinct from the HIF-α CAD.

1.3.4 Recognition of ARD substrates by FIH

Shortly after the commencement of this PhD research, Coleman et al. (2007) published crystal structures of FIH in complex with peptide fragments of the Notch1 ARD [95], spanning the target Asn and adjacent residues from Site 1 (Asn1945) or Site 2 (Asn2012). Unfortunately, the Notch peptides utilised in this study terminate shortly after the target Asn, and therefore only contain residues corresponding to those at the N-terminal FIH-contact site in HIF-1α. Although it is likely that Notch makes additional contacts with FIH, elucidation of these sites may require structural analyses of the full-length Notch ARD, or longer peptides that include additional residues C-terminal to the target Asn. Cockman *et al*. reported that attempts were made with FIH and the full-length Notch ARD, but these failed to yield suitable crystals. Nevertheless, the structural data obtained with the Notch1 peptides provide some important insights into ARD recognition by FIH.

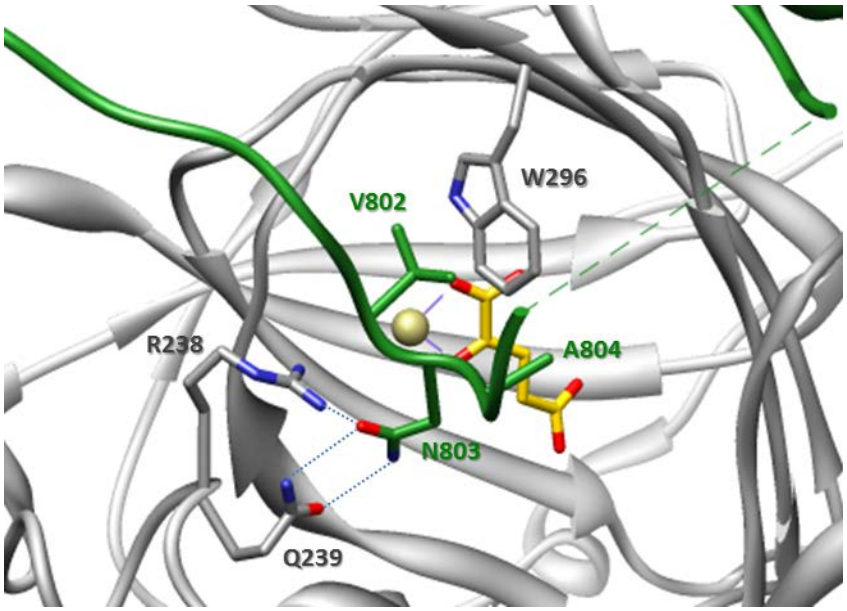

Figure 1.7 Precise positioning of HIF Asn803 within the active site of FIH

Close up view of the HIF CAD peptide (green, visible residues 798-805) bound within the active site of FIH (grey). Upon binding, the side chain of Trp296 in FIH must rotate in order to accommodate Val802 from the CAD. A backbone interaction (not shown) between Val802 and Ala804 creates a turn in the peptide backbone that projects Asn803 toward the Fe(II) centre. The Asn is held in place by hydrogen bonds (represented by dotted blue lines) with Arg238 and Gln239 in FIH. The Fe(II) is shown in gold, and the 2OG in yellow. Image was generated from the crystal structure of the FIH-HIF complex (PDB ID: 1H2L [116]) using UCSF Chimera software [92].

It is likely that the FIH-Notch interaction also occurs via an induced fit mechanism. FIH undergoes subtle structural alterations upon binding to the Notch peptides, akin to those that occur with the HIF-1α CAD. The arrangement of cofactors and positioning of the target Asn within the active site of FIH indicates that the mechanism of catalysis is also similar, with hydroxylation occurring at the β-carbon. In particular, the structural organisation of the peptide backbone is almost identical for equivalent regions of HIF and Notch when bound to FIH (Figure 1.8A).

Since individual ankyrin repeats are unable to adopt an ankyrin fold autonomously, the Notch peptides utilised in this study would presumably be unstructured in an unbound state, and therefore undergo only minor conformational changes upon binding to FIH [93]. However, native ARDs exhibit a conserved secondary and tertiary structure (described in Section 1.2.1), and as such, an interaction between FIH and the full-length Notch ARD would likely require a far more extensive structural rearrangement for hydroxylation to occur. As highlighted in Figure 1.8B, this is likely to include an extension of the β-hairpin loop region, as well as partial unfolding of the α-helix N-terminal to the hydroxylation site. Structures of FIH in complex with the full-length ARD would provide invaluable insights into how ARD recognition is achieved, however, these have not yet been described.

1.3.5 Identification of a FIH substrate motif

Sequence alignment of the hydroxylation sites from HIF and ARD substrates reveals considerable variation in the identity of residues proximal to the target asparagine (Figure 1.9). As a result, the consensus is largely degenerate. Nonetheless, strong conservation of several residues is observed, namely those at the -8, -2 and -1 positions relative to the target asparagine. Of these, only the -8 Leu is completely invariant in FIH substrates. Crystal structures of HIF and Notch peptides in complex with FIH reveal that this residue makes distinct contacts with a hydrophobic pocket on the surface of FIH, which may be required for binding [95, 116]. As described in Section 1.3.4, the -1 Val is likely to be important for positioning the target Asn within the active site, and may therefore contribute to the efficiency of FIH-catalysed ARD hydroxylation, as is the case for HIF-α

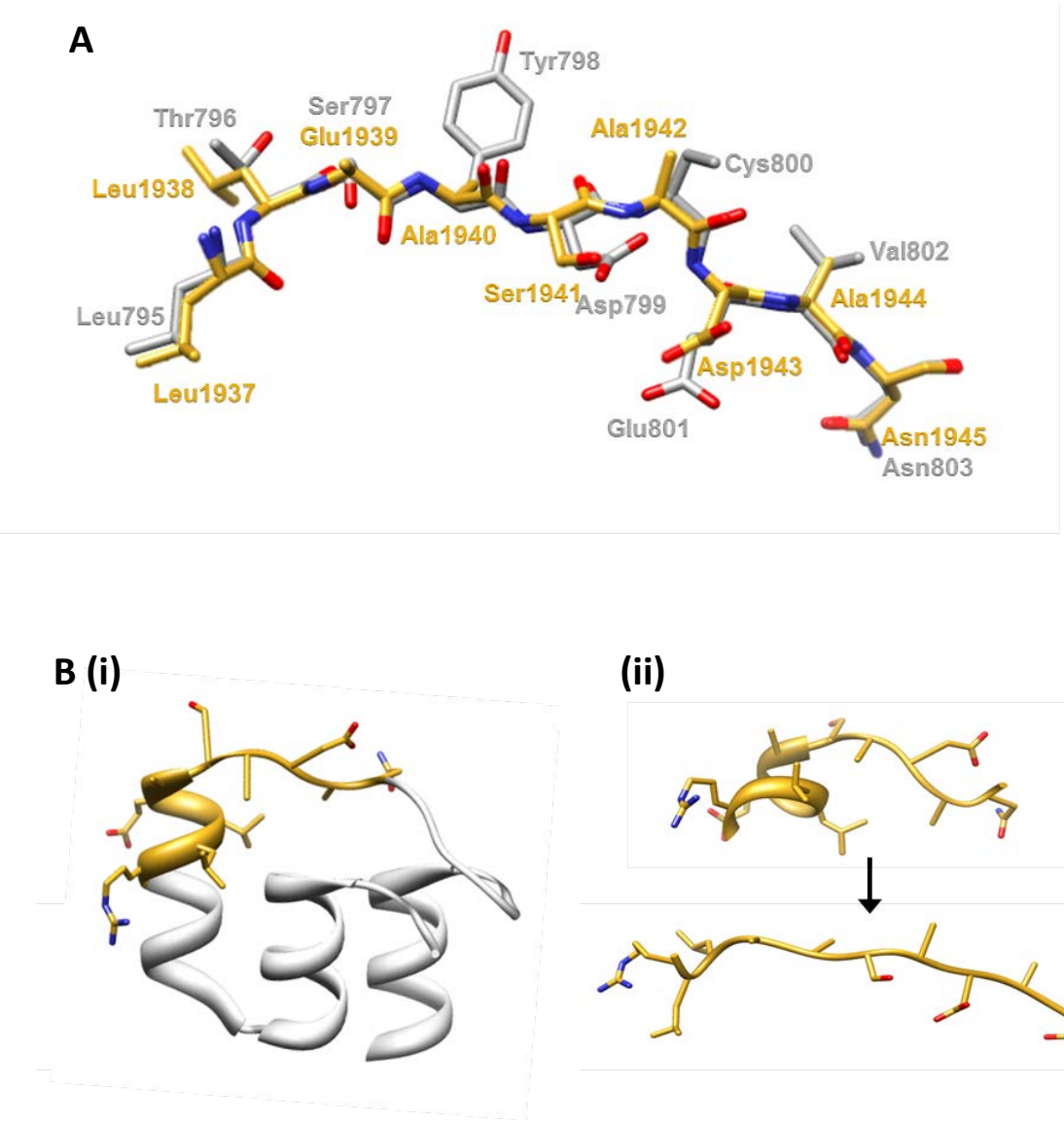

Figure 1.8 Structure of mNotch1 and hHIF-1α peptides in complex with FIH

A. Superimposed ball-and-stick representations of mNotch1 (1937-1945, yellow) and hHIF-1α (795-803, grey) peptides, taken from the crystal structures of these peptides in complex with FIH [PDB IDs: 1H2L [116] and 3P3N [95]]. Figure generated using UCSF Chimera software [92], and adapted from Coleman *et al*., 2007 [95].

B. The residues that comprise the Notch peptide described in A are highlighted in yellow to show their conformation in the context of a of a folded ankyrin repeat (i), in order to demonstrate the extensive conformation changes required for binding to FIH (ii).

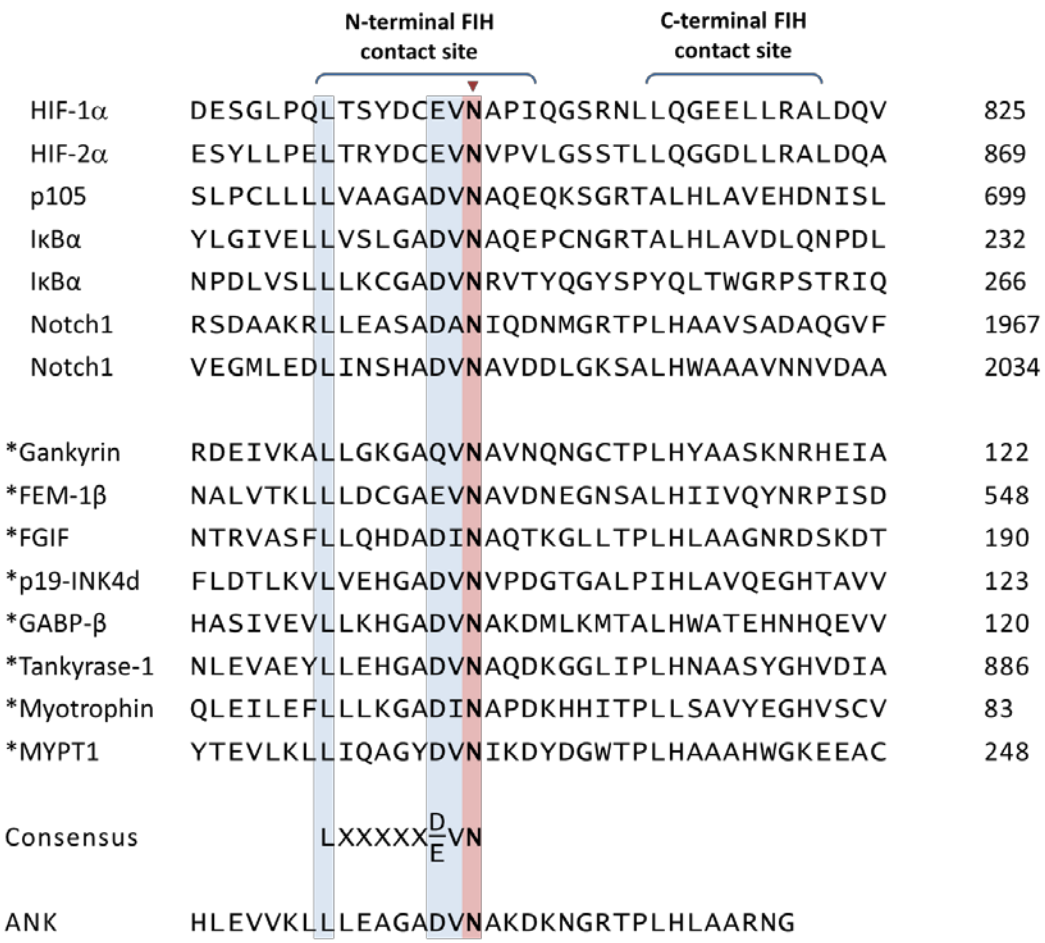

Figure 1.9 Substrate consensus sequence for FIH

Sequence alignment of hydroxylation sites from selected FIH substrates (those identified prior to the commencement of this work). The asterisk (*) denotes peptide substrates, for which hydroxylation of the full-length ARD has not been demonstrated. The target asparagine is in bold and is indicated by the red arrow (▼), while the numbers to the right specify the amino acid number of the most C-terminal residue shown. Conserved residues that form the consensus sequence for hydroxylation by FIH are highlighted [102]. The consensus sequence for ankyrin repeats (ANK) is included for comparison [88], and shows that all of the key residues required for hydroxylation by FIH are common in ankyrin repeats.

[127]. The reason for conservation of an acidic residue at the -2 position is not apparent from crystal structures. Although this residue engages in a backbone hydrogen bond with FIH, there is no evidence that the identity of the side-chain is important for binding or hydroxylation. Nonetheless, its presence is strongly correlated with hydroxylation by FIH. Thus, as concluded by Coleman *et al*. (2007), the preferred FIH substrate motif may be described as LXXXXX$\frac{\mathrm{D}}{\mathrm{E}}$VN [95].

Whilst this motif may facilitate the identification of novel ankyrin repeat substrates for FIH, it is by no means absolute. Not all ankyrin repeats that conform to the consensus are hydroxylated by FIH, and neither the acidic residue at the -2 position, or the -1 Val are completely conserved in HIF and ARD substrates (Figure 1.9), indicating that other factors, such as stability, must also be taken into consideration. Furthermore, these residues form part of the consensus sequence for the ankyrin repeat, and as such, their conservation in ARD substrates may not necessarily reflect any contribution to hydroxylation by FIH, but may be due to their importance in preserving the ankyrin fold. Clearly, further experiments are required to refine the consensus sequence for FIH, through the identification of specific residues involved in binding and catalysis.

1.4 Further investigation of ARD substrates is required

FIH was identified approximately a decade ago as an oxygen sensor for the mammalian hypoxic response pathway, and its role in regulating the activity of the HIF transcription factors is now well-established [129]. However, the recent discovery of ARD substrates and the somewhat unexpected phenotype of the $FIH^{-/-}$ mice have highlighted the possibility that FIH has yet uncharacterised roles in a number of other cellular pathways, and may provide an important link between these pathways and hypoxia [85, 130].

Given the large number of ARD substrates identified to date, and the diversity of their cellular roles, the consequences of FIH-catalysed ARD hydroxylation could potentially be wide-spread. Further investigation of this novel class of substrate is required in order to understand the specific physiological roles that FIH might be playing, and how these relate to its role as an oxygen sensor. Accordingly, this thesis aims to explore several important aspects of ARD hydroxylation, as detailed below.

1.4.1 Thesis Aims

The overall aim of this project is to characterise ankyrin repeat proteins as substrates for FIH. In particular, to determine how these proteins differ from HIF in terms of their recognition and hydroxylation by FIH, and to investigate potential mechanisms of cross-talk between ARD proteins and the HIF pathway.

The specific aims are as follows:

1) Analyse and compare the binding affinity, hydroxylation efficiency and oxygen sensitivity of FIH with respect to HIF and ARD substrates.

2) Examine the importance of primary, secondary and tertiary structure in FIH-substrate interactions and thus identify key molecular determinants of recognition and hydroxylation by FIH.

3) Identify and characterise novel ARD substrates of FIH. Specifically, the prediction that FIH-catalysed hydroxylation of ARDs extends beyond metazoa to include proteins encoded by viruses, and whether the expression of ARD proteins during viral infection has consequences for HIF regulation.

1.4.2 Differences in hydroxylation and binding of Notch and HIF-α by FIH

A key question that has arisen following the identification of ARD hydroxylation, is which of the two classes of substrate (HIF vs. ARD proteins) represents the 'preferred' substrate for FIH *in vivo*? This question is of renewed importance in light of the recently published FIH knockout mouse [85]. Prior to the commencement of this thesis, little was known about ARD proteins in terms of their recognition and hydroxylation by FIH. Preliminary data from affinity pull-downs and co-immunoprecipitation (CoIP) experiments performed in our laboratory indicated that FIH has a higher affinity for ARD proteins than for the HIF CAD, although ARD substrates are less efficient at promoting FIH-dependent 2OG turnover in the context of *in vitro* hydroxylation assays. The results from these experiments, although informative, provide only qualitative data about FIH-substrate interactions. Further experiments are required to extend these findings and identify key

differences in the properties of HIF and ARD proteins as substrates for FIH, and help understand substrate preference *in vivo*.

Therefore, the first part of this thesis (Chapter 3) presents a detailed analysis of the binding affinity, hydroxylation efficiency and oxygen sensitivity of FIH with respect to HIF and ARD substrates, using the Notch receptor family as examples of the latter. A range of biochemical and biophysical techniques were employed, including CO_2 capture assays to measure the kinetic parameters and oxygen-sensitivity of ARD hydroxylation, as well as fluorescence polarisation-based binding assays to accurately determine affinity constants for FIH-substrate interactions. The information obtained from these experiments is particularly relevant for understanding how FIH chooses between substrates within a cellular context, and whether these modifications are differentially regulated depending on oxygen availability.

A portion of this work was part of a collaborative project with Dr. Peppi Koivunen from the University of Oulu in Finland, and was published in the International Journal of Biochemistry and Cell Biology in 2009 (refer to Appendix 1 for a copy of the paper).

1.4.3 Molecular determinants of FIH substrate specificity

Initial characterisation of FIH substrate recognition was based primarily on the HIF proteins as substrates. The identification of ARD substrates has highlighted the ability of FIH to hydroxylate proteins that are distinct from HIF in terms of primary, secondary and tertiary structure. As discussed in section 1.3, crystal structures have now been solved for FIH in complex with peptides from both the HIF-1α CAD [116] and the ARD of Notch1 [95]. Despite similarities in the stereochemistry of these interactions, it is predicted that the full-length Notch ARD may be recognised in a manner that is, at least to some extent, distinct from shorter peptide fragments or indeed the HIF CAD.

In contrast with the HIF CAD, which lacks any discernible structure in the absence of FIH, ARD proteins exhibit conserved secondary and tertiary structures (described in section 1.2.1). How important this structural context is for the presentation and hydroxylation of the target asparagine is unknown at this stage. Likewise, the primary sequence

requirements for hydroxylation are unclear. A consensus sequence for FIH substrates has been described (refer to section 1.3.5), however, it is lacking in detail and requires further refinement.

These issues are addressed in Chapter 4 of this thesis, which presents a thorough investigation of the molecular determinants of recognition and hydroxylation by FIH. A series of point-mutants and chimeric substrate proteins were generated and analysed for their ability to bind FIH, and to promote 2OG turnover in *in vitro* hydroxylation assays. A biophysical approach was also employed to investigate the importance of protein structure and stability in substrate recognition. Collectively, these experiments highlight the importance of residues proximal to the asparagine in determining hydroxylation, and identify additional substrate-specific elements that contribute to distinct properties of HIF and ARD proteins as substrates for FIH. These distinct features are likely to influence FIH substrate choice *in vivo*, and therefore have important consequences for HIF regulation.

This work is presented as a manuscript that was recently accepted for publication by the Journal of Biological Chemistry.

1.4.4 Investigation of viral ARD proteins as substrates for FIH

The third and final aim of this thesis was to characterise FIH-catalysed hydroxylation of viral ARD proteins. The major focus of this thesis was understanding substrate recognition by FIH, specifically ARD substrates compared with HIF. Therefore, the identification and characterisation of new substrates, particularly those from quite different but relevant organisms, may be particularly informative. A bioinformatic search by our collaborator, Jonathan Gleadle from Flinders University in South Australia, identified a number of potential ARD substrates in the Orf virus. Whilst the vast majority of ankyrin repeats are found in eukaryotes, numerous copies of the repeat motif have been identified in the proteomes of bacteria and viruses [SMART protein database, [87]]. In particular, ARD proteins are highly expressed in poxviruses [131]. Close inspection of amino acid sequences from poxviral ARD proteins revealed a number of promising candidates for hydroxylation by FIH, including several ARD proteins from one virus in particular, Orf.

Orf virus is a strain of parapoxvirus that causes localised skin infections in sheep, goats, and to a lesser extent, humans [132]. Although the specific functions of the Orf virus ARD proteins have yet to be fully characterised, it is possible that hydroxylation by FIH may serve to regulate their activity, should they prove to be substrates. Furthermore, if these proteins are able to interact with FIH, and do so with the high affinity observed for other ARD proteins, there may be consequences for HIF regulation following virus infection.

Chapter 5 of this thesis investigates several of the Orf virus ARD proteins as novel substrates for FIH. These proteins were also analysed for their ability to bind FIH and, in doing so, regulate the activity of the HIF transcription factors through sequestration of FIH. These experiments not only provide the first direct evidence for hydroxylation of a non-metazoan protein by FIH, but may reveal a novel mechanism through which a virus can alter a host signalling pathway. This work was performed in collaboration with Jonathan Gleadle, as well as Ellena Whelan and Andrew Mercer from the University of Otago in New Zealand.

Chapter 2

Materials and Methods

2.1 List of Abbreviations

A_{280}	absorbance at 280 nm
Amp	ampicillin
ARD	ankyrin repeat domain
ATP	adenosine triphosphate
BSA	bovine serum albumin
Carb	carbenicillin
CD	circular dichroism
cpm	counts per minute
CAD	carboxy-terminal transactivation domain
dNTP	deoxyribonucleotide triphosphate
DTT	dithiothreitol
ECL	enhanced chemiluminescence
EDTA	ethylene diamine tetra acetic acid
EtBr	ethidium bromide
FIH	Factor Inhibiting HIF
FITC	fluorescein isothiocyanate
6H	6 x Histidine
HEPES	4-(2-Hydroethyl) piperazine-1- ethanesulphonic acid
HIF	Hypoxia Inducible Factor
HRP	Horseradish Peroxidase
IPTG	isopropyl-β-D-thiogalactopyranoside
Kan	kanamycin
LB	Luria Broth
MBP	maltose-binding protein
MQ	milliQ
MS	mass spectrometry
Ni^{2+}	nickel
Ni-IDA	nickel iminodiactic acid
NOG	N-oxalylglycine
NP-40	Nonidet P-40 or Octylphenoxy Polyethoxy Ethanol (Igepal CA-630)
OD_{600}	optical density at 600 nm
ODDD	oxygen-dependent degradation domain
ORFV	Orf Virus
2OG	2-oxoglutarate (α-ketoglutaric acid)
PAGE	polyacrylamide gel electrophoresis
PBS	phosphate buffered saline 20 mM sodium phosphate, 137 mM NaCl
PBT	phosphate buffered saline with 0.1% tween-20
PMSF	phenylmethyl sulphonyl fluoride
PNK	polynucleotide kinase
RT	room temperature
SDS	sodium dodecyl sulphate
Tween-20	polyoxyethylene-sorbitan monolaurate
Tris	Tris (hydroxymethyl) aminomethane
Trx	thioredoxin
Trx-6H	thioredoxin followed by 6 Histidine residues
WCEB	whole cell extract buffer

2.2 Materials

2.2.1 Equipment

SDS-PAGE Equipment	Biorad
Cell Disruptor	Microfluidics M-110L Pneumatic Microfluidizer
Sonicator	Sonifer cell-disruptor B-30
Wet Transfer Apparatus	Biorad
X-ray Film & Developer	Agfa CP1000
Scintillation Counter	LKB Wallac 1214 RACKBETA
Microplate Readers	BMG POLARstar Galaxy Perkin Elmer VICTOR™ X5
CD Spectrometer	Jasco J-815
Real-Time PCR System	Applied Biosystems ABI-7500 StepOnePlus System

2.2.2 Consumables

PD-10 Desalting Columns	GE Healthcare
Empty PD10 Columns	GE Healthcare
Centrifugal Filter Units	Amicon® Ultra (Millipore)
Bottle-top filters (0.45 μm, 500 ml)	Corning
Nitrocellulose Membrane	PALL BioTrace™ NT

2.2.3 Commercial Kits

Qiagen	QIAquick® Gel Extraction Kit QIAprep ® Spin Mini Kit QIAfilter ™ Spin Midi Kit RNeasy® Mini Kit
Promega	pGem®-T Easy Kit
Stratagene	Quikchange site-directed mutagenesis kit
Invitrogen	Superscript III cDNA synthesis kit

2.2.4 Chemicals and Reagents

All chemicals were purchased from Sigma unless specified below.

1Kb+ DNA Ladder	Invitrogen (Life Technologies)
10 x PCR enhancer	Invitrogen (Life Technologies)
^{14}C-labelled 2-oxoglutarate	Perkin Elmer
Amylose-agarose resin	Scientifix
BigDye Terminator (version 3)	Invitrogen (Life Technologies)
dNTPs	Finnzymes
DTT	BioVectra
ECL Reagent (Supersignal)	Pierce (Thermo Scientific)
IPTG	BioVectra
Ni-IDA-agarose resin	Scientifix
Oligo-dTs	Promega
Precision Plus Protein Dual Colour Marker	BioRad
Random dNTP hexamer	Geneworks (Perkin Elmer)
Restore - Western Blot Stripping Buffer	Pierce (Thermo Scientific)
RNAprotect Cell Reagent	Qiagen
RNase ZAP	Amersham
SUPERase-In	Ambion
SYBR®-Green Mastermix	Applied Biosystems
Ultima Gold XR Scintillation Fluid	Packard Bioscience

2.2.5 Enzymes

Sigma	Lysozyme
New England Biolabs	T4 DNA Ligase, Taq DNA Polymerase Restriction Enzymes (*Nco*I, *Not*I, *Xho*I, *Bgl*II)
Roche	*Asp*718 Restriction Enzyme
Stratagene	Pfu Turbo™ DNA Polymerase Pfu Ultra™ DNA Polymerase
Invitrogen (Life Technologies)	Superscript™ III Reverse Transcriptase Calf Intestinal Phosphatase AcTEV Protease
Boehringer Mannheim	Klenow DNA Polymerase

2.2.6 Antibodies

Primary Antibodies

FIH	No. 8: rabbit polyclonal sera generated in our laboratory against MBP-tagged full-length hFIH (1:1000 in PBT, overnight at 4°C)
	Novus Biologicals (NB100-428): purified rabbit polyclonal raised against full-length hFIH (1:1000 in PBT, overnight at 4°C)
Trx	Sigma (T0803): purified rabbit polyclonal raised against full-length *E. coli* thioredoxin (1:5000 in PBT, overnight at 4°C)
α-Tubulin	Novus Biologicals (NB600-506): purified rat monoclonal antibody (1:10 000 in PBT, overnight at 4°C)
ARNT	BAMBI: rabbit polyclonal sera generated by IMVS Antibody Services against the N-terminus (aa39-58) of hARNT1 (1:1000 in PBT + 0.5% skim milk, overnight at 4°C)
HIF-1α	BD Biosciences (610958): purified mouse polyclonal raised against the C-terminus (aa610-727) of hHIF-1α (1:1000 in PBT + 0.5% skim milk, overnight at 4°C)

Secondary Antibodies

anti-rabbit IgG	Pierce (31460): goat polyclonal, HRP conjugated (1:20 000 in PBT, 1 hour at RT)
anti-mouse IgG	Pierce (31430): goat polyclonal, HRP conjugated (1:20 000 in PBT, 1 hour at RT)
anti-rat IgG	Abcam (ab6845): goat polyclonal, HRP conjugated (1:20 000 in PBT, 1 hour at RT)

2.2.7 Buffers and Solutions

Coomassie Stain:	0.03% coomassie blue, 8.75% acetic acid, 50% methanol
Destain:	5% acetic acid, 50% methanol
DNA load buffer (6x):	50% glycerol, 0.01% bromophenol blue, 0.01% xylene cyanol 0.1 mM EDTA pH 8.0
Amylose Lysis Buffer:	20 mM Tris pH 8, 150 mM NaCl, 1 mM PMSF*
Amylose Elution Buffer:	20 mM Tris pH 8, 150 mM NaCl, 10 mM maltose
Standard Assay Buffer:	20 mM Tris pH 8, 150 mM NaCl
Nickel Lysis Buffer:	20 mM Tris pH 8, 500 mM NaCl, 5 mM imidazole, 0.5 mM DTT,* 1 mM PMSF*
Nickel Wash Buffer:	20 mM Tris pH 8, 500 mM NaCl, 10 mM imidazole
Nickel Elution Buffer:	20 mM Tris pH 8, 500 mM NaCl, 250 mM imidazole
Crude Lysis Buffer:	2% SDS, 100 mM DTT
Pull-down Buffer:	20 mM Tris pH 7.5, 150 mM NaCl, 10% glycerol, 1% NP40
Ligation Buffer:	500 mM Tris pH 7.5, 10 mM $MgCl_2$, 10 mM DTT, 50 μg/ml BSA
SDS load buffer (2x):	20% glycerol, 1% bromophenol blue, 4% SDS, 62.5 mM Tris pH 6.8, 2 mM EDTA, 100 mM DTT*
Tricine load buffer (5x):	50% glycerol, 0.1% bromophenol blue, 10% SDS, 250 mM Tris pH 8.3, 150 mM DTT*
CD Buffer:	5 mM Sodium Phosphate (pH 8.0)
TEV Buffer:	50 mM Tris pH 8, 0.5 mM EDTA, 1 mM DTT*
Wet Transfer Buffer:	50 mM Tris, 2.85% glycine
WCEB:	20 mM HEPES, 0.42 mM NaCl, 0.5% NP-40, 25% glycerol, 1.7 mM EDTA, 1.5 mM $MgCl_2$, 1 mM PMSF,* 1 mM DTT,* 2 μg/ml aprotinin,* 4 μg/ml bestatin,* 5 μg/ml leupeptin,* 1 μg/ml pepstatin*

* add immediately prior to use

2.2.8 Bacterial Growth Media

LB	Luria Broth 1% tryptone, 0.5% yeast extract, 1% NaCl, pH 7.5, autoclaved
LB-Amp	LB with 100 μg/ml of Ampicillin
LB-Kan	LB with 50 μg/ml of Kanamycin
LB-Carb	LB with 100 μg/ml Carbenicillin
LB-Agar	LB with 1.5% agar
SOC	Super Optimal broth with Catabolite repression 2% tryptone, 0.5% yeast extract, 10 mM NaCl, 2.5 mM KCl, 10 mM $MgCl_2$, 10 mM $MgSO_4$, 0.2% glucose, pH 7.5, autoclaved

2.2.9 Plasmids

pGem-T Easy

The pGem-T Easy plasmid (Promega) is pre-linearised with EcoRV and modified by the addition of a deoxy thymidine phosphate at each 3' end. These single 3'T overhangs enable efficient insertion of PCR products pre-treated with Taq polymerase to add a single deoxy adenosine phosphate at the 3' ends of the amplified fragments.

Bacterial Expression Plasmids

pET32a(+)

The pET32a(+) vector (Novagen) encodes an amino-terminal thioredoxin-6-histidine (Trx-6H) tag that enables purification of a fusion partner by Ni^{2+}-affinity chromatography. It contains a T7 promoter followed by a *lac* operon, allowing transcription by T7 RNA polymerase and induction of protein expression by the lactose analogue IPTG. Thus, pET32a(+) constructs are expressed at high levels in BL21 (DE3) *E. coli*, which express T7 polymerase, also under *lac* operon control.

pET32-TEV

The pET32-TEV vector was generated through the insertion of a TEV protease recognition sequence (ENLYFQG) between the *Kpn*I and *Nco*I restriction sites of the pET32a(+) vector to replace the original enterokinase site. This plasmid was constructed by Fiona Whelan and is described in her PhD thesis [133].

pET32-TEV-Kpn1

This vector was constructed by the insertion of a TEV protease recognition sequence (ENLYFQG) between the *Bgl*II and *Kpn*I restriction sites of the pET32a(+) vector, permitting use of the *Kpn*I site for cloning. The TEV site was inserted using complimentary 5'-phosphorylated oligos (5'-GATCTGGAAAACCTGTACTTCCAGGGCG-3', 5'-GTACCGCCCTGGAAGTACAGGTTTTCCA-3'), which annealed to produce a fragment with sticky ends compatible with the *Bgl*II and *Kpn*I-cut plasmid. The original frame of the multiple cloning site was maintined.

pMBP

The pMBP vector was obtained from Richard Bruick and is described in Sheffield *et al*., 1999 [134]. It encodes maltose-binding protein (MBP) that creates an N-terminal fusion to the inserted protein of interest, enabling purification of the fusion protein by amylose affinity chromatography. The promoter is under the control of the *lac* operator, which permits IPTG-inducible expression. The mRNA is not transcribed by T7 polymerase, thus expression can be achieved in *E. Coli* strains that do not carry the λDE3 lysogen.

pAC28-H6-TEV

This plasmid is a modified version of the pAC28 vector [135], and is described in Wilkins *et al*., 2012 [136]. It encodes an N-terminal 6H tag that enables purification of a fusion partner by Ni^{2+}-affinity chromatography, but can be cleaved with TEV protease. The mRNA is transcribed by T7 polymerase, and is under the control of the *lac* operon, allowing induction of protein expression by the lactose analogue IPTG. Thus, pAC28-H6-TEV constructs are expressed at high levels in BL21 (DE3) *E. coli*, which express T7 polymerase, also under *lac* operon control.

FIH Expression Plasmids

pMBP-hFIH: generated by Dr. Richard Bruick through insertion of full-length human FIH between the *Nco*I and *Xho*I sites of pMBP. Described in Lando et al., 2002 [58].

pET32-TEV-hFIH: full-length human FIH was subcloned from pMBP into pET32-TEV between the *Nco*I and *Xho*I restriction sites. Described in Linke et al., 2007 [105].

pMBP-mFIH: full-length mouse FIH was amplified by PCR from a mouse E10.5 cDNA library (Invitrogen) using the PCR primers described below, and cloned into pMBP between the *Nco*I and *Xho*I restriction sites.

mFIH-1 FL F: 5'-TATACCATGGCGGCGACGGC-3'

mFIH-1 FL R: 5'-ATCTCGAGTTAGTTGTAACGGCC-3'

pAC28-H6-TEV-mFIH: full-length mFIH was subcloned from pMBP into pAC28-H6-TEV between the *Nco*I and *Xho*I restriction sites. Described in Wilkins *et al*., 2012 [136].

pET32-TEV-hFIH L340R: generated by QuikChange site-directed mutagenesis (Stratagene) of pET32-TEV-hFIH using the following primer and its reverse compliment: hFIH-1 L340R: 5'-GTGGGGCCCTTGAGGAACACAATGATCAAGGGC-3'

HIF-1α Expression Plasmids

pET32-hHIF-1α CAD (737-826) wildtype, RLL781-783AAA and LL782-783AA: kindly provided by Sarah Linke and described in Wilkins *et al*., 2012 [136].

pET32a-TEV-mHIF-1α CAD-50 and CAD-90: the last 50 amino acids (787-836) and the last 90 amino acids (747-836) of the mouse HIF-1α CAD were amplified by PCR from a mouse E10.5 cDNA library (Invitrogen) using the primers described below and cloned into pET32-TEV between the *Nco*I and *Not*I restriction sites.

mHIF-1α 787F: 5'-TACCATGGCCGATTTAGCATGC-3'

mHIF-1α 747F: 5'-ATCCATGGCATTATTGCAGCAACC-3'

mHIF-1α 836R: 5'-TAGCGGCCGCTCAGTTAACTTGATCCAAAGC-3'

pET32-mHIF-1α CAD-90 N813A: generated by QuikChange site-directed mutagenesis (Stratagene) of pET32-mHIF-1α CAD-90 using the following primer and its reverse compliment: mHIF-1α N813A 5'-CGATTGTGAAGTTGCTGCTCCCATACAAGG-3'

pET32a-hHIF-1α ODDD/C-TAD: amino acids 356-826 of human HIF-1α comprising the ODDD and CTAD were amplified from human 293T cell cDNA using the primers described below, and cloned into pET32 between the *Kpn*I and *Xho*I restriction sites.

hHIF-1α Q326 F: 5'-TGTCGGTACCCAAACAGAATGTGTCCTTAAACCGG-3'
hHIF-1α N826 R: 5'-AAGCCTCGAGTCAGTTAACTTGATCCAAAGCTCTGAG-3'

Notch Expression Plasmids

pET32-Notch1 RAM (1753-1847): generated and kindly provided by Sarah Linke, and described in Zheng *et al.*, 2008 [94].

pET32-Notch ARD Constructs: pET32-mNotch1 ANK1-7 (1862-2104), pET32-mNotch2 ANK1-7 (1817-2061), pET32-mNotch3 ANK1-7 (1781-2026) and pET32-mNotch4 ANK1-7 (1570-1815) were constructed by inserting the respective PCR products into pET32a(+) between the *Kpn*I and *Xho*I sites. The following PCR primers were used to amplify the specified products from a mouse E10.5 cDNA library (Invitrogen).

mNotch1 1862F: 5'-TGTCGGTACCATGGATGTCAATGTTCGAGGACC-3'
mNotch1 2104R: 5'-AAGCCTCGAGTCAATCCAAAAGCCGCACGATATCGTGG-3'

mNotch2 1817F: 5'-TGTCGGTACCCTGGACGTGAATGTCCGAGG-3'
mNotch2 2061R: 5'-AAGCCTCGAGTCAGTCCAGGAGGCGAACGATGTCATGC-3'

mNotch3 1781F: 5'-TGTCGGTACCGTGGATGTCAACGTCCGAGG-3'
mNotch3 2026R: 5'-AAGCCTCGAGTCAGTCCAGCAACCGCACAATGTCCTGC-3'

mNotch4 1570F: 5'-TGTCGGTACCCTGGATGTGGACACCTGTGG-3'
mNotch4 1815R: 5'-AAGCCTCGAGTCATTCCAGCAGCGTTAGCAGGTCCCAG-3'

pAC28-H6-TEV-Notch1 ANK1-7 wildtype and N2012Q: mNotch1 ANK1-7 wildtype and N2012Q were sub-cloned from pET32a(+) into pAC28-H6-TEV between the *Kpn*I and *Xho*I restriction sites. Described in Wilkins *et al*., 2012 [136].

Notch ARD mutant constructs: pET32-mNotch1 ANK1-7 N1945A, N2012A and N1945A/N2012A, N1945Q, N2012Q, N1945Q/N2012Q, A1944P/N2012Q, I1946Q/N2012Q and A1944P/I1946Q/N2012Q, pET32-mNotch2 ANK1-7 N1902A, N1969A and N1902A/N1969A, pET32-mNotch3 ANK1-7 N1867A, N1934A and N1867A/N1934A, pET32-mNotch4 ANK1-7 P1655A, Q1657I and P1655A/Q1657I mutants were generated by QuikChange site-directed mutagenesis (Stratagene) using the following primers and their reverse compliments:

mNotch1 N1945A: 5'-GTGCAGATGCCGCCATCCAGGACAAC-3'
mNotch1 N2012A: 5'-CATGCTGACGTCGCTGCCGTGGATG-3'
mNotch1 N1945Q: 5'-GTGCAGATGCCCAGATCCAGGACAAC-3'
mNotch1 N2012Q: 5'-CATGCTGACGTCCAGGCCGTGGATG-3'
mNotch1 A1944P: 5'-GGCCAGTGCAGATCCCAACATCCAGGAC-3'
mNotch1 I1946Q: 5'-GTGCAGATGCCAACCAGCAGGACAACATGGGCCG-3'
mNotch1 A-P/I-Q: 5'-GTGCAGATCCCAACCAGCAGGACAACATGGGCCG-3'

mNotch2 N1902A: 5'-GGTGCGGATGCAGCTGCCCAGGACAACATGG-3'
mNotch2 N1969A: 5'-CAAGCAGATGTCGCTGCAGTGGATG-3'

mNotch3 N1867A: 5'-GGGCGGACACCGCCGCCCAGGATCATTCG-3'
mNotch3 N1934A: 5'-CATGCCGATGTCGCTGCAGTGGATG-3'

mNotch4 P1655A: 5'-GGCTGGAGCCAACGCCAACCAGCCAGA-3'
mNotch4 Q1657I: 5'-GAGCCAACCCCAACATCCCAGACCGCGCTGGG-3'
mNotch4 P-A/Q-I: 5'-GAGCCAACGCCAACATCCCAGACCGCGCTGGG-3'

Gankyrin Expression Plamids

pET32-Gankyrin: generated by Iain Murchland through insertion of full-length human Gankyrin between the *Eco*RI and *Xho*I sites of pET32a(+).

pAC28-H6-TEV-Gankyrin: full-length human Gankyrin was sub-cloned from pET32a(+) into pAC28-H6-TEV between the *Eco*RI and *Xho*I restriction sites.

Chimeric Constructs

pET32-HIF/Notch helix: this construct was generated by PCR and is described in Wilkins *et al*., 2012 [136]. Briefly, primers were designed to amplify the mHIF-1α CAD (747-836), and simultaneously replace the last 18 amino acids (819-836) with helix 3A from the mNotch1 ARD (residues 1950-1963). The resultant chimera was then cloned into pET32a(+) between the *Nco*I and *Xho*I restriction sites.

pET32-Notch/HIF linker: this construct was generated by overlap extension PCR and is described in Wilkins *et al*., 2012 [136]. Briefly, one of the β-hairpin regions (residues 1940-1953) in pET32-mNotch1 ANK1-7 N2012Q was replaced with a linker region comprised of mHIF-1α residues 808-825.

pAC28-H6-TEV-Notch/HIF linker: the Notch/HIF linker chimera was subcloned from pET32a(+) into pAC28-H6-TEV between the *Kpn*I and *Xho*I restriction sites.

Orf Virus Expression Plasmids

pAPEX-Flag008, 123 and 126: also called pVU655, pVU657 and pVU661, respectively. Kindly provided by Andrew Mercer and described in Sonnberg *et al*., 2008 [137]. These constructs were generated by insertion of the 008, 123 and 126 genes from Orf virus strain NZ2 into the mammalian expression vector pAPEX3, which was also modified to include a Flag-tag at its N-terminus.

pET32-ORFV ARD constructs: pET32-ORFV 008 full-Length (1-516), pET32-ORFV 008 ARD (1-325), pET32-ORFV 123 ARD (1-366) and pET32a-ORFV 126 ARD (1-342) were generated by inserting the respective PCR products (amplified from the corresponding pAPEXFlag constructs) into pET32a(+) using restriction sites (underlined) incorporated in the following PCR primers:

Orf 008 1F	5’-TGTCGGTACCATGCTCTCGCGGGAGTCCGTCGTGGTCCC-3’ (*Kpn*I)
Orf008 325R	5’-AAGCCCATGGTCAGTGCTCGAGCTCCGCGCCCATGCG-3’ (*Nco*I)
Orf008 516R	5’-AAGCCCATGGTCAGGGGCGGGTCAGCATGGCG-3’ (*Nco*I)
Orf123 1F	5’-TTAGCCATGGAAAACAACGACGGCAACG-3’ (*Nco*I)
Orf123 366R	5’-AAGCCTCGAGTCAGGCGTCCGCGGGAGG-3’ (*Xho*I)
Orf126 1F	5’-TTAGAGATCTGATGGCCGATGAGAGAGAGG-3’ (*Bgl*II)
Orf126 386R	5’-AGCAGTCGACTCAGGCCGCGCTCGGCGTGC-3’ (*Sal*I)

2.2.10 Oligonucleotides

The following primers were used for sequencing, overlap-extension PCR and colony PCR.

S-tag:	5’-GGTTCTGGTTCTGGCCATT-3’
T7 Terminator:	5’-GCTAGTTATTGCTCAGCGG-3’
MBP 5’ Seq:	5’-CTGAAAGACGCGCAGAC-3’
BS M13-20:	5’-GTAAAACGACGGCCAGT-3’
BS Reverse:	5’-AACAGCTATGACCATG-3’

Primers for qPCR are described in Section 2.3.2.

2.2.11 Bacterial Strains

DH5α *E. coli*

This strain was used for plasmid amplification and cloning. Genotype: F^- Φ80d*lacZ*ΔM15, Δ(*lacZYA-argF)* U169, *deo*R, recA1, relA1, endA1, *thi*-1, *gyrA*96, sup*E*44, *hsd*R17($r_K^-m_K^+$), λ^-.

BL21(DE3) *E. coli*

This strain was used for recombinant protein expression. Genotype: *E. coli* B F^- *dcm ompT* *hsdS*($r_B^-m_B^-$) *gal* λ(DE3).

2.2.12 Peptides

The following table lists the amino acid sequences of synthetic peptides (Auspep) representing the hydroxylation sites in mNotch1-3 (Sites 1 and 2). The asparaginyl residues targeted by FIH are underlined.

	Peptide	Sequence
mNotch1	S1: N1945	RSDAAKRLLEASADA<u>N</u>IQDN
	L1: N1945	RSDAAKRLLEASADA<u>N</u>IQDNMGRTPLHAAVSADA
	S2: N2012	VEGMLEDLINSHADV<u>N</u>AVDD
	L2: N2012	VEGMLEDLINSHADV<u>N</u>AVDDLGKSALHWAAAVN
mNotch2	L1: N1902	RADAAKRLLDAGADA<u>N</u>AQDNMGRCPLHAAVAADA
	L1: N1969	VEGMVAELINCQADV<u>N</u>AVDDHGKSALHWAAAVN
mNotch3	L1: N1867	RADAAKRLLDAGADT<u>N</u>AQDHSGRTPLHTAVTADA
	L1: N1934	VEGMVEELIASHADV<u>N</u>AVDELGKSALHWAAAVN

2.3 Methods

2.3.1 RNA Techniques

All manipulation of RNA was performed with designated RNase-free microcentrifuge tubes, filter-tips and reagents, and any materials that came into contact with RNA were cleaned with RNase ZAP prior to use.

2.3.1.1 Total RNA isolation from sheep LT cells

Primary lamb testis (LT) cells, either uninfected or infected with Orf virus NZ2, were prepared by Ellena Whelan from the University of Otago in New Zealand, stabilised in RNAprotect cell reagent (~250 μl/1x10^6 cells) and shipped to our laboratory at room temperature. Upon arrival, samples were centrifuged (5000 x g for 5 mins) and the RNAprotect reagent removed by pipetting. Total RNA was isolated from the cell pellet using the RNeasy Mini Kit (Qiagen), and purified RNA stored at -20°C in RNase-free water.

2.3.1.2 Verification of RNA quality

RNA concentration was determined by measurement of optical absorbance at 260 nm (A_{260}) with an absorbance factor of 40 μg/ml. Purity was assessed by the A_{260}/A_{280} ratio, with values >1.6 considered to be of reasonable purity. The integrity of the RNA was analysed by 1% agarose gel electrophoresis with ethidium bromide staining, enabling visualisation of bands corresponding to the 28S and 18S ribosomal RNAs under UV light.

2.3.2 DNA Techniques

Preparation of plasmid DNA was performed using either the QIAprep Spin Mini Kit or the QIAfilter Spin Midi Kit (Qiagen). The concentration of DNA was determined by optical absorbance at 260 nm, with an absorbance factor of 50 μg/ml. All restriction digests were performed according to manufacturers' instructions. DNA was assessed for size and purity using 1xTBE agarose gel electrophoresis and ethidium bromide staining according to standard procedures. Gel purifications were performed using the QIAquick gel extraction kit (Qiagen).

2.3.2.1 cDNA Synthesis

1 μg of RNA was added to 1 μl of random dNTP hexamer (300 ng/μl) and 1 μl oligo-dTs (500 ng/μl), and the volume made up to 19 μl with MQ water. RNA was denatured at 70°C for 10 minutes then cooled on ice for 5 minutes to allow primer annealing. Reagents for reverse transcription were then added: 6 μl Superscript III buffer (5x), 2 μl DTT (0.1M), 1 μl SUPERase-In and 1 μl Superscript III Reverse Transcriptase or MQ water in the 'no RT' control reactions. Reactions were then incubated at 50°C for 2.5 hours, followed by heat inactivation at 70°C for 15 minutes. cDNA samples were stored at -20°C.

2.3.2.2 Polymerase Chain Reaction (PCR)

Standard 25 μl reactions consisted of 2.5 μl Pfu Turbo buffer (10x), 2.5 μl 10x PCR enhancer, 1 μl dNTPs (10 mM), 1 μl of each primer (100 ng/μl), 0.5 μl Pfu Turbo DNA Polymerase (5U/μl) and finally 1 μl of cDNA template (100 ng) obtained from either sheep LT cells, 293T cells (Rachel Hampton-Smith) or a mouse E10.5 cDNA library (Invitrogen). Normal cycling parameters were: 95°C for 5 minutes, 30 x (95°C for 30 seconds, 50-65°C for 30 seconds, 72°C for 1 minute), 72°C for 5 minutes, hold at 4°C. PCR products were separated and visualised by agarose gel electrophoresis and ethidium bromide staining. PCR products of the expected size were excised from the gel and purified using the QIAquick gel extraction kit (Qiagen).

2.3.2.3 Quantitative Real-Time PCR (qPCR)

Quantitative PCR was performed in triplicate on cDNA samples from ORFV-infected and uninfected LT cells. A single reaction for each 'no RT' sample was also included as a negative control. Reactions were set up on ice, and each contained 10 μl of 2x Fast SYBR Green Mastermix (Applied Biosystems), 1 μl of cDNA (or 'no RT' control), 0.4 μl of each primer (10 μM) and RNase-free water to a final volume of 20 μl. To minimise error from pipetting, all reactions were prepared using a mastermix of SYBR green and cDNA, with the primers and water added from a separate mastermix. Reactions were run on a StepOnePlus thermo-cycler (Applied Biosystems), with the following cycling parameters: 95°C for 20 seconds, 40 x (95°C for 3 seconds, 60°C for 30 seconds). After 40 cycles were complete, the temperature was increased from 60°C to 95°C in 0.5°C increments, with

fluorescence measured at each increment to give a melting curve that was used to estimate the accuracy of the reaction in amplifying a single product. PCR products were also visualised by 2% agarose gel electrophoresis and ethidium bromide staining. Relative amounts of target gene mRNA were determined using StepOne and Q-Gene software [138].

The following sets of qPCR primers were designed using Primer 3 software [139], as described in Appendix 5. Efficiency of amplification was verified by analysis of standard curves using StepOnePlus software (Applied Biosystems).

	Forward Primer (5'-3')	Reverse Primer (5'-3')	Amplicon
RPLP0	GCGACCTGGAAGTCCAACTA	TGTCTGCTCCCACAATGAAG	82 bp
VEGF	TTGCCTTGCTGCTCTACCTT	AGATGTCCACCAGGGTCTCA	147 bp
PHD3	TTACCTCCTGTCCCTCATCG	GTTCCATTTCCTGGGTAGCA	114 bp
GLUT1	ATCCTCATTGCCGTGGTG	GCCTTCTCGAAGATGCTTGT	89 bp
POLR2A	TACTCAGCACCAGCATCACC	AACTCCCCGTCCTCTGTGAT	92 bp
GAPDH	CACAGTCAAGGCAGAGAACG	TACTCAGCACCAGCATCACC	112 bp
ARNT1	TTCCCTTGTCTTCCTGCATC	AACCCAGCCTCAGTTTTTCA	97 bp
β-ACTIN	CTGCCTGACGGCCAGG	GATTCCATACCCAAGAAGGAAGG	89 bp

2.3.2.4 Ligations

Reactions contained 1 μl of 10x ligation buffer, 1 μl of T4 DNA ligase (2U/μl), 1 μl of ATP (10 mM) and a 1:3 molar ratio of vector to insert, with 100-200ng total DNA per reaction. Reactions were made up to 10 μl with MQ water and incubated overnight at 16°C.

2.3.2.5 A-tailing and pGem-T Easy Ligations

5 μl of purified PCR product (approximately 150 ng) was mixed with 1.5 μl 10x Thermopol buffer, 0.9 μl $MgCl_2$ (25 mM), 1 μl dATP (0.25 mM) and 1 μl Taq DNA Polymerase (5U/μl). Reactions were made up to 15 μl with MQ water and incubated at 70°C for 30 minutes. 5.5 μl of A-tailed PCR product was then used in a ligation with 1 μl of pGem-T Easy, 1 μl of T4 DNA ligase and 7.5 μl of the supplied 2x ligation buffer. Ligations were incubated at 4°C overnight, then transformed into competent Dh5α *E. coli* and plated onto LB-

agar/Amp, which had been spread with 100 μl IPTG (0.1 M) and 20 μl X-gal (50 mg/ml) 30 mins prior to use. White colonies were selected for plasmid preparation and sequencing.

2.3.2.6 Cloning of Oligonucleotides

Oligonucleotides were purchased already 5'-phosphorylated or were phosphorylated as follows: 20 μl of oligo (20 pmol/μl) was added to 1 μl PNK (Polynucleotide Kinase), 3 μl 10x PNK Buffer and 1.5 μl ATP (10 mM). The reaction volume was made up to 30 μl with MQ water and incubated at 37°C for 1 hour, then heat inactivated at 65°C for 10 minutes. To anneal the oligos, 24.5 μl of each phosphorylated oligo was added to a microcentrifuge tube with NaCl added to a final concentration of 50 mM. The mixture was incubated at 95°C for 5 minutes, then slowly cooled to room temperature (~1 hour). Phosphorylated, annealed oligos were then serially diluted and used in a series of ligations. Following transformation into Dh5α *E. coli*, the colonies produced from the lowest dilution of oligo yielding at least 2 fold more colonies than the no-insert ligation control (which were least likely to contain multiple insert clones) were picked for plasmid amplification.

2.3.2.7 Transformations

Approximately 10 ng of plasmid DNA or 10 μl of ligation mixture was added to 40 μl of chemically competent DH5α or BL21 *E. coli* that had been thawed on ice. Tubes were gently flicked and left on ice for 10 minutes, after which the cells were heat-shocked at 42°C for 45 seconds. Cells were returned to ice for 20 minutes, then 450 μl of SOC medium was added. Samples were then rocked at 37°C for 30 mins, and 150 μl was plated onto selective LB-agar plates and grown at 37°C overnight.

2.3.2.8 Sequencing

In a standard sequencing reaction, 1 μl of BigDye Terminator reaction mix (V3.1) was added to 4 μl of 5x sequencing buffer, 100 ng of sequencing primer and 400 ng of DNA template, then made up to 20 μl with MQ water. Reactions were placed into a thermal cycler with the following cycling parameters: 96°C for 3 minutes, 25 x (96°C for 30 seconds, 50°C for 15 seconds, 60°C for 4 minutes), hold at 4°C. After completion of the cycles, 80 μl of 75% isopropanol was added, and the mixture was incubated at room

temperature for 25 minutes. Extension products were pelleted by centrifugation at 15,000 x g for 20 minutes, and the supernatant removed completely. 250 μl of 75% isopropanol was then added to wash the pellet, followed by centrifugation for a further 10 minutes at 15,000 x g. The supernatant was removed immediately following centrifugation, and the pellets were dried for 1 minute on a 95°C heat-block. The samples were then sent to the Australian Genome Research Facility (AGRF) for analysis by capillary separation.

2.3.2.9 Site-Directed Mutagenesis / Overlap-Extension PCR

Single amino acid substitutions were made using the QuikChange Site-directed Mutagenesis Kit (Stratagene). Larger insertions and deletions were generated using overlap extension PCR as follows. First round PCR reactions consisted of 2.5 μl 10x Pfu Turbo Buffer, 1 μl dNTPs (10 mM), 100 ng of each primer, 1 μl Pfu Turbo DNA Polymerase (5U/μl) and 10 ng of template DNA. Reaction volume was brought to 25 μl with MQ water and cycling parameters were: 95°C for 2 minutes, 40 x (95°C for 30 seconds, 55°C for 30 seconds, 72°C for 1 minute), 72°C for 10 minutes, hold at 4°C. Reactions were separated by 1% agarose gel electrophoresis, and the bands corresponding to the desired product excised and purified using the QIAquick gel extraction kit (Qiagen). For the second round PCR, 8.5 μl of each of the two PCR products from the first reactions were combined in a microcentrifuge tube with 2 μl 10x NEB Buffer 2. This mixture was heated for 5 minutes at 95°C to separate the DNA, then slowly cooled to room temperature (~1 hour) to allow proper annealing of the overlapping strands. Following this, 1 μl Klenow DNA Polymerase (2U/μl) and 1 μl dNTPs (10 mM) were added, and the reaction placed at 25°C for 20 minutes to enable elongation of the DNA, then placed at 70°C for 10 minutes to heat-inactivate the Klenow. 2 μl of this product was then used as a template for another PCR, with 2.5 μl 10 x Pfu Turbo buffer, 1 μl dNTPs (10 mM), 100 ng of each primer and 1 μl Pfu Turbo DNA Polymerase (5U/μl). Reaction volume was brought to 25 μl with MQ water and cycling parameters were as follows: 95°C for 3 minutes, 40 x (95°C for 30 seconds, 62°C for 30 seconds, 72°C for 1 minute), 72°C for 15 minutes, hold at 4°C. Reaction products were then visualised by 1% agarose gel electrophoresis, and the desired product excised and purified with the Qiagen gel extraction kit.

2.3.3 Protein Techniques

2.3.3.1 Small-scale protein induction

Colonies from BL21(DE3) transformation plates were selected and grown in 3 ml of LB-Carb or LB-Kan with 2% glucose overnight at 30°C with shaking. The following day, 250 μl of culture was transferred to a microcentrifuge tube and centrifuged at 3,000 x g for 2 minutes at room temperature. The cell pellet was resuspended in 250 μl fresh LB, and 200 μl of this suspension was used to inoculate 10 ml LB-Carb/LB-Kan, which was then shaken at 30°C until OD_{600} = 0.5 (~2 hours). At this stage, 1 ml of the uninduced culture was transferred to a microcentrifuge tube and placed on ice. The remaining 9 ml culture was divided evenly into 2 flasks and IPTG added to each to give a final concentration of 0.5 mM. These cultures were then incubated further at 30°C or 37°C with shaking. At time-points of 1, 3 and 5 hours following the addition of IPTG, 600 μl of each sample was removed, 100 μl of which was used to measure the OD_{600} and the remaining 500 μl was transferred to a microcentrifuge tube and placed on ice. When all samples were collected, cells were pelleted by centrifugation at 3,000 x g for 2 minutes at room temperature, and media was removed by aspiration. Cell pellets were resuspended in a crude lysis buffer made up of 2% SDS and 100 mM DTT, using 50 μl per OD unit per ml of culture. Cells were lysed by heating at 95°C for 10 minutes, then cooled on ice for 20 minutes and heated again at 95°C for 5 minutes. While still warm, 5 μl of each crude protein sample was transferred to a fresh tube, and 5 μl of 2x SDS sample buffer was added. Samples were then stored at -20°C, and later analysed by 10% SDS-PAGE with Coomassie staining.

2.3.3.2 Large-scale protein induction

Colonies from BL21(DE3) *E. coli* that had been freshly transformed with the desired expression plasmid were used to inoculate a 50 ml culture (LB-Carb/2% glucose), which was grown at 37°C overnight with shaking. The following day, 30 ml of the overnight culture was transferred to a fresh tube and centrifuged (2500 x g for 5 mins at RT), and the cell pellet resuspended in 20 ml fresh LB. 10 ml of this suspension was used to inoculate 500 ml LB-Carb, and this was then shaken at 37°C for approximately 1.5 hours until the OD_{600} reached 0.5 (0.4-0.6 was considered an acceptable range). IPTG was then added to a final concentration of 1 mM to induce protein expression, and the induction was carried out at 30°C with shaking for 4 hours. Cultures were then centrifuged (5000 x g

for 20 mins at RT), the supernatant removed and the cell pellet stored at -20°C until required. Induction of MBP-FIH fusion proteins was carried out as described above, except that no glucose was added in the overnight culture and protein expression was induced with 0.2 mM IPTG.

2.3.3.3 Nickel-affinity purification of His-tagged proteins

Frozen cell pellets derived from 500 ml of induced bacterial culture were thawed on ice, resuspended in 30 ml Nickel Lysis Buffer (see Section 2.2.7) and cells lysed with a Microfluidics cell-disruptor. Lysate was then clarified by centrifugation (15,000 rcf for 45 minutes at 4°C) and the supernatant mixed with 1 ml Ni-IDA-agarose resin and rocked for 1 hour at 4°C. The slurry was then poured into an empty PD-10 column (GE Healthcare), drained and washed with 50 ml Nickel Lysis Buffer followed by 50 ml Nickel Wash Buffer. Proteins were eluted using 2.5 ml of Nickel Elution Buffer, which was applied to the resin, rocked for 30 minutes at 4°C and then eluted. The eluted 6H-fusion protein was then buffer exchanged using a Sephadex G-25M PD-10 column (GE Healthcare) into Standard Assay Buffer, and stored at 4°C.

2.3.3.4 Amylose-affinity purification of MBP-tagged proteins

Frozen cell pellets derived from 500 ml of induced bacterial culture were thawed on ice, resuspended in 30 ml Amylose Lysis Buffer (see Section 2.2.7) and cells lysed with a Microfluidics cell-disruptor. Lysate was then clarified by centrifugation (15,000 rcf for 45 minutes at 4°C) and the supernatant mixed with 1 ml amylose-agarose resin and rocked for 1 hour at 4°C. The slurry was then poured into an empty PD-10 column (GE Healthcare), drained and washed with 50 ml Amylose Lysis Buffer followed by 50 ml Standard Assay Buffer. Proteins were eluted using 2.5 ml of Amylose Elution Buffer, which was applied to the resin, rocked for 30 minutes at 4°C and then eluted. The eluted MBP-fusion protein was then buffer exchanged using a Sephadex G-25M PD-10 column (GE Healthcare) into Standard Assay Buffer, and stored at 4°C.

2.3.3.5 Protein Quantification

The ExPasy ProtParam tool (http://kr.expasy.org/cgi-bin/protparam) was used to calculate extinction coefficients (A_{280} for 1 g/L) for recombinant proteins. These were used to determine protein concentrations for samples based on optical absorbance at 280 nm (A_{280}). These values were considered together with the purity and integrity of proteins as assessed by SDS-PAGE and coomassie staining.

2.3.3.6 Denaturing SDS-PAGE

To assess protein size and purity, denaturing SDS-PAGE was performed using 10% polyacrylamide Tris/Glycine gels. For experiments requiring optimal resolution of very low molecular weight proteins, either 12.5% polyacrylamide Tris/Tricine gels or Precast gradient gels (Bio-Rad) were used. SDS-PAGE was carried out according to standard laboratory protocols and proteins were visualised by Coomassie Stain (~1 hour at RT) followed by overnight incubation in Destain.

2.3.3.7 Western Blot Analysis

Samples of purified recombinant protein or whole-cell protein extracts were separated by 10% SDS-PAGE and transferred immediately to nitrocellulose membrane using the Bio-Rad Criterion wet-transfer system according to standard laboratory protocols. Membranes were blocked for 1 hour at RT with 10% skim milk, and incubated in primary antibody (conditions described in section 2.2.6). Membranes were then washed 3 times in 30 ml PBT for 5 mins at RT with gentle rocking, then incubated for 60 minutes at RT with the appropriate HRP-conjugated secondary antibody (refer to 2.2.6). This was followed by 3 further washes in 30 ml PBT and a 5 minute incubation in Pierce SuperSignal ECL reagent. Membranes were then blotted dry between two pieces of Whatman paper, exposed to AGFA X-ray film and developed.

For sequential immunoblot detection of different proteins, membranes were incubated for 10 minutes in Western blot stripping buffer (Pierce), washed 3 times (5 mins each) in 30 ml PBT, and re-probed with a different primary antibody.

2.3.3.8 In Vitro Affinity Pull-down Assays

In a standard affinity pulldown, 10 μl recombinant MBP-FIH (~8 μM) was mixed with 25 μl of Ni-IDA-agarose resin upon which 6H-tagged bait proteins had been retained following purification. The volume was made up to 200 μl by addition of whole cell extract buffer (WCEB) and mixtures were rocked gently at 4°C for 1 hour to enable complex formation. Samples were then centrifuged to pellet the resin (30 seconds, 1,500 rpm, RT) and the supernatant aspirated. Resins were washed 3-4 times with 1 ml Pull-down buffer (see section 2.2.6) for 1 minute at 4°C with gentle rocking. To elute the captured complexes, 40 μl Nickel Elution Buffer was added to each resin sample and rocked for 10 minutes at 4°C. The eluted protein (30 μl) was then transferred to a fresh microcentrifuge tube along with 30 μl of 2x SDS load buffer and heated at 95°C for 2 minutes. Samples were stored at -20°C before subsequent analysis by 10% Tris/Glycine SDS-PAGE with Western blotting as described in section 2.3.3.7.

For pulldowns performed with hydroxylated/non-hydroxylated Notch1 as bait, Trx-6H-mNotch1 ARD protein (~5 mg) was combined with untagged FIH (5 μM), cofactors (used at standard final concentrations as per CO_2 capture assay protocol; refer to section 2.3.3.11) , and an equivalent amount (40 μM) of either 2OG or the FIH inhibitor *N*-oxalylglycine (NOG), to a final reaction volume of 3 ml. Reactions were incubated for 2 hours at 37°C. Hydroxylated/ non-hydroxylated proteins were purified from the reaction mixture by nickel-affinity chromatography and retained on the Ni-IDA resin for use as bait to capture recombinant MBP-hFIH in pulldown assays as described above.

2.3.3.9 Fluorescence Polarisation

Fluorescence Polarisation (FP) assays were performed using a fluorescently labelled Notch1 peptide as the tracer. The peptide (FITC-βAla-RSDAAKRLLEASADANIQDNMGRTPLH AAVSADA) was synthesised by Auspep, and consisted of residues 1930-1963 of the mouse Notch1 ARD (corresponding to FIH hydroxylation site 1), N-terminally labelled with a fluorescein isothiocyanate (FITC) fluorophore linked via a β-alanine residue. Assays were set up in triplicate in black 96-well trays (Nunc), which were blocked prior to use with a

1% casein solution. FP measurements were made using a POLARstar Galaxy microplate reader (BMG Labtech), and data analyses performed using GraphPad PRISM software. In saturation binding experiments, a fixed concentration of the fluorescent tracer (400 nM) was incubated with an increasing concentration of MBP-FIH for 30 min at room temperature in standard assay buffer (150 mM NaCl, 20 mM Tris, pH 8). In competition binding experiments, a fixed concentration of MBP-FIH (5 μM) was pre-incubated with serial dilutions of a competing substrate protein for 30 minutes prior to the addition of the fluorescent tracer. The tracer was added at a final concentration of 400 nM, and the mixture incubated at room temperature for a further 30 mins before FP measurements were taken. Equilibrium dissociation constants were determined using non-linear regression analyses (Graphpad PRISM), with data fit to a one-site binding curve for K_d estimation or to a one-site competitive binding curve for K_i estimation.

2.3.3.10 Circular Dichroism

His-tagged proteins for circular dichroism (CD) analysis were expressed in bacteria from pET32 or pAC28-H6-TEV and purified by Ni-2+ affinity chromatography. To obtain protein of sufficiently high purity, proteins were subjected to an additional wash prior to elution from the Ni^{2+}-resin in 150 mM NaCl, 20 mM Tris pH 8.0 and 50 mM imidazole. Purified proteins were buffer exchanged into 5 mM sodium phosphate, pH 8.0 using a Sephadex G-25M PD-10 column (GE Healthcare) or by overnight dialysis.

CD spectra were recorded on a JASCO J-815 CD spectrometer. Measurements were carried out at 20°C in a 0.1 cm path length quartz cuvette, with protein concentrations ranging from 0.05-0.4 mg/ml in 5 mM sodium phosphate, pH 8.0. Spectra were recorded in the wavelength range of 300 to 185 nm at 0.2 nm intervals, and each spectrum was an average of 5 scans. Spectra were baseline-corrected by subtraction of the spectrum for buffer alone, and smoothed using the 'means-movement' smoothing method in the Spectra Manager software. Data were expressed as the mean residue ellipticity ([θ], deg cm^2 $dmol^{-1}$) and in some cases normalised to the ellipticity measured at 207 nm to minimise interference from small differences in protein concentration [140]. The experimental data in the 190-260 nm range were analysed using DICHROWEB [141], and the CDSSTR deconvolution method was used to estimate the secondary structural content

using reference set 7 [142]. For each protein, a minimum of 3 scans was performed from at least 2 independent protein preparations.
Thermal denaturation experiments were performed at protein concentrations of 0.2 mg/ml in 5 mM sodium phosphate buffer, pH 8.0. The ellipticity at 220 nm (θ_{220}) was monitored continuously as the temperature increased from 4°C to 90°C at a ramp rate of 1°C/minute. Data were baseline-corrected and expressed as a percentage of the θ_{220} value measured at 4°C. Graphpad PRISM software was employed to fit data to a sigmoidal curve and estimate apparent T_m values, as denaturation was irreversible.

2.3.3.11 CO_2 capture assays

CO_2 capture assays for *in vitro* analysis of FIH-catalysed hydroxylation were performed as described in Linke et al., 2007 [105]. Briefly, MBP-FIH and Trx-6H-tagged substrate proteins were expressed in bacteria, purified by affinity chromatography, and buffer exchanged into Standard Assay Buffer. Substrate (20 μl) and enzyme (10 μl) were aliquoted into V-shaped, polypropylene, screw-capped, rubber-sealed tubes and kept on ice. Samples in which the FIH was replaced by buffer were also included to control for background decarboxylation of 2OG.

Cofactors (5 μl) were added from a mastermix, containing 400 mM Tris (pH 7.0), 0.32% BSA, 4 mM DTT, 32 mM ascorbic acid and 80 μM $FeSO_4$, to give final concentrations of 50 mM, 0.04%, 0.5 mM, 4 mM and 10 μM, respectively. Reactions were initiated by the addition of 5 μl of 320 μM [^{14}C]-2OG, giving a total reaction volume of 40 μl. The specific activity of the 2OG (54.5 mCi/mmol; Perkin Elmer Life Sciences) was high enough to permit a 1:2 dilution in unlabelled 2OG, while still allowing detection by scintillation counting. Thus, the final concentration of 2OG was 40 μM, with a specific activity of 18 mCi/mmol.

Immediately following the addition of the 2OG solution, a $Ca(OH)_2$–soaked filter paper was placed into the tube, suspended above the reaction. The lid was capped tightly and the reaction placed at 37°C for the specified incubation time. All reactions were timed to the second and terminated by removal of the filter. Filters were dried at room temperature for 40 minutes, after which time 130 μl UltimaGold™ XR scintillation fluid

was applied directly onto the filter. Each filter was counted in scintillation vials using a 1214 RACKBETA liquid scintillation counter (LKB WALLAC).

To simply infer whether a suspected substrate can be hydroxylated by FIH, assays were performed with maximal amounts of enzyme and substrate, and lengthy incubation periods (60 mins). For kinetic experiments, the concentration of FIH was optimised to ensure that activity was linear over the assay time (usually 20 minutes) and that less than 10% of substrate was consumed. The data were converted to V_o (nmol 2OG turnover/mg FIH/minute) and Graphpad PRISM software was employed to fit data to a hyperbolic curve and estimate kinetic constants (apparent K_m and V_{max}).

2.3.3.12 Hydroxylation of substrates for mass spectrometry analysis

Affinity-purified Trx-6His-tagged mNotch2 and mNotch3 ARD proteins were treated with a saturating amount of MBP-FIH and cofactors under the same conditions as in the CO_2 capture assay, but using non-radiolabelled 2OG. Samples with buffer in place of FIH were also included to control for non-specific oxidations that may have occurred during sample preparation. Reactions were incubated at 37°C for 1 hour, at which point more MBP-FIH was added and reactions were incubated for a further hour to achieve maximal substrate hydroxylation. EDTA (1 mM) was then added to each sample, along with 10 μl of 5x Tris/ Tricine loading buffer containing 150 mM fresh DTT (30 mM final concentration). Samples were then reduced for 10 mins at 70°C, then alkylated by the addition of 30 mM iodoacetamide (prepared fresh) and heated for a further 10 mins at 70°C. Proteins were separated by 10% Tris/Tricine SDS-PAGE and visualised by coomassie staining. Bands corresponding to the substrate proteins were excised and sent to our collaborators in the Gorman laboratory at the Queensland Institute of Medical Research (QIMR) for in-gel tryptic digestion and analysis by mass spectrometry using using HPLC separation together with matrix-assisted laser desorption/ionisation (MALDI), electrospray ionisation (ESI) and linear trap quadrupole (LTQ)-Orbitrap MS and MS/MS. Detailed methods for MS analysis are described in Wilkins et al., 2009 [100].

Chapter 3

Differences in hydroxylation and binding of HIF and ARD substrates by FIH

3.1 Introduction

As discussed in Chapter 1, FIH is an oxygen-dependent asparaginyl hydroxylase with two distinct classes of substrates: HIF-α transcription factors, and ankyrin repeat domain (ARD) proteins. Hydroxylation of HIF by FIH is well characterised, both in terms of its functional outcomes and its kinetic parameters. In contrast, ARD substrates have only recently been identified, and comparatively little is known about these proteins in terms of their hydroxylation by FIH. A distinguishing feature of ARD proteins is that they are structurally dissimilar to the HIF-α CAD [60, 61, 93]. We hypothesise that distinct structural properties of the ARD will contribute to differences in recognition and ultimately hydroxylation by FIH.

To this end, this chapter presents a detailed comparison of the catalytic properties of FIH with respect to HIF and ARD substrates. CO_2 capture assays were employed to measure the kinetic parameters and oxygen-sensitivity of ARD hydroxylation, and a fluorescence polarisation-based binding assay was developed to accurately determine affinity constants for FIH-substrate interactions. Previous work in our laboratory has characterised hydroxylation of the Notch receptor family by FIH, and consequently, Notch1-3 proteins were employed in these analyses as representative ARD substrates. Given the large number of potential substrates within any cell, the relative affinity of FIH for each substrate and the efficiency of hydroxylation will be crucial determinants of substrate selection and modification. As such, the data presented in this chapter are of particular importance in understanding how FIH discriminates between HIF and ARD substrates within a cellular context.

3.2 Results

Prior to investigating differences in the hydroxylation of Notch and HIF substrates, preliminary experiments were performed to complete the initial characterisation of Notch hydroxylation, by confirming hydroxylation of Notch2 and 3 and determining the target asparagine residues.

3.2.1 Identification of hydroxylation sites in Notch2 and Notch3

Previous work in our laboratory identified mouse Notch1 as a novel substrate for FIH (refer to section 1.2.3). Analysis of the Notch1 ARD by mass spectrometry has shown that two asparaginyl residues (Asn1945 and Asn2012) are hydroxylated by FIH, both *in vitro* and in mammalian cells [94, 95]. Preliminary data from my Honours research indicate that Notch2 and 3 are also likely to be FIH substrates, producing high activity in CO_2 capture assays similar to other FIH substrates [143]. However, the specific sites of hydroxylation were not identified. Given the high degree of amino acid sequence similarity in the ARDs of Notch1-3 (Figure 3.1), specifically the conserved asparagines and surrounding residues, it is likely that FIH hydroxylates Notch 2 and 3 in positions equivalent to Asn1945 and Asn2012 in Notch1.

To determine whether this is indeed the case, site-directed mutagenesis was performed to substitute Asn1902 and Asn1969 in mNotch2, and Asn1867 and Asn1934 in mNotch3, with alanine residues. Wildtype Notch ARD proteins, as well as single and double Asn-Ala mutants, were expressed in *E. coli* with an N-terminal Thioredoxin-6-histidine (Trx-6His) tag and purified by nickel-affinity chromatography. Analysis of purified proteins by SDS-PAGE and coomassie staining confirmed good yields of soluble protein that was at least 80% pure (Figure 3.2, *left-hand panels*). Equivalent amounts of wildtype and mutant proteins were then tested as substrates for FIH in CO_2 capture assays (*right-hand panel*).

The CO_2 capture assay

The CO_2 capture assay provides an indirect measure of substrate hydroxylation by FIH. The assay quantifies the amount of [^{14}C]-CO_2 liberated from the oxidative decarboxylation of [^{14}C]-labelled 2OG, which occurs in a FIH-dependent manner, and is stoichiometrically

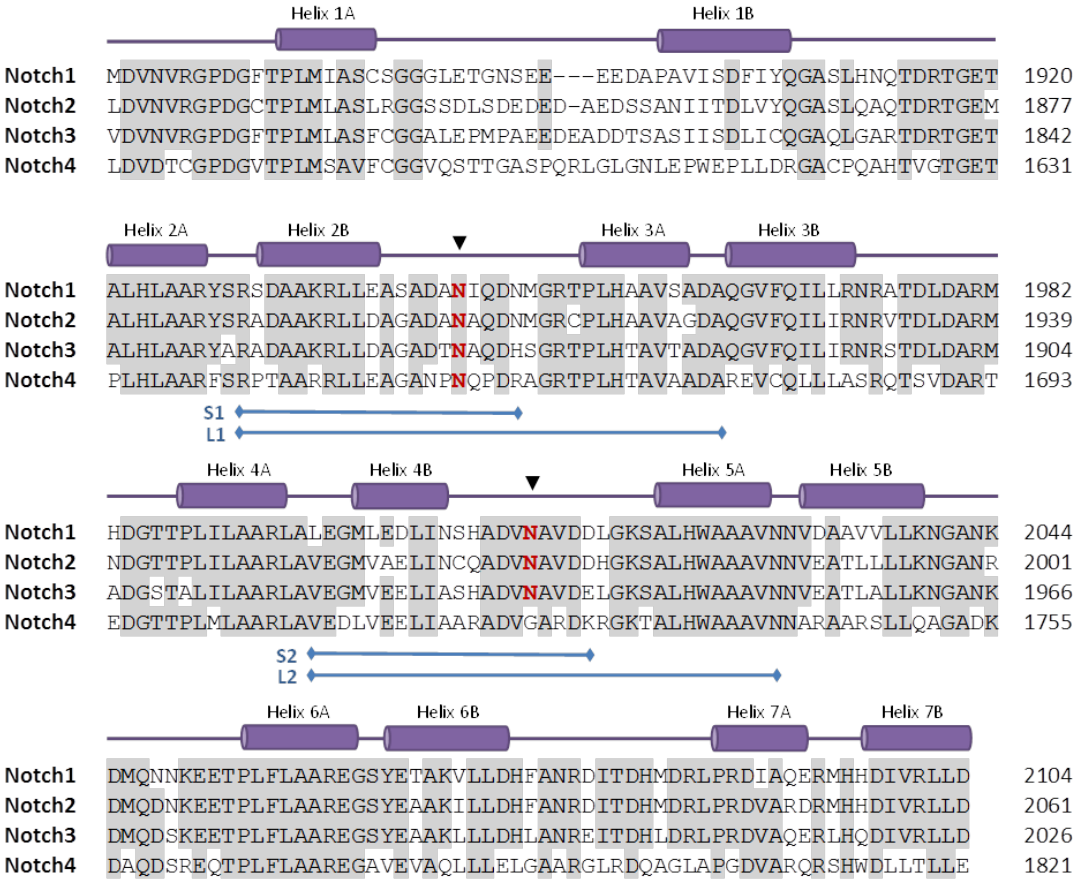

Figure 3.1 Potential sites for hydroxylation by FIH in mouse Notch1-4

Alignment of amino acid sequences from the ankyrin repeat domains (ARDs) of mouse Notch1 (NP_032740.3), Notch2 (NP_035058.2), Notch3 (NP_032742.1) and Notch4 (NP_035059.2) by ClustalW [144]. Residues conserved in >3 Notch homologues are highlighted in grey. Numbers to the right correspond to the amino acid positions. Barrels above the sequences indicate the position of helices based on the crystal structure of the human Notch1 ARD [145]. Hydroxylation of mNotch1 at N1945 (Site 1) and N2012 (Site 2) by FIH has been confirmed by mass spectrometry [94, 95], and these sites are indicated by black triangles. Bars below the alignment indicate residues that correspond to long (L1 and L2) and short (S1 and S2) peptides for mNotch1-3 at both hydroxylation sites.

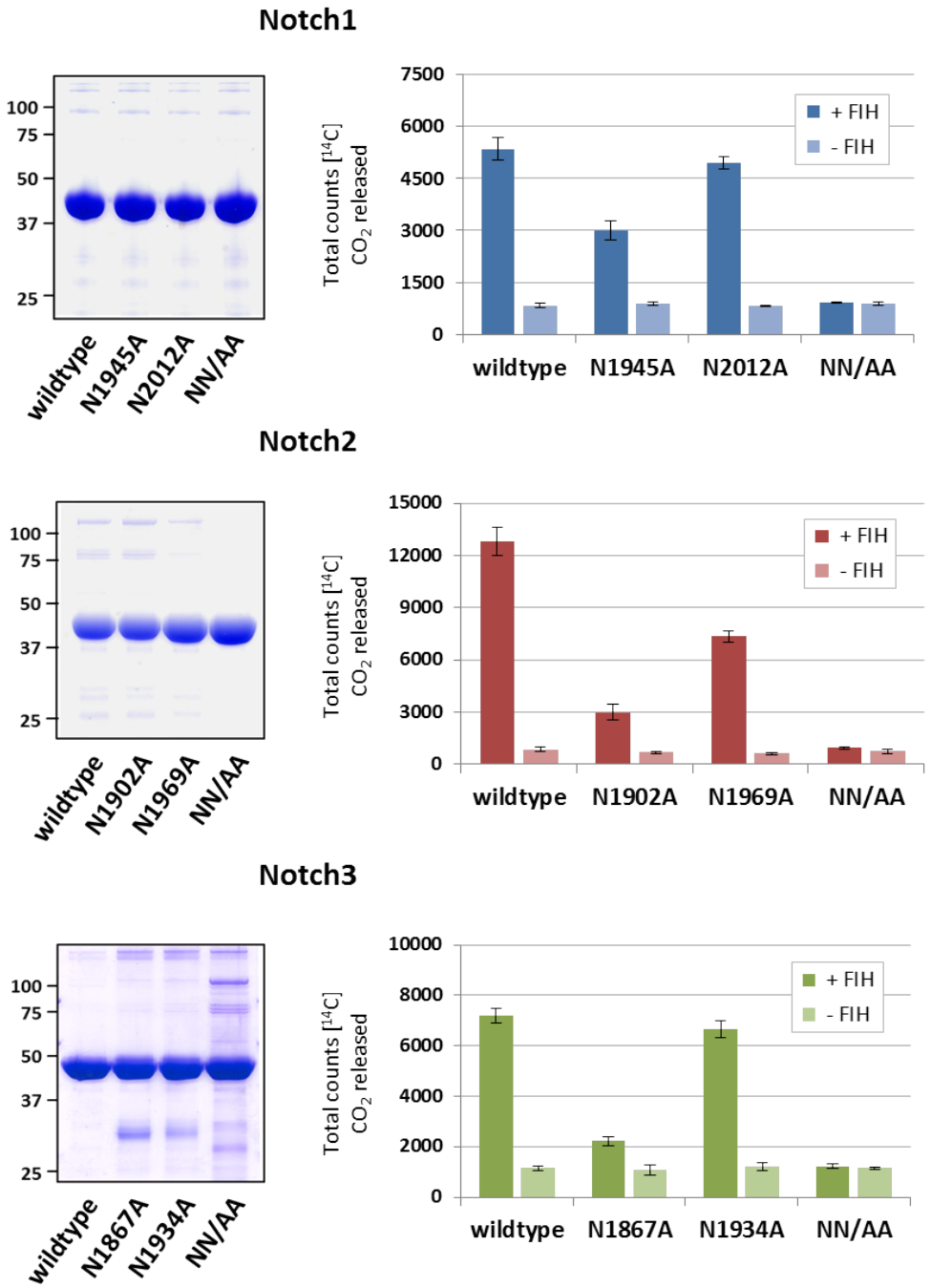

Figure 3.2 FIH hydroxylates Sites 1 and 2 in the ARDs of Notch1–3

Left-hand panels: Affinity-purified mNotch1-3 ARD proteins and their Asn to Ala single and double mutants were assessed for purity by coomassie staining of SDS-PAGE gels loaded with equivalent amounts of each protein. Right hand panels: Purified wildtype and mutant ARD proteins (30 μM) were analysed for hydroxylation by MBP-hFIH (1 μM) based on their ability to promote FIH-dependent decarboxylation of [^{14}C]-2OG in CO_2 capture assays. Data are the mean of triplicate reactions ± SD, and are representative of 3 independent experiments.

coupled to substrate hydroxylation (i.e. 1 molecule of [^{14}C]-CO_2 is produced per molecule of hydroxylated product) [146, 147]. FIH is typically expressed in *E.coli* with an N-terminal maltose binding protein (MBP)-tag, and purified by amylose-affinity chromatography. In a standard assay, MBP-FIH, substrate, essential cofactors (iron and ascorbic acid) and [^{14}C]-2OG are combined in sealed microcentrifuge tubes with a $Ca(OH)_2$-soaked filter paper suspended above each reaction. Any [^{14}C]-CO_2 released from the reaction is 'captured' by formation of the precipitate Ca[^{14}C]-CO_3 on the filter, and quantified by scintillation counting. The assay has been optimised for FIH in our laboratory, and previous work by Sarah Linke has verified that under standard assay conditions, FIH does not oxidise 2OG in the absence of a protein substrate [105, 127].

Hydroxylation sites in Notch2 and Notch3 are in equivalent positions to those in Notch1

The CO_2 capture assay results are shown in Figure 3.2 (*right-hand panel*), and are similar to those previously reported for Notch1 [94, 95]. Specifically, mutation of the Site 1 asparagine in Notch1, 2 and 3 resulted in a major reduction in FIH activity. Mutation of Site 2 alone also reduced activity, but to a much lesser extent, suggesting that hydroxylation of the Site 2 asparagine is less efficient. No activity was observed above background level for any of the double Asn-Ala mutants, indicating that these are likely to be the only sites of FIH-catalysed hydroxylation in these proteins. Overall, the data support hydroxylation of Notch1-3 at two conserved asparagine residues, and in each case, FIH displays a preference for Site 1 over Site 2. Interestingly, FIH appears to hydroxylate Notch2 substrates *in vitro* at a higher efficiency than it does Notch1 or Notch3, liberating nearly twice the amount of [^{14}C]-CO_2 in three independent experiments, despite the addition of similar amounts of protein substrate in each assay. Such a significant and consistent difference is unlikely to be due simply to variation within the assay.

Mass spectrometry confirms hydroxylation sites in Notch2-3

For confirmation of *in vitro* hydroxylation by mass spectrometry (MS), Trx-6H-tagged Notch2 and Notch3 wildtype ARD proteins were treated with MBP-FIH and cofactors under the same conditions as the CO_2 capture assay, but using un-labelled 2OG in place of [^{14}C]-2OG. Negative control reactions were performed under identical conditions but with

the addition of buffer in place of FIH. Following incubation at 37°C, proteins were reduced, alkylated and visualised by 10% Tris/Tricine SDS-PAGE with coomassie staining. The bands corresponding to hydroxylated/un-hydroxylated Notch2 and Notch3 were excised and sent to our collaborators, Professor Jeffrey Gorman and Johana Chicher, at the Queensland Institute of Medical Research for in-gel tryptic digestion and MS analysis. MALDI-TOF-MS analyses (Figure 3.3) revealed an additional mass of 16 daltons in tryptic peptides from Notch2 and Notch3 ARD proteins treated with FIH (*lower spectra*) compared to '- FIH' samples (*upper spectra*), consistent with hydroxylation at Asn1902 and Asn1969 in Notch2, as well as Asn1867 and Asn1934 in Notch3. Mass changes corresponding to FIH-independent methionyl and aspartyl oxidations were also detected, as indicated in Figure 3.3. Hydroxylated residues (as well as non-specific oxidations) were subsequently confirmed by MALDI-MS–MS and LQT-Orbitrap analysis (see supplemental data for Wilkins et al., 2009; Appendix 1). Together with the *in vitro* hydroxylation of Asn-Ala point mutants these data confirm that both Notch2 and 3 are hydroxylated by FIH at asparaginyl residues equivalent to those at Sites 1 and 2 in Notch1.

3.2.2 Differences in binding and hydroxylation of Notch and HIF substrates by FIH

CO_2 capture assays were next employed to characterise and compare the *in vitro* hydroxylation of Notch and HIF-1α substrates by FIH. Trx-6H-tagged mNotch1 ARD and mHIF-1α CAD proteins, as well as MBP-mFIH were expressed in *E. coli* and purified by nickel- and amylose-affinity chromatography, respectively. Accurate quantification of purified proteins is essential for kinetic analyses, and was achieved using molar extinction coefficients calculated using the ExPASy ProtParam tool [148], and optical absorbance at 280 nm. The purity of recombinant proteins (typically >80%) was also taken into consideration, and was assessed by SDS-PAGE with coomassie staining (Figure 3.4A). Kinetic analyses were employed to compare the rates of 2OG turnover and relative affinities of FIH for Notch and HIF substrates, as indicated by the apparent V_{max} and K_m values, respectively. Assays were performed with varying concentrations of substrate, and a limiting amount of FIH (120 nM) to ensure that release of [^{14}C]-CO_2 (and therefore FIH activity) was linear with time for both HIF and Notch. As shown in Figure 3.4B, the maximal rate of 2OG turnover by FIH is roughly 5-fold higher with HIF as a substrate than

A. Notch2 Site 1 (N1902)

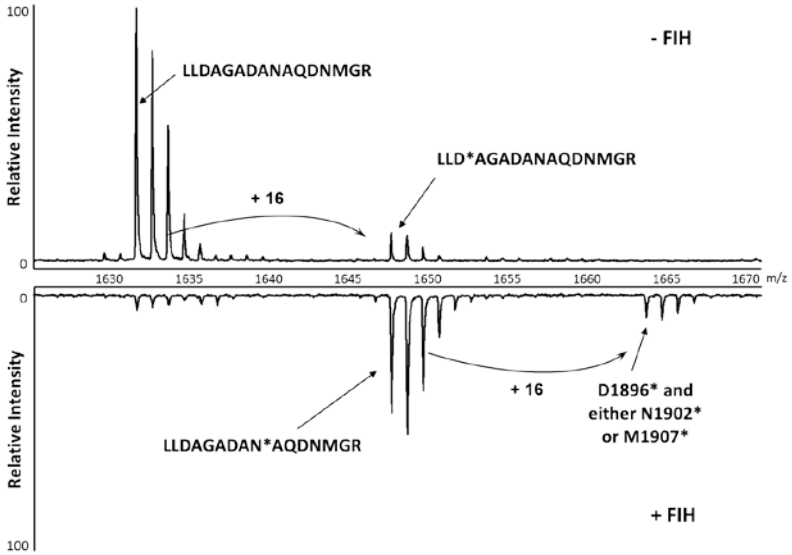

B. Notch2 Site 2 (N1969)

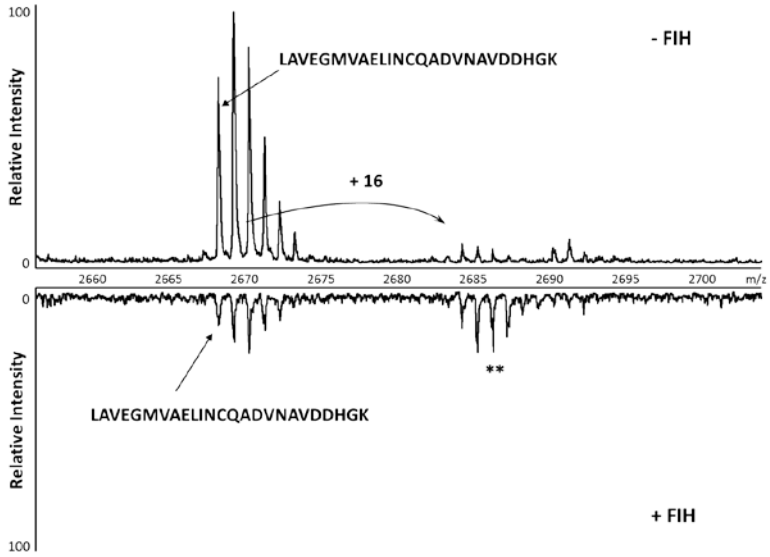

C. Notch3 Site 1 (N1867)

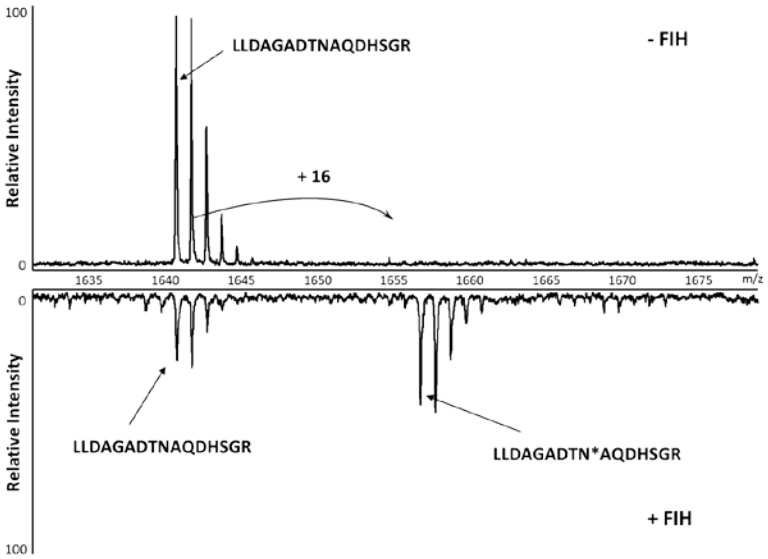

D. Notch3 Site 2 (N1934)

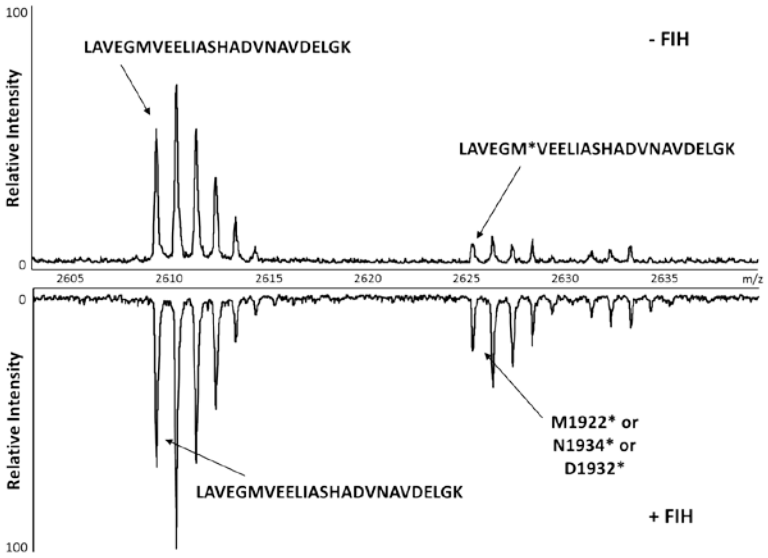

Figure 3.3 MS identification of hydroxylation sites in Notch2 and Notch3

HPLC-MALDI-TOF-MS spectra showing hydroxylated (*lower spectra*) and un-hydroxylated (*upper spectra*) forms of tryptic peptides encompassing either Site 1 or Site 2 from Notch2-3. A mass change of +16 was observed between ions, consistent with asparaginyl hydroxylation by FIH. The specific amino acids modified with +16, including those independent of FIH, were confirmed by MALDI-TOF/TOF-MS-MS where indicated (*). MALDI-TOF-MS spectra are shown for ions representing: (A) residues 1894–1909 of Notch2 detected under non-hydroxylated (*m*/*z* 1647.7) and hydroxylated (*m*/*z* 1631.7) conditions; (B) residues 1952–1976 of Notch2 detected under non-hydroxylated (*m*/*z* 2668.3) and hydroxylated (*m*/*z* 2684.3) conditions (peaks denoted ** are likely to contain hydroxylated N1969, as demonstrated by LQT-MS–MS (see Appendix 1); (C) residues 1859–1874 of Notch3 detected under non-hydroxylated (*m*/*z* 1640.7) and hydroxylated (*m*/*z* 1756.7) conditions; and (D) residues 1917–1941 of Notch3 detected under non-hydroxylated (*m*/*z* 2609.3) and hydroxylated (*m*/*z* 2625.3) conditions.

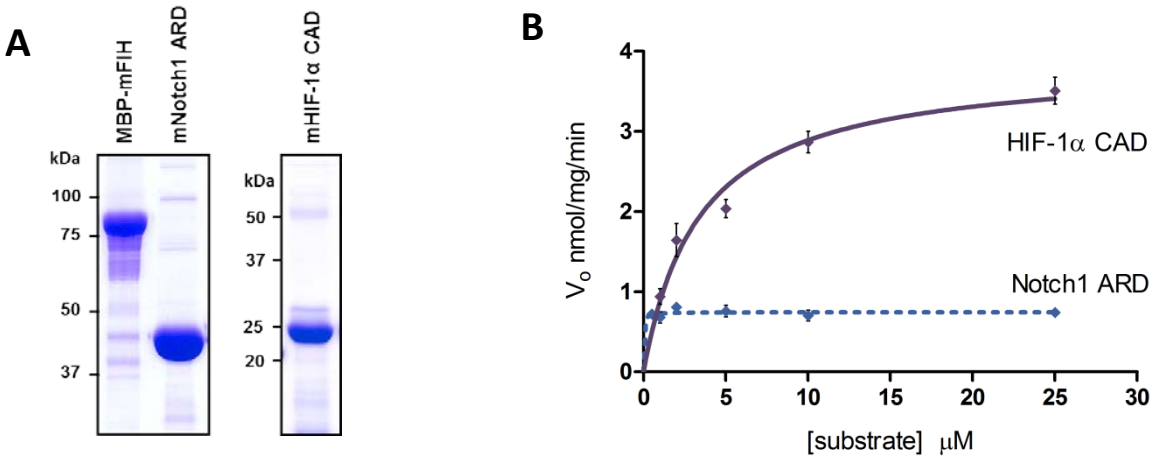

	K_m (μM)	V_{max} (nmol/mg/min)	k_{cat} (min^{-1})	k_{cat}/K_m ($\mu M^{-1}min^{-1}$)
HIF-1α CAD	3.7 ± 1.4	4.7 ± 1.5	0.5 ± 0.2	0.12 ± 0.02
Notch1 ARD	< 0.5	1.1 ± 0.2	0.1 ± 0.02	> 0.2

Figure 3.4 Kinetic parameters of HIF and Notch hydroxylation by FIH

A. MBP-mFIH, Trx-6H- mNotch1 ARD and Trx-6H- mHIF-1α CAD proteins were purified by affinity chromatography and visualised by 10% (*left panel*) or 12% (*right panel*) Tris/Glycine SDS-PAGE with coomassie staining. B. Proteins from A were analysed in CO_2 capture assays at concentrations ranging from 0.5 to 25.0 μM. Reactions were incubated for 22 min at 37 °C and contained 120 nM MBP-mFIH and saturating concentrations of all cofactors except oxygen. Data are expressed as V_o (nmol/min/mg FIH), and kinetic constants (K_m and k_{cat}) were calculated using Graphpad PRISM software. A representative curve (mean of triplicates ± SD) is shown for each protein, and values presented in the table are the mean of three independent experiments ± SD.

with Notch, with V_{max} values of 4.7 and 1.1 nmol/mg/min, respectively. Whilst the apparent K_m value of FIH for the HIF-1α CAD was ~ 4 μM, the K_m value for the Notch ARD was found to be too low to be determined accurately with this assay (Figure 3.4B). The lowest non-limiting substrate concentration at which hydroxylation-coupled turnover of 2OG could be reliably assayed was 0.5 μM, and at this concentration, the rate of FIH catalysis was consistently found to have reached its plateau.

To more accurately determine the K_m value of FIH for Notch substrates, we established a collaboration with Dr Peppi Karppinen from the University of Oulu in Finland, who has previously published kinetic analyses of HIF hydroxylation by both the PHDs [67, 149] and FIH [66] using a more sensitive version of the CO_2 capture assay. Kinetic analyses performed by Jana Hyvarinen from Dr Karppinen's laboratory (presented in Wilkins et al., 2009; Appendix 1) narrowed down the K_m value of FIH for the Notch1 ARD to less than 0.2 μM. However, it was still too low to be accurately determined, despite the increased sensitivity of the assay.

3.2.3 Catalytic properties of FIH with peptide substrates

It was hypothesised that the markedly higher affinity that FIH displays for the Notch1 ARD over the HIF CAD is likely due to structural differences between the two proteins. Nevertheless, crystallographic analyses indicate that peptide fragments encompassing the hydroxylation sites in Notch1 and HIF-1α bind to the active site of FIH in a similar manner [95, 116]. As such, it was predicted that peptides isolated from Site1 or Site2 in Notch (removed from the structural context of the ARD) would have an affinity for FIH that was more comparable to that of the HIF-1α CAD.

To investigate this possibility, K_m and V_{max} values were determined using short synthetic peptides corresponding to the two hydroxylation sites in Notch1 (refer to Figure 3.1), and were compared to peptides of similar length from HIF-1α (Table 3.1). Consistent with the hypothesis, FIH was found to have a similar affinity for all short (20-mer) peptide substrates, with K_m values of 110 μM for both Notch1 Site 1 and Site 2 peptides, compared with 120 μM for the short HIF-1α peptide. Interestingly, increasing the length

Table 3.1 Amino acid sequences for Notch1 and HIF-1α synthetic peptide substrates

Synthetic Peptide		Sequence
mNotch1	N1945 short	RSDAAKRLLEASADANIQDN
	N1945 long	RSDAAKRLLEASADANIQDNMGRTPLHAAVSADA
	N2012 short	VEGMLEDLINSHADVNAVDD
	N2012 long	VEGMLEDLINSHADVNAVDDLGKSALHWAAAVN
hHIF-1α	N803 short	DESGLPQLTSYDCEVNAPI
	N803 long	DESGLPQLTSYDCEVNAPIQGSRNLLQGEELLRALDQVN

Target Asn residues are underlined in the peptide sequence

Table 3.2 K_m and V_{max} values of FIH for Notch1 and HIF-1α synthetic peptide substrates

Peptide Substrate		K_m (μM)	V_{max} (% of ref)
mNotch1	N1945 short	110 ± 20	< 10
	N1945 long	0.7 ± 0.6	30 ± 5
	N2012 short	110 ± 1	< 10
	N2012 long	13 ± 3	50 ± 5
hHIF-1α	N803 short	120 ± 30	30 ± 5
	N803 long	50 ± 3	110 ± 5

Data from kinetic experiments performed by our collaborators (Dr Peppi Karppinen and Jaana Hyvarinen) from the University of Oulu in Finland, published in Wilkins et al., 2009 [100] and used with permission. Activity of human FIH (purified from insect cells) was determined in the presence of increasing substrate concentrations, with cofactors other than oxygen at saturating concentrations. Values are mean ± SD from >3 independent experiments. The V_{max} values are expressed as a percentage relative to the value obtained for the DES35 HIF-1α peptide described in Koivunen at el., 2004 [66].

of the peptide substrates to 35 amino acids reduced the K_m over 150-fold to 0.7 μM for Notch1 Site 1, while the K_m for Site 2 decreased around 10-fold to 13 μM. In comparison, a similar increase in length for the HIF-1α peptide only improved the binding affinity 2-fold, reducing K_m from 120 to 50 μM. The increase in peptide length also correlated with an increase in V_{max} for all substrates (Table 3.2).

Overall, increasing the length of peptide substrates led to a dramatic improvement in the affinity of FIH for the Notch peptides, but had much less influence on the ability of FIH to bind the HIF peptides. The longer peptides, which presumably enable additional interactions beyond the catalytic binding pocket, result in FIH displaying a significantly lower K_m for the Notch substrates than for the HIF-1α CAD, consistent with previous experiments (Figure 3.4). Nonetheless, the K_m values for the long Notch peptides are still higher than the K_m value of FIH for the full-length Notch1 ARD, likely reflecting a preference for the ankyrin fold over an unstructured peptide.

3.2.4 The K_m of FIH for oxygen is lower with Notch1 than with HIF-1α as a substrate

As discussed previously (section 1.1.6), the K_m of FIH for oxygen (90 μM) correlates well with its important role as an oxygen sensor for the HIF pathway [66]. However, the K_m values of FIH for oxygen with ARD substrates such as Notch have not been reported. These values have important implications for understanding the physiological role of FIH, including the range of oxygen concentrations at which it is active, and the potential for differential substrate hydroxylation dependent on oxygen concentration. This is especially relevant since binding of the peptide substrate results in a conformational change to FIH, which may alter the affinity for the subsequent binding of oxygen [66, 116]. Therefore, as part of our collaboration, Dr Karppinen determined the K_m value of FIH for oxygen using the mNotch1 ARD protein as a substrate. In marked contrast to the 90 μM obtained for HIF-1α, the K_m of FIH for oxygen with the Notch1 ARD as a substrate was 12 μM, almost 8-fold lower (see Appendix 1 for kinetic curves). Thus, FIH has a significantly higher affinity for oxygen *in vitro* with Notch1 as a substrate than with HIF-1α, suggesting that Notch is likely to become hydroxylated efficiently even under relatively severe hypoxic conditions, where HIF-α hydroxylation would be reduced.

3.2.5 FIH has a higher binding affinity for Notch1-3 than HIF-1α

Since it was not possible to determine accurate K_m values for the Notch1 ARD in CO_2 capture assays due to the high affinity of the Notch-FIH interaction, I established a sensitive fluorescence polarisation (FP)-based assay for determining the relative binding affinities of FIH for its various substrates. The development and optimisation of this assay is described in Appendix 2, and is based on FP being dependent on the size of the fluorescent component being measured. Briefly, proteins of interest (e.g. FIH substrates) compete with a fluorescent peptide tracer for binding to FIH. As the concentration of the competing protein is increased, the FP value decreases in proportion to the amount of tracer displaced from FIH (the free tracer is much smaller than when complexed with FIH, and thus FP decreases). The data are fit to a one-site competitive binding curve (using Graphpad PRISM software) in order to determine K_i values, which give a measure of the relative binding affinity for FIH, and should correlate directly to K_m values.

As with the K_m values, the K_i values obtained for all FIH substrates lay within the low μM range. The mean K_i values for the Notch1, 2 and 3 ARD proteins were 1.1, 0.4 and 0.9 μM, respectively (Figure 3.5A). This demonstrates a small, yet statistically significant difference in the ability of FIH to bind the Notch1-3 proteins, with Notch2 having the highest affinity. A markedly lower affinity was observed for HIF-1α, with a K_i value at least 50-fold higher than that obtained for Notch1, also consistent with the K_m values (refer to section 3.2.1). Although Notch4 is not a substrate for FIH [94, 143], the FP assays indicated that it is able to bind to FIH. The mean K_i for the Notch4 ARD was found to be 9.5 μM, almost an order of magnitude higher than the values for Notch1-3, but significantly lower than the K_i for HIF-1α. These data demonstrate that FIH binds Notch ARD proteins with a relatively high affinity compared with HIF, regardless of whether or not they are hydroxylated.

3.2.6 FIH has a higher affinity for Notch in its non-hydroxylated state

In vitro affinity pulldown assays were performed to characterise the relative binding affinity of FIH for hydroxylated versus non-hydroxylated Notch. Ideally, FP competition

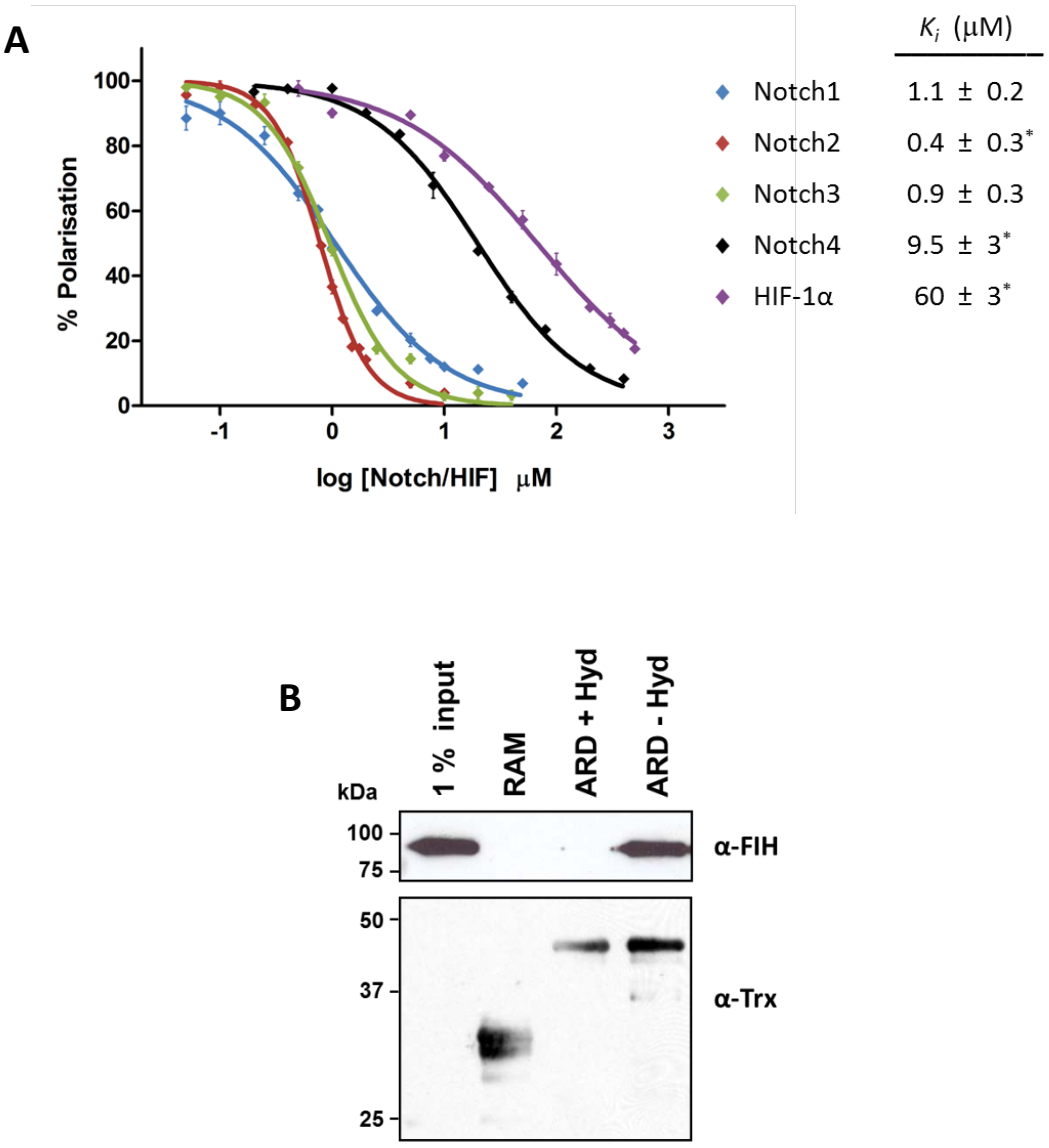

Figure 3.6 Relative binding affinity of FIH for Notch and HIF substrates

A. Serial dilutions of purified Trx-6H-tagged hHIF-1α (356-826) and mNotch1-4 ARD proteins were assayed for their ability to compete with a fluorescent peptide for binding to MBP-hFIH in fluorescence polarisation (FP) competition binding assays. Data were expressed as a percentage of the maximum polarisation and subjected to non-linear regression analysis using Graphpad PRISM software. A representative curve is shown for each protein, but K_i values are the mean of 3 independent experiments ± SD. Unpaired two-tailed Student's t-tests were performed using the data for Notch1 as a reference (* value significant at $p < 0.05$). B. *In vitro* affinity pull-down assays were performed using Trx-6H-tagged Notch RAM, hydroxylated ARD (+ Hyd) or un-hydroxylated ARD (- Hyd) as bait to capture recombinant MBP-hFIH. Complexes were separated by SDS-PAGE and visualised by immunoblotting to detect bound FIH (*upper panel*) or Trx-tagged bait proteins (*lower panel*).

binding assays would have been used for this analysis, but the low yields of protein obtained after *in vitro* hydroxylation meant that this was not feasible. Unlike FP, pull-down assays are not quantitative, but are relatively straightforward to perform and provide valuable qualitative information about protein-protein interactions.

Trx-6H-Notch1 ARD was expressed in *E.coli* and affinity-purified, then treated with FIH and cofactors in the presence of either 2OG to promote hydroxylation, or the FIH inhibitor N-oxalylglycine (NOG) to prevent hydroxylation [66, 150]. Hydroxylated and un-hydroxylated Notch proteins were immobilised on Ni-IDA resin, and used as bait to pull-down purified MBP-FIH. The Notch RAM domain, which does not interact with FIH [94], was included as a negative control. Complexes were separated by SDS-PAGE and analysed by immunoblotting to detect captured MBP-FIH (Figure 3.5B, *upper panel*) or Trx-6H-tagged bait proteins (*lower panel*). As shown in Figure 3.5B, FIH was captured efficiently by the un-hydroxylated Notch ARD. In contrast, the hydroxylated protein was able to capture only a very small amount of MBP-FIH, whilst the Notch RAM domain did not interact with FIH at all. The results demonstrate that FIH has a much greater affinity for Notch1 in its un-hydroxylated state. Whilst it is not particularly surprising for an enzyme to have a higher affinity for its substrate compared with the product of the reaction, it does suggest that the binding affinity of FIH for ARD substrates is likely to be dependent on hydroxylation, and hence regulated by oxygen availability.

3.2.7 Dimerisation of FIH is required for catalysis on Notch and HIF substrates

Previous studies have demonstrated that FIH forms homodimers in solution, and that its ability to do so is essential for hydroxylation of HIF [115, 118]. To determine whether dimerisation is also required for hydroxylation of Notch, an L340R point mutation, previously shown to disrupt the hydrophobic dimer interface in FIH [118], was generated by site-directed mutagenesis. MBP tagged wildtype FIH, as well as the L340R mutant, were expressed in *E. coli* and purified by amylose-affinity chromatograpy. Purified proteins were then analysed for their ability to catalyse hydroxylation-coupled turnover of 2OG in CO_2 capture assays using the HIF-1α CAD and Notch1 ARD as substrates (Figure 3.6).

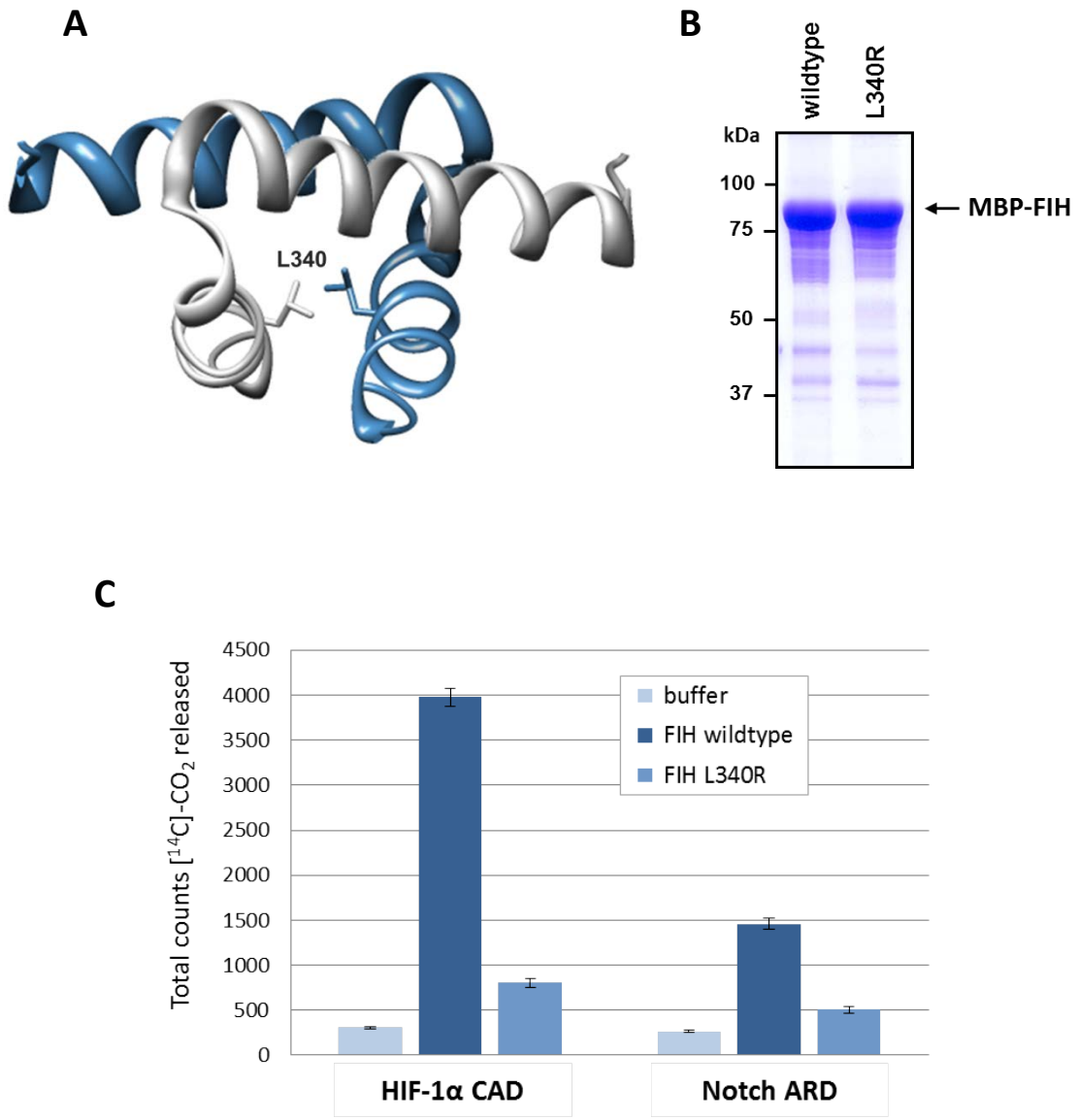

Figure 3.6 Dimerisation of FIH is required for activity on HIF and Notch substrates

A. Crystal structure of the FIH dimerisation interface, which is mediated by hydrophobic interactions between two C-terminal helices of each FIH monomer (blue and grey). The positions of the two Leu340 residues are highlighted to demonstrate how their mutation to Arg disrupts the interface. Image adapted from Lancaster *et al.*, 2004 [118] and generated using UCSF Chimera software [92] from the crystal structure of FIH (visible residues 307-349, PDB ID: 1H2K [116]). B. Affinity-purified MBP-FIH wildtype and L340R proteins were visualised by 10% Tris/Glycine SDS-PAGE with coomassie staining. C. An equivalent amount (1 μM) of FIH proteins from (B) were tested for their activity on Trx-6H-tagged HIF-1α and Notch1 ARD substrates (15 μM) in CO_2 capture assays. Data are the mean of triplicate reactions ± SD and are representative of 2 independent experiments.

Consistent with previous results, the L340R mutation reduced hydroxylation of the HIF-1α CAD to a level that was only just above background, and led to a similar reduction in activity on the Notch1 ARD. These data indicate that dimerisation of FIH is required for hydroxylation of both HIF and Notch substrates, and is therefore likely to have an important influence on the active site of the enzyme.

3.3 Discussion

3.3.1 Summary of Results

This work defines the kinetic parameters of FIH-catalysed hydroxylation of the Notch receptor family as representative ARD substrates. Preliminary experiments confirm the *in vitro* hydroxylation of Notch2-3 by FIH, and demonstrate hydroxylation at two asparagine residues located at equivalent positions to Sites 1 and 2 in the ARD of Notch1. The Site 1 asparagine appears to be hydroxylated more efficiently in the context of the full-length ARD, as well as shorter peptides encompassing the individual hydroxylation sites, consistent with results previously obtained for Notch 1 [94, 95].

Dimerisation of FIH was found to be essential for hydroxylation of both Notch and HIF substrates. However, a direct comparison of HIF and Notch hydroxylation by FIH in kinetic CO_2 capture assays and binding affinities using FP-based interaction assays showed that HIF has a higher maximum rate of hydroxylation, but displays a considerably lower affinity for FIH than Notch1-3, suggesting that Notch is likely to be the preferred substrate. Although Notch4 is not hydroxylated *in vitro*, it is still able to bind to FIH, and does so with a relatively high affinity compared with the HIF CAD. Finally, FIH has a higher affinity for oxygen with Notch as a substrate than with HIF, indicating that FIH-catalysed hydroxylation of Notch and HIF substrates is likely to be differentially regulated by oxygen availability. As discussed below, these data contribute important insights into FIH substrate specificity, particularly with respect to substrate choice in cells.

3.3.2 FIH has a preference for hydroxylation of Site 1 in Notch1-3

The mass spectrometry data presented in this thesis indicate that FIH hydroxylates two asparaginyl residues in Notch2 (N1902, N1969) and Notch3 (N1867, N1934), in equivalent positions to Sites 1 and 2 in Notch1. In contrast to the HIF-α CAD, most ARD substrates identified to date contain multiple sites of hydroxylation by FIH (refer to Table 1.1). This is not all that surprising given the repetitive nature of the ARD. Nonetheless, it is interesting to note that the extent of hydroxylation often differs between sites within the same ARD [86, 101, 104]. Consistent with previous analyses of Notch1, mutation of the Site 1 asparagine in Notch2-3 leads to a greater reduction in FIH activity than mutation of Site 2 (Figure 3.4), suggesting that Site 1 is preferentially hydroxylated by FIH [94, 95].

The differences in Site 1 and Site 2 hydroxylation may, in part, reflect the fact that one site within the folded ARD is more accessible than the other. Structural studies of Notch1 have indicated that the ARD folds via a discrete two-stage process with folding of repeats 3-5 (surrounding Site 2) preceding those around Site 1, thus placing Site 2 in a more stable position within the ARD [151, 152]. Similarly, the predominant site of hydroxylation in IκBα is located between ankyrin repeats 5 and 6, which are inherently less stable than the remainder of the ARD [86, 153]. Given the significant structural rearrangement required to enable an ARD to bind FIH in an extended conformation [95], it follows that the more accessible site would be preferred. The suggestion that ankyrin repeat stability is a determinant of hydroxylation is supported by a recent study of synthetic consensus ARDs, in which the more stable ARDs were found to be less susceptible to hydroxylation by FIH [113]. Even so, a similar preference for Site 1 over Site 2 is observed in the context of isolated peptides, which are unlikely to be folded, indicating that primary sequence determinants in the vicinity of the target Asn also make important contributions to hydroxylation.

3.3.3 FIH displays differential catalytic properties with Notch and HIF substrates

Kinetic analyses of FIH with the Notch1 ARD and the HIF-1α CAD reveal marked differences in their relative affinities for FIH, as well as their maximal rates of hydroxylation. The V_{max} (and k_{cat}) for FIH with the HIF-1α CAD was found to be

approximately 5-fold greater than that measured with the Notch1 ARD. However, FIH displays much higher affinity for Notch than for HIF. Whilst the K_m for the Notch ARD could not accurately be determined, the kinetic analyses presented in Figure 3.5 indicate that it is lower than 0.5 μM, although even this is a conservative estimate, as FIH activity had already reached its V_{max} at this concentration.

Similar experiments performed by our collaborators Dr Peppi Karppinen and Jaana Hyvarinen, found the K_m to be < 0.2 μM, suggesting that there is likely to be at least an order of magnitude difference in affinity between the two substrates. Consequently, the k_{cat}/K_m value, which gives a measure of enzyme efficiency, is at least 2-fold lower for HIF than for Notch. Therefore, whilst HIF is the better substrate for FIH at saturating substrate concentrations, these data imply that Notch is more efficiently hydroxylated and is likely to be the favoured substrate for FIH in a cellular context.

However, whilst FIH is predicted to display a preference for hydroxylation of ARD proteins such as Notch, studies have consistently demonstrated that HIF is efficiently hydroxylated in cells, whereas hydroxylation of ARD proteins is often incomplete [86, 95, 154]. A possible explanation for this lies in the function of the ARD as a protein-protein interaction domain [89]. Perhaps the high affinity FIH displays for ARD proteins reflects a need to compete with other proteins in order to gain access to hydroxylation sites, as opposed to a 'preference' for ARD hydroxylation over HIF.

3.3.4 Of mice and men

The K_m value determined for the mHIF-1α CAD in this study (~4 μM) is considerably lower than previously reported values (35-50 μM) for HIF-1α substrates [66, 127]. Although the affinity of FIH for HIF varies to some extent depending on the length of the peptide substrate [66, 100], this is unlikely to be the sole cause of this discrepancy. Similar kinetic experiments performed by Sarah Linke in our laboratory using an equivalent fragment of the human HIF-1α protein (last 90 amino acids) have determined the K_m to be 35 μM [136]. The most likely explanation is the difference in species-origin of the recombinant proteins. This study employed mouse orthologues of both FIH and HIF, whereas other studies have predominantly used human proteins. It is not completely clear whether the

differences in affinity are due to sequence variation between orthologues of FIH, HIF or a combination of the two. It is of interest to note that mouse FIH displays a higher binding affinity for mouse Notch substrates in FP assays, compared to human FIH (data not shown), although in most cases the difference is less than 2-fold.

The mouse and human orthologues of both FIH and HIF-1α are very similar, with amino acid sequence homology of 97% and 92%, respectively. Consequently, a number of previous studies, both by our laboratory and others, have used FIH and HIF-α proteins from mouse or human origin interchangeably (e.g. to demonstrate hydroxylation of a mouse substrate protein by the human enzyme) [58, 95]. The minor variations in sequence do not appear to alter the overall function of either protein; both human and mouse HIF-α subunits are regulated by FIH-catalysed asparaginyl hydroxylation, with similar consequences for expression of HIF target genes. Nevertheless, this study highlights key differences between the catalytic properties of mouse and human FIH on their respective HIF-α substrates, and highlights the need for more careful consideration of species differences in the future. A clear understanding of these differences will be essential for characterising and interpreting the phenotype of the $FIH^{-/-}$ mouse [85], and determining whether it provides an accurate representation of what occurs in a human context.

3.3.5 FIH has a high binding affinity for many ARD proteins

Whilst the K_m value determined for mouse HIF-1α is lower than previously reported, it is still considerably higher than the K_m value for the Notch ARD. This trend is consistent with other studies, which also show that FIH has a much higher affinity for the Notch ARD than for HIF [94, 95]. This robust affinity may be a general property of ARD substrates. The ARD proteins Gankyrin, FGIF and ANK44 interact with FIH in CoIP experiments and *in vitro* affinity pull-down assays under conditions that fail to efficiently capture HIF-1α (Rachel Hampton-Smith, personal communication), and similar findings have been reported by others [86, 101].

The work presented in this thesis suggests that this high affinity may also extend to ARD proteins that are not substrates for FIH. The ARD of Notch4 is not hydroxylated by FIH *in vitro*, but was found to interact with FIH in FP binding assays. The affinity was lower than that observed for Notch1-3, but was still several-fold higher than for HIF-1α (K_i values of 9.5 and 60 μM, respectively). This is in contrast with an earlier report that Notch4 was incapable of interacting with FIH in CoIP experiments [95]. However, this discrepancy is likely due to the higher sensitivity of the FP binding assay. As mentioned previously, the functional consequence of the inability of Notch4 to be hydroxylated is unclear, as no specific role for Notch4 has yet been elucidated that is distinct from the other Notch family members, but may become apparent if/when a role for ARD hydroxylation is identified. Until then, the Notch receptor family, in particular Notch4, provide a useful tool for the investigation of sequence elements that contribute to binding FIH, as opposed to catalysis.

3.3.6 A regulatory role for the FIH-ARD interaction

The ability of FIH to bind ARD proteins that are not substrates highlights the possibility that there may be dual physiological roles for binding versus hydroxylation of ARD proteins *in vivo.* Notably, numerous ARD proteins, including Notch1, have been shown to compete with the HIF-1α CAD for hydroxylation by FIH when co-expressed in transfected cells [94, 95, 98, 103]. This led Coleman et al. (2007) to hypothesise that competition by ARD proteins serves to fine-tune the HIF response [95]. However, this would not be feasible as a regulatory mechanism if FIH displayed a constitutively high affinity for ARD proteins, as the ubiquitous expression of a large pool of competitors would lead to inefficient hydroxylation of HIF under all oxygen conditions.

Thus, the finding that FIH has a considerably lower affinity for ARD proteins in their hydroxylated state (Figure 3.7B) is of particular importance, as it enables the hydroxylation status of the ARD pool to determine the level of FIH available for modification of HIF-α. In normoxic conditions, the majority of cellular ARD proteins will be hydroxylated, thus reducing their ability to bind and sequester FIH from HIF-α. In contrast, hypoxia will decrease the proportion of the ARD pool that is hydroxylated, leading to increased sequestration of FIH from HIF.

However, in order for this to occur, the hydroxylation status of the ARD pool would have to be equally sensitive (or more sensitive) to decreasing oxygen levels than hydroxylation of HIF. On the contrary, kinetic analyses performed by our collaborators determined the $K_m[O_2]$ of FIH for Notch to be 12 μM, which is almost 8-fold lower than the value of 90 μM determined for HIF-1α. As such, hydroxylation of Notch is likely to be less sensitive to decreasing oxygen levels than hydroxylation of HIF. It will therefore be important to determine whether the affinity of FIH for oxygen is similar for hydroxylation of other ARD substrates, as this may have important consequences for HIF regulation.

3.3.7 Structural determinants of hydroxylation by FIH

The distinct kinetic properties of HIF and Notch as substrates for FIH are particularly interesting in light of the structural differences between the two proteins. The higher affinity of FIH for Notch suggests that it may have a preference for binding to the ankyrin fold, as opposed to the structurally disordered HIF CAD. In support of this, short (20-mer) peptides from Site 1 and Site 2 in Notch, which presumably lack any secondary or tertiary structure, have a similarly low affinity for FIH as peptides from HIF-1α (K_m values of 110-120 μM). Interestingly, increasing the C-terminal length of these Notch peptide substrates by only 15 amino acids leads to a dramatic increase in affinity for FIH, with K_m values of 0.7 μM and 13 μM for Site 1 and Site 2, respectively.

Whilst Notch and HIF peptides bind in a similar manner within the active site of FIH (refer to section 1.3.4), these longer Notch peptides presumably enable further interactions beyond the catalytic binding pocket. Crystal structures indicate that residues C-terminal to the hydroxylation site in HIF-1α form a helix that makes additional contacts on the surface of FIH. However, increasing the length of HIF peptide substrates to include this helix had much less influence on the K_m or V_{max} values than the equivalent increase in length of Notch peptides, suggesting that hydroxylation of HIF is largely dependent on residues proximal to the target asparagine. Structural analyses of FIH bound to the full-length Notch ARD, or longer peptides that include additional residues C-terminal to the target asparagine would be helpful in elucidating any distinct interaction surfaces outside of the active site that promote a high affinity interaction with ARD proteins.

While it is clear from this work that the substrate properties of HIF and ARD proteins are influenced considerably by their structure, the relative importance of primary, secondary and tertiary structure remain largely uncharacterised and are addressed in the next chapter.

Taken together, the data presented in this chapter demonstrate that FIH-catalysed hydroxylation of Notch, and presumably other ARD substrates, differs considerably from hydroxylation of HIF, both in terms of the affinity of the interaction and its sensitivity to oxygen availability. Whilst the functional outcome of ARD hydroxylation remains unclear, the differential properties of ARD substrates are predicted to have important consequences for HIF activity in cells. The extent to which ARD proteins shape the HIF-mediated response to hypoxia will depend on the specific repertoire of ARD proteins expressed in a particular cell-type, their relative binding affinities for FIH, the number of accessible hydroxylation sites, and the overall oxygen sensitivity of the ARD pool. This adds a further layer of complexity to regulation of the HIF pathway, and provides numerous opportunities for cross-talk between HIF signalling and ARD-mediated pathways.

Chapter 4

Structural determinants of FIH substrate recognition and hydroxylation

4.1 Foreword

This chapter presents a detailed investigation of the molecular determinants of recognition and hydroxylation by FIH, with a focus on key differences between HIF and ARD substrates. To investigate the relative importance of primary, secondary and tertiary structure, a series of point-mutants and chimeric substrate proteins were generated and analysed for their ability to bind FIH, and to promote 2OG turnover in *in vitro* hydroxylation assays. A biophysical approach was also employed to investigate the importance of protein structure and stability in substrate recognition. Collectively, these experiments identify substrate-specific recognition elements that contribute to the distinct properties of HIF and ARD proteins as substrates for FIH.

This work is presented as a manuscript that was recently accepted for publication by the Journal of Biological Chemistry. Whilst the majority of the experimental data presented in this paper was generated by myself, a section of work performed by Sarah Linke (characterising a conserved RLL motif in the HIF CAD; Figures 6 and 7) is also included. This chapter is referenced separately from the rest of the thesis, with the references listed at the end of the paper.

4.2 Statement of Author Contributions

Factor inhibiting HIF (**FIH**) recognises distinct molecular features within hypoxia inducible factor (HIF)-α versus ankyrin repeat substrates.

Author	**Contribution**	**Signature**
Sarah Wilkins	Primary role in designing and performing experiments. Contributed to analysis and interpretation of data. Responsible for writing and editing the manuscript.	
Sarah Karttunen	Primary role in designing and performing experiments (Figures 6 and 7). Contributed to data analysis and interpretation. Assisted with proof-reading of the manuscript.	
Rachel Hampton-Smith	Designed and performed experiments (Figures 2C & S1). Contributed to data analysis and interpretation.	
Iain Murchland	Performed molecular dynamics simulations (Figures 5B, 5C & S4). Contributed to data analysis and preparation of the manuscript.	
Anne Chapman-Smith	Provided intellectual discussion, as well as direction and assistance with CD spectroscopy. Assisted with proof-reading of the manuscript.	
Daniel Peet	Provided intellectual discussion. Contributed to the design of experiments, interpretation of data, as well as preparation and editing of the manuscript.	

4.3 Wilkins *et al*. (2012)

Wilkins, S.E., Karttunen, S., Hampton-Smith, R.J., Murchland, I., Chapman-Smith, A. & Daniel J. Peet, D.J. (2012) Factor Inhibiting HIF (FIH) Recognizes Distinct Molecular Features within Hypoxia inducible Factor-α (HIF- α) *versus* Ankyrin Repeat Substrates.
The Journal of Biological Chemistry, v. 287 (12), pp. 8769 -8781

NOTE:
This publication is included on pages 105-124 in the print copy of the thesis held in the University of Adelaide Library.

It is also available online to authorised users at:

http://dx.doi.org/10.1074/jbc.M111.294678

Chapter 5

Characterisation of Orf virus ARD proteins as substrates for FIH

5.1 Introduction

Extensive analyses of ARD proteins as substrates for FIH (detailed in Chapters 3 and 4) have provided crucial insights into the molecular determinants of recognition and hydroxylation by FIH. In particular, a putative FIH hydroxylation motif has been defined ($LXXXX\pi\frac{D}{E}\phi N$[†]) based on sequence homology between hydroxylation sites in HIF and ARD substrates. This consensus motif was recently employed by Jonathan Gleadle (a close collaborator of our laboratory) in a bioinformatic search for novel FIH substrates. The search identified a large number of ankyrin repeat proteins, several of which were of particular interest to our laboratory. Amongst these were a family of ankyrin repeat proteins encoded by a species of poxvirus known as Orf.

ARD proteins are relatively uncommon in viruses (compared to eukaryotes and/or bacteria), but are over-represented in the proteomes of vertebrate poxviruses [131]. The reason for their prevalence is poorly understood, as is their contribution to viral pathogenesis. Nonetheless, they provide an interesting avenue for investigation of FIH substrate specificity. As the known substrate repertoire of FIH is currently limited to proteins encoded by metazoa, it is of considerable interest to determine whether FIH-dependent hydroxylation of ARD proteins extends to those encoded by intracellular pathogens such as viruses.

5.1.1 Poxviruses

Poxviruses (*Poxviridae*) are a family of double-stranded DNA viruses that cause acute infections in wide range of animal hosts (see [155] for review). They are unique amongst DNA viruses in that they replicate exclusively within the cytoplasm of the infected cell, via a mechanism that is largely independent of host machinery [156]. Poxviruses that infect vertebrates belong to the sub-family *Chordopoxvirinae*, and include several species that are pathogenic for humans [157]. The most well-known of these is the Variola virus, which causes small-pox, although the closely related Vaccinia virus has been the most extensively studied [158]. This chapter will focus on the Orf virus, which is the prototypical member of the *Parapoxvirus* genus.

[†] amino acid nomenclature: π = small, uncharged; ϕ = hydrophobic

5.1.2 Orf Virus

Orf virus (ORFV) is one of several zoonotic parapoxviruses. It predominantly infects sheep and goats, giving rise to a debilitating skin condition known as contagious ecthyma or 'scabby mouth' [132, 159]. Infections are characterised by highly vascularised (bloody), pustular or scabby lesions, which occur on the lips, nostrils, or genitals of affected animals, and occasionally on the hands and forearms of humans that come into contact with diseased animals [128, 160]. The virus infects its host through broken or damaged skin, and replicates locally in regenerating epidermal keratinocytes [128]. Infections are rarely fatal, but are a major economic burden and animal-welfare concern within the livestock industry, and an occupational hazard for animal handlers and farmers.

Like other poxviruses, ORFV has evolved a number of complex strategies to evade host anti-viral defence mechanisms, and establish a cellular environment that is favourable for replication (reviewed in [161, 162]). Its genome encodes numerous proteins that function at both a cellular and systemic level to modulate host immune and inflammatory responses [163-167], and interfere with key cellular processes such as cell cycle regulation [168] and apoptosis [169]. Recent studies suggest that the ORFV ARD proteins may contribute to some of these processes, via manipulation of the host cell ubiquitylation machinery [137, 170].

5.1.3 Orf Virus ARD Proteins

ORFV encodes five ARD proteins, 008, 123, 126, 128 and 129, which are similar in size and share a common domain arrangement. The N-terminal portion of each protein contains 9-10 ankyrin repeats, whilst the C-terminus contains an F-box motif [171]. The F-box motif mediates a specific interaction with Skp1, a component of the cellular SCF (Skp1-Cullin1-F-box) ubiquitin-ligase complex. The precise outcome of this interaction is unknown. However, it is thought to enable the ORFV F-box/ARD proteins to function in a similar manner to mammalian F-box proteins, by recruiting specific protein substrates to the SCF complex for polyubiquitylation and subsequent degradation by the 26S proteasome [172, 173]. In this scenario, the ARD would function in a recognition capacity by interacting with ubiquitylation targets, and would thus dictate the substrate specificity of the complex. The versatility of the ARD as a protein-protein interaction motif could enable

them to direct the poly-ubiquitylation and degradation of a wide range of cellular proteins, and in doing so modulate diverse cellular responses to viral infection.

Given the likelihood that the ORFV ARD proteins are substrates for FIH, hydroxylation may serve to regulate their activity (e.g. by influencing their ability to interact with protein targets). Furthermore, if they are able to interact with FIH with the high affinity observed for other ARD proteins, they could potentially sequester FIH from other substrates, or alternatively, promote its poly-ubiquitylation and degradation in response to virus infection. Either of these outcomes could have important consequences for HIF regulation following ORFV infection.

5.1.4 Activation of HIF by viruses

Activation of the HIF pathway has been shown to occur in response to infection by a number of viruses, including human papillomavirus [174], hepatitis B and C [175-177], and human immunodeficiency virus [178, 179]. In most cases, HIF-1α protein is stabilised in a hypoxia- independent manner during viral infection, and contributes to virus-associated changes in gene expression. Such a mechanism has not previously been demonstrated for ORFV, however, it would be consistent with other strategies employed by the virus to modulate host cell physiology. In common with other members of the *Parapoxvirus* genus, ORFV encodes a viral homologue of VEGF, which stimulates angiogenesis and plays a critical role in virus infection [180-184] . Upregulation of endogenous *VEGF*, as well as other HIF targets involved in angiogenesis or vascularisation, could serve to augment this response.

5.1.5 Chapter Aims

Therefore, in addition to investigating the ORFV ARD proteins as substrates for FIH, this chapter will investigate their ability to activate the HIF pathway through sequestration or degradation of FIH. This could provide a novel FIH-dependent mechanism for HIF activation by an intracellular pathogen. Three specific hypotheses will be addressed:

1. FIH can bind and hydroxylate the ORFV ANK proteins
2. FIH is targeted for polyubiquitylation and degradation during ORFV infection
3. ORFV activates HIF target gene expression in a FIH-dependent manner

This work was performed in collaboration with Professor Andrew Mercer from the University of Otago in New Zealand, an expert on the Orf virus and associated ARD proteins, as well as Professor Jonathan Gleadle from the University of South Australia.

5.2 Results

5.2.1 Hypothesis 1: FIH can bind and hydroxylate the ORFV ARD proteins

The bioinformatic search performed by Jonathan Gleadle identified potential hydroxylation sites in all five of the ORFV ARD/F-box proteins (Figure 5.1). Preliminary experiments were designed to analyse *in vitro* hydroxylation of 008 as a representative of the ORFV ARD/F-box protein family, and the first step in this process was to generate recombinant protein for use in CO_2 capture assays.

Expression and Purification of the 008 ARD

A pApex-based plasmid containing the full-length 008 gene (pVU655) was obtained from the Mercer group at the University of Otago [137]. This construct was not suitable for bacterial expression, and so the 008 coding sequence was sub-cloned into the pET32 expression plasmid to produce the full-length 008 protein in *E. coli* with an N-terminal Trx-6H tag. A truncated construct encoding the predicted ARD (refer to Figure 5.1) was also generated. A small-scale trial induction and Ni^{2+}-affinity purification were performed for each protein in order to optimise induction conditions and asses yield.

Analysis of crude bacterial lysates by SDS-PAGE/coomassie staining showed intense bands corresponding to either Trx-6H-008 (Figure 5.2A) or Trx-6H-008 ARD (Figure 5.2B), which were present in the induced, but not the uninduced, samples. Both bands ran slightly lower than their expected molecular weights of 52 kDa and 73 kDa, respectively. However, this was deduced to be a gel artefact. A high yield of Trx-6H-008 ARD was obtained following Ni^{2+}-affinity purification under native conditions (~15 mg/L culture), and the protein ran as a single discrete species of >90% purity (Figure 5.2B, lane 5). In contrast, the full-length 008 protein was largely insoluble, and little to no protein was obtained following affinity-purification (Figure 5.2A, lanes 5-6). Several attempts were

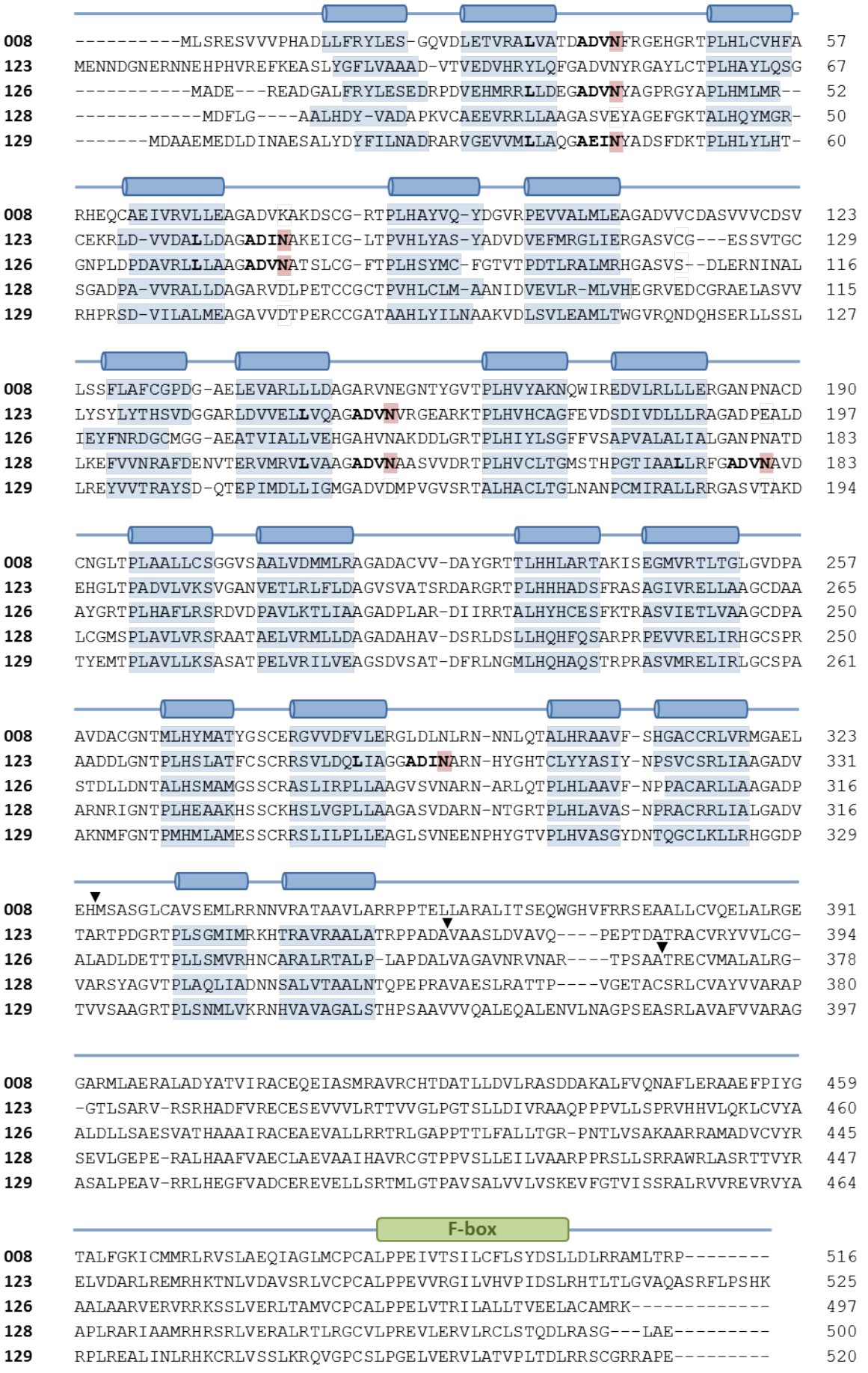
F-box

Figure 5.1 The Orf virus ARD proteins are potential substrates for FIH

A. Alignment of the amino acid sequences for the ARD/F-box proteins 008, 123, 126, 128 and 129 of the ORFV strain NZ2 (Genbank accession numbers: ABA00524, ABA00641, ABA00642, ABA00646 and ABA00647). Ankyrin repeat helices (indicated by blue shading and barrels above the sequence) were predicted using the PSIPRED secondary structure prediction server [185], and were mostly consistent with previous predictions by Mercer at al. (2005) using the SMART protein database [87, 171]. The position of the C-terminal F-box motif is also shown [171]. Numbers to the right indicate relative position in amino acid sequence, and black arrowheads (▼) indicate the terminal residue in ARD constructs generated for 008, 123 and 126 proteins. Pink highlighting denotes asparagine residues that could potentially be hydroxylated by FIH based on their position within the ankyrin repeat sequence and homology to the FIH consensus hydroxylation motif, LXXXXπ(D/E)ϕN (where ϕ and π represent hydrophobic and small, uncharged amino acids, respectively).

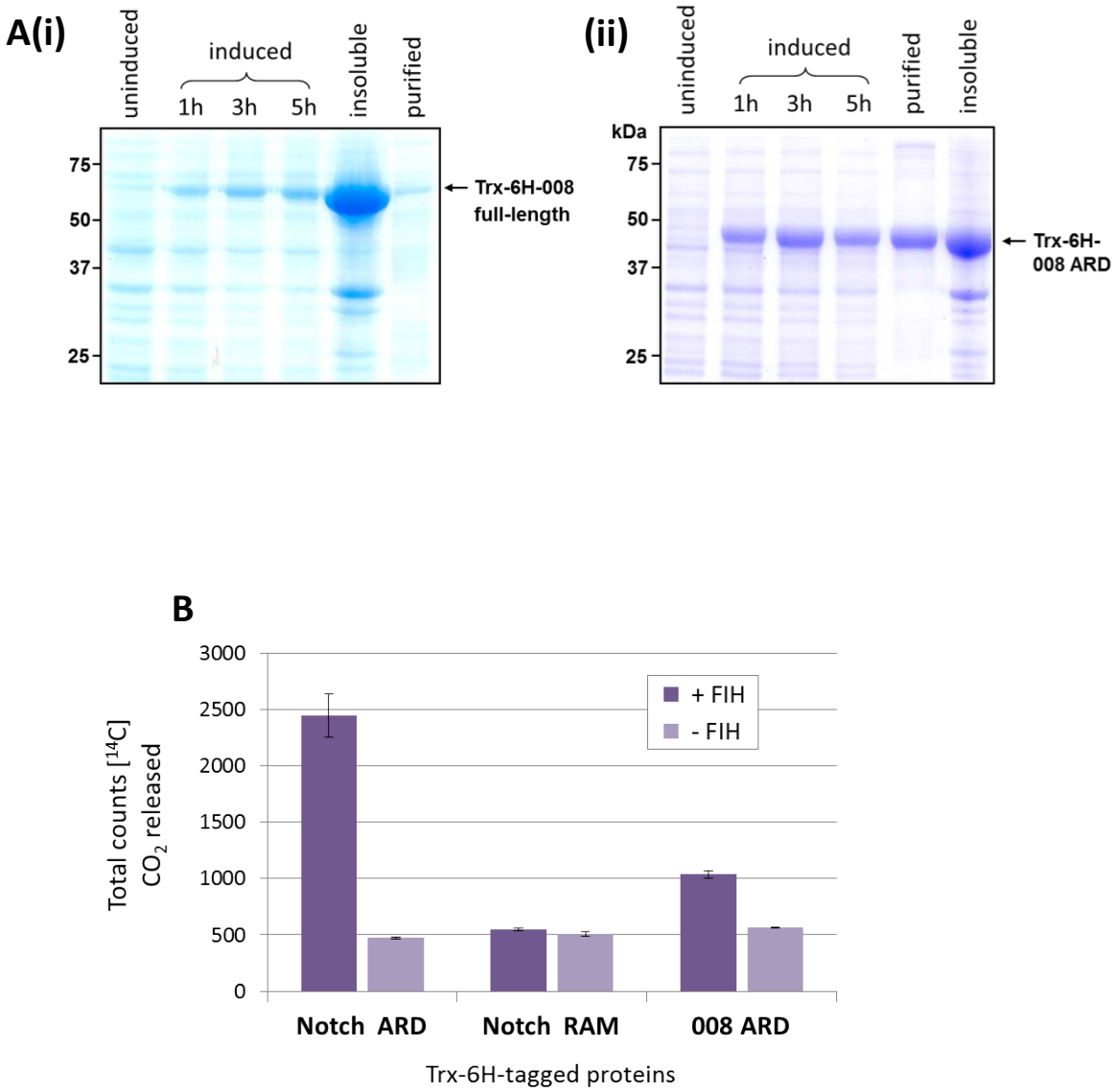

Figure 5.2 Purification and Hydroxylation of ORFV008

A. SDS-PAGE analyses of small-scale induction and purification of Trx-6H-tagged 008 full-length (i) and ARD (ii) proteins. Samples show crude bacterial lysates from BL21(DE3) *E. coli* before (uninduced) and 1, 3 and 5 h after IPTG induction, insoluble and Ni^{2+}-affinity purified proteins, separated by 10% SDS-PAGE and stained with coomassie. B. Equivalent concentrations (20 μM) of Trx-6H-ORFV008 ARD, Trx-6H-Notch ARD (positive control) and Trx-6H-Notch RAM (negative control) were assayed for hydroxylation by MBP-hFIH (1 μM) in CO_2 capture assays. Data are the mean of triplicate reactions ± SD, and are representative of 3 independent experiments.

made to increase the yield of soluble full-length 008 protein by altering the induction conditions (IPTG concentration, induction time and temperatures of 25^{o}C, 30^{o}C and 37^{o}C) or including a low concentration of detergent in the lysis buffer. However, these were largely unsuccessful (data not shown). Therefore, the ARD construct was chosen for use in further experiments, and a large-scale expression and purification was performed to generate sufficient protein for use in CO_2 capture assays.

CO_2 capture assays infer that 008 is a substrate for FIH in vitro

CO_2 capture assays were performed to determine whether Trx-6H-008 ARD is a direct substrate for FIH *in vitro*, based on its ability to promote FIH-dependent turnover of 2OG. The ARD and RAM domain of mNotch1 were included as positive and negative controls, respectively. Trx-6H-tagged proteins were expressed in *E. coli*, purified by Ni^{2+}-affinity chromatography, and equal concentrations (20 μM) assayed for hydroxylation by MBP-hFIH. As shown in Figure 5.2B, the Notch RAM domain was unable to promote decarboxylation of 2OG above background levels, whilst the Notch ARD displayed robust activity. The 008 ARD stimulated a small but statistically significant amount of 2OG turnover. The activity was low in comparison with the Notch ARD, but was consistently greater (~2 fold) than background. These results were consistent with ORFV008 being a substrate for FIH *in vitro,* although hydroxylation appears to be relatively inefficient in comparison with Notch.

ORFV 123 and 126 are also hydroxylated by FIH

Following on from the analysis of 008, two additional members of the ORFV ARD/F-box protein family (123 and 126) were tested as *in vitro* substrates for FIH. Full-length constructs were not generated for either these proteins, given the difficulties encountered with obtaining soluble full-length protein for 008. Rather, the predicted ARDs of 123 and 126 (refer to Figure 5.1A) were amplified from their respective pApex plasmids (pVU661 and pVU657) and sub-cloned into pET32 for direct comparison with 008. Trx-6H-123 ARD and Trx-6H-126 ARD proteins were expressed in BL21(DE3) *E. coli,* purified by Ni^{2+}-affinity chromatography, and visualised by SDS-PAGE with coomassie staining (Figure 5.3A). Relatively high yields of soluble protein were obtained for both constructs (~12 mg/L culture), and each produced a band at the expected molecular

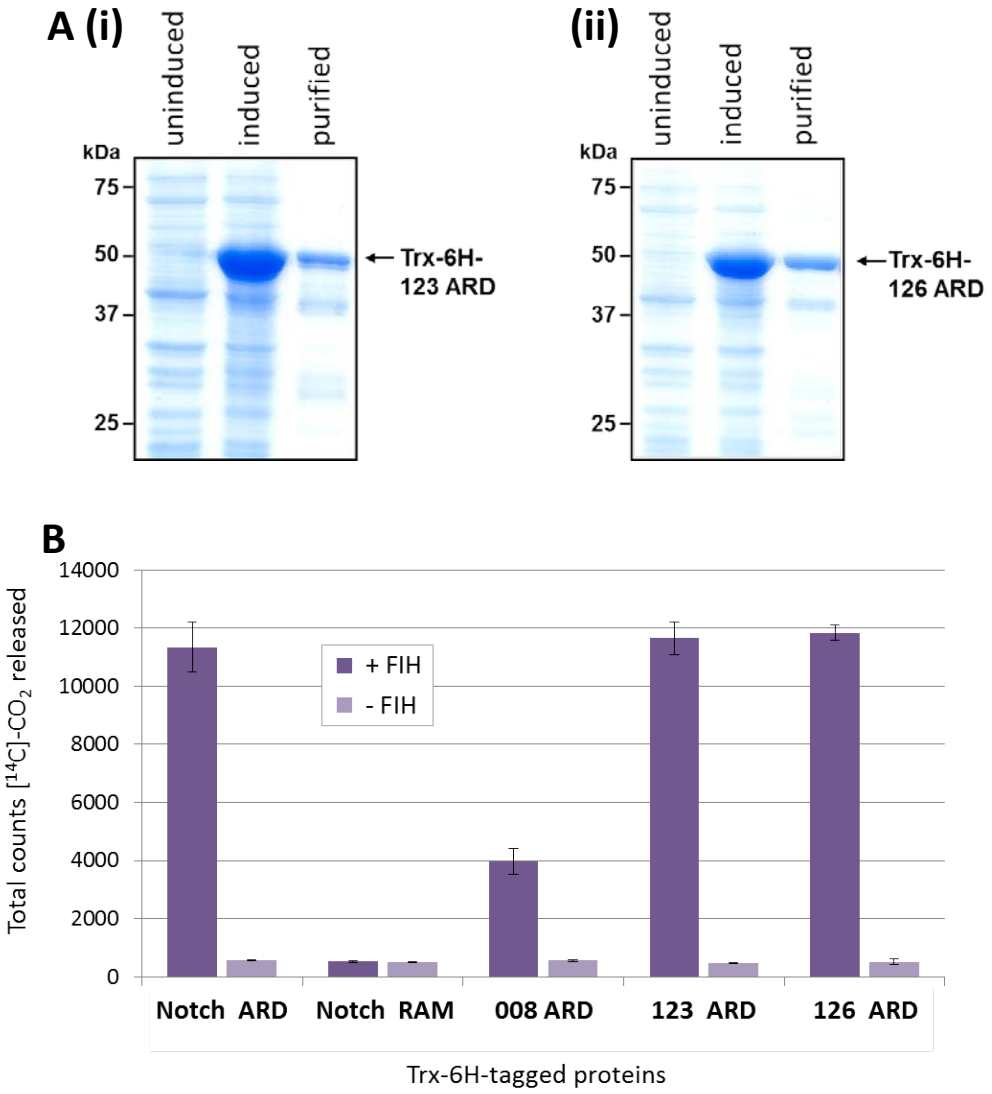

Figure 5.3 Purification and Hydroxylation of ORFV123 and ORFV126

A. SDS-PAGE analyses of small-scale induction and purification of Trx-6H-tagged 123 (i) and 126 (ii) ARD proteins. Samples show crude bacterial lysates from BL21(DE3) *E. coli* before (uninduced) and after 5 hours of IPTG induction, as well as Ni^{2+}-affinity purified proteins, separated by 10% SDS-PAGE and stained with coomassie. B. Equivalent concentrations (50 μM) of Trx-6H-tagged proteins (mNotch1 ARD, mNotch1 RAM, ORFV008 ARD, ORFV123 ARD and ORFV126 ARD) were assayed for hydroxylation by MBP-hFIH (2 μM) in CO_2 capture assays. Data are the mean of triplicate reactions ± SD, and are representative of 3 independent experiments.

weight (52 kDa for Trx-6H-123 ARD and 53 kDa for Trx-6H-126 ARD). Although some degradation of both proteins was evident from the SDS-PAGE analyses, this was minimised in future protein preparations by the addition of protease inhibitors (data not shown).

The expression of the ARDs of 123 and 126 were scaled up, and the purified proteins were then analysed for *in vitro* hydroxylation by FIH. A CO_2 capture assay was performed using maximal amounts (50 μM) of Trx-6H-ORFV008 ARD, Trx-6H-ORFV123 ARD and Trx-6H-ORFV126 ARD, as well as a saturating amount of MBP-hFIH (2 μM). As shown in Figure 5.3B, both the 123 and 126 ARD proteins promoted FIH-dependent turnover of 2OG, at comparable levels to those observed for the Notch1 ARD. Once again, a small, but significant, level of 2OG turnover was stimulated by Trx-6H-008 ARD. Taken together, these data strongly infer that the ORFV ARD proteins are substrates for FIH *in vitro*.

The ORFV ARD proteins bind FIH with high affinity in vitro

To complement the hydroxylation analyses, *in vitro* affinity-pulldown assays were performed to investigate the relative binding affinities of the ORFV ARD proteins for FIH. Trx-6H-tagged 'bait' proteins were immobilised on Ni^{2+}-resin and incubated with affinity-purified MBP-hFIH. Resultant complexes were washed, eluted and separated by SDS-PAGE, and the captured FIH detected by Western blot. As shown in Figure 5.4, FIH was pulled-down by all three ORFV ARD proteins as well as the ARD of Notch, but not by the Notch RAM domain, which we have previously shown does not interact with FIH. Despite the low levels of activity displayed by the 008 protein in CO_2 capture assays, it bound to FIH with a similar affinity (albeit slightly lower) to the Notch ARD. In fact, all three of the ORFV ARD proteins form stable complexes with FIH, indicating a relatively high affinity interaction. This result was particularly interesting, given the potential repercussions of FIH sequestration or recruitment by the ARD/F-box proteins.

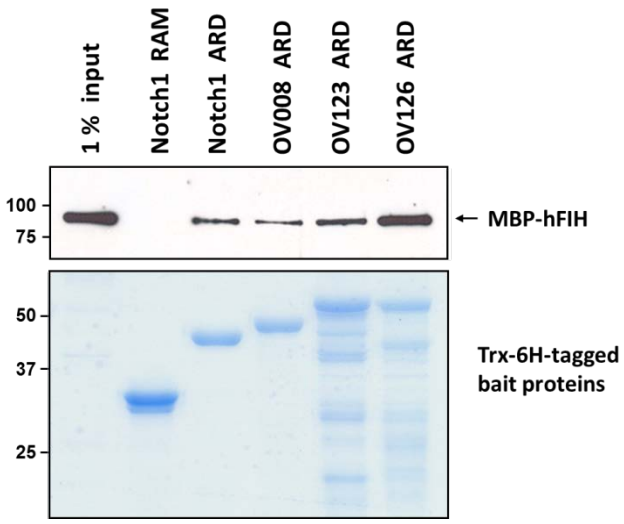

Figure 5.4 FIH can bind the ORFV ARD proteins *in vitro*

Affinity pull-down assay in which Trx-6H-tagged bait proteins were retained on Ni^{2+}-resin following purification and incubated with recombinant MBP-FIH. Captured complexes were analysed by SDS-PAGE and immunoblotting with an anti-FIH antibody (Novus; *upper panel*) or coomassie staining (*lower panel*) to visualise bait proteins. A representative pulldown of 4 independent experiments is shown. The RAM domain of Notch, which does not interact with FIH and is not hydroxylated [94], was used as a negative control. The input lane contains 1% of the total amount of MBP-FIH incubated with the bait resin.

5.2.2 Hypothesis 2: FIH is targeted for degradation in response to ORFV infection

Given the role of cellular F-box proteins in recruiting substrates to the SCF ubiquitin ligase complex, and the robust affinity with which FIH binds the ORFV ARD/F-box proteins, it was hypothesised that FIH might be targeted for poly-ubiquitylation and degradation in response to ORFV infection. A key preliminary experiment, which would either support or disprove this hypothesis, was to compare the relative levels of FIH protein in ORFV-infected versus uninfected cells.

An important consideration in these experiments was the choice of cell-type. Whilst FIH is ubiquitously expressed, ORFV exhibits a fairly narrow host range, and cannot productively infect most established cell-lines. The Mercer group typically utilise primary lamb testis (LT) cells to propagate and analyse virus isolates. However, use of this cell-type would require an antibody capable of detecting sheep FIH. The polyclonal antibody routinely used in our laboratory (from Novus Biologicals) was raised against the full-length human protein, and its cross-reactivity with species other than mouse had not previously been tested. Therefore, preliminary experiments were performed to confirm that the Novus antibody was indeed capable of detecting sheep FIH in cell-lysates (Appendix 3). Following on from this, LT cell lysates were analysed for changes in FIH protein levels in response to ORFV infection.

Analysis of FIH levels after ORFV infection

Virus infections were performed by our collaborators at the University of Otago, and cell-lysates sent to our laboratory for Western blot analyses. In the first experiment, lysates from LT cells were harvested at 6 hours and 20 hours post-infection with ORFV, and after 20 hours of treatment with PBS as an uninfected control. Extracts from the human neuroblastoma cell-line SK-N-BE2C (kindly provided by Teresa Otto) were included in the Western blot analyses as an antibody control. As shown in Figure 5.5A, FIH protein levels were noticeably diminished in ORFV-infected lysates compared to the PBS control, with the lowest level of protein observed at 20 hours post-infection. In contrast, a relatively uniform level of protein was detected by the ARNT antibody across infected and uninfected samples. This result, although preliminary, is consistent with the hypothesis that FIH is selectively degraded in response to ORFV infection.

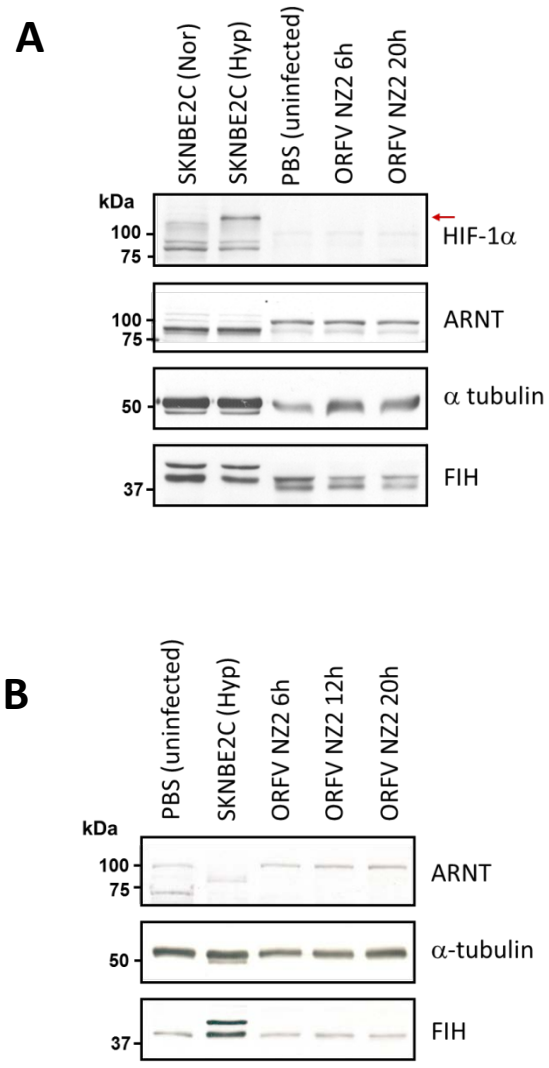

Figure 5.5 Detection of FIH in lysates from ORFV-infected and uninfected LT cells

Primary lamb testis (LT) cells were infected with ORFV strain NZ2, or treated with PBS as an uninfected control. Equivalent numbers of cells were harvested in denaturing laemmli buffer after 6, 12 and 20 hours of infection, or 20 hours of PBS treatment. Equivalent volumes of LT cell-lysates, as well as extracts from hypoxia (Hyp) or normoxia (Nor) treated SK-N-BE2Cs, were separated by SDS-PAGE and subjected to sequential immunoblot analyses of proteins as labelled. The red arrow indicates the expected molecular weight for human HIF-1α. A and B are data from two independent experiments.

However, the same result was not obtained in a repeat experiment. Rather, analyses of LT cell lysates harvested at 6, 12 and 20 hours post-infection revealed equivalent levels of FIH to the uninfected (PBS-treated) control (Figure 5.5B). Similar results were also obtained following ORFV infection of a human osteosarcoma (TK-143b) cell-line (data not shown). Taken together, these results indicate that degradation of FIH is not a consistent outcome of ORFV infection. Interestingly, HIF-1α protein (visible in extracts from hypoxia treated SK-NB-E2Cs, Figure 5.5A) was not detected in any of the LT lysates, suggesting that it is not stabilised in response to ORFV infection. However, it is also possible that the antibody (which was raised against amino acids 610-727 of human HIF-1α) is unable to detect sheep HIF-1a, given that the sheep and human sequences are only 82% similar within the immunogenic region.

5.2.3 Hypothesis 3: The HIF pathway is activated in response to ORFV infection

The lack of any consistent reduction in FIH protein levels as a result of ORFV infection suggests that degradation of FIH is not a specific mechanism employed by the virus to activate the HIF pathway, although clearly more quantitative experiments are required to determine whether any change in FIH levels occur. Nonetheless, FIH interacts with the ORFV ARD/F-box proteins with a similarly high affinity to that observed for the Notch ARD, which has previously been shown to sequester FIH away from HIF in mammalian cells [94, 95]. As discussed in Section 1.1.8, the hydroxylase activity of FIH is of particular importance in repressing the low levels of HIF that escape prolyl hydroxylation and proteasomal degradation in normoxia. As such, sequestration of FIH by the ORFV ARD/F-box proteins would limit the amount of FIH available for hydroxylation of HIF-1α, which would likely result in activation of the HIF pathway in response to ORFV infection.

To address this possibility, quantitative PCR (qPCR) experiments were designed to compare the expression of particular HIF target genes in ORFV-infected versus uninfected LT cells. As with previous experiments, ORFV infections of LT cells were performed by our collaborators at the University of Otago in New Zealand, and lysates from infected cells sent to our laboratory for RNA extraction and qPCR analyses. Although fairly low yields of total RNA were typically obtained (2-5 μg RNA/1 x 10^6 cells), the RNA was of high purity as

assessed by gel electrophoresis and the ratio of absorbance at 260 and 280 nm. An equivalent amount of total RNA from ORFV-infected and uninfected cells was reverse-transcribed, and expression of three well-characterised HIF target genes (*VEGF, PHD3* and *GLUT1)* analysed by qPCR. Importantly, the expression of each of these target genes has previously been shown to be upregulated in a HIF-dependent manner following depletion of FIH by siRNA in normoxia [83]. The design and validation of specific primer sets is described in Appendix 4.

The relative expression of VEGF and PHD3 increases with ORFV infection

In two independent experiments (Figure 5.6A and B), infection of LT cells with ORFV led to an increase in *VEGF* expression relative to the reference gene *RPLP0* (*ribosomal protein P0*). A similar trend was observed for *PHD3*, although the level of induction was less consistent between experiments. This is possibly due to the lower expression of *PHD3*, particularly in the second experiment, in which the levels of *PHD3* mRNA were at the lower limits of detection. Nevertheless, these results support the hypothesis that HIF is activated in response to ORFV infection. Interestingly, similar effects on HIF target gene expression, specifically *VEGF*, were observed following infection of LT cells with Vaccinia virus (Figure 5.6D), suggesting that vertebrate poxviruses may employ a common mechanism of HIF pathway activation, possibly through sequestration of FIH by virally encoded ARD proteins.

Global mRNA regulation by ORFV

Analysis of raw data from initial qPCR experiments indicated that the amount of mRNA for the reference gene, *RPLP0,* was not constant across samples, and was considerably lower at 20 h post-infection than in the other two samples. In an attempt to resolve this issue, the expression levels of three other house-keeping genes (*β-actin, GAPDH* and *POLR2A*) were analysed in the same ORFV-infected and uninfected LT cells as in previous experiments (Figures 5.6A and B). Once again, the expression of all three genes (as well as *RPLP0*) was reduced in response to ORFV infection (Figure 5.6C).

In each case, a similar trend was observed, with an approximate 2-fold reduction in mRNA at 6 and 12 hours post-infection, and a further reduction by 20 hours to around one tenth

A

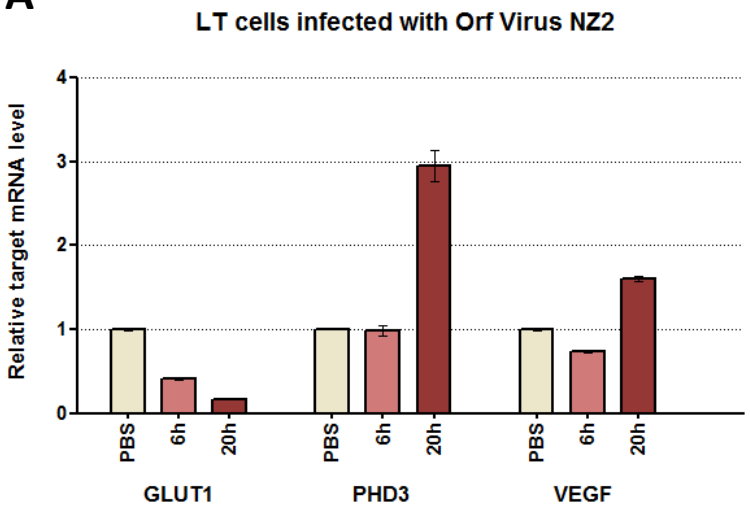
LT cells infected with Orf Virus NZ2
Relative target mRNA level
0
1
2
3
4
PBS
6h
20h
GLUT1
PHD3
VEGF

B

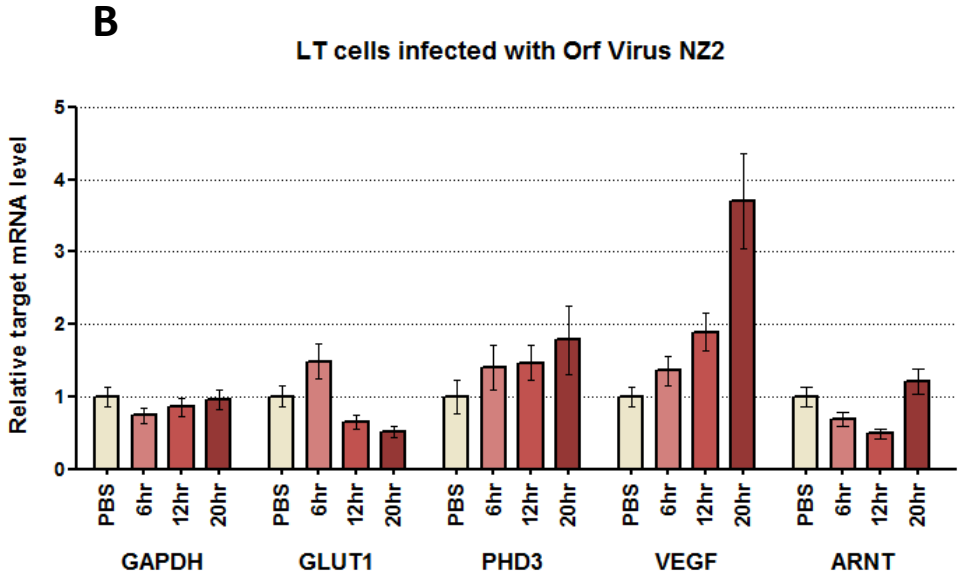
LT cells infected with Orf Virus NZ2
Relative target mRNA level
0
1
2
3
4
5
PBS
6hr
12hr
20hr
GAPDH
GLUT1
PHD3
VEGF
ARNT

C

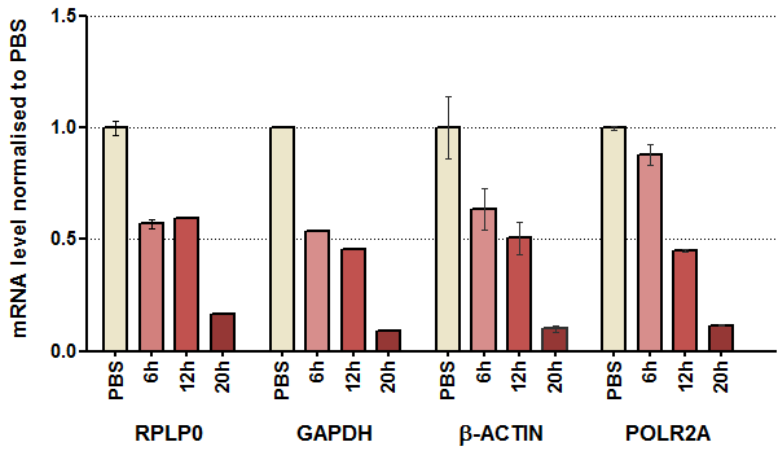
LT cells infected with Orf Virus NZ2
mRNA level normalised to PBS
0.0
0.5
1.0
1.5
PBS
6h
12h
20h
RPLP0
GAPDH
β-ACTIN
POLR2A

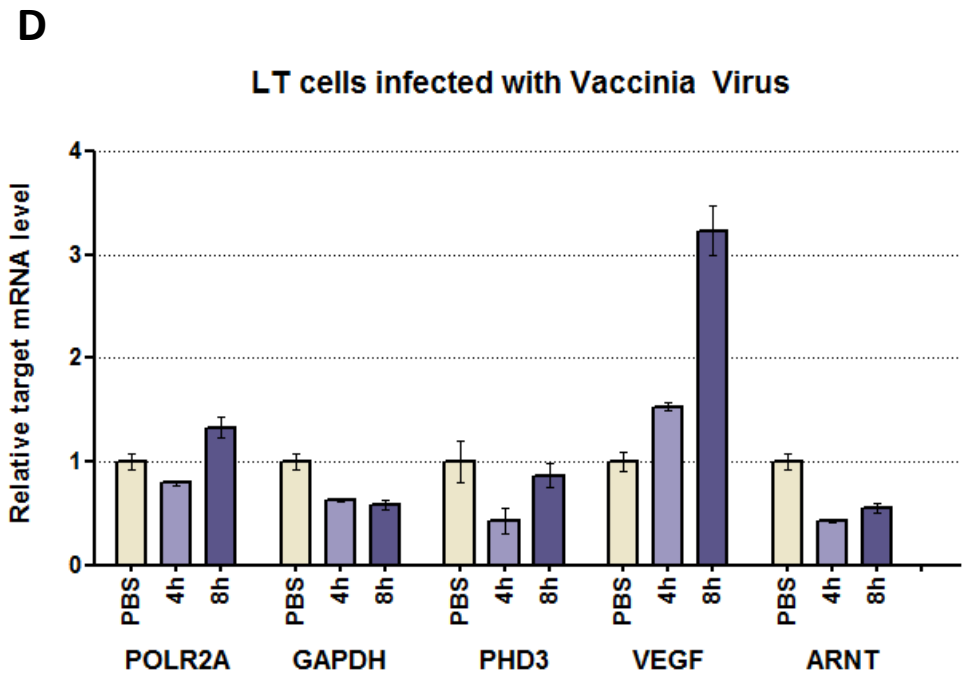

Figure 5.6 Analysis of HIF target gene expression by qPCR

In two independent experiments (A and B), LT cells were infected with the NZ2 strain of ORFV and total RNA isolated after 6, 12 and 20 hours of infection, or after 20 hours of PBS treatment as an uninfected control. Equivalent amounts of RNA were reverse transcribed and subjected to qPCR analyses. Expression levels of each gene are shown normalised to the reference genes *RPLP0* and *β-Actin,* and are expressed as the fold change relative to uninfected (PBS-treated) samples. Data are the mean of triplicate reactions ± SEM. C. RNA samples from B were subjected to qPCR analysis to investigate the expression levels of of several house-keeping genes in uninfected and ORFV-infected LT cells. Expression levels of each gene were not normalised to a reference gene, but instead the raw data were expressed as the fold change relative to the uninfected sample. Data are the mean of triplicate reactions ± SEM. D. In a single preliminary experiment, LT cells were infected with the Copenhagen strain of Vaccinia virus (VACV) and total RNA isolated after 4 and 8 hours of infection, or 8 hours of PBS treatment as an uninfected control. Isolated total RNA was reverse transcribed and gene expression analysed by qPCR. Expression levels of each gene are shown normalised to *β-Actin,* and are expressed as the fold change relative to the uninfected (PBS-treated) sample. Data are the mean of triplicate reactions ± SEM.

the amount in the uninfected control. Given these results, it seems likely that ORFV has a global influence on mRNA expression. Consequently, the absolute levels of mRNA for *VEGF* and *PHD3* are actually lower in ORFV infected samples compared to the uninfected control. Nonetheless, they are reduced to a lesser extent by ORFV infection than all four reference genes, and thus appear to be regulated by an additional mechanism, possibly involving virus-induced activation of the HIF pathway.

5.3 Discussion

This section of work characterises a novel functional interaction between FIH and the Orf virus ARD proteins. Preliminary experiments revealed that members of this family are substrates for FIH *in vitro,* and are capable of binding to FIH with a relatively high affinity. Based on these findings, as well as the known association of the ORFV ARD/F-box proteins with the cellular SCF ubiquitin ligase complex [137], we envisaged several functional outcomes for the interaction between FIH and the ORFV ARD proteins (Figure 5.7), and addressed each of these as separate hypotheses.

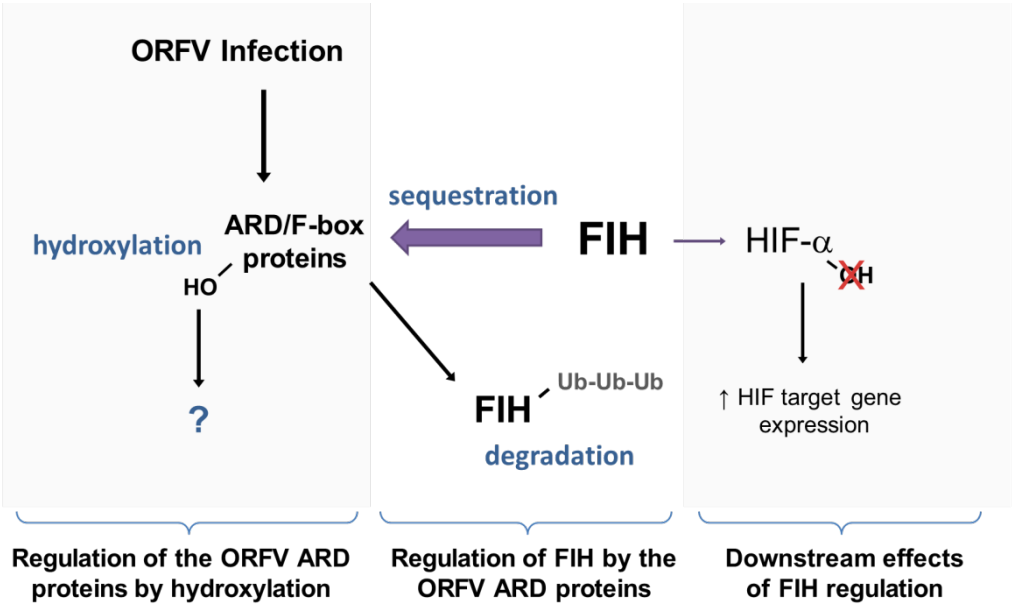

Figure 5.7 Possible outcomes of the FIH/ORFV ARD interaction

The schematic diagram on the previous page illustrates the specific hypotheses addressed in this chapter. Firstly, that FIH regulates the ORFV ARD proteins via hydroxylation. Secondly, that the ORFV ARD proteins in turn regulate FIH, either through sequestration, or by targeting FIH for degradation via the ubiquitin-proteasome pathway. Thirdly, that sequestration or degradation of FIH would limit its availability for hydroxylation of HIF-α, providing a FIH-dependent mechanism for upregulation of the HIF pathway in response to ORFV infection.

5.3.1 Hypothesis 1: FIH regulates the ORFV ARD proteins via hydroxylation

The ORFV ARD proteins are novel substrates for FIH

The first part of this chapter sought to investigate the ORFV ARD proteins as substrates for FIH. The *in vitro* hydroxylation of 008, 123 and 126 was demonstrated by their ability to promote FIH-dependent turnover of 2OG in CO_2 capture assays. Although this assay does not provide a direct measure of hydroxylation, it has been validated previously by mass spectrometry as a reliable method for determining hydroxylation of FIH substrates [58, 94, 100]. As such, these data (presented in Figures 5.2 and 5.3) strongly support the hypothesis that the ORFV ARD/F-box proteins are indeed novel substrates, and provide the first evidence for hydroxylation of a non-metazoan protein by FIH.

Identification of target asparagine residues

The ARDs of 008, 123 and 126 each contain multiple asparagine residues in positions analogous to proven sites of FIH-catalysed hydroxylation in other ARD substrates, a number of which also conform to the consensus substrate motif (Figure 5.8). However, residues outside of the consensus must also be taken into consideration. In particular, the work presented in Chapter 4 of this thesis highlights the importance of the amino acid directly C-terminal (+1) to the target asparagine. This residue, which tends to be small and uncharged, plays an important role in positioning the asparagine within the active site of FIH [136]. Notably, the single candidate hydroxylation site in ORFV 008 (Asn41) has a phenylalanine at this position, which may not be easily accommodated by FIH due to its size. This could explain the low levels of activity generated by the 008 protein in CO_2

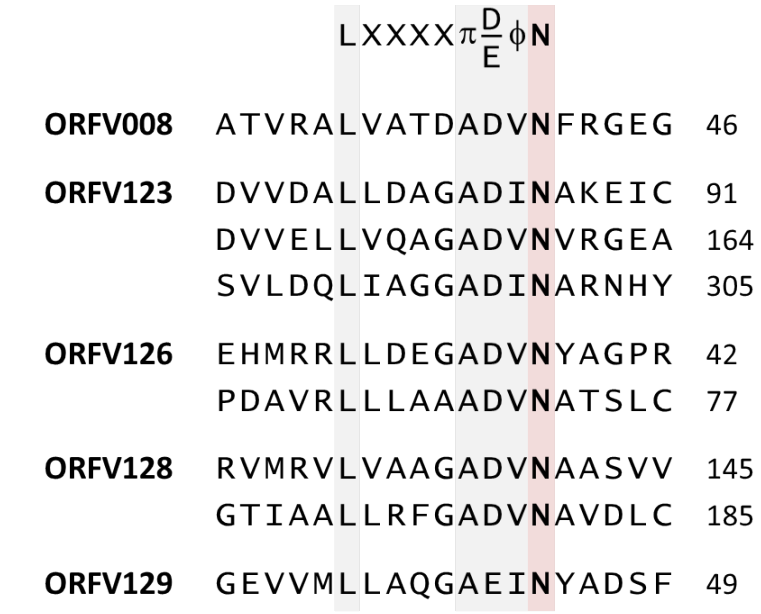

Figure 5.8 Potential hydroxylation sites in ORFV ARD proteins

Alignment of the potential FIH hydroxylation sites in ORFV ARD proteins, which were identified in a bioinformatic search using the substrate consensus motif LXXXXπ(D/E)ϕN. The target asparagine residues are highlighted in pink, whilst other key residues that make up the consensus are highlighted in grey. Numbers to the right indicate relative positions in the amino acid sequences for ORFV ARD proteins.

capture assays. In contrast, the ORFV 123 and 126 proteins each contain multiple sites that are identical in sequence to confirmed sites of hydroxylation in other ARD substrates.

Nonetheless, primary sequence is not the sole determinant of catalysis by FIH. Other factors, such as ankyrin repeat stability, are likely to contribute to determining whether or not a particular site will be hydroxylated [113, 136]. Ultimately, analysis of these proteins by mass spectrometry (MS) will be essential, both to formally demonstrate hydroxylation and to identify the target asparagine residues. These experiments are already underway in our laboratory to confirm the *in vitro* hydroxylation of 008, 123 and 126. To demonstrate hydroxylation in a more physiological context, tagged ARD/F-box proteins will be purified from LT cells following ORFV infection, and subjected to similar MS analysis. It will also be important to determine whether hydroxylation extends to the other two members of the ORFV ARD/F-box protein family (128 and 129), or to poxviral ARD proteins in general.

Contribution of ARD hydroxylation to ORFV infection

Once hydroxylation has been confirmed, and the target Asn residues identified, a key experiment will be to determine the extent to which hydroxylation of the ARD/F-box proteins influences ORFV infection. This would involve infecting cultured LT cells with wildtype ORFV, or a recombinant virus expressing ARD proteins that have been mutated to prevent hydroxylation (i.e. by site-directed mutagenesis of the target asparagine residues), combined with treatment of cells with FIH inhibitors [136, 150]. Virus infection would be monitored by assessment of plaque morphology and analysis of replication kinetics using multi-cycle growth curves [186-188]. *In viv*o analyses could be also performed by infecting sheep and comparing the clinical outcomes of infection (e.g. lesion size and time to resolution) with the wildtype or mutant virus [164].

If FIH-dependent hydroxylation is found to alter the rate or severity of ORFV infection, then further experiments will be carried out to determine the specific effects of hydroxylation on the function of the ARD/F-box proteins. This may require further characterisation of their role in modulating the ubiquitin-proteasome pathway. Whilst all five family members have been shown to interact with functional SCF complexes, protein targets have yet to be identified [137]. Efforts are already underway in the Mercer

laboratory to determine the substrate repertoire of the ORFV ARD/F-box proteins. Once identified, changes to substrate ubiquitylation and degradation can be characterised in the presence and absence of hydroxylation of the ORFV ARD/F-box proteins.

Hydroxylation of ARD proteins in other poxviruses

Given the abundance of ARD proteins expressed by vertebrate poxviruses, and the wide-spread nature of cellular ARD hydroxylation, it seems likely that most species will encode at least one ARD protein with the potential to be hydroxylated by FIH [102, 131]. Although the specific functions of most poxviral ARD proteins have yet to be elucidated, recent studies have indicated that the vast majority contain F-box-like motifs, and are likely to have a general role in regulating the host ubiquitin-proteasome pathway [131, 171]. Hydroxylation could therefore provide a common mechanism by which FIH could modulate the activity of these proteins (i.e. by altering their ability to recruit target proteins to the SCF complex), and in doing so, either contribute to or counteract viral infection. To explore this possibility, the experiments described above for identification of ORFV ARD substrates and investigation of their role in virus infection could be extended to other vertebrate poxviruses. Of particular interest are viruses that are highly prevalent within animal populations and/or zoonotic for humans, such as Cowpox, Monkeypox and Vaccinia [157]. Although nearly all poxviruses contain ARD proteins, the number and sequence of encoded ARD proteins vary. Therefore, the extent to which hydroxylation influences virus infection may also differ between species.

5.3.2 Hypothesis 2: ORFV ARD proteins regulate FIH via degradation or sequestration

Regulation of FIH by sequestration

Having demonstrated that FIH is capable of hydroxylating the ORFV ARD/F-box proteins, we sought to investigate whether the ORFV proteins might in turn be able to regulate FIH. Cellular ARD substrates typically bind FIH with a high affinity, and several (including Notch) can compete with the HIF-1α CAD for hydroxylation when co-expressed in transfected cells [94, 95, 103]. We predicted that this property might extend to the ORFV ARD/F-box proteins, and thus investigated their relative affinities for FIH. In support of

the hypothesis, *in vitro* affinity pulldowns (Figure 5.4) indicate that FIH can interact with the ARDs of 008, 123 and 126 with an affinity that is similar to, if not greater than, the Notch1 ARD. Furthermore, although FIH is normally cytoplasmic [84, 127, 189], transient expression of the ORFV ARD proteins in HeLa cells leads to sequestration of FIH to defined areas of the nucleus, where it co-localises with ORFV 008, 126 and 128 (Andrew Mercer, personal communication). Collectively, these data provide strong evidence for sequestration of FIH by the ORFV ARD proteins.

Regulation of FIH by degradation

Given the ability of the ORFV/ARD proteins to bind FIH, and their putative role in recruiting proteins to the cellular SCF ubiquitin ligase complex, we hypothesised that FIH might be targeted for polyubiquitylation and degradation following ORFV infection. To address this possibility, western blot analyses were employed to compare the relative levels of FIH protein in lysates from ORFV-infected versus uninfected LT cells. Unfortunately, these experiments yielded conflicting results; one experiment showed an obvious reduction in FIH levels by 20 hours post infection, whilst another showed no visible change in FIH levels across infected and uninfected samples (Figure 5.5).

The reason for this discrepancy is unclear. It is possible that the time course of ORFV infection was simply not long enough to observe consistent degradation of FIH. In bovine testes cells, synthesis of ORFV-encoded proteins commences at around 10 hours post infection, but does not reach its peak until 14-16 hours [190]. Consequently, at 20 hours post infection with ORFV, the ARD/F-box proteins may not be expressed at high enough levels in LT cells to cause significant degradation of FIH. If degradation is occurring within this time-frame, the change may be too small to be detected accurately or reproducibly by this method.

To obtain a more definitive result, it will be necessary to repeat these experiments over a longer time-course of ORFV infection, and include replicates. A more quantitative detection method (e.g. fluorescently labelled antibodies, or ECL with quantitative detection rather than autoradiography) could also be used, and may enable more accurate detection of minor changes in protein levels. Additional experiments could be employed to determine whether FIH is a direct substrate for polyubiquitylation by the

cellular SCF ubiquitin ligase complex, and would involve analysis of endogenous FIH (immunoprecipitated from ORFV-infected cells) by SDS-PAGE and immunoblotting with a ubiquitin-specific antibody [137, 191].

F-box proteins typically interact quite transiently with substrate proteins to enable dissociation of the ubiquitylated product and rapid turnover by the proteasome [192]. However, the affinity pulldown assays presented in this thesis demonstrate that FIH forms a relatively stable complex with the ORFV ARD/F-box proteins (Figure 5.4). Subsequent experiments by our collaborators have shown that the interaction is sufficiently robust to enable co-immunoprecipiation of endogenous FIH from 293T cells with transiently transfected full-length ORFV 008, 123 and 126 proteins (Andrew Mercer, personal communication).

A number of other poxvirus ARD/F-box proteins, including myxoma virus M-T5 and M150R, variola virus G1R and cowpox virus CP77, have been shown to engage in specific protein-protein interactions without any evidence for ubiquitination or degradation of the target protein [193-196]. Furthermore, another recently identified substrate for FIH is the mammalian protein ASB4 (ankyrin repeat and SOCS box protein 4), which like the ORFV ARD/F-box proteins, is the substrate recognition component of an E3 ubiquitin ligase complex. Although an endogenous interaction with FIH was demonstrated in 293T cells, ASB4 was found to have no effect on FIH ubiquitination or degradation [99]. Taken together, these data argue against a role for the ORFV ARD proteins in promoting the polyubiquitylation and degradation of FIH during ORFV infection, but support an alternative mechanism of FIH regulation via sequestration, as discussed below.

5.3.3 Hypothesis 3: ORFV activates the HIF pathway via sequestration of FIH

A strong interaction between the ORFV ARD proteins and FIH could lead to competitive inhibition of FIH activity on endogenous substrates. Although this could potentially influence the hydroxylation of a range of FIH substrates, HIF is currently the only substrate for which a clear functional outcome for hydroxylation has been demonstrated. As discussed previously, FIH-catalysed hydroxylation of the HIF CAD is involved in

repressing its transcriptional activity in normoxia [56, 57]. As such, we predicted that sequestration (or degradation) of FIH by the ORFV ARD/F-box proteins would limit the amount of FIH available for hydroxylation of HIF-1α, and lead to upregulation of endogenous HIF target genes.

To investigate this, we analysed the expression of three well-characterised HIF target genes (*VEGF, PHD3* and *GLUT1*) by qPCR in ORFV-infected versus uninfected LT cells. Consistent with our hypothesis, the relative levels of *VEGF* and *PHD3* expression were increased with ORFV infection. *GLUT1* was not induced, although this is not entirely surprising given that only a subset of HIF targets is regulated by FIH, and levels of *Glut1* are not altered in cells lacking endogenous FIH (27). Similar effects on HIF target gene expression were observed following infection of LT cells with Vaccinia virus (Figure 5.6D), suggesting that other poxviruses may employ a similar mechanism of HIF pathway activation.

Interestingly, the qPCR experiments suggest that ORFV may have a global influence on gene expression. Analysis of raw qPCR data (prior to normalisation to a reference gene) revealed that the levels of all analysed transcripts decrease in a time-dependent manner following ORFV-infection, relative to total RNA input (Figure 5.6). A number of other viruses have been shown to inhibit host gene expression through various mechanisms involving degradation of cellular mRNAs [197, 198] or inhibition of cellular mRNA synthesis [199, 200]. Notably, Vaccinia virus encodes two hydrolase enzymes that promote widespread mRNA turnover by de-capping cellular mRNAs and exposing them to exonucleases [201-203], and homologues of these enzymes have been identified in other poxviruses, including ORFV [204].

Regardless of its cause, the apparent global reduction in mRNA expression has important consequences for the interpretation of data from these experiments. Since the mRNA levels of all four reference genes were decreased by ORFV infection, the normalised qPCR data show an increase in the expression of *VEGF* and *PHD3* with ORFV-infection, despite the fact that the absolute levels of mRNA are actually lower in infected samples compared to the uninfected controls. Nevertheless, the data clearly indicate that *VEGF* and *PHD3* are differentially regulated by ORFV infection compared to other transcripts.

Whilst the results imply a global reduction in mRNA levels following ORFV infection, *VEGF* and *PHD3* are affected by this downregulation to a lesser extent, most likely due to increased transcription by HIF. Although these data are preliminary, they provide support for a FIH-dependent mechanism of HIF activation in response to ORFV infection.

These findings raise the possibility of a novel approach for treatment of poxviral infections. Whilst most poxviruses cause relatively benign infections in humans, they are a significant cause of morbidity and mortality in domestic animals, and there is high demand for the development of safe and effective therapeutics [205]. There is already considerable interest in pharmacological modulation of the HIF pathway as a treatment for oncogenic and ischemic disease [206, 207], and given the preliminary evidence for HIF upregulation by poxviruses, HIF antagonists (or FIH agonists) may also provide an effective strategy for treating poxvirus infections. However, before this can be considered, it will be critical to determine the precise involvement of FIH and the HIF pathway in poxvirus infection.

Firstly, it will be important to demonstrate that the observed effects on gene expression are HIF-dependent. This could be achieved using siRNA to knockdown HIF-1α and HIF-2α subunits (either separately or in combination), followed by HIF CAD reporter assays [56, 136], either in ORFV-infected cells, or in cells with transiently over-expressed ORFV ARD/F-box proteins, as this should be sufficient to promote sequestration of FIH. The qPCR experiments could also be extended to include a broader range of HIF target genes, although a more comprehensive analysis of changes in gene expression would be provided by microarray analysis or high throughput sequencing [208]. To definitively demonstrate a role for FIH, HIF activation could be monitored by qPCR in ORFV-infected LT cells treated with siRNA to knockdown endogenous FIH. Alternatively, overexpression of FIH could be performed to saturate the ORFV ARD/F-box proteins and prevent FIH from being sequestered from HIF following ORFV infection.

As discussed previously, a number of viruses activate the HIF pathway via stabilisation of HIF-1α protein and/or increases in transcription. HIF-1α protein levels can also be regulated in an oxygen-independent manner by pro-inflammatory cytokines signalling

through the NFκB, PI3-kinase and ERK/MAP kinase pathways [209-211]. Consequently, we investigated HIF protein levels by western blot, but found no evidence for stabilisation of HIF-1α protein in response to ORFV infection (Figure 5.4), supporting a novel FIH-dependent mechanism of HIF activation. However, it is possible that HIF-1α levels do increase with ORFV infection, but the increased level of HIF-1α protein is still below the limit of detection by western blot. Furthermore, as discussed previously, the antibody used in these experiments (BD biosciences polyclonal) may not have been able to detect sheep HIF-1α. Future experiments should include lysates from hypoxia-treated LT cells as a control for induction of HIF-1α protein, and would benefit from using an alternative antibody that has been validated for detection of sheep HIF-1α [212]. Similar experiments will be also performed to investigate levels of HIF-2α protein in ORFV-infected and uninfected cells.

Given that the major focus of this thesis is FIH substrate specificity with respect to HIF and ARD proteins, the involvement of the HIF pathway in ORFV infection is of particular interest. However, it is likely that sequestration of FIH by the ORFV ARD proteins will have consequences for other substrates in addition to HIF-α. At this stage, HIF is the only FIH substrate for which a clear outcome for hydroxylation has been defined [56, 57]. Nevertheless, it is clear from the phenotype of the $FIH^{-/-}$ mice that FIH is likely to be involved in regulating other cellular pathways [85]. In particular, a key role for FIH in regulation of metabolism has been identified. It is interesting to note that an increase in cellular ATP levels (which occurs in response to knockdown of FIH in MEFs) has also been shown to occur in response to Vaccinia virus infection, and is important for virus replication [213]. Further characterisation of the physiological role of FIH may reveal alternative pathways that could be exploited by viruses to facilitate replication or infection.

Summary and Conclusions

Taken together, this work provides important insights into the molecular mechanisms underlying Orf infection, and the complex strategies employed by viruses to manipulate host-cell pathways. In particular, it reveals a potential FIH-dependent mechanism of cross-talk between the ORFV ARD proteins and the HIF pathway, which may aid virus infection. This mechanism is likely to extend to most vertebrate poxviruses, and possibly other intracellular pathogens encoding proteins with ankyrin repeats. Although much of the data presented here are preliminary, they provide provocative evidence that FIH may have an important role in virus infection, and are worthy of a more intensive investigation.

Final Discussion

FIH targets an extensive family of ankyrin repeat proteins

The work presented in this thesis contributes to a growing body of research that identifies ARD proteins as a novel and extensive class of FIH substrate. With more than 25 ARD substrates already characterised, it appears that FIH-catalysed hydroxylation is common to the majority of ARD proteins within the human proteome [102, 214], and likely extends to a range of ARD proteins encoded by viruses and other intracellular pathogens. The identification of this alternative class of substrate has challenged our understanding of the physiological role of FIH, and raised important questions as to the contribution of ARD hydroxylation to cellular oxygen sensing.

Substrate choice - it's an ARD decision

FIH has a much higher affinity for many of the ARD substrates than it does for HIF, suggesting that ARD proteins are likely to be the preferred class of substrate [94, 95, 100]. At a molecular level, this is mediated by a combination of primary, secondary and tertiary structural elements within the ARD, with important contributions from residues that make contacts outside of the catalytic binding pocket [136]. Notably, the magnitude of this difference in affinity is lessened *in vivo* by the presence of the RLL motif in the HIF-α CAD. The requirement of this motif for normoxic repression of the CAD by FIH likely reflects its ability to promote a higher-affinity interaction with FIH in the crowded environment of a cell, thus reducing competition from ARD substrates [136].

FIH has recently been reported to engage in high-affinity interactions with two other proteins, Mint3 and matrix metalloproteinase-14 (MMP14), neither of which contains an ARD or any sequence resembling a hydroxylation motif. The affinity is sufficiently robust to enable both proteins to competitively inhibit hydroxylation of HIF-1α, both *in vitro* and in mammalian cells. The *in vitro* result is of particular interest, as it suggests that these proteins do not require molecular crowding to promote a high-affinity interaction with FIH, and may therefore bind in a manner that is more similar to ARD proteins than HIF. The specific interaction sites have not yet been identified, but may provide important insights into recognition by FIH.

Structural preference for FIH substrates

Whilst FIH displays a strong binding affinity for the intact ankyrin fold, this conformation is not permissive to hydroxylation, and transient unfolding must occur to enable catalysis [95, 113, 136]. In contrast, the HIF CAD lacks any discernible structure in the absence of FIH, but adopts several ankyrin-like features in the transition state, including a helix C-terminal to the target asparagine [60, 61, 116]. Overall, it seems that the most favourable conformation for substrate recognition by FIH would involve a compromise between flexibility and a stable ankyrin fold. This complicates the prediction of new substrates based on specific structural features, as recognition by FIH may depend less heavily on the native conformation of the substrate, and more-so on its ability to adapt to fit the active site, which is likely to involve at least some degree of conformational flexibility.

Specific recognition and regulation of HIF and ARD substrates

An important consequence of structural differences between HIF and ARD substrates is that it enables their hydroxylation by FIH to be differentially regulated in a cellular context. Cells could take advantage of differences in recognition, for example, by expressing factors capable of binding to and masking the RLL motif in the HIF-α CAD, thus specifically preventing FIH from interacting with HIF without altering its ability to bind ARD proteins. This could provide an alternative mechanism for activation of the HIF pathway that is not dependent on cellular oxygen concentration. Given the importance of the HIF pathway in normal physiology and disease, it seems likely that the cell would employ additional mechanisms to ensure its activity is tightly regulated. Similar mechanisms could also be employed to specifically regulate hydroxylation of ARD proteins, although the functional consequences of this are unclear at this stage.

Contribution of ARD proteins to oxygen sensing

Although a clear outcome for ARD hydroxylation has not yet been demonstrated, it is possible that it does have a defined signalling output in specific cases. As such, a few select ARD substrates may be directly involved in mediating cellular responses to hypoxia. In support of this possibility, recent work by our laboratory has identified a potential role for FIH in regulating members of the TRP (transient receptor potential) family of ion channels. FIH hydroxylates ankyrin repeats in several TRP channels of the vanilloid (TRPV)

subfamily ([215], Sarah Linke, personal communication), and it appears that both binding and hydroxylation by FIH have consequences for TRPV-channel activity. This discovery is particularly interesting given the key role of oxygen-sensitive ion channels in mediating acute responses to hypoxia [216].

Nevertheless, it seems unlikely that ARD hydroxylation will function in a switch-like manner in response to hypoxia, as is observed with hydroxylation of the HIF-α CAD. As FIH-catalysed hydroxylation does not appear to be reversible [154], loss of hydroxylation under hypoxic conditions will be largely dependent on the rate of product turnover. HIF-α protein has an extremely short half-life in normoxia (~5 mins) due to efficient hydroxylation by the PHDs, which allows for rapid accumulation of non-hydroxylated protein in hypoxia. However, most cellular proteins have much longer half-lives [217], and thus, loss of hydroxylation would be predicted to occur gradually over time during hypoxia. A recent study has shown this to be the case for Notch and Rabankyrin [154]. Even so, it is possible that this is not the case for all ARD substrates, some of which may be regulated by hypoxia in a similar manner to HIF.

Whilst the longer half-life of some ARD proteins argues against a global role for ARD hydroxylation in mediating rapid cellular responses to hypoxia, it may be of significance with regard to the changes in cellular physiology that occur in response to re-oxygenation, especially following periods of prolonged hypoxia where the hydroxylated ARD pool would be considerably depleted. Firstly, the proportion of the ARD pool that is still hydroxylated upon re-oxygenation may provide a 'memory' of the severity or duration of the preceding hypoxic episode.

Furthermore, the higher affinity that ARD proteins display for FIH in their non-hydroxylated state suggests that they will be hydroxylated preferentially by FIH upon re-oxygenation, which could have consequences for the function of specific ARD substrates. Notably, the inflammatory response to reperfusion of ischemic tissue is mediated in part by the NFκB signalling pathway [218], several members of which have been identified as substrates for FIH [86]. As such, it may be interesting to investigate the influence of FIH on re-oxygenation induced NFκB activity in endothelial cells. Oxygen levels also influence

the differentiation of stem and progenitor cell populations during development, although the lack of any apparent developmental defects in the FIH knockout mice argue against an essential role for FIH in regulating this process [219].

Regulation of HIF signalling by the ARD-FIH interaction

As described in detail in section 3.3.4, the presence of numerous ARD proteins within a cell, and their hydroxylation by FIH, is hypothesised to fine-tune the HIF response by regulating the availability of FIH for hydroxylation of HIF-α [95]. In particular, competition from the ARD pool is predicted to introduce an oxygen threshold, below which HIF-α is not efficiently hydroxylated and thus CAD-dependent gene expression is activated [214]. Given that the hydroxylation status of an ARD strongly influences its ability to bind and sequester FIH, the exact oxygen concentration that provides this threshold for CAD regulation will be determined by the number of accessible hydroxylation sites in ARD proteins, their relative affinity for FIH, and the overall oxygen sensitivity of the ARD pool. This highly complex regulatory mechanism would therefore be dependent on the specific repertoire of ARD proteins expressed by a particular cell at any given time. Since this is likely to vary considerably between different cell types and at different stages of development, it may well contribute to cell-specific differences in HIF regulation [126].

Another potential consequence of this mechanism of HIF regulation is that it enables cross-talk between HIF signalling and events/pathways that alter cellular levels of ARD proteins. For example, activation of Notch signalling in 293T cells has been found to increase recruitment of HIF-1 to target promoters (without altering HIF-α protein levels), leading to activation of CAD-regulated genes in normoxia [94, 108]. This is thought to be due to enhanced sequestration of FIH by the Notch ICD. The work presented in this thesis support a similar mechanism of HIF upregulation by the Orf virus ARD proteins in response to virus infection.

Given the diverse range of signalling pathways that regulate or are mediated by ARD proteins, the consequences of this cross-talk could be wide-spread, enabling the HIF pathway to contribute to a broad range of cellular processes, independent of hypoxia. These modes of cross-talk may be particularly significant in physiological or pathological situations where HIF-α is stabilised in normoxia, such as in Von Hippel Lindau (VHL)

disease [220-222], or in response to growth factors/cytokines signalling through the PI3K/Akt pathway [223-225].

Sequestration of FIH by ARD proteins also has the potential to alter its subcellular localisation. Although FIH is normally expressed predominantly within the cytoplasm of cells [127, 189], nuclear translocation of FIH has been observed in response to transient expression of the Notch1 ICD, and several of the ORFV ARD proteins [94]. Since ankyrin repeats have been proposed to function as an atypical nuclear localisation signal [226], this property may extend to a number of other ARD proteins that bind FIH with a suitably high affinity. This is particularly interesting in light of recent reports that the subcellular localisation of FIH correlates with disease prognosis in several types of cancer, including breast cancer [227, 228], pancreatic endocrine tumors [229] and clear cell renal cell carcinoma [230]. As such, further characterisation of ARD-FIH interactions may provide new avenues for the development of novel cancer therapeutics.

Which class of FIH substrate is more important?

The ambiguity surrounding the phenotype of the FIH knockout mouse raises important questions as to which of the two classes of substrate (HIF-α / ARD proteins) accounts for the majority of FIH's physiological function. From an evolutionary perspective, the absence of a functional homologue of FIH in animals lacking a HIF-α CAD suggests that retention of FIH is driven by a strong requirement for HIF-CAD regulation [231, 232]. Indeed, the role of FIH in repressing HIF transactivation in normoxia is clearly important, and is the only defined outcome for FIH-catalysed hydroxylation to date. As such, it is tempting to assume that HIF is its primary target, and that ARD hydroxylation merely contributes to HIF regulation (as described above). However, our current understanding of ARD hydroxylation remains relatively limited, and further research into this novel class of substrate is required before any definitive conclusions can be drawn.

Insights from the FIH knockout mouse

The $FIH^{-/-}$ knockout mouse phenotype revealed an unanticipated role for FIH as a key regulator of metabolism [85]. As described in section 1.1.9, $FIH^{-/-}$ mice display multiple symptoms of hypermetabolism, very few of which are consistent with the expected metabolic effects of HIF activation *in vivo*. These point to a potential role for alternative substrates such as ARD proteins in contributing to the phenotype.

ARD proteins have been implicated in multiple aspects of metabolism, ranging from control of insulin sensitivity, to glucose and fatty acid oxidation [233-239]. Interestingly, the $FIH^{-/-}$ phenotype bears striking resemblance to the phenotype of transgenic mice over-expressing ASB4 (an ARD substrate for FIH) in pro-opiomelanocortin (POMC) neurons of the arcuate nucleus, a region of the hypothalamus responsible for the control of appetite and metabolism [240]. Similar to $FIH^{-/-}$ mice, the ASB4 transgenic mice displayed increased food consumption accompanied by an elevated metabolic rate, but were resistant to high-fat-diet-induced obesity.

The strong similarity between the two phenotypes is particularly interesting in light of the observation that a neural-specific knockout of FIH can recapitulate some of the major metabolic phenotypes of the global null animals [85], which suggests that FIH functions largely through the central nervous system to regulate metabolism. It could be interesting to look for differences in ASB4 activity in $FIH^{-/-}$ mice, or to see whether over-expression of FIH within the hypothalamus (for example, using a lentiviral system for gene delivery of FIH under the control of a hypothalamus-specific promoter) is able to reverse the metabolic phenotype of the ASB4 transgenic mice.

Despite the lack of classical HIF responses in the FIH null mice, the possibility that HIF activation is responsible for some aspects of the hypermetabolic phenotype cannot be ruled out; there could well be overlapping contributions from both HIF and ARD substrates. In a recent study by Zhang et al. (2011), over-expression of HIF-1α or HIF-2α (in combination with ARNT) in the hypothalamus of C57BL/6 mice was found to confer resistance to high-fat-diet-induced obesity, one of the major symptoms of metabolic alteration exhibited by the $FIH^{-/-}$ mice. Nevertheless, other effects of this gain-of-function were not described, and the mechanism behind the observed metabolic effects was not

elucidated. Thus, it may well involve processes such as glycolysis that were not upregulated in the FIH$^{-/-}$ mice.

Interpreting the FIH$^{-/-}$ mouse phenotype

In order to determine the relative importance and contribution of HIF and ARD substrates to the physiological role of FIH, it may be beneficial to generate variants of FIH with altered substrate recognition capabilities (e.g. able to hydroxylate one class of substrate but not the other). Such mutants could be expressed in FIH$^{-/-}$ MEFs, or used to generate a 'knock-in' mouse, and would be extremely valuable in discerning the HIF-specific effects of FIH-catalysed hydroxylation from those that are dependent on ARD substrates (although these may overlap to some extent).

This may be difficult to achieve using a directed approach, as the particular residues in FIH that contribute to substrate-specific recognition have not been defined. Nevertheless, work by Briony Davenport from our laboratory has identified a functional homologue of FIH in the red flour beetle (*Tribolium Castanium*) that is capable of hydroxylating mammalian ARD substrates, but not the HIF-α CAD. Investigation of key sequence differences between the beetle and human orthologues of FIH may provide crucial insights into the specificity of substrate recognition, and facilitate the design of FIH mutants that would be useful in these experiments. Of course, the results would need to be interpreted with caution. It would be somewhat narrow minded to assume that HIF and ARD proteins constitute the only cellular substrates for FIH. Even so, these experiments would still be extremely valuable in deciphering the different cellular roles of FIH.

Therapeutic Targeting of FIH

The central role of FIH and the PHDs as oxygen sensors and key regulators of the HIF pathway have made them attractive targets for therapeutic manipulation (reviewed in [206, 241]). Inhibition of the HIF hydroxylases is predicted to promote red-blood cell growth and tissue vascularisation (via activation of HIF target genes such as *EPO* and *VEGF*), which may be useful for treatment of anaemia and ischemic disease, respectively. Several PHD inhibitors are already in stage 2 clinical trials for the treatment of anaemia

[242], and there is considerable interest in developing specific inhibitors for FIH. Given that FIH and the PHDs influence different subsets of HIF target genes [83], pharmacological inhibition of both may lead to a more robust response. Conversely, elevated HIF expression is a hallmark of many solid tumors, and is often associated with an aggressive tumor phenotype [243, 244]. As such, hydroxylase agonists are sought to reduce HIF-mediated tumor vascularisation [245].

Although the function of ARD hydroxylation is not clear, this extensive class of substrate must be taken into consideration in the design of small molecules directed toward FIH, not only because of the potential for wide-ranging off-target effects, but because the FIH-ARD interaction itself is a promising target for modulation of the HIF pathway. Molecules that specifically disrupt the interaction between ARD proteins and FIH are predicted to increase HIF CAD hydroxylation, and may be useful both as cancer therapeutics, and as an anti-viral for treating poxvirus infections. In contrast, stabilisation of the ARD-FIH interaction should lead to sequestration of FIH and activation of the HIF pathway.

Given the lack of classical HIF effects such as angiogenesis or erythropoiesis in the $FIH^{-/-}$ mice [85], targeting FIH to treat anaemia or ischemic disease is unlikely to be as effective as inhibition of the PHDs, or direct activation of HIF with specific agonists. Nevertheless, the increased glucose tolerance and insulin sensitivity of the knockout mice suggest that FIH antagonists may provide novel therapeutics for treatment of metabolic diseases such as clinical obesity or type 2 diabetes. Since it is unclear which class of FIH substrate is predominantly responsible for its metabolic effects, a general FIH inhibitor that targets both would be ideal.

Ultimately, identification of the full array of substrates and an intricate understanding of their recognition and modification by FIH will be essential to predict and interpret the functional consequences of specific FIH agonists or antagonists.

In conclusion, the work presented in this thesis demonstrates marked differences in the catalytic properties of FIH with HIF and ARD substrates. The robust nature of the FIH-ARD interaction is likely to have important consequences for ARD function, as well as HIF pathway regulation. Investigation of the molecular determinants of substrate recognition has identified specific structural features in HIF and ARD substrates that are recognised differentially by FIH. These likely enable FIH to discriminate between its substrates in a cellular context, but may also provide novel avenues for the design of small-molecules for therapeutic targeting of FIH in ischemic, oncogenic and metabolic disease. This work also identifies a potential role for FIH in poxviral infections, via hydroxylation of viral ARD proteins, or through a novel FIH-dependent mechanism of HIF activation.

Together this body of work provides several novel and important insights into the recognition and hydroxylation of ARD proteins by FIH, and potential mechanisms of cross-talk between this alternative class of substrate and the HIF pathway. These data further our understanding of the role of FIH as an oxygen sensor, its involvement in normal physiology and disease, its potential for manipulation, and the possible benefits and consequences of therapeutic targeting.

Appendices

Appendix 1 - Wilkins *et al.* (2009)

ELSEVIER LICENSE
TERMS AND CONDITIONS

This is a License Agreement between Sarah E Wilkins ("You") and Elsevier ("Elsevier") provided by Copyright Clearance Center ("CCC"). The license consists of your order details, the terms and conditions provided by Elsevier, and the payment terms and conditions.

Supplier	Elsevier Limited The Boulevard,Langford Lane Kidlington,Oxford,OX5 1GB,UK
Registered Company Number	1982084
Customer name	Sarah E Wilkins
Customer address	Molecular Life Science Building University of Adelaide, SA, Australia 5005
License number	2850480399660
License date	Feb 15, 2012
Licensed content publisher	Elsevier
Licensed content publication	The International Journal of Biochemistry & Cell Biology
Licensed content title	Differences in hydroxylation and binding of Notch and HIF-1α demonstrate substrate selectivity for factor inhibiting HIF-1 (FIH-1)
Licensed content author	Sarah E. Wilkins, Jaana Hyvärinen, Johana Chicher, Jeffrey J. Gorman, Daniel J. Peet, Rebecca L. Bilton, Peppi Koivunen
Licensed content date	July 2009
Licensed content volume number	41
Licensed content issue number	7
Number of pages	9
Start Page	1563
End Page	1571
Type of Use	reuse in a thesis/dissertation
Portion	full article
Format	both print and electronic
Are you the author of this Elsevier article?	Yes

The International Journal of Biochemistry & Cell Biology 41 (2009) 1563–1571

Contents lists available at ScienceDirect

The International Journal of Biochemistry & Cell Biology

journal homepage: www.elsevier.com/locate/biocel

Differences in hydroxylation and binding of Notch and HIF-1α demonstrate substrate selectivity for factor inhibiting HIF-1 (FIH-1)

Sarah E. Wilkins[a,1], Jaana Hyvärinen[b,1], Johana Chicher[c], Jeffrey J. Gorman[c], Daniel J. Peet[a], Rebecca L. Bilton[a,1], Peppi Koivunen[b,*,1]

[a] School of Molecular and Biomedical Science and the Australian Research Council Special Research Centre for the Molecular Genetics of Development, University of Adelaide, Adelaide, SA 5005, Australia
[b] Oulu Centre for Cell-Matrix Research, Biocenter Oulu and Department of Medical Biochemistry and Molecular Biology, University of Oulu, FIN-90014 Oulu, Finland
[c] Protein Discovery Centre, Queensland Institute of Medical Research, PO Royal Brisbane Hospital, QLD, 4029 Australia

ARTICLE INFO

Article history:
Received 6 November 2008
Received in revised form 8 January 2009
Accepted 12 January 2009
Available online 20 January 2009

Keywords:
FIH-1
HIF
Hydroxylation
Notch
Oxygen

ABSTRACT

FIH-1, factor inhibiting hypoxia-inducible factor-1 (HIF-1), regulates oxygen sensing by hydroxylating an asparagine within HIF-α. It also hydroxylates asparagines in many proteins containing ankyrin repeats, including Notch1–3, p105 and IκBα. Relative binding affinity and hydroxylation rate are crucial determinants of substrate selection and modification. We determined the contributions of substrate sequence composition and length and of oxygen concentration to the FIH-1-binding and/or hydroxylation of Notch1–4 and compared them with those for HIF-1α. We also demonstrated hydroxylation of two asparagines in Notch2 and 3, corresponding to Sites 1 and 2 of Notch1, by mass spectrometry for the first time.

Our data demonstrate that substrate length has a much greater influence on FIH-1-dependent hydroxylation of Notch than of HIF-1α, predominantly through binding affinity rather than maximal reaction velocity. The K_m value of FIH-1 for Notch1, <0.2 μM, is at least 250-fold lower than that of 50 μM for HIF-1α. Site 1 of Notch1–3 appeared the preferred site of FIH-1 hydroxylation in these substrates. Interestingly, binding of Notch4 to FIH-1 was observed with an affinity almost 10-fold lower than for Notch1–3, but no hydroxylation was detected. Importantly, we demonstrate that the K_m of FIH-1 for oxygen at the preferred Site 1 of Notch1–3, 10–19 μM, is an order of magnitude lower than that for Site 2 or HIF-1α. Hence, at least during *in vitro* hydroxylation, Notch is likely to become efficiently hydroxylated by FIH-1 even under relatively severe hypoxic conditions, where HIF-1α hydroxylation would be reduced.

© 2009 Elsevier Ltd. All rights reserved.

1. Introduction

Factor inhibiting HIF-1 (FIH-1) hydroxylates a specific asparagine in the C-terminal trans-activation domain (C-TAD) of the hypoxia-inducible factor (HIF) α-subunits (Mahon et al., 2001; Lando et al., 2002a; Hewitson et al., 2002). This hydroxylation is oxygen-dependent, as FIH-1 requires molecular dioxygen in addition to Fe^{2+}, 2-oxoglutarate and ascorbate (Lando et al., 2002a,b; Hewitson et al., 2002; Koivunen et al., 2004). The resulting hydroxy-asparagine prevents binding of the transcriptional co-activator CBP/p300 to the HIF-α subunit (HIF-α) and inhibits transcriptional activation of HIF target-genes involved in angiogenesis, vascularisation and anaerobic energy production (Lando et al., 2002b; Ratcliffe and Kaelin, 2008; Myllyharju and Kivirikko, 2004). HIF-α is also regulated by oxygen-dependent prolyl hydroxylation mediated by three HIF prolyl 4-hydroxylases (HIF-P4Hs 1–3) which, like FIH-1 and the collagen prolyl 4-hydroxylases (P4Hs), belong to a group of 2-oxoglutarate-dependent dioxygenases which share the same cofactors (for reviews, see Ratcliffe and Kaelin, 2008; Myllyharju and Kivirikko, 2004). The hydroxylation of two prolines in the oxygen-dependent degradation domain (ODDD) of HIF-α leads to polyubiquitylation and degradation (Epstein et al., 2001; Bruick and McKnight, 2001; Ivan et al., 2001, 2002; Jaakkola et al., 2001) Thus, HIF-α is both rapidly degraded and transcriptionally repressed in normoxia, but stabilised and active in hypoxia, when oxygen-dependent hydroxylation is inhibited.

We previously reported that FIH-1 has unique catalytic and inhibitory properties (Koivunen et al., 2004, 2006, 2007; Linke et al., 2004; Hirsilä et al., 2003). It also requires a relatively long

Abbreviations: ANK, ankyrin repeat domain; C-TAD, C-terminal trans-activation domain; FIH-1, factor inhibiting HIF-1; FP, fluorescence polarisation; h, human; HIF, hypoxia-inducible factor; HIF-α, hypoxia-inducible factor α subunit; HIF-P4H, HIF prolyl 4-hydroxylase; ODDD, oxygen-dependent degradation domain; m, mouse; P4H, prolyl 4-hydroxylase; SD, standard deviation.

* Corresponding author. Tel.: +358 8 5375822; fax: +358 8 5375811.
E-mail address: Peppi.Koivunen@oulu.fi (P. Koivunen).

[1] These authors contributed equally to the work.

1357-2725/$ – see front matter © 2009 Elsevier Ltd. All rights reserved.
doi:10.1016/j.biocel.2009.01.005

substrate for efficient hydroxylation of the HIF-1α subunit by comparison with the HIF-P4Hs. Thus the K_m of a 35-residue HIF-1α peptide for FIH-1 was 100 μM, whereas the HIF-P4Hs have at least 10-fold higher affinity, given that the K_m for a 19-residue peptide was 5–10 μM (Koivunen et al., 2004, 2006; Hirsilä et al., 2003). In contrast, FIH-1 has a higher affinity for oxygen than the HIF-P4Hs, with a K_m value of 90 μM compared with 230–250 μM for the latter when using synthetic peptides as substrates (Koivunen et al., 2004; Hirsilä et al., 2003). Interestingly, both the oxygen sensitivity of the HIF-P4Hs and their substrate affinity increased with substrate length (Koivunen et al., 2006), likely due to inclusion of residues important for recognition.

Hydroxylation of asparagines by FIH-1 has been demonstrated in two proteins containing ankyrin repeat domains (ANKs), p105 and IκBα; although no clear function has been identified for this hydroxylation (Cockman et al., 2006). Likewise, *in vitro* hydroxylation of peptide sequences from ANK-containing proteins gankyrin, myosin phosphatase target subunit, myotrophin, fetal globin-inducing factor and tankyrase-1 has been demonstrated (Cockman et al., 2006). It has recently been reported that FIH-1 hydroxylates two asparagines within the ANKs of Notch1, at Sites 1 and 2 (Coleman et al., 2007; Zheng et al., 2008). These residues are important for Notch-mediated transcriptional activation and its role in neurogenesis and myogenesis. FIH-1 negatively regulates Notch activity during myogenesis, promoting differentiation (Zheng et al., 2008), although its specific role remains unclear. Furthermore, FIH-1 has been implicated in cross-talk between the hypoxia and Notch signalling pathways (Coleman et al., 2007; Zheng et al., 2008).

ANK comprises a conserved motif, often between 1 and 7 tandem repeats of 33-residues containing two anti-parallel α-helices separated by a short loop and followed by a longer, β-hairpin-like loop which connects each tandem repeat (for reviews, see Mosavi et al., 2004; Li et al., 2006). The asparagines targeted by FIH-1 lie within these loops and are semi-conserved within the ANK consensus sequence (Cockman et al., 2006; Coleman et al., 2007; Zheng et al., 2008; Mosavi et al., 2004). A unifying trait of ANKs is that they typically play a role in mediating protein–protein interactions, although the proteins they are found in are involved in diverse processes including cell adhesion, cell cycle regulation, transcriptional regulation, cytoskeletal organization, tumour suppression, cell development and differentiation (Mosavi et al., 2004; Li et al., 2006; Bray, 2006).

The ANK structure is distinct from that of the unstructured HIF-α C-TAD (Freedman et al., 2002; Dames et al., 2002), illustrating the accommodating nature of FIH-1, although peptides of both substrates adopt extremely similar conformations upon FIH-1 binding (Coleman et al., 2007). Interestingly, not all ANK proteins are substrates. For example, mouse (m) Notch4 possesses an asparagine at the corresponding Site 1 of mNotch1–3 (Fig. 1), but it does not conform to the FIH-1 target consensus sequence $L^{-8}(D/E)^{-2}X^{-1}N$ and does not appear to be hydroxylated by FIH-1 *in vitro* (Coleman et al., 2007; Zheng et al., 2008). It is likely, however, that many ANK proteins are FIH-1 substrates, and the question remains as to what role their hydroxylation plays and how it is regulated.

One proposed function for the ANK substrates is that they sequester FIH-1 and thus increase HIF-α transcriptional activity by reducing its asparagine hydroxylation (Coleman et al., 2007). Furthermore, as FIH-1 has an order of magnitude lower affinity for Notch after it is hydroxylated, the hydroxylation status adds another level of oxygen-dependent complexity to the modulation of HIF-α signalling (Coleman et al., 2007; Zheng et al., 2008). The hydroxylation status of Notch, and hence its ability to sequester FIH-1 from HIF-α, is dependent on the relative sensitivity of FIH-1 activity to changes in oxygen for each substrate. Although the K_m of FIH-1 for oxygen has been reported for HIF-1α (Koivunen et al., 2004), it has not been reported for Notch or any ANK substrate.

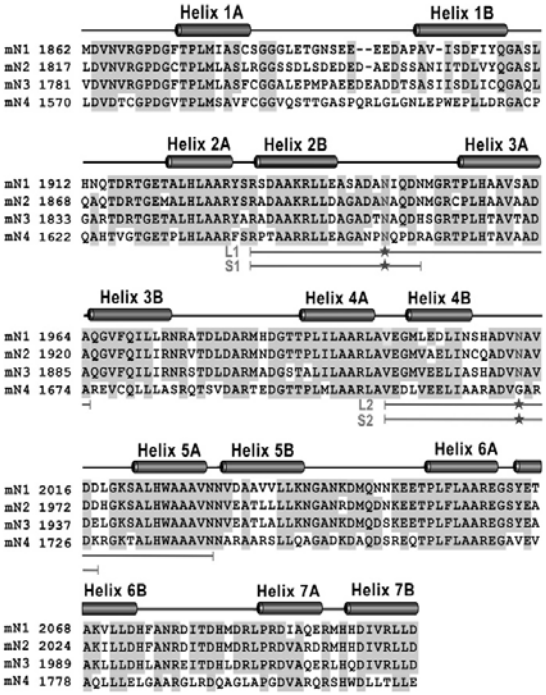

Fig. 1. Amino acid sequence alignment of mouse full-length ankyrin repeat domains (ANKs) by ClustalW. mNotch1–4 ANK1-7 (mN1–4) (NP_032740, NP_035058, NP_032742, NP_035059) include Sites 1 and 2 of asparaginyl hydroxylation by FIH-1. Conserved residues are highlighted. Numbers indicate relative amino acid positions. Barrels indicate the positions of helices based on the human Notch1 structure (Ehebauer et al., 2005). Bars indicate the positions of the long peptides (L1 and L2) for mNotch1–3 and the short peptides (S1 and S2) for mNotch1 at both hydroxylation sites. Stars indicate the position of the hydroxylated asparagines. Hydroxylation of the mNotch1 N1945 and N2012 by hFIH-1 has been confirmed by mass spectrometry (Coleman et al., 2007; Zheng et al., 2008). Notch4 did not serve as a substrate in the previously reported *in vitro* hydroxylation assays, even though it contains an asparagine at the equivalent Site 1 (Coleman et al., 2007; Zheng et al., 2008).

Given the large number of potential substrates within any cell, the relative affinity of FIH-1 for each substrate and the hydroxylation efficiency will be crucial determinants of substrate selection and modification. This is particularly important given the contribution of hypoxia to numerous diseases and to therapeutic targeting of the HIF hydroxylases. Furthermore, given that there are constantly changing oxygen gradients within cells and tissues, determination of the K_m values of FIH-1 for oxygen with different substrates will help decipher how FIH-1 differentially hydroxylates multiple substrates within a cell.

We report here on the kinetic parameters of FIH-1-mediated hydroxylation of Notch and compare them with those for HIF-1α. Specifically, substrate sequence composition and length, and, crucially, oxygen concentration were investigated to determine their contribution to FIH-1-binding and hydroxylation of Notch1–4, and the hydroxylation sites for Notch2 and 3 were determined by mass spectrometry.

2. Materials and methods

2.1. Notch1–4 and HIF-1α (poly)peptide substrates

Sequences of the synthetic peptides representing the asparaginyl hydroxylation sites in mNotch1–3 (Sites 1 and

Table 1
Amino acid sequences of the synthetic peptides.

Substrate	Peptide	Sequence
mNotch1	S1: N1945	RSDAAKRLLEASADANIQDN
	L1: N1945	RSDAAKRLLEASADANIQDNMGRTPLHAAVSADA
	L1: N1945A	RSDAAKRLLEASADAAIQDNMGRTPLHAAVSADA
	S2: N2012	VEGMLEDLINSHADVNAVDD
	L2: N2012	VEGMLEDLINSHADVNAVDDLGKSALHWAAAVN
	L2: N2012A	VEGMLEDLINSHADVAAVDDLGKSALHWAAAVN
mNotch2	L1: N1902	RADAAKRLLDAGADANAQDNMGRCPLHAAVAADA
	L2: N1969	VEGMVAELINCQADVNAVDDHGKSALHWAAAVN
mNotch3	L1: N1867	RADAAKRLLDAGADTNAQDHSGRTPLHTAVTADA
	L2: N1934	VEGMVEELIASHADVNAVDELGKSALHWAAAVN
hHIF-1α	S: N803	DESGLPQLTSYDCEVNAPI
	L: N803	DESGLPQLTSYDCEVNAPIQGSRNLLQGEELLRALDQVN
	L: N803A	DESGLPQLTSYDCEVAAPIQGSRNLLQGEELLRALDQVN
	DES35[a]	DESGLPQLTSYDCEVNAPIQGSRNLLQGEELLRAL

The asparagines to be hydroxylated are underlined in the amino acid sequences.
[a] Characterised by Koivunen et al. (2004).

2) and human (h)HIF-1α (Auspep or Innovagen) are listed in Table 1.

Plasmids coding for thioredoxin (Trx)-6His-tagged mNotch1–4 ANK1–7 have been generated previously (Zheng et al., 2008). Mutations of mNotch2 (N1902A, N1969A) and mNotch3 (N1867A, N1934A) and double mutants were generated in a similar fashion to mNotch1 (N1945A, N2012A) described previously (Zheng et al., 2008). A cDNA fragment encoding residues 356–826 of the hHIF-1α ODDD/C-TAD was generated by PCR with primers 5′-GCGCATATGCAAACAGAATGTGTCCTTAAACCGG-3′ and 5′-GCGCTCGAGGTTAACTTGATCCAAAGCTCTGAG-3′. The His-tags of the mNotch1–4 ANK1–7 and hHIF-1α ODDD/C-TAD polypeptides were exploited in their purification by nickel affinity chromatography (Linke et al., 2007). Recombinant polypeptide concentrations were calculated using their extinction coefficients and absorbance at 280 nm or by RotiQuant (Roth), and purity was assessed by densitometry of Coomassie-stained SDS/PAGE gels.

2.2. Expression and purification of recombinant FIH-1

Expression and purification of the maltose binding protein MBP-hFIH-1 from *Escherichia coli* and hFIH-1-FLAGHis from insect cells has been described earlier (Lando et al., 2002a; Koivunen et al., 2004).

2.3. FIH-1 activity assays

hFIH-1 activity was assayed by a method based on the hydroxylation-coupled decarboxylation of 2-oxo[1-^{14}C]glutarate (Koivunen et al., 2004; Linke et al., 2007).

2.4. Fluorescence polarisation (FP) competition binding assay

Fluorescein-labelled peptide mNotch1 L1:N1945 (Auspep) (400 nM) was used as a tracer in FP competition assays in 150 mM NaCl, 20 mM Tris pH 8.0, with MBP-hFIH-1 (5 μM) and various concentrations of each polypeptide. Unpaired, two-tailed Student's *t*-tests were performed using the data for Notch1 as a reference.

2.5. Mass spectrometry

In vitro hydroxylation of mNotch2 and 3 ANK1–7 in the presence or absence of FIH-1, subsequent separation of the protein by SDS-PAGE, in-gel tryptic digestion, robotic spotting onto MALDI targets and analysis by nanoHPLC-MALDI-TOF/TOF-MS and -MS/MS and nanoHPLC-ESI-LQT-Orbitrap-FTMS and -MS/MS experiments were performed as for those described previously for Notch1 (Zheng et al., 2008).

3. Results and discussion

3.1. Hydroxylation of Notch1 and HIF-1α substrates by FIH-1 is differentially influenced by peptide substrate length

To characterise the FIH-1-mediated hydroxylation of the Notch substrates, short (S1 and S2) and long (L1 and L2) peptides encompassing the Notch1 Site 1 and Site 2 asparagines were synthesised (Fig. 1, Table 1). Peptides of similar length for HIF-1α were generated for comparison, and asparagine-to-alanine mutants of all the long peptides were employed as negative controls (Table 1). The K_m values, reflecting FIH-1 affinity, and the relative V_{max} values were determined as previously described (Koivunen et al., 2004).

FIH-1 was found to have a similar affinity for both short peptide substrates, with K_m values of 110 μM for both Notch1 S1 and S2 peptides, compared with 120 μM for the HIF-1α peptide (Table 2). Given that length is known to influence the affinity of HIF-1α peptide interaction with both the FIH-1 and HIF-P4H enzymes (Koivunen et al., 2004, 2006), we investigated whether this phenomenon was common to other FIH-1 substrates. Increasing the substrate length reduced the K_m over 150-fold to 0.7 μM for the Notch1 Site 1 L1 peptide, while the K_m for Site 2 L2 decreased about 10-fold to 13 μM (Table 2). In comparison, a similar increase in length for the HIF-1α peptide only improved the binding efficiency 2-fold, reducing K_m from 120 to 50 μM (Table 2). Thus, increased length led to a dramatic improvement in the affinity of FIH-1 for binding the Notch peptides, as with HIF-P4Hs and HIF-α (Koivunen et al., 2006), while it had much less influence on the ability of FIH-1 to bind the HIF peptide. The longer peptides, which presumably enable additional interactions beyond the catalytic binding pocket, result in FIH-1 displaying a significantly lower K_m for the Notch substrates than for the HIF-1α C-TAD.

The V_{max} values of FIH-1 for the short Notch1 peptides were less than 10% of the reference HIF-1α DES35 peptide, while the V_{max} for the short HIF-1α peptide was 30% of the reference (Table 2). An increase in substrate length correlated with an increase in V_{max} for all the substrates. The V_{max} values of the Notch1 L2 and L1 peptides were 50 and 30% of DES35, respectively, compared with 110% for the long HIF-1α peptide (Table 2). Reaction velocity does not necessarily correlate with higher affinity, as the Notch1 L1

Table 2
K_m values of FIH-1 for Notch1 and HIF-1α synthetic peptide substrates[a].

Substrate	Peptide	K_m (μM)	V_{max} (%)[b]
mNotch1	S1: N1945	110 ± 20	<10
	L1: N1945	0.7 ± 0.6	30 ± 5
	L1: N1945A	No[c]	
	S2: N2012	110 ± 1	<10
	L2: N2012	13 ± 3	50 ± 5
	L2: N2012A	No[c]	
hHIF-1α	S: N803	120 ± 30	30 ± 5
	L: N803	50 ± 3	110 ± 5
	L: N803A	No[c]	

FIH-1 activity was determined in the presence of increasing substrate concentrations, with cofactors other than oxygen at saturating concentrations. 2-oxoglutarate with a specific activity of 1100 dpm/nmol was used. The values are means ± SD from three to four independent experiments.
[a] Human FIH-1 produced and purified from insect cells was used as the catalyst.
[b] The V_{max} values are expressed relative to that obtained for the DES35 HIF-1α peptide (Koivunen et al., 2004).
[c] The peptide did not function as a substrate for FIH-1.

peptide had the lowest K_m, and the lowest V_{max} value (Table 2). Taken together, our data display clear differences between Notch and HIF-1α substrates in terms of their FIH-1-binding and hydroxylation, which, given the use of peptide substrates, are likely to reflect differences in primary sequence rather than tertiary structure.

These data also indicate a 20-fold difference between the K_m values for the Notch1 L1 and L2 peptides, with relatively little difference in V_{max}, indicating that FIH-1 has a much higher affinity for Site 1 than for Site 2 in these peptides. Given that these data were generated using peptides that encompass a single asparagine and possess no secondary structure, the influence of tertiary structure was further investigated using recombinant polypeptide substrates.

3.2. Affinity of FIH-1 for Notch but not HIF-1α substrates is increased with long recombinant polypeptides

Hydroxylation of Notch1 was studied using a recombinant (mNotch1 ANK1–7) substrate that contains both acceptor asparagines, partially spans the Notch1 intracellular domain, contains all seven ANKs, and had previously been shown to fold into a typical ANK structure (Ehebauer et al., 2005). The K_m value of FIH-1 for Notch1 ANK1–7 was found to be too low to be determined accurately with this assay (Table 3). The lowest non-limiting substrate concentration at which hydroxylation-coupled decarboxylation of 2-oxo[1-^{14}C]glutarate could be reliably assayed was 0.2 μM, and at this concentration the rate of FIH-1 catalysis was repeatedly found to have already reached its plateau. We conclude that the K_m for Notch1 ANK1–7 is less than 0.2 μM (Table 3), considerably lower than for the L1 and L2 peptides, and orders of magnitude lower than those for the short peptides (compare Tables 2 and 3). The increased affinity of FIH-1 for longer substrates may reflect a preference for the ankyrin repeat structure in addition to the primary amino acid sequence distal to the asparagine.

In contrast to the high affinity of FIH-1 for Notch1 ANK1–7, the K_m of the recombinant human HIF-1α ODDD/C-TAD for FIH-1 was found to be 50 μM, identical to that for the HIF-1α long peptide (compare Tables 2 and 3). Thus, unlike the case for the Notch polypeptides, a further increase in length did not increase the affinity of FIH-1 for HIF-1α. The affinity of FIH-1 for C-TAD may be influenced predominantly by residues close to the asparagine involved in the direct interaction with FIH-1, but impervious to additional increases in length due to the inherently unfolded nature of the C-TAD (Freedman et al., 2002; Dames et al., 2002). This demonstrates another significant difference in hydroxylation of Notch1 relative to HIF-1α, and is also in contrast to HIF prolyl hydroxylation, where the substrate length markedly reduces the K_m for HIF-P4Hs (Koivunen et al., 2006).

Table 3
K_m values of FIH-1 for recombinant Notch1 ANK1–7 and HIF-1α ODDD/C-TAD polypeptide substrates[a].

Substrate	Recombinant protein	K_m (μM)
mNotch1	ANK1–7	<0.2
	ANK1–7 N1945A	0.4 ± 0.03
	ANK1–7 N2012A	<0.2
	ANK1–7 N1945A, N2012A	No[b]
hHIF-1α	ODDD/C-TAD	50 ± 7

FIH-1 activity was determined in the presence of increasing substrate concentrations, with cofactors other than oxygen at saturating concentrations. To ensure that the substrate was not limiting, the concentration of enzyme was adjusted so that the maximum hydroxylation level obtained was 40%. 2-oxoglutarate with a specific activity of 11,100 dpm/nmol was used. The values are means ± SD from a minimum of three independent experiments.

[a] Human FIH-1 produced and purified from insect cells was used as the catalyst.

[b] The polypeptide did not function as a substrate for FIH-1.

The V_{max} values for the Notch1 and HIF-1α polypeptides did not differ greatly from those obtained with the peptide substrates, implying that hydroxylation velocity is predominantly determined by the primary sequence (compare Tables 2 and 3). V_{max} for Notch1 ANK1–7 was 50% of that for DES35 compared with 135% for the HIF-1α polypeptide.

Our results demonstrate that substrate length has a much greater influence on the FIH-1-dependent hydroxylation of Notch than on that of HIF-α, and this effect is predominantly through substrate binding affinity rather than the maximal hydroxylation velocity by FIH-1. Our results also confirm and extend previous observations that FIH-1 has a 250-fold higher affinity for Notch than for HIF-α, supporting the proposal that FIH-1 may be sequestered away from HIF-α by Notch proteins, thus inhibiting the function of HIF-α both *in vitro* and *in vivo* (Coleman et al., 2007; Zheng et al., 2008). Since it is currently unknown whether this is a general phenomenon for all FIH-1 substrates containing ANKs, it will be important to determine their affinities in order to understand their potential role in regulating FIH-1 and HIF-α activity. The 60% lower V_{max} value of FIH-1 for Notch1 than for the HIF-1α polypeptide is unlikely to affect substrate sequestering, however, as this will be influenced predominantly by the different substrate affinities.

3.3. FIH-1 preferentially hydroxylates Site 1 rather than Site 2 in Notch1–3

The two FIH-1 hydroxylation sites in Notch1 lie within homologous ANK regions, yet we and others have demonstrated that peptides encompassing a single hydroxylation site display significant differences with respect to their efficiency of hydroxylation (Coleman et al., 2007; Zheng et al., 2008). We studied here for the first time the hydroxylation of both sites within a single structured substrate, using mNotch1 ANK1–7 polypeptides with single alanine substitutions as substrates for FIH-1. As shown for the wild-type substrate, the K_m of <0.2 μM for the Site 2 mutant (N2012A), representing hydroxylation at Site 1 (N1945), was too low to be determined accurately with this assay (Table 3). By comparison, and following the trend observed with peptides, the K_m for the Site 1 mutant (N1945A), representing Site 2 hydroxylation of Notch1, was higher, 0.4 μM (Table 3). Although the magnitude of this difference could not be determined accurately, we conclude that FIH-1 has a higher affinity for Site 1 *in vitro*, and most likely a preference for it *in vivo*, especially at concentrations below and around the K_m value. These data are consistent with K_d values of 4.0 and 48.9 μM determined *in vitro* in the absence of Fe^{2+} and 2-oxoglutarate for Notch1 Sites 1 and 2, respectively (Coleman et al., 2007), and likewise the preference of FIH-1 for residue Asn-244 (Site 2) rather than Asn-210 (Site 1), as reported for IκBα (Cockman et al., 2006).

The large difference in the K_m values for the long Site 1 and 2 peptides (Table 2) is clearly due to differences in the primary sequence of the specific contact residues, since the peptides are unlikely to form stable ankyrin folds. The variations in K_m observed with the folded recombinant polypeptides (Table 3), above those for the peptide substrates, may nevertheless reflect in part the fact that one site within the folded ankyrin repeat is more accessible than the other. Structural studies of Notch have indicated that the ankyrin domain folds via a discrete two-stage process with folding at the repeats surrounding Site 2 preceding those around Site 1 (Kukkola et al., 2004; Lubman et al., 2005), thus placing Site 2 in a more stable position within the ankyrin domain. Given that the ANK substrates must undergo significant structural rearrangement in order to bind to FIH-1 in an extended conformation (Coleman et al., 2007), it would follow that the more accessible site would be preferred.

3.4. FIH-1 hydroxylates Notch2 and Notch3 at two asparagines in positions equivalent to those in Notch1

The Notch2 and Notch3 proteins, but not Notch4, have been reported to be hydroxylated by FIH-1, although their specific sites and hydroxylation kinetics have not been characterised. To identify the FIH-1 hydroxylation sites in Notch2 and 3, wild type and mutant ANK1–7 polypeptides with asparagine-to-alanine substitutions in equivalent positions to Sites 1 and 2 in Notch1 were expressed (Fig. 2A–C). As for Notch1, FIH-1-mediated hydroxylation of both sites in Notch2 and 3 was demonstrated *in vitro* (Fig. 2A–C). Mutation of the asparagine at Site 1 alone resulted in a major reduction in relative enzyme activity, whereas mutation of Site 2 alone led to only a moderate change. Mutation of both asparagines, however, abolished all hydroxylase activity, suggesting that, as in Notch1, both sites in Notch2 and 3 can be hydroxylated by FIH-1 and that Site 1 is preferred over Site 2 (Table 3; Coleman et al., 2007; Zheng et al., 2008). MALDI-MS of tryptic peptides of Notch2 and 3 incubated in the presence of FIH-1 demonstrated a mass change of +16 compared with untreated samples, consistent with asparaginyl hydroxylation at positions 1902 and 1969 of Notch2, and 1867 and 1934 of Notch3 (Fig. 3A–D). The identity of the hydroxylated residues was subsequently confirmed by MALDI-MS–MS (data not shown) and LQT-Orbitrap analysis (Supplementary Fig. 1A–D). Together with the *in vitro* hydroxylation results, these data confirm that both Notch2 and 3 become hydroxylated by FIH-1 at positions equivalent to those of Sites 1 and 2 in Notch1.

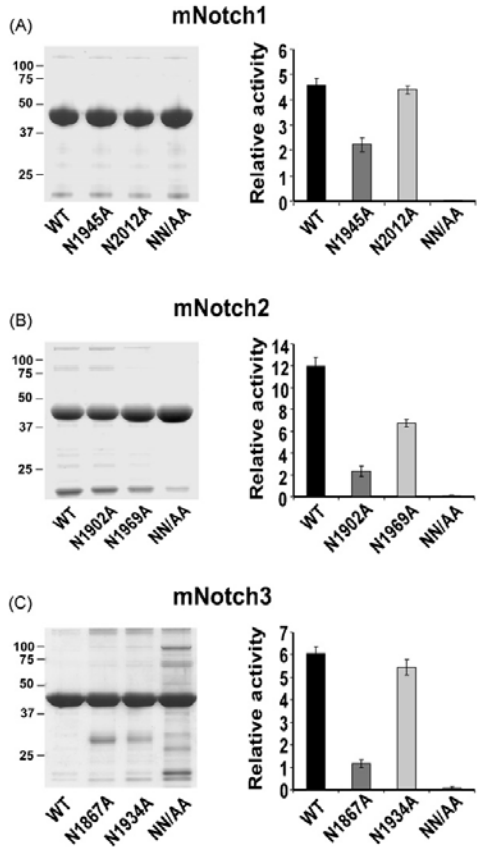

Fig. 2. FIH-1 hydroxylates Sites 1 and 2 in the full-length ANK1–7 of Notch1–3, with a preference for Site 1. (Left hand panels) Purified recombinant mNotch1–3 ANK1–7 proteins coding for residues 1862–2104, 1817–2061 and 1781–2026, (A–C respectively), and their asparagine-to-alanine single and double mutants were assessed for purity by Coomassie blue staining of SDS-PAGE gels loaded with equivalent concentrations of each protein. (Right hand panels) Purified substrates (30 μM) were analysed for MBP-hFIH-1-catalysed hydroxylation-coupled stoichiometric release of $^{14}CO_2$ from 2-oxo[1-^{14}C]glutarate. Cofactors other than oxygen were at saturating concentrations and 1 μM enzyme was used. The data are mean relative activities of triplicate reactions ± standard deviation, and are representative of three independent experiments.

Table 4
K_m values of FIH-1 for Notch2 and 3 synthetic peptides[a].

Substrate	Peptide	K_m (μM)	V_{max} (%)[b]
mNotch2	L1: N1902	2.2 ± 0.8	90 ± 5
	L2: N1969	40 ± 10	155 ± 5
mNotch3	L1: N1867	0.5 ± 0.2	120 ± 20
	L2: N1934	50 ± 10	130 ± 10

FIH-1 activity was determined in the presence of increasing substrate concentrations, with cofactors other than oxygen at saturating concentrations. 2-oxoglutarate with a specific activity of 1100 dpm/nmol was used. The values are means ± SD from three independent experiments.

[a] Human FIH-1 produced and purified from insect cells was used as the catalyst.

[b] The V_{max} values are expressed relative to that obtained for the DES35 HIF-1α peptide (Koivunen et al., 2004).

We next determined the K_m and V_{max} values of FIH-1 for Sites 1 and 2 in Notch2 and 3 and compared them with those for Notch1. As the K_m values for the long Notch1 synthetic peptides were markedly lower than those for the short peptides (Table 2), and bearing in mind the limits of our assay, we synthesised long peptides corresponding to Sites 1 and 2 (L1 and L2) in Notch2 and 3 (Fig. 1, Table 1). No major differences in hydroxylation were apparent between Notch1–3 peptides *in vitro*. The K_m values for Site 1 were 2.2 and 0.5 μM for Notch2 and 3, respectively, similar to that of 0.7 μM for Notch1 (Tables 2 and 4), while those for Site 2 were 40 and 50 μM for Notch2 and 3, respectively, which are in the same order of magnitude as that of 13 μM for Notch1 (Tables 2 and 4). The affinity of FIH-1 for Site 1 in all the Notch substrates was at least 18-fold higher than for Site 2 as evaluated from the K_m values.

Surprisingly, the V_{max} values for the Site 2 peptides of Notch1–3 were slightly higher than those for Site 1 (Tables 2 and 4). These values were dissimilar to the relative activities obtained for the full-length mNotch1–3 ANK1–7 ankyrin substrates, for which the relative activity of Site 1 was clearly higher than that of Site 2 (Fig. 2A–C) most likely reflecting a preference for the ankyrin structure. Notch2 and 3 peptides demonstrated higher V_{max} values for both sites than the corresponding Notch1 peptides and the full-length Notch1 ANK domain (Tables 2–4), suggesting that Notch2 and 3 are more efficiently hydroxylated than Notch1 at saturating substrate concentrations, and indeed this has been shown to be the case for Notch2 (Zheng et al., 2008; S. Wilkins, personal communication). It will be intriguing to investigate whether these trends are replicated in a cellular environment.

3.5. FIH-1 has a higher binding affinity for Notch1–3 than for Notch4 or HIF-1α

To complement our FIH-1 hydroxylation studies, we developed a sensitive assay for determining the relative FIH-1-binding affinities of Notch and HIF-1α recombinant polypeptides. Of particular interest were the relative binding affinities for the different Notch polypeptides, since it was not possible to determine accurate K_m values for Notch1 ANK1–7 with the hydroxylation assay due to the high affinity of the Notch–FIH-1 interaction. Quantitative analyses were performed and IC_{50} values measured with a fluorescence polarisation competition binding assay, and K_i values were sub-

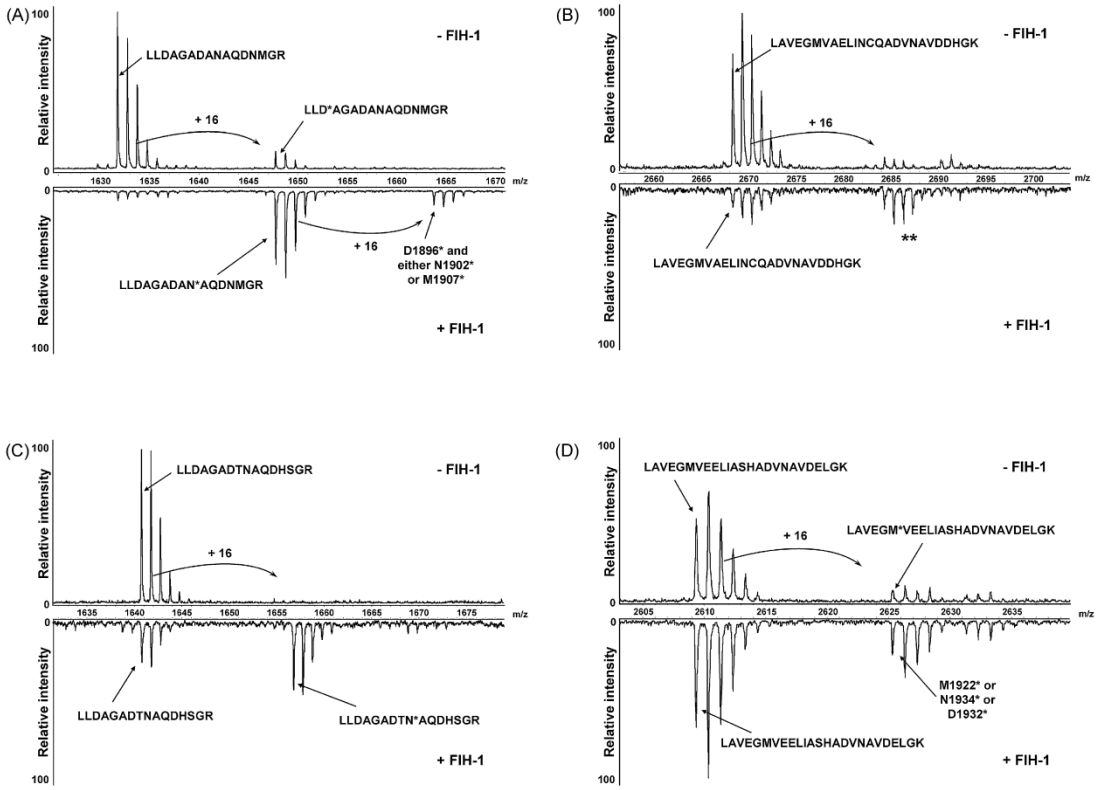

Fig. 3. Identification of FIH-1-dependent hydroxylation of asparaginyl residues at Sites 1 and 2 of mNotch2 and 3 by MALDI mass spectrometry. Notch2 and 3 ANK1–7 proteins incubated in the absence or presence of FIH-1 (− FIH-1, upper panels; + FIH-1, lower panels) were subjected to reduction, alkylation, SDS-PAGE and in-gel tryptic digestion. The tryptic peptides were then extracted in 0.1% trifluoroacetic acid for fractionation using a 120 min multistage gradient nanoHPLC. The eluted peptides were robotically mixed with CHCA-diluted matrix and arrayed onto MALDI target plates. A hand-spotted calibration standard mixture was used to calibrate the spectra. For peptides encompassing either Site 1 or Site 2, nanoHPLC-MALDI-TOF-MS demonstrated a mass change of +16 u between ions, consistent with asparaginyl hydroxylation by FIH-1. The modifications, including those independent of FIH-1, were confirmed by MALDI-TOF/TOF-MS–MS where indicated (*). MALDI-TOF-MS spectra are shown for ions representing: (A) residues 1894–1909 of Notch2 detected under non-hydroxylated (m/z 1647.7) and hydroxylated (m/z 1631.7) conditions; (B) residues 1952–1976 of Notch2 detected under non-hydroxylated (m/z 2668.3) and hydroxylated (m/z 2684.3) conditions (peaks denoted (**) are likely to contain hydroxylated N1969, as demonstrated by LQT-MS–MS (see Supplementary Fig. 1B)); (C) residues 1859–1874 of Notch3 detected under non-hydroxylated (m/z 1640.7) and hydroxylated (m/z 1756.7) conditions; and (D) residues 1917–1941 of Notch3 detected under non-hydroxylated (m/z 2609.3) and hydroxylated (m/z 2625.3) conditions.

sequently determined as a measure of relative binding affinity for FIH-1. Polypeptide substrates were used to compete with a fluorescently-labelled Notch1 L1 peptide for FIH-1 binding (Fig. 4A and B). As with the K_m values, the K_i values obtained for all the FIH-1 substrates lay within the μM range. The mean K_i values for Notch1, 2 and 3 were 1.1, 0.4 and 0.9 μM, respectively (Table 5). This demonstrates a small, yet statistically significant difference in the ability of FIH-1 to bind the Notch1–3 proteins, with Notch2 having the highest affinity. A markedly lower affinity was observed for the HIF-1αODDD/CTAD protein, with a mean K_i of 60 μM, at least 50-fold higher than those obtained for Notch1–3, a result that is consistent with our K_m values. Collectively, these data further support the proposal that hypoxic signalling may be regulated by Notch sequestering FIH-1 away from HIF-α (Coleman et al., 2007; Zheng et al., 2008). Subtle differences in the efficiency of FIH-1-binding and/or hydroxylation of Notch substrates add a level of complexity to this regulation, as do their differential temporal and spatial expression patterns.

Although Notch4 is not a substrate of FIH-1, we nonetheless demonstrated that it is able to bind to FIH-1, albeit with a K_i of 9.5 μM, implying an order of magnitude lower affinity than those for Notch1–3 (Table 5). This is in contrast to an earlier report that Notch4 was incapable of interacting with FIH-1 (Coleman et al., 2007). We believe this discrepancy is likely to be due to the higher sensitivity of the FP binding assay. Like Notch1–3, Notch4 binds FIH-1 with a higher affinity than it does HIF-1α. The functional consequence of the inability of Notch4 to be hydroxylated is unclear, as

Table 5
IC_{50} and K_i values of FIH-1 for Notch1–4 and HIF-1α recombinant polypeptides[a].

Substrate	IC_{50} (μM)	K_i (μM)
mNotch1 ANK1–7	1.3 ± 0.2	1.1 ± 0.2
mNotch2 ANK1–7	0.5 ± 0.3	0.4 ± 0.3[b]
mNotch3 ANK1–7	1.1 ± 0.4	0.9 ± 0.3
mNotch4 ANK1–7	10.9 ± 3.4	9.5 ± 3[b]
hHIF-1α ODDD/C-TAD	69 ± 3	60 ± 3[b]

IC_{50} concentrations were determined by non-linear regression analysis using Prism software (Graph Pad Software) and the K_i constants were determined according to the Cheng–Prusoff equation. The values are means ± SD from three independent experiments.

[a] Human FIH-1 produced and purified from *E. coli* was used.

[b] $p < 0.05$ compared to mNotch1 ANK1–7.

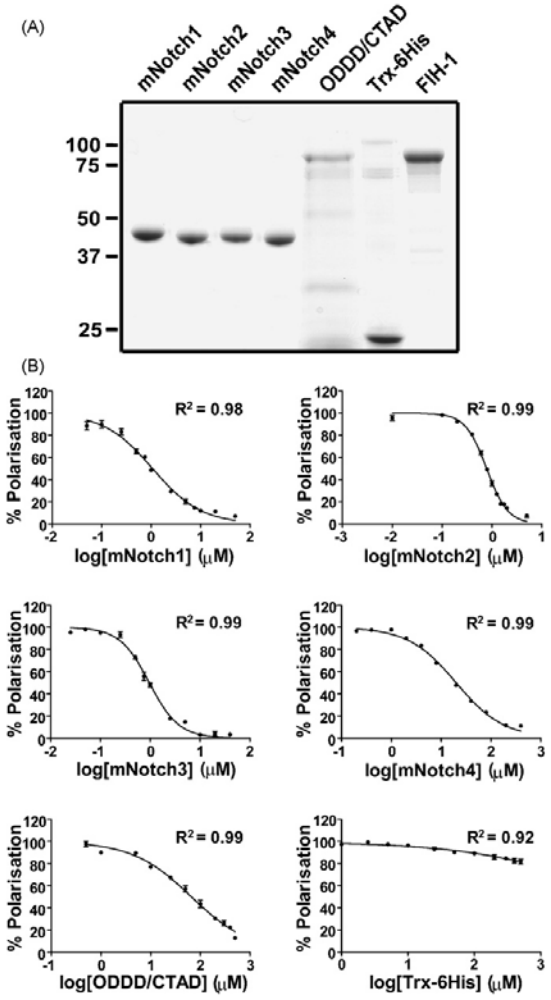

Fig. 4. Binding affinity of FIH-1 for Notch and HIF-1α recombinant polypeptides. Purified Trx-6His-tagged recombinant polypeptides for mNotch1–4 ANK1–7 with residues 1862–2104, 1817–2061, 1781–2026 and 1570–1815, respectively, hHIF-1α ODDD/C-TAD and the Trx-6His tag alone were (A) assessed for purity by Coomassie blue staining of SDS-PAGE gels loaded with equivalent amounts of each protein, and (B) serially diluted and used in fluorescence polarisation (FP) competition assays. Competitive binding for FIH-1 was assayed and the data were normalised, expressed as percentages of the maximum polarisation and subjected to non-linear regression analysis using Prism software (Graph Pad Software). The curve was fitted to a dose–response model with a variable slope. The data are mean % polarisations of triplicate reactions ± S.E.M., and are representative of three independent experiments.

no specific role for Notch4 has yet been elucidated that is distinct from those of the other family members. The data nevertheless indicate that Notch4 may be able to act as a regulator of FIH-1 substrate hydroxylation by competing with other substrates, including HIF-1α, for binding to FIH-1. The ability of FIH-1 to bind proteins that are not substrates highlights the possibility that there may be dual physiological roles for binding versus catalysis by FIH-1 *in vivo*. It is of interest to note that hydroxylation of Notch4 by FIH-1 can be achieved by mutation of single amino acids within close proximity to the target asparagine (S. Wilkins, personal communication).

3.6. The K_m of FIH-1 for oxygen is lower with Notch1 than with HIF-1α as a substrate

We have previously reported that the K_m of FIH-1 for oxygen correlates well with its important role in hypoxia sensing (Koivunen et al., 2004). However the K_m values of FIH-1 for oxygen with non-HIF-α substrates have not been reported. This value has important implications for understanding the physiological role of FIH-1, including the range of oxygen concentrations at which it is active and whether its activity is influenced by the nature or the length of the substrate. Especially since we have shown previously that the K_m of HIF-P4H-2 for oxygen is 250 μM when determined with a 19-residue synthetic peptide substrate, but 100 μM with recombinant HIF-1αODDD (Koivunen et al., 2006; Hirsilä et al., 2003). Since differences in the K_m for oxygen are also likely to contribute to substrate selection by FIH-1 within cells, we determined the K_m value of FIH-1 for oxygen using the mNotch1 ANK1–7 wild-type and mutant polypeptides and hHIF-1αODDD/CTAD as substrates. In marked contrast to the 90 μM obtained for HIF-1αODDD/CTAD, which is identical to the value previously observed for the HIF-1α synthetic peptide (Koivunen et al., 2004), the K_m of FIH-1 for oxygen for Notch1 ANK1–7 was almost 8-fold lower, 12 μM (Table 6, Fig. 5A and D). This demonstrates that FIH-1 has a significantly higher affinity for oxygen with Notch1 as a substrate than with HIF-1α. This is an important finding for cellular oxygen sensing, demonstrating that the sensitivity of FIH-1 to hypoxia varies depending on its substrate. Interestingly, when the mNotch1 N1945A mutant polypeptide was used as a substrate the K_m for oxygen was 90 μM, identical to that of HIF-1αODDD/CTAD (Table 6, Fig. 5C). However, the K_m of FIH-1 for oxygen obtained with the N2012A mutant polypeptide was 10 μM (Table 6, Fig. 5B), almost identical to that for the wild-type polypeptide. Like the hydroxylation affinity, the oxygen sensitivity of FIH-1 for Notch1 appears to be predominantly dictated by Site 1.

Finally, determination of the K_m values of FIH-1 for oxygen using the Notch2 and 3 long peptides as substrates demonstrated that the hydroxylation sites in Notch2 and 3 are similar in their oxygen affinity to those of Notch1. The K_m values for the Site 1 peptides (L1: N1902 and L1: N1867) were 19 and 12 μM, respectively, while those for Site 2 (L2: N1969 and L2: N1934) were higher, 70 and 110 μM, respectively (Table 6). Hence, in the context of *in vitro* hydroxylation, FIH-1 has a higher affinity for oxygen at Site 1 of all the Notch family substrates than at Site 2 or HIF-1α. The Site 1 positions in all the Notch proteins are thus likely to become hydroxylated efficiently even under relatively severe hypoxic conditions, where HIF-α hydroxylation would be reduced.

It is of interest to note that the higher affinity of FIH-1 for the Notch1–3 substrates than for HIF-1α also correlates with a higher

Table 6
K_m values of FIH-1 for oxygen using Notch1 and HIF-1α recombinant polypeptides or Notch2 and 3 synthetic peptide substrates[a].

Substrate	(Poly) peptide	K_m (μM)
mNotch1	ANK1–7	12 ± 3
	ANK1–7 N1945A	90 ± 30
	ANK1–7 N2012A	10 ± 3
mNotch2	L1: N1902	19 ± 4
	L2: N1969	70 ± 20
mNotch3	L1: N1867	12 ± 4
	L2: N1934	110 ± 20
hHIF-1α	ODDD/C-TAD	90 ± 25

K_m values of FIH-1 for O_2 were determined at five O_2 concentrations (20, 40, 80, 212 and 454 μM) with saturating concentrations of the various substrates and cofactors. The values are means ± SD from a minimum of three independent experiments.

[a] Human FIH-1 produced and purified from insect cells was used as the catalyst.

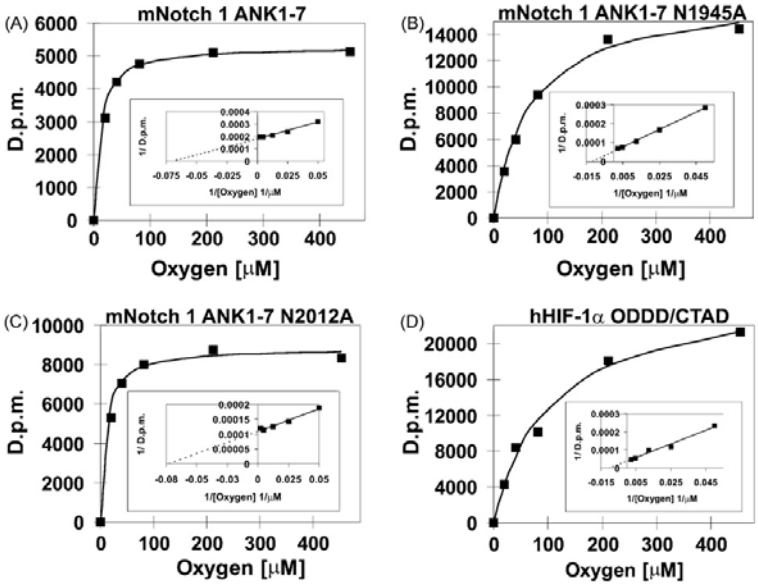

Fig. 5. Determination of the K_m value of FIH-1 for oxygen using the recombinant full-length Notch1 ANK1–7, its Site 1 and 2 asparagine mutants and the HIF-1α ODDD/C-TAD polypeptides as substrates. Effect of oxygen concentration on the reaction velocity of FIH-1 using (A) mNotch1 ANK1–7, (B) mNotch1 ANK1–7 N1945A, (C) mNotch1 ANK1–7 N2012A and (D) hHIF-1α ODDD/C-TAD as substrates. K_m values calculated from three independent experiments are given in Table 5 as means ± standard deviation (SD) of the values obtained from Michaelis–Menten and Lineweaver–Burk plots. The V_{max} values obtained from these plots cannot be compared directly as the determinations were made with different enzyme preparations, the specific activities of which may not be identical.

affinity for oxygen. Thus it may follow that a substrate that binds with a higher affinity 'induces' a conformation of FIH-1 that displays a higher affinity for oxygen, although the verification of this would require analysis of the affinities of additional ANK-containing FIH-1 substrates.

In conclusion, our data indicate that the K_m values of FIH-1 for oxygen at the preferred Site 1 of all three hydroxylated Notch family members are almost an order of magnitude lower than those at Site 2 and those for HIF-1α. Despite of this difference, it is however clear from previous functional studies that FIH-1 dependent hydroxylation of endogenous HIF-α occurs and it modulates HIF-α activity in cells during normoxia and hypoxia (Dayan et al., 2006; Stolze et al., 2004). The variation in the K_m values for oxygen between these two substrates supports the proposed order of binding to FIH-1 and other 2-oxoglutarate-dependent dioxygenases (Myllyharju and Kivirikko, 2004; Schofield and Ratcliffe, 2005), with the peptide substrate preceding the binding of oxygen to the active site and thus influencing it through a conformational change. This may have important implications for the cellular hypoxia response, as hydroxylation of Notch, specifically at its Site 1, is less sensitive to decreases in available oxygen than is the hydroxylation of HIF-α. Hence, as oxygen levels decrease, hydroxylation of the HIF-1α C-TAD will be inhibited much earlier than that of Notch at Site 1, adding another level of complexity and a new possibility for fine tuning the hypoxia response in physiological or pathological conditions.

Considering that the affinity of FIH-1 for Notch decreases upon its hydroxylation (Coleman et al., 2007; Zheng et al., 2008), this may influence the ability of Notch to sequester FIH-1 away from HIF-α and thus regulate transcriptional output from C-TAD. Once oxygen concentrations have decreased to levels low enough to inhibit Notch hydroxylation and thus increase its affinity for FIH-1, the oxygen levels at which HIF-α can be efficiently hydroxylated will long be surpassed. Thus the functional effect of FIH-1 sequestration by Notch may be redundant in terms of hypoxic signalling, although it may be more significant in situations such as sudden changes in oxygen levels rather than gradual decreases, in chronic hypoxia (Coleman et al., 2007), or upon re-oxygenation.

Taken together, these data demonstrate that hydroxylation of the Notch proteins by FIH-1, and presumably other substrates containing ankyrin repeats, differs considerably in terms of affinity and dependence on oxygen from that of the HIF substrates. Given the large number and diversity of potential substrates *in vivo*, the ultimate outcome will be determined by substrate availability, the affinity of FIH-1 for each substrate, hydroxylation efficiency and the concentration of oxygen and the other cofactors within the cell. Subsequent in cellulo analysis will demonstrate the importance of these *in vitro* differences in FIH-1 hydroxylation and substrate preference under physiological hypoxia.

Acknowledgements

We thank Tanja Aatsinki, Anne Kokko, Eeva Lehtimäki, Riitta Polojärvi and Minna Siurua for their expert technical assistance, Sarah Linke for critical discussion and Johanna Myllyharju, for the opportunity to carry out this work in her laboratory and for critical comments on the manuscript. This work was supported by grants 120156, 200471 and 202469 from the Research Councils for Biosciences and Environment and for Health, Academy of Finland to PK and Johanna Myllyharju, the S. Jusélius Foundation to PK and JM, the Finnish Cultural Foundation to PK, and the NHMRC of Australia and the National Heart Foundation of Australia to DJP.

Appendix A. Supplementary data

Supplementary data associated with this article can be found, in the online version, at doi:10.1016/j.biocel.2009.01.005.

References

Bray SJ. Notch signalling: a simple pathway becomes complex. Nat Rev Mol Cell Biol 2006;7:678–89.

Bruick RK, McKnight SL. A conserved family of prolyl-4-hydroxylases that modify HIF. Science 2001;294:1337–40.

Cockman ME, Lancaster DE, Stolze IP, Hewitson KS, McDonough MA, Coleman ML, et al. Posttranslational hydroxylation of ankyrin repeats in IkappaB proteins by the hypoxia-inducible factor (HIF) asparaginyl hydroxylase, factor inhibiting HIF (FIH). Proc Natl Acad Sci USA 2006;103:14767–72.

Coleman ML, McDonough MA, Hewitson KS, Coles C, Mecinovic J, Edelmann M, et al. Asparaginyl hydroxylation of the Notch ankyrin repeat domain by factor inhibiting hypoxia-inducible factor. J Biol Chem 2007;282:24027–38.

Dames SA, Martinez-Yamout M, De Guzman RN, Dyson HJ, Wright PE. Structural basis for Hif-1 alpha/CBP recognition in the cellular hypoxic response. Proc Natl Acad Sci USA 2002;99:5271–6.

Dayan F, Roux D, Brahimi-Horn MC, Pouyssegur J, Mazure NM. The oxygen sensor factor-inhibiting hypoxia-inducible factor-1 controls expression of distinct genes through the bifunctional transcriptional character of hypoxia-inducible factor-1alpha. Cancer Res 2006;66:3688–98.

Ehebauer MT, Chirgadze DY, Hayward P, Martinez Arias A, Blundell TL. High-resolution crystal structure of the human Notch1 ankyrin domain. Biochem J 2005;392:13–20.

Epstein ACR, Gleadle JM, McNeill LA, Hewitson KS, O'Rourke J, Mole DR, et al. *C. elegans* EGL-9 and mammalian homologs define a family of dioxygenases that regulate HIF by prolyl hydroxylation. Cell 2001;107:43–54.

Freedman SJ, Sun ZY, Poy F, Kung AL, Livingston DM, Wagner G, et al. Structural basis for recruitment of CBP/p300 by hypoxia-inducible factor-1 alpha. Proc Natl Acad Sci USA 2002;99:5367–72.

Hewitson KS, McNeill LA, Riordan MV, Tian Y-M, Bullock AN, Welford RW, et al. Hypoxia-inducible factor (HIF) asparagine hydroxylase is identical to factor inhibiting HIF (FIH) and is related to the cupin structural family. J Biol Chem 2002;277:26351–5.

Hirsilä M, Koivunen P, Günzler V, Kivirikko KI, Myllyharju J. Characterization of the human prolyl 4-hydroxylases that modify the hypoxia-inducible factor. J Biol Chem 2003;278:30772–80.

Ivan M, Haberberger T, Gervasi DC, Michelson KS, Günzler V, Kondo K, et al. Biochemical purification and pharmacological inhibition of a mammalian prolyl hydroxylase acting on hypoxia-inducible factor. Proc Natl Acad Sci USA 2002;99:13459–64.

Ivan M, Kondo K, Yang H, Kim W, Valiando J, Ohh M, et al. HIFalpha targeted for VHL-mediated destruction by proline hydroxylation: implications for O_2 sensing. Science 2001;292:464–8.

Jaakkola P, Mole DR, Tian Y-M, Wilson MI, Gielbert J, Gaskell SJ, et al. Targeting of HIF-alpha to the von Hippel-Lindau ubiquitylation complex by O_2-regulated prolyl hydroxylation. Science 2001;292:468–72.

Koivunen P, Hirsilä M, Günzler V, Kivirikko KI, Myllyharju J. Catalytic properties of the asparaginyl hydroxylase (FIH) in the oxygen sensing pathway are distinct from those of its prolyl 4-hydroxylases. J Biol Chem 2004;279:9899–904.

Koivunen P, Hirsilä M, Kivirikko KI, Myllyharju J. The length of peptide substrates has a marked effect on hydroxylation by the hypoxia-inducible factor prolyl 4-hydroxylases. J Biol Chem 2006;281:28712–20.

Koivunen P, Hirsilä M, Remes AM, Hassinen IE, Kivirikko KI, Myllyharju J. Inhibition of hypoxia-inducible factor (HIF) hydroxylases by citric acid cycle intermediates: possible links between cell metabolism and stabilization of HIF. J Biol Chem 2007;282:4524–32.

Kukkola L, Koivunen P, Pakkanen O, Page AP, Myllyharju J. Collagen prolyl 4-hydroxylase tetramers and dimers show identical decreases in K_m values for peptide substrates with increasing chain length: mutation of one of the two catalytic sites in the tetramer inactivates the enzyme by more than half. J Biol Chem 2004;279:18656–61.

Lando D, Peet DJ, Gorman JJ, Whelan DA, Whitelaw ML, Bruick RK. FIH-1 is an asparaginyl hydroxylase enzyme that regulates the transcriptional activity of hypoxia-inducible factor. Genes Dev 2002a;16:1466–71.

Lando D, Peet DJ, Whelan DA, Gorman JJ, Whitelaw ML. Asparagine hydroxylation of the HIF transactivation domain a hypoxic switch. Science 2002b;295:858–61.

Li J, Mahajan A, Tsai MD. Ankyrin repeat: a unique motif mediating protein–protein interactions. Biochemistry 2006;45:15168–78.

Linke S, Hampton-Smith RJ, Peet DJ. Characterization of ankyrin repeat-containing proteins as substrates of the asparaginyl hydroxylase factor inhibiting hypoxia-inducible transcription factor. Methods Enzymol 2007;435:61–85.

Linke S, Stojkoski C, Kewley RJ, Booker GW, Whitelaw ML, Peet DJ. Substrate requirements of the oxygen-sensing asparaginyl hydroxylase factor-inhibiting hypoxia-inducible factor. J Biol Chem 2004;279:14391–7.

Lubman OY, Kopan R, Waksman G, Korolev S. The crystal structure of a partial mouse Notch-1 ankyrin domain: repeats 4 through 7 preserve an ankyrin fold. Protein Sci 2005;14:1274–81.

Mahon PC, Hirota K, Semenza GL. FIH-1: a novel protein that interacts with HIF-1alpha and VHL to mediate repression of HIF-1 transcriptional activity. Genes Dev 2001;15:2675–86.

Mosavi LK, Cammett TJ, Desrosiers DC, Peng ZY. The ankyrin repeat as molecular architecture for protein recognition. Protein Sci 2004;13:1435–48.

Myllyharju J, Kivirikko KI. Collagens, modifying enzymes and their mutations in humans, flies and worms. Trends Genet 2004;20:33–43.

Ratcliffe PJ, Kaelin Jr WG. Oxygen sensing by metazoans: the central role of the HIF hydroxylase pathway. Mol Cell 2008;30:393–402.

Schofield CJ, Ratcliffe PJ. Signalling hypoxia by HIF hydroxylases. Biochem Biophys Res Commun 2005;338:617–26.

Stolze IP, Tian YM, Appelhoff RJ, Turley H, Wykoff CC, Gleadle JM, et al. Genetic analysis of the role of the asparaginyl hydroxylase factor inhibiting hypoxia-inducible factor (HIF) in regulating HIF transcriptional target genes. J Biol Chem 2004;279:42719–25.

Zheng X, Linke S, Dias J, Zheng X, Gradin K, Wallis TP, et al. Interaction with factor inhibiting HIF-1 defines an additional mode of cross-coupling between the Notch and hypoxia signalling pathways. Proc Natl Acad Sci USA 2008;105:3368–73.

Supplementary Data

Supplementary Fig. S1. Confirmation of hydroxylation by FIH-1 of Site 1 and 2 asparagines of Notch2 and 3 by Orbitrap-FT mass spectrometry. Non-hydroxylated and hydroxylated tryptic peptides were obtained from in-gel tryptic digestions of mNotch2 and 3 ANK1-7 following incubation in the absence or presence of FIH-1 (- FIH-1, upper panels; + FIH-1, lower panels). Tryptic peptides were separated using a 120 min multistage gradient HPLC on-line with an LTQ-Orbitrap. Double-charged precursor ions were observed with high accuracy by the Orbitrap-FT-MS and subsequently subjected to MS/MS in the LTQ compartment of the instrument. The LTQ-MS/MS fragmentation spectra of ions represent: (A) residues 1894-1909 of Notch2 for which precursor ions were observed for non-hydroxylated (m/z 816.38) and hydroxylated (m/z 824.37) forms (addition of a mass corresponding to the FIH-1-dependent hydroxylation of N1902 is indicated by the presence of y and b-ions at +16 u accompanying y8-y14 and b9-b15); (B) residues 1952-1976 of Notch2 for which precursor ions were observed for non-hydroxylated (m/z 1335.14) and hydroxylated (m/z 1343.14) forms (addition of a mass corresponding to the FIH-1-dependent hydroxylation of N1969 is indicated by the presence of y and b-ions at +16 u accompanying y8-y18 and b18); (C) residues 1859-1874 of Notch3 for which precursor ions were observed for non-hydroxylated (m/z 820.88) and hydroxylated (m/z 828.88) forms (addition of a mass corresponding to the FIH-1-dependent hydroxylation of N1867 is indicated by the presence of y and b-ions at +16 u accompanying y8-y14 and b11-15 and +8 u on double-charged (+2) y12-14); and (D) residues 1917-1941 of Notch3 for which precursor ions were observed for non-hydroxylated (m/z 1305.66) and hydroxylated (m/z 1313.66) forms (addition of a mass corresponding to the FIH-1-dependent hydroxylation of N1934 is indicated by the presence of y and b-ions at +16 u accompanying y8-y18 and b18). The mass additions to ions are indicated by dotted lines and asterisks in the + FIH-1 sections of panels A-D.

A

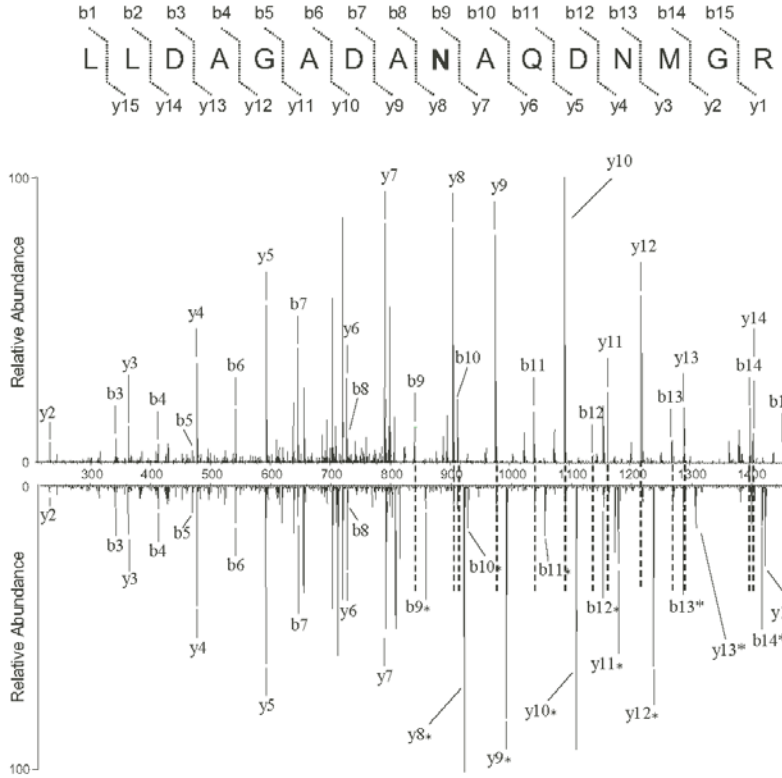
b1 b2 b3 b4 b5 b6 b7 b8 b9 b10 b11 b12 b13 b14 b15
L L D A G A D A N A Q D N M G R
y15 y14 y13 y12 y11 y10 y9 y8 y7 y6 y5 y4 y3 y2 y1
Relative Abundance
m/z
- FIH-1
+ FIH-1

B

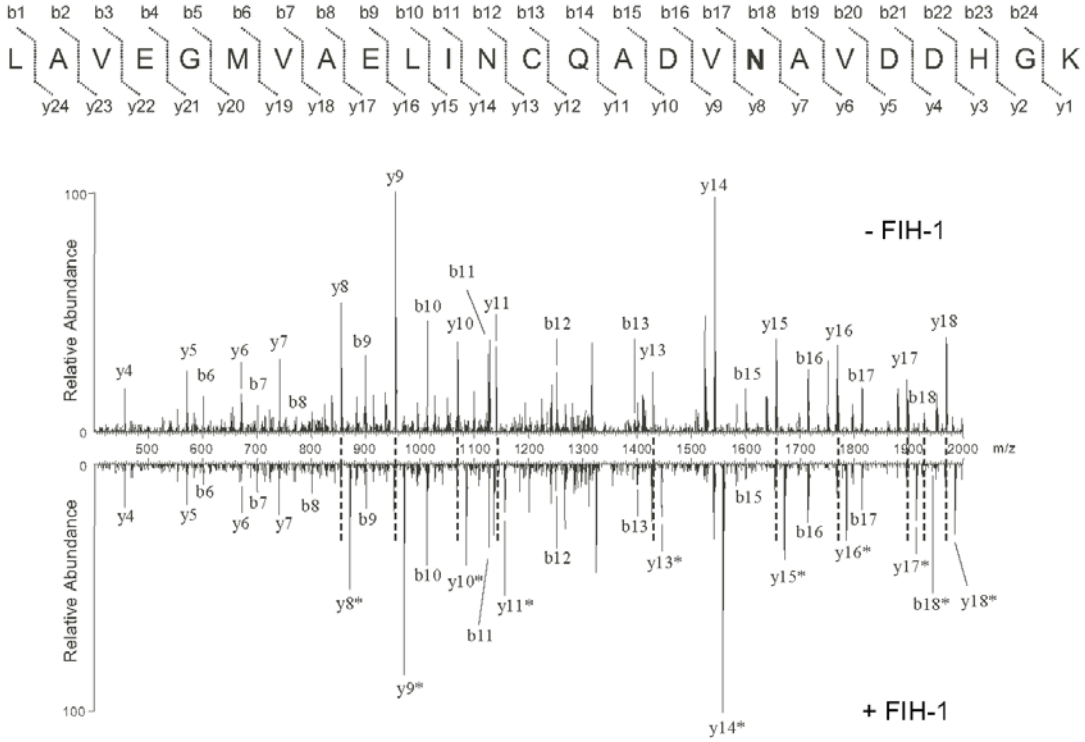
b1 b2 b3 b4 b5 b6 b7 b8 b9 b10 b11 b12 b13 b14 b15 b16 b17 b18 b19 b20 b21 b22 b23 b24
L A V E G M V A E L I N C Q A D V N A V D D H G K
y24 y23 y22 y21 y20 y19 y18 y17 y16 y15 y14 y13 y12 y11 y10 y9 y8 y7 y6 y5 y4 y3 y2 y1
Relative Abundance
m/z
- FIH-1
+ FIH-1

C

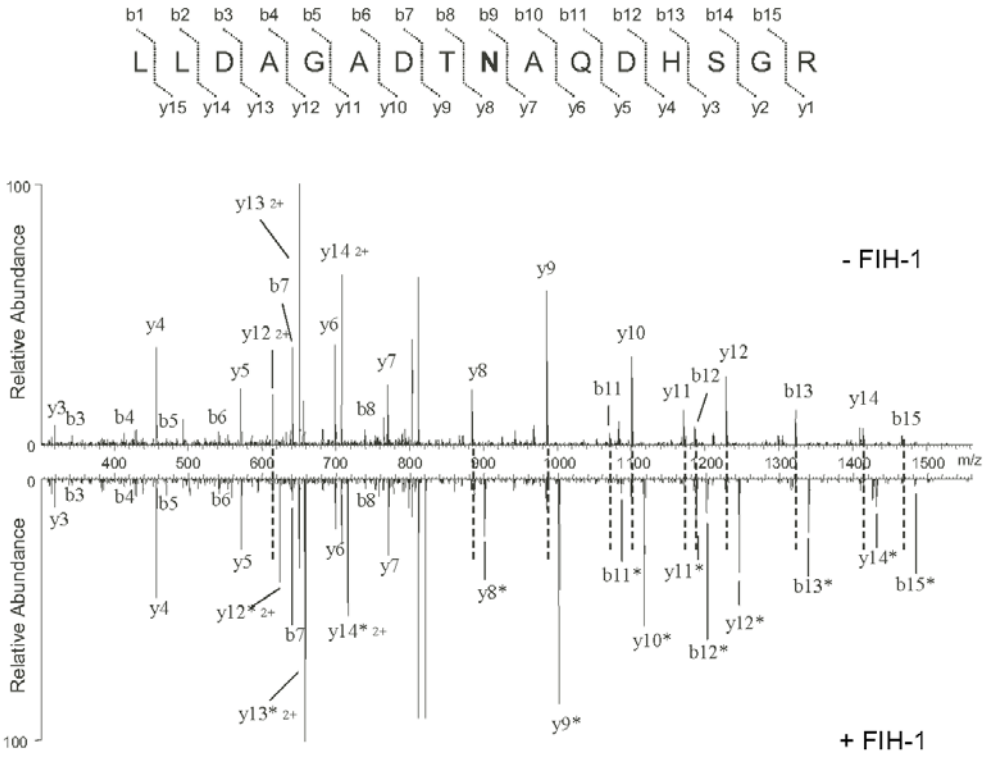
b1 b2 b3 b4 b5 b6 b7 b8 b9 b10 b11 b12 b13 b14 b15
L L D A G A D T N A Q D H S G R
y15 y14 y13 y12 y11 y10 y9 y8 y7 y6 y5 y4 y3 y2 y1
Relative Abundance
m/z
- FIH-1
+ FIH-1

D

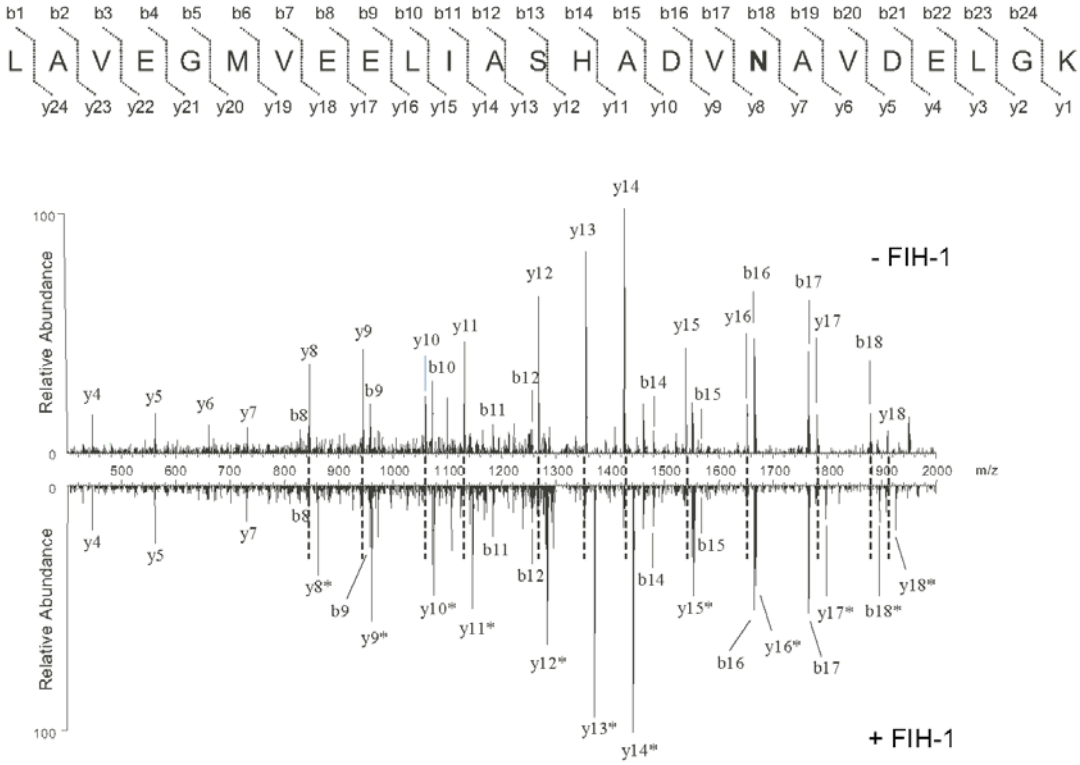
b1 b2 b3 b4 b5 b6 b7 b8 b9 b10 b11 b12 b13 b14 b15 b16 b17 b18 b19 b20 b21 b22 b23 b24
L A V E G M V E E L I A S H A D V N A V D E L G K
y24 y23 y22 y21 y20 y19 y18 y17 y16 y15 y14 y13 y12 y11 y10 y9 y8 y7 y6 y5 y4 y3 y2 y1
Relative Abundance
m/z
- FIH-1
+ FIH-1

Appendix 2 Development of a FP-based binding assay

Measurement of protein-protein interactions using FP

Fluorescence polarisation (FP) is a technique that monitors the rotational motion of molecules in solution as a means of quantifying bimolecular interactions (reviewed in [246, 247]). The underlying principle of FP is that a fluorescent molecule, when excited with plane-polarised light, will emit light with a degree of polarisation that is inversely proportional to its rate of rotation. As illustrated in Figure A2.1, small fluorescent ligands (e.g. a fluorescently-labelled peptide) rotate rapidly when free in solution. Consequently, excitation with polarised light leads to emission of light that is largely depolarised, due to reorientation of the fluorophore during its excited state. If the fluorescent ligand binds to an interacting protein, its rate of rotation will be significantly reduced due to the greater molecular weight of the complex. As such, the fluorophore will re-orient to a much lesser extent in the excited state, and the emitted light will remain largely depolarised.
This property of FP enables it to be used for equilibrium-binding studies of a known ligand-protein interaction. In a mixture of fluorescent ligand and interacting protein, the observed polarisation will be proportional to the amount of bound ligand. As such, titrating increasing amounts of interacting protein enables the generation of a binding curve, which can be used to calculate the equilibrium binding constant (K_d) for the interaction. This technique can also be used to perform competition binding assays, which measure the decrease in FP caused by a competing protein that displaces the labelled ligand (Figure A2.1).

Development and optimisation of FP binding assays for FIH

To determine equilibrium binding constants for FIH-substrate interactions, a FP-based competition binding assay was developed, in which protein substrates were assayed for their ability to compete with a fluorescently-labelled Notch peptide for binding to FIH. The fluorescent peptide, commonly referred to as the tracer, must be relatively small (< 5 kDa), such that binding to FIH results in a large increase in polarisation. A 35 amino acid peptide consisting of residues 1930-1963 of the mouse Notch1 ARD (corresponding to FIH hydroxylation site 1) was chosen for use as the tracer. The peptide was commercially synthesised (Auspep), and labelled N-terminally with a fluorescein isothiocyanate (FITC).

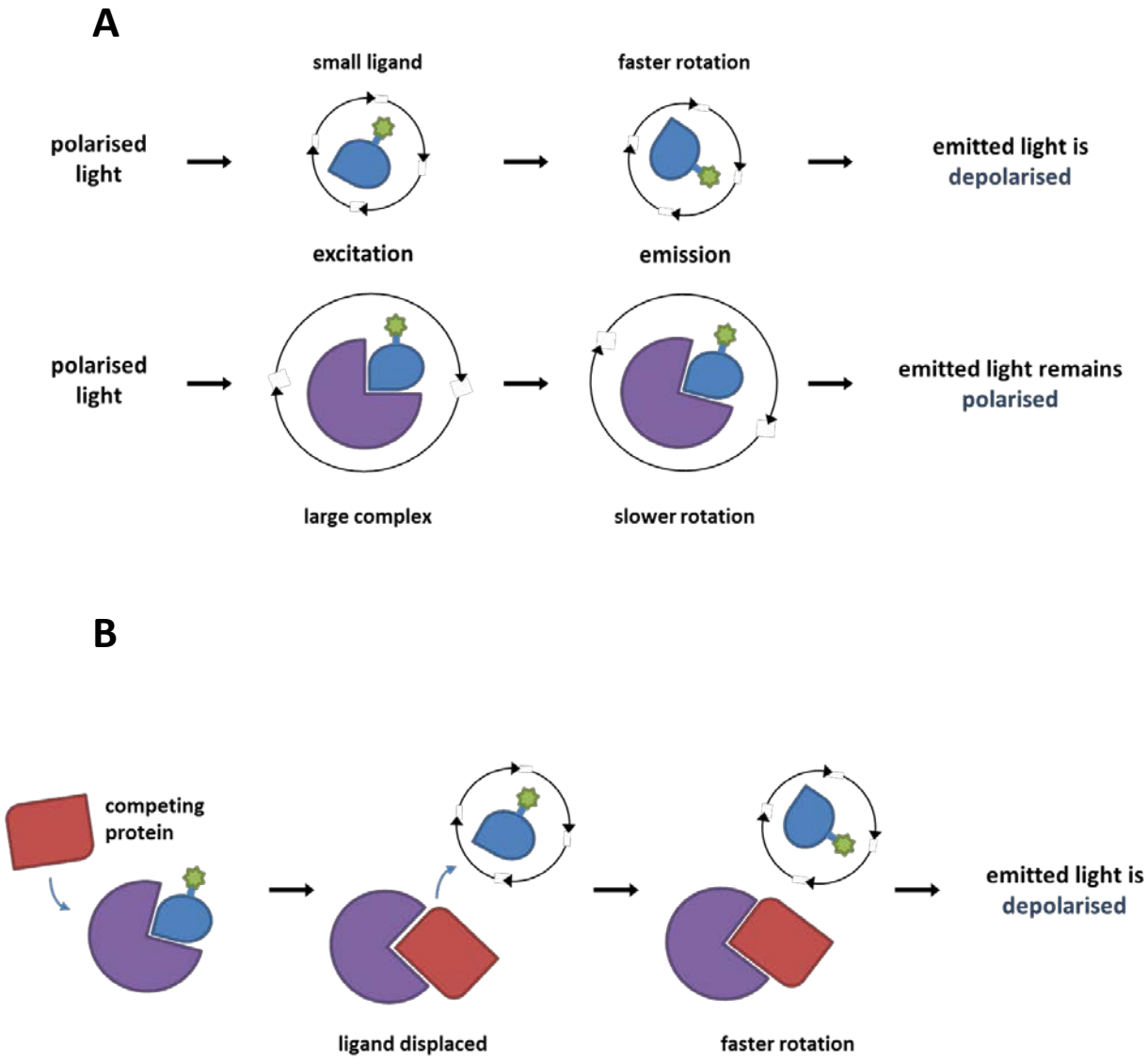

Figure A2.1 Principles of fluorescence polarisation

A. Schematic depicting the basic principle of fluorescence polarisation. When a small molecule (blue) with a fluorescent label (green star) is excited by polarised light, it will emit light that is predominantly depolarised due to rapid rotation of the molecule in the excited state. Binding to an interacting protein (purple) causes an apparent increase in the molecular weight of the fluorescent molecule, resulting in a slower rate of rotation and the emission of light that retains its polarisation. B. In FP competition binding assays, the addition of a competing protein (red) leads to displacement of the fluorescent ligand. The unbound ligand rotates rapidly in solution, and consequently, when excited by polarised light will emit light that is largely depolarised. Figure adapted from Moerke *et al*., 2009 [246].

Preliminary experiments were performed to measure binding of the FITC-Notch peptide tracer to MBP-FIH, using a fixed amount of tracer (400 nM) and increasing concentrations of MBP-hFIH, ranging from 500 nM to 35 μM. Assays were performed under oxygenated conditions, but without the addition of cofactors (2OG, ascorbate and Fe^{II}) to prevent the formation of hydroxylated product, which might complicate the results. Most cofactors, with the exception of Fe(II), are not required for substrate binding, and previous work in our laboratory indicates that bacterially expressed MBP-FIH co-purifies with Fe(II) already bound within its active site (Sarah Linke, personal communication).

Assays were incubated at room temperature for 30 minutes to enable binding to reach equilibrium, at which point FP measurements were made using a microplate reader (BMG Labtech). As shown in Figure A2.2, the addition of MBP-FIH, but not MBP alone, led to an increase in polarisation, which reached its plateau (corresponding to complete binding of all labelled ligand) at a concentration of approximately 20 μM MBP-FIH. The data were fitted to a one-site equilibrium binding curve using Graphpad PRISM software, and the mean K_d (concentration of FIH at which 50% of the tracer is bound) from 3 independent experiments was found to be 2.6 μM. This value is relatively consistent with the K_m of 0.7 μM for the unlabelled peptide (Notch1 Site 1 long), which had previously been determined in CO_2 capture assays (refer to section 3.2.1), although it is possible that addition of the fluorophore reduced the affinity of the interaction to some extent.

Based on these data, a concentration of 5 μM MBP-hFIH was chosen for subsequent competition binding assays. This concentration produced approximately 80% of the change in polarisation between the free tracer and the completely bound state, providing a large window for measurement of displacement of the tracer. In competition binding experiments, 5 μM MBP-FIH was pre-incubated with serial dilutions of an interacting protein (e.g. substrate) for 30 minutes prior to the addition of the fluorescent tracer (400 nM). Assays were incubated at room temperature for a further 30 mins before FP measurements were taken, to enable equilibrium to be reached. Data were subjected to non-linear regression analysis (Graphpad PRISM), with data fit to a one-site competitive binding curve for estimation of IC_{50} values (concentration of protein required to displace 50% of the fluorescent tracer from FIH).

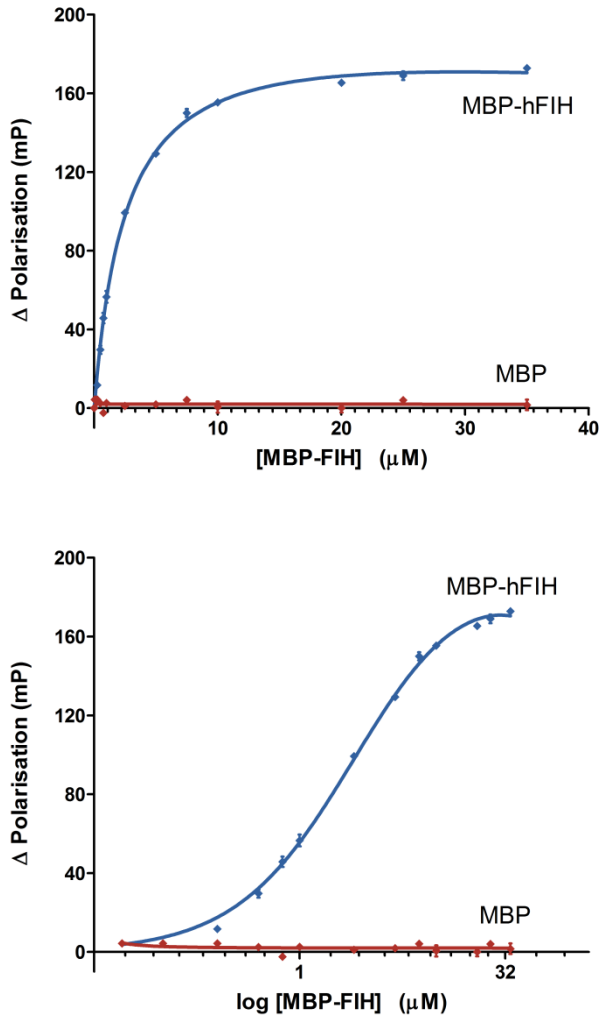

Figure A2.2 Determination of the K_d for the FIH-tracer interaction

FP assay were performed to measure the equilibrium binding constant (K_d) of FIH for a fluorescently-labelled Notch peptide tracer. A constant amount of tracer (400 nM) was titrated with increasing concentrations of MBP-FIH, or MBP alone as a negative control. Data were expressed as the change (Δ) in polarisation by subtraction of polarisation measured for the tracer alone (i.e. without the addition of FIH). Data were then subjected to non-linear regression analysis and fit to a one-site binding curve using Graphpad PRISM software. A representative curve from three independent experiments is shown, plotted on either a linear scale (*upper panel*) or a logarithmic scale (*lower panel*), resulting in hyperbolic and sigmoidal curves, respectively.

The equilibrium dissociation constant (K_i) was calculated from the IC_{50} value (by PRISM software) using the Cheng-Prusoff equation:

$$K_i = \frac{IC_{50}}{1 + \frac{[L]}{K_d}}$$

This takes into account the concentration of the fluorescent tracer [L], as well as the K_d of the FIH-tracer interaction. These values are more comparable to K_m values determined from kinetic hydroxylation assays.

Data from FP competition binding assays are presented in section 3.2.4, but as an example, the dissociation curve for the Notch1 ARD is presented in Figure A2.3. As the concentration of Notch1 increases, the polarisation (expressed as a percentage of the initial value) decreases until the tracer is completely displaced from FIH. At this point, the curve reaches its plateau, and the polarisation values are equivalent to the values obtained for the fluorescent tracer alone in solution (i.e. in the absence of FIH). As with CO_2 capture assays, substrate proteins for FP experiments were expressed with an N-terminal Trx-6H-tag and purified by nickel-affinity chromatography. Thus, a competition binding experiment was performed using the Trx-6H-tag alone as a control. As shown in Figure A2.3, only a very small amount of non-specific binding was observed at high concentrations (>50 μM), indicating that the assay is specific for FIH-interacting proteins, and that the Trx-6His-tag does not interact with MBP-FIH.

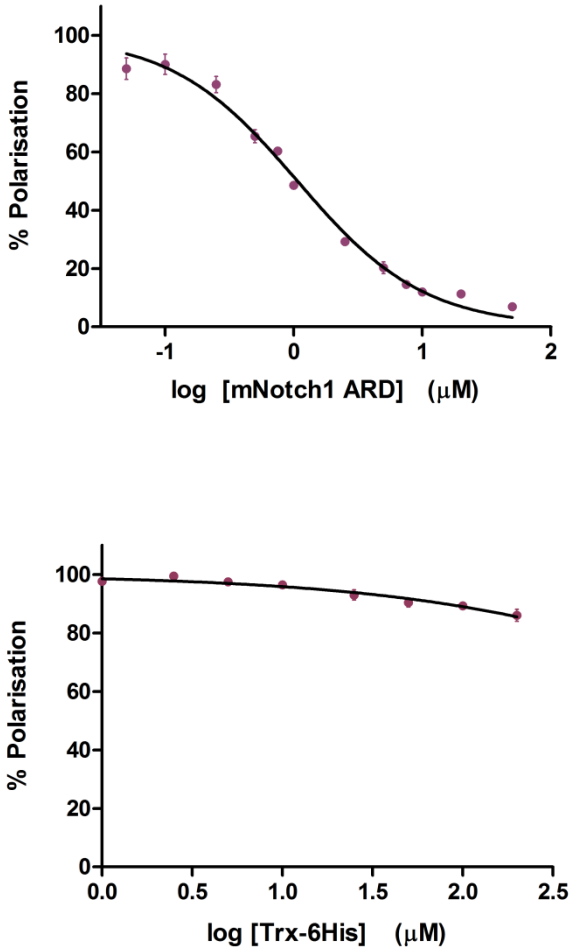

Figure A2.3 Analysis of FIH binding to Notch and Trx in FP assays

Affinity-purified Trx-6H-tagged Notch1 ARD (*upper panel*) and Trx-6His alone (*lower panel*) were assayed for their ability to compete with a fluorescently labelled Notch peptide in FP competition binding assays. A constant amount of tracer (400 nM) and MBP-hFIH (5 μM) were titrated with increasing concentrations of the Trx-6H-tagged protein. Data are background corrected by subtraction of polarisation measured for the peptide alone, and expressed as a percentage of the initial polarisation in presence of FIH but absence of any competing protein, then fit to a one-site competitive binding curve using Graphpad PRISM software. Data are the mean of triplicate reactions ± SD and are representative of three independent experiments.

Appendix 3 Detection of sheep FIH

Species cross-reactivity of the Novus anti-FIH polyclonal antibody

As described in section 5.2.2, investigation of FIH protein levels in LT cell lysates required an antibody capable of detecting ovine FIH. Polyclonal antibodies available at the time were raised against the full-length human enzyme, however, the high degree of homology (97%) between the amino acid sequences for sheep and human FIH suggested that at least some of the epitopes were likely to be conserved between the two species (Figure A3.1). Nevertheless, preliminary experiments were performed to determine which, if any, of our anti-FIH antibodies was capable of detecting sheep FIH in cell-lysates.

Protein extracts from foetal sheep tissues (kindly provided by Kimberley Botting from the Morrison group at the University of South Australia) were separated by SDS-PAGE and analysed by Western blot (Figure A3.2), using either the Novus anti-FIH polyclonal antibody (*left panel*), or our own anti-FIH 'No. 8' rabbit sera (*right panel*) to detect FIH. Lysate from 293T cells (expressing endogenous FIH) was included as a positive control, as was a sample of bacterially expressed and affinity-purified MBP-hFIH. As shown in Figure A3.2, both antibodies were able to detect the recombinant protein, as well as a doublet (commonly seen for FIH) in the 293T cell lysate at the expected molecular weight (~40 kDa) for FIH. A doublet of roughly the equivalent molecular weight was observed in both of the sheep protein extracts, and was picked up more strongly by the Novus antibody than the #8 antisera. Thus, the Novus antibody was deemed most suitable for detection of sheep FIH, and was employed in subsequent analyses of Orf-infected LT cells.

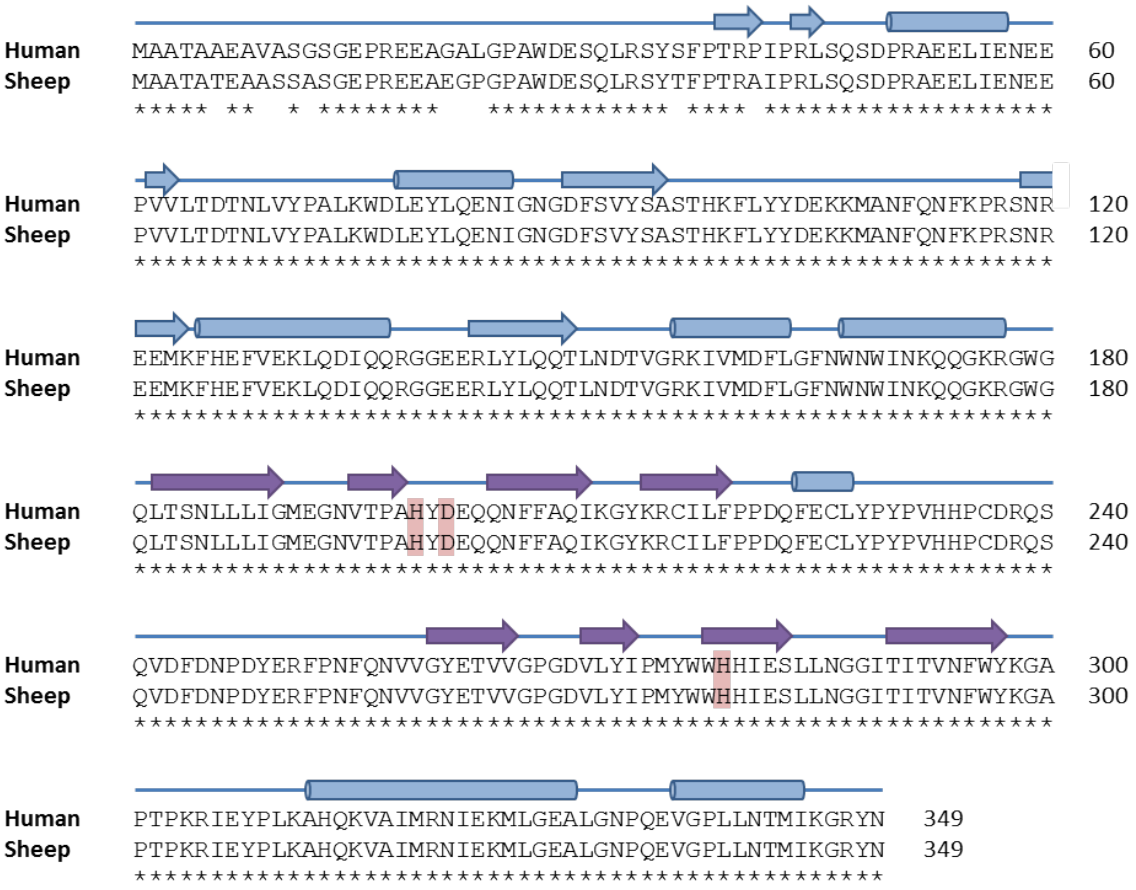

Figure A3.1 Amino acid sequence alignment of human and sheep FIH

The cDNA sequence for human FIH (Genbank ID: NM_017902) was used in a BLAST search of the sheep EST database (http://www.ncbi.nlm.nih.gov/blast). The search identified two overlapping ESTs (DY482626 and GT874196) that give complete coverage of the FIH coding sequence (CDS). The combined sequence was translated, and the resultant amino acid sequence (for sheep FIH) aligned with the human FIH amino acid sequence (Genbank ID: NP_060372) using clustalW. The homology between the two sequences (indicated by asterisks below the alignment) was found to be 97%. Importantly, among the conserved residues are those that form the catalytic triad involved in binding Fe(II), and these are shaded in pink. Residues that form α-helices and β-strands (according to the crystal structure of hFIH reported by Elkins et al. [116]) are indicated by cylinders and arrows, respectively, above the sequence. Purple arrows denote the 8 β-strands that comprise the DSBH.

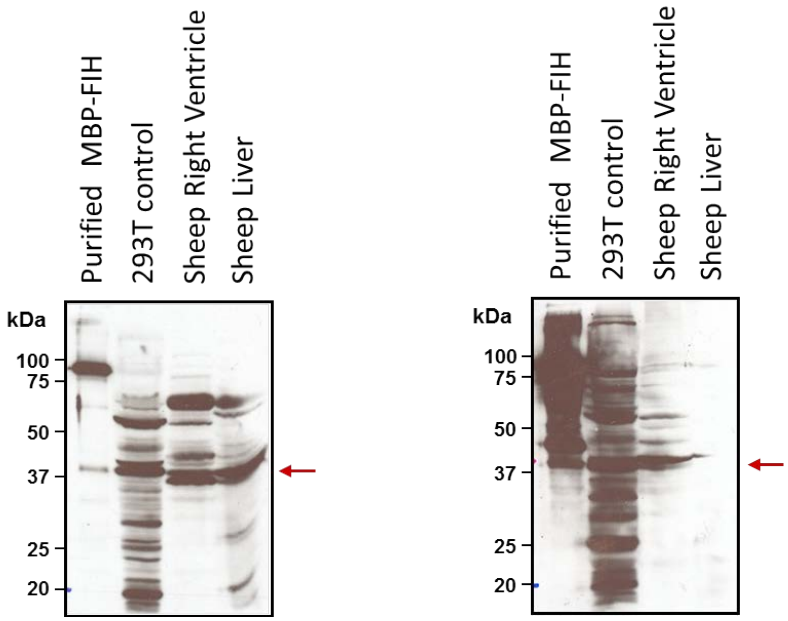

Figure A3.2 Detection of ovine FIH in extracts from sheep tissue

Equivalent volumes of total protein extracts from fetal sheep right-ventricle and liver tissue were analysed by SDS-PAGE and immunoblotting with either the Novus anti-FIH polyclonal antibody (left panel) or our own polyclonal serum (right panel). 293T cell lysate was used as a control, as was a sample of MBP-hFIH that had been affinity-purified from bacteria. MBP-FIH commonly degrades over time to produce a 40kDa band at around the same size as endogenous FIH (indicated by red arrow). The polyclonal serum was raised against MBP-hFIH and detects a large number of degradation products that are not seen with the Novus antibody.

Appendix 4 Primer design for qPCR experiments

At this time this work commenced, the sheep genome had not yet been fully sequenced. As such, efforts to design primers for qPCR were hampered by the limited amount of publicly available sequence information for the sheep genome. Consequently, cDNA sequences for genes of interest were identified by BLAST searches of the sheep EST database (http://blast.ncbi.nlm.nih.gov/), and only those with a high degree of similarity to the human sequence were selected for analysis. Primer3 software [139] was used to design primers that would amplify products of 80-120 bp within regions of particularly high similarity (>90%), and spanning at least one predicted exon boundary. Primers for *β-Actin,* described in Sutton *et al.* (2011), were obtained from the Thomas lab at the University of Adelaide [248]. These were originally designed for analysis of mouse *β-Actin* by qPCR, but were found to be suitable for amplification of the sheep cDNA sequence. Primer design for *VEGF* was complicated by the fact that ORFV encodes its own homologue of *VEGF.* Therefore, primers were designed towards a region of low homology to the viral *VEGF* gene. The specificity of each primer set was verified by visualisation of a single PCR product of the expected size by gel electrophoreisis (data not shown), and confirmed by sequencing of amplified products.

Egl nine homolog 3 (EGLN3, PHD3)

```
Hs PHD3     AGAAAATTGCCCTGGAGTACATCGTGCCCTGTCTGCACGAGGTGGGCTTCTGCTACCTGG   420
Oa EST      AGAAAATCGCCCTGGAGTACATCGTGCCCTGTCTGCACGAGGTCGGCTTCTGCTACCTGG   229
            ******* ********************************** ****************

Hs PHD3     ACAACTTCCTGGGCGAGGTGGTGGGCGACTGCGTCCTGGAGCGCGTCAAGCAGCTGCACT   480
Oa EST      ATAACTTCCTGGGCGAGGTGGTGGGCGACTGCGTCCTGGAGCGCGTGAAGCAGCTGCACT   289
            * ****************************************** *************

Hs PHD3     GCACCGGGGCCCTGCGGGACGGCCAGCTGGCGGGGCCGCGCGCCGGCGTCTCCAAGCGAC   540
Oa EST      GCAACGGGGCCCTGCGGGACGGCCAGCTGGCCGGGCCCCGCGCCGGCGTCTCCAAGCGGC   349
            *** ************************** ***** ******************** *

Hs PHD3     ACCTGCGGGGCGACCAGATCACGTGGATCGGGGGCAACGAGGAGGGCTGCGAGGCCATCA   600
Oa EST      ACCTGCGGGGTGATCAGATCACGTGGATCGGGGGCAACGAGGAAGGCTGTGAGGCCATCA   409
            ********** ** ***************************** ***** **********

                        >>>>>>>>>>>>>>>>>>>
Hs PHD3     GCTTCCTCCTGTCCCTCATCGACAGGCTGGTCCTCTACTGCGGGAGCCGGCTGGGCAAAT   660
Oa EST      GTTACCTCCTGTCCCTCATCGATAGGCTGGTCTTGTACTGCGGGAGCCGGCTGGGCAAAT   469
            * * ****************** ********* * *************************

                                                <<<<<<<<<<<<<<<<<<<
                            ▼
Hs PHD3     ACTACGTCAAGGAGAGGTCTAAGGCAATGGTGGCTTGCTATCCGGGAAATGGAACAGGTT   720
Oa EST      ACTACGTCAAGGAAAGGTCCAAGGCGATGGTGGCTTGCTACCCAGGAAATGGAACAGGCT   529
            ************* ***** ***** ************** ** ************** *

Hs PHD3     ATGTTCGCCACGTGGACAACCCCAACGGTGATGGTCGCTGCATCACCTGCATCTACTATC   780
Oa EST      ATGTTCGACATGTGGACAACCCCAACGGTGACGGCCGCTGTATCACCTGCATCTACTATC   589
            ******* ** ******************** ** ***** ********************

                            ▼
Hs PHD3     TGAACAAGAATTGGGATGCCAAGCTACATGGTGGGATCCTGCGGATATTTCCAGAGGGGA   840
Oa EST      TGAACAAGAACTGGGATGCCAAGCGACATGGCGGGGTCCTGCGAATATTTCCAGAAGGGA   649
            ********** ************* ****** *** ******* *********** ****

Hs PHD3     AATCATTCATAGCAGATGTGGAGCCCATTTTTGACAGACTCCTGTTCTTCTGGTCAGATC   900
Oa EST      AATCATTCATAGCGGACGTGGAGCCCATTTTTGACAGACTGTTGTTCTTCTGGTCAGACC   709
            ************* ** ********************** ***************** *
```

>>>>>>>> Forward primer <<<<<<<< Reverse primer

▼ Exon boundary ⋆ Identical nucleotide

Genbank Accession Numbers: Hs EGLN3: NM_022073, Oa EST: EE830671

Solute carrier family 2, member 1 (SLC2A1, GLUT1)

```
Hs GLUT1    TGGCCCCTGCTGCTGAGCATCATCTTCATCCCGGCCCTGCTGCAGTGCATCGTGCTGCCC   1140
Oa EST      TGGCCCCTGCTGCTGAGCGTCATCTTCATCCCGGCCCTGTTGCAGTGCATCCTGCTGCCC   166
            ****************** ****************** *********** ********

Hs GLUT1    TTCTGCCCCGAGAGTCCCCGCTTCCTGCTCATCAACCGCAACGAGGAGAACCGGGCCAAG   1200
Oa EST      TTCTGCCCCGAGAGCCCCCGCTTCCTGCTCATTAACCGCAACGAGGAGAACCGGGCCAAG   226
            ************** ***************** ***************************

Hs GLUT1    AGTGTGCTAAAGAAGCTGCGCGGGACAGCTGACGTGACCCATGACCTGCAGGAGATGAAG   1260
Oa EST      AGCGTGCTGAAGAAGCTGCGTGGGACCGCGGACGTGACCCGCGACCTGCAGGAGATGAAG   286
            ** ***** ************ ***** ** **********  ******************

Hs GLUT1    GAAGAGAGTCGGCAGATGATGCGGGAGAAGAAGGTCACCATCCTGGAGCTGTTCCGCTCC   1320
Oa EST      GAGGAGAGCCGGCAGATGATGCGAGAGAAGAAGGTCACCATCCTGGAGCTGTTCCGCTCG   346
            ** ***** ************** ************************************

                                >>>>>>>>>>>>>>>>>>
Hs GLUT1    CCCGCCTACCGCCAGCCCATCCTCATCGCTGTGGTGCTGCAGCTGTCCCAGCAGCTGTCT   1380
Oa EST      GCCGCCTACCGCCAGCCCATCCTCATTGCCGTGGTGCTGCAGCTGTCCCAGCAGCTGTCC   406
             ************************* ** ****************************

                                                <<<<<<<<<<<<<<<<<<<
Hs GLUT1    GGCATCAACGCTGTCTTCTATTACTCCACGAGCATCTTCGAGAAGGCGGGGGTGCAGCAG   1440
Oa EST      GGCATCAACGCTGTTTTCTATTACTCCACAAGCATCTTCGAGAAGGCGGGGGTGCAGCAG   466
            ************** ************** ******************************

Hs GLUT1    CCTGTGTATGCCACCATTGGCTCCGGTATCGTCAACACGGCCTTCACTGTCGTGTCGCTG   1500
Oa EST      CCCGTGTACGCCACCATCGGCTCCGGCATCGTCAACACAGCCTTCACTGTCGTGTCGCTG   526
            ** ***** ******** ******** *********** **********************

Hs GLUT1    TTTGTGGTGGAGCGAGCAGGCCGGCGGACCCTGCACCTCATAGGCCTCGCTGGCATGGCG   1560
Oa EST      TTTGTGGTGGAGCGAGCCGGCCGGCGGACCCTGCACCTCATAGGCCTGGCCGGCATGGCT   586
            ***************** ***************************** ** ********

Hs GLUT1    GGTTGTGCCATACTCATGACCATCGCGCTAGCACTGCTGGAGCAGCTACCCTGGATGTCC   1620
Oa EST      GGCTGTGCGGTGCTCATGACCATCGCGCTGGCGCTGCTGGAGCAACTGCCCTGGATGTCC   646
            ** *****  * ***************** ** *********** ** ************
```

>>>>>>>> Forward primer <<<<<<<< Reverse primer

▼ Exon boundary ⋆ Identical nucleotide

Genbank Accession Numbers: Hs SLC2A1: NM_006516, Oa EST: GT643538

Vascular endothelial growth factor A (VEGF)

```
                                                                >>>>>>>>
Hs VEGFA      GGTCGGGCCTCCGAAACCATGAACTTTCTGCTGTCTTGGGTGCATTGGAGCCTTGCCTTG   1080
Oa VEGFA      ------------------ATGAACTTTCTGCTCTCTTGGGTGCATTGGAGCCTTGCCTTG   42
                                 ************** ***************************

              >>>>>>>>>>>>
Hs VEGFA      CTGCTCTACCTCCACCATGCCAAGTGGTCCCAGGCTGCACCCATGGCAGAAGGAGGAGGG   1140
Oa VEGFA      CTGCTCTACCTTCACCATGCCAAGTGGTCCCAGGCTGCACCCATGGCAGAAGGAGG---G   99
              *********** ******************************************   *

Hs VEGFA      CAGAATCATCACGAAGTGGTGAAGTTCATGGATGTCTATCAGCGCAGCTACTGCCATCCA   1200
Oa VEGFA      CAGAAACCCCATGAAGTGATGAAGTTCATGGATGTCTACCAGCGCAGCTTCTGCCGTCCC   159
              ***** *  ** ****** ****************** ********** ***** ***

                <<<<<<<<<<<<<<<<<<<<
Hs VEGFA      ATCGAGACCCTGGTGGACATCTTCCAGGAGTACCCTGATGAGATCGAGTACATCTTCAAG   1260
Oa VEGFA      ATTGAGACCCTGGTGGACATCTTCCAGGAGTACCCAGATGAGATTGAGTTCATTTTCAAG   219
              ** ******************************** ******** **** *** ******

Hs VEGFA      CCATCCTGTGTGCCCCTGATGCGATGCGGGGGCTGCTGCAATGACGAGGGCCTGGAGTGT   1320
Oa VEGFA      CCGTCCTGTGTGCCCCTGATGCGGTGCGGGGGCTGCTGTAATGACGAAAGTCTGGAGTGT   279
              ** ******************** ************** ********  * *********

Hs VEGFA      GTGCCCACTGAGGAGTCCAACATCACCATGCAGATTATGCGGATCAAACCTCACCAAGGC   1380
Oa VEGFA      GTGCCCACTGAGGAGTTCAACATCACCATGCAGATTATGCGGATCAAACCTCACCAAAGC   339
              **************** ****************************************** **
```

Homology to ORFV VEGF homologue

```
                                        >>>>>>>>>>>>>>>>>>>>
Oa VEGFA      TCTGCTCTCTTGGGTGCATTGGAGCCTTGCCTTGCTGCTCTACCTTCACCATGCCAAGTG 68
ORFV VEGF     TATAACGCCCAACTTTTAAGGGTGAGGCGCCATGAAGTTGC-TCGTCGGCATACTA-GTA 298
              * *     *     *  *  ** *    *** **  * *    * **  *** * * **

Oa VEGFA      GTCCCAGGCT-GCACCCATGGCAGAAGGAGGGCAGAAACCCCATGAAGTGATGAAGTTCA 127
ORFV VEGF     GCCGTGTGCTTGCACCAGTATCTGCTGAACGCGGACAGCAACACGAAAGGATG--GTCC- 355
              * *    *** *****  *  * *  * * *     * *  ** ***  ****  ** *

                                                <<<<<<<<<<<<<<<<<<<<
Oa VEGFA      TGGATGTCTACCAGCGCAGCTTCTGCCGTCCCATTGAGACCCTGGTGGACATCTTCCAGG 187
ORFV VEGF     --GAAGTGCTGAAAGGCAGCGAGTGCAAGCCTAGGCCGATTGTTGTTCCTGTAAGCGAGA 413
                ** **     *  *****   ***   ** *    **   * **     *   * **
```

>>>>>>>> Forward primer <<<<<<<< Reverse primer

▼ Exon boundary ⋆ Identical nucleotide

Genbank Accession Numbers: Hs VEGFA: NM_001025366, Oa VEGFA: NM_001025110

ORFV NZ2 VEGF-E: S67520

Aryl hydrocarbon receptor nuclear translocator (ARNT)

```
Hs ARNT     AAAAGCAAATCTTTCTGTAAACAGAATAAAAGTTCCTCTCCCTTCCCTTCCCTCACCCCT   2637
Oa EST      AAAAGCACATCTTTCTGTAAACAGAATAAAAGTTCCTCTCCCTTCCCTTCCCTCTCCCCT   90
            ******* ********************************************** *****

                                                >>>>>>>>>>>>>>>>>>>>
Hs ARNT     GACATGTACCCCCTTTCCCTTCTGGCTGTTCCCCTGCTCTGTTGCCTCTCTAAGGTAACA   2697
Oa EST      CATGTATACCCCCTTTCCCTTCTGACCTTTCCCTTGTCTTCCTGCATCTCTGAGATAACA   150
             *  * ******************  *  ***** **   *  *** ***** ** *****

                                                            <<<<<<<<<<<<<<<
Hs ARNT     TTTATAGAAGAAATGGAATGAATCTCCAAGGCTTTTAGGACTGTCTGAAAATTTGAGGCT   2757
Oa EST      TTTATAGAAGAAATGGAGTGACTCCTCAACGCTTTGGGGACCCTTTGAAAAACTGAGGCT   210
            ***************** *** **  *** *****  ****  * ******  *******

            <<<<<
Hs ARNT     GGGTGAAGTTAA-AACACCTTTCCTTATGTCTCCTGACCTGAAATT-GTATAGTGTTGAT   2815
Oa EST      GGGTTAGGTTAAGAATGTCTTTCCTTATGTCTCCTGACCAGAAATTTATGCAGAAACGAT   270
            **** * ***** **   ********************** ******  *  **    ***

Hs ARNT     TTGTGCTGAGATCAAGAGGCAGGTTAGAAGAACCTGACATCCACTGTTTGCCTTGGATAG   2875
Oa EST      TTGTGCTGGG-TCAAGGAGCAGGTTAGAAAA------CATTCACTATTTCCTTTGGATAC   323
            ******** * *****  ********** *      *** **** *** * *******

Hs ARNT     TATGGCTTGTTTTTGGAAAGAAATTCTGAAGAGAGTGGAGGAGAGGAGAAATGTCCTCA-   2934
Oa EST      TATGGCTTATTTTTGGAAAGATATTCTTAATAAGGTGAGAGAGAGGAGAAATGTCCTCAA   383
            ******** ************ ***** ** *  ***   ******************

Hs ARNT     TATTTGAGGACCATGAAACATTGTAGGTATATATGGGGCTTTAGCAAGTTTGAGCATAGG   2994
Oa EST      TGTTTGAGGACCATGAAACATGGCAGGTGTA-ATGGGGTTTTTGGAAGT--GAGTACAGG   440
            * ******************* * **** ** ****** *** * ****  *** * ***

Hs ARNT     CTCTTTTTGCTGCCTGTGAGCAGTCCCTCTGGAAAGAAACATGTGAGTAAGTGAGAGAGA   3054
Oa EST      TGCTTTTTGCTGCCTGTGAGCAATTCCTCTGGAATGAAATATGAG--------------   485
              ******************* * ********* **** *** *
```

>>>>>>>> Forward primer <<<<<<<< Reverse primer

▼ Exon boundary * Identical nucleotide

Genbank Accession Numbers: Hs ARNT: NM_001197325, Oa EST: EE799134

Ribosomal protein, large, P0 (RPLP0)

```
                                >>>>>>>>>>>>>>>>>>>>                                  ▼
Hs RPLP0        CCCAGGGAAGACAGGGCGACCTGGAAGTCCAACTACTTCCTTAAGATCATCCAACTATTG    300
Oa EST          CCCAGGGAAGACAGGGCGACCTGGAAGTCCAACTACTTCCTTAAGATCATCCAACTTCTG    127
                ************************************************************  **

                                <<<<<<<<<<<<<<<<<<<<
Hs RPLP0        GATGATTATCCGAAATGTTTCATTGTGGGAGCAGACAATGTGGGCTCCAAGCAGATGCAG    360
Oa EST          GATGATTATCCAAAATGCTTCATTGTGGGAGCAGACAATGTGGGCTCCAAGCAGATGCAG    187
                *********** ***** ****************************************

Hs RPLP0        CAGATCCGCATGTCCCTTCGCGGGAAGGCTGTGGTGCTGATGGGCAAGAACACCATGATG    420
Oa EST          CAGATCCGCATGTCGCTGCGCGGGAAGGCTGTGGTGCTGATGGGCAAGAACACGATGATG    247
                ************** ** ********************************** ******

                                                                     ▼
Hs RPLP0        CGCAAGGCCATCCGAGGGCACCTGGAAAACAACCCAGCTCTGGAGAAACTGCTGCCTCAT    480
Oa EST          CGCAAGGCCATCCGAGGGCATCTGGAAAACAACCCGGCTCTGGAGAAACTGTTGCCTCAC    307
                ******************** ************** *************** *******

Hs RPLP0        ATCCGGGGGAATGTGGGCTTTGTGTTCACCAAGGAGGACCTCACTGAGATCAGGGACATG    540
Oa EST          ATCCGGGGAAATGTGGGCTTCGTGTTCACCAAGGAGGACCTCACTGAGATCAGGGACATG    367
                ******** *********** ************************************

                ▼
Hs RPLP0        TTGCTGGCCAATAAGGTGCCAGCTGCTGCCCGTGCTGGTGCCATTGCCCCATGTGAAGTC    600
Oa EST          CTGCTGGCCAATAAGGTGCCGGCTGCCGCCCGTGCTGGTGCCATAGCGCCGTGCGAAGTC    427
                 ****************** ***** ***************** ** ** ** ******

Hs RPLP0        ACTGTGCCAGCCCAGAACACTGGTCTCGGGCCCGAGAAGACCTCCTTTTTCCAGGCTTTA    660
Oa EST          ACTGTGCCAGCCCAGAACACTGGTCTGGGGCCCGAGAAGACATCCTTCTTCCAGGCTTTA    487
                ************************** ************** ***** ************

                                                  ▼
Hs RPLP0        GGTATCACCACTAAAATCTCCAGGGGCACCATTGAAATCCTGAGTGATGTGCAGCTGATC    720
Oa EST          GGCATCACCACTAAGATCTCCAGGGGCACAATTGAAATCCTGAGCGATGTGCAGCTGATT    547
                ** *********** ************** ************** **************

Hs RPLP0        AAGACTGGAGACAAAGTGGGAGCCAGCGAAGCCACGCTGCTGAACATGCTCAACATCTCC    780
Oa EST          AAGACCGGAGACAAGGTGGGCGCCAGCGAAGCCACGCTGCTGAACATGCTGAACATCTCC    607
                ***** ******** ***** ****************************** *********
```

>>>>>>>> Forward primer <<<<<<<< Reverse primer

▼ Exon boundary ⋆ Identical nucleotide

Genbank Accession Numbers: Hs RPLP0: NM_053275, Oa EST: GT881993

β-Actin (ACTB)

```
Mm Actb     TTGTGATGGACTCCGGAGACGGGGTCACCCACACTGTGCCCATCTACGAGGGCTATGCTC   590
Oa ACTB     TCGTGATGGACTCCGGTGACGGGGTCACCCACACGGTGCCCATCTACGAGGGGTACGCCC   597
            * ************** ***************** ***************** ** ** *

Mm Actb     TCCCTCACGCCATCCTGCGTCTGGACCTGGCTGGCCGGGACCTGACAGACTACCTCATGA   650
Oa ACTB     TCCCCCACGCCATCCTGCGTCTGGACCTGGCTGGCCGGGACCTGACGGACTACCTCATGA   657
            **** ****************************************** *************

Mm Actb     AGATCCTGACCGAGCGTGGCTACAGCTTCACCACCACAGCTGAGAGGGAAATCGTGCGTG   710
Oa ACTB     AGATCCTCACGGAGCGTGGCTACAGCTTCACCACCACGGCCGAGCGGGAAATCGTCCGTG   717
            ******* ** ************************** ** *** ********** ****

Mm Actb     ACATCAAAGAGAAGCTGTGCTATGTTGCTCTAGACTTCGAGCAGGAGATGGCCACTGCCG   770
Oa ACTB     ACATCAAGGAGAAGCTCTGCTACGTGGCCCTGGACTTCGAGCAGGAGATGGCCACCGCGG   777
            ******* ******** ***** ** ** ** ************************ ** *

                                                >>>>>>>>>>>>>>>
Mm Actb     CATCCTCTTCCTCCCTGGAGAAGAGCTATGAGCTGCCTGACGGCCAGGTCATCACTATTG   830
Oa ACTB     CCTCCAGCTCCTCCCTGGAGAAGAGCTACGAGCTGCCGGACGGGCAGGTCATCACCATCG   837
            * ***   ******************** ******** ***** *********** ** *

                                                <<<<<<<<<<<<<<<<<<<
                                                            ▼
Mm Actb     GCAACGAGCGGTTCCGATGCCCTGAGGCTCTTTTCCAGCCTTCCTTCTTGGGTATGGAAT   890
Oa ACTB     GCAATGAGCGGTTCCGCTGCCCTGAGGCTCTCTTCCAGCCTTCCTTCCTGGGCATGGAAT   897
            **** *********** ************** *************** **** *******

            <
Mm Actb     CCTGTGGCATCCATGAAACTACATTCAATTCCATCATGAAGTGTGACGTTGACATCCGTA   950
Oa ACTB     CCTGCGGCATTCACGAAACTACCTTCAATTCCATCATGAAGTGTGACGTCGACATCCGCA   957
            **** ***** ** ******** ************************** ******** *

Mm Actb     AAGACCTCTATGCCAACACAGTGCTGTCTGGTGGTACCACCATGTACCCAGGCATTGCTG   1010
Oa ACTB     AAGACCTCTACGCCAACACGGTGCTGTCCGGCGGGACCACCATGTACCCTGGCATCGCAG   1017
            ********** ******** ******** ** ** ************** ***** ** *

                                                            ▼
Mm Actb     ACAGGATGCAGAAGGAGATTACTGCTCTGGCTCCTAGCACCATGAAGATCAAGATCATTG   1070
Oa ACTB     ACAGGATGCAGAAAGAGATCACTGCCCTGGCACCCAGCACGATGAAGATCAAGATCATCG   1077
            ************* ***** ***** ***** ** ***** ***************** *
```

>>>>>>>> Forward primer <<<<<<<< Reverse primer

▼ Exon boundary * Identical nucleotide

Genbank Accession Numbers: Mm Actb: NM_007393, Oa ACTB: NM_001009784

Polymerase (RNA) II (DNA directed) polypeptide A (POLR2A)

```
Hs POLR2A     CTGAAAAGATCAATGCTGGTTTTGGTGACGACTTGAACTGCATCTTTAATGATGACAATG   4140
Oa EST        ---AAAAGATCAATGCTG-CTTCGGTGACGACTTGAACTGCATCTTTAACGATGATAACG   67
                 ***************  ** ************************** ***** ** *

Hs POLR2A     CAGAGAAGCTGGTGCTCCGTATTCGCATCATGAACAGCGATGAGAACAAGATGCAAGAGG   4200
Oa EST        CAGAGAAGCTGGTGCTCCGGATCCGCATCATGAACAGTGATGAAAACAAGATGCAAGAGG   127
              ******************* ** ************** ***** ****************

Hs POLR2A     AGGAAGAGGTGGTGGACAAGATGGATGATGATGTCTTCCTGCGCTGCATCGAGTCCAACA   4260
Oa EST        AGGAAGAGGTGGTGGACAAGATGGACGACGACGTCTTCCTGCGCTGCATCGAGTCCAACA   187
              ************************* ** ** ****************************

                                >>>>>>>>>>>>>>>>>>>>
Hs POLR2A     TGCTGACAGATATGACCCTGCAGGGCATCGAGCAGATCAGCAAGGTGTACATGCACTTGC   4320
Oa EST        TGCTGACGGACATGACCCTGCAGGGCATAGAGCAGATCAGCAAGGTGTACATGCACTTGC   247
              ******* ** ***************** ********************************

                                                <<<<<<<<<<<<<<<<<<<<
Hs POLR2A     CACAGACAGACAACAAGAAGAAGATCATCATCACGGAGGATGGGGAATTCAAGGCCCTGC   4380
Oa EST        CGCAGACTGACAACAAGAAGAAGATCATCATCACAGAGGACGGGGAGTTCAAGGCCCTGC   307
              * ***** ************************** ***** ***** *************

Hs POLR2A     AGGAGTGGATCCTGGAGACGGACGGCGTGAGCTTGATGCGGGTGCTGAGTGAGAAGGACG   4440
Oa EST        AGGAGTGGATCCTGGAGACGGACGGTGTGAGCCTGATGCGCGTGCTGAGTGAGAAGGATG   367
              ************************* ****** ******* ***************** *

Hs POLR2A     TGGACCCCGTACGCACCACGTCCAATGACATTGTGGAGATCTTCACGGTGCTGGGCATTG   4500
Oa EST        TGGACCCTGTGCGCACCACATCCAACGACATCGTGGAGATCTTCACGGTGCTGGGCATTG   427
              ******* ** ******** ***** ***** ****************************

Hs POLR2A     AAGCCGTGCGGAAGGCCCTGGAGCGGGAGCTGTACCACGTCATCTCCTTTGATGGCTCCT   4560
Oa EST        AGGCTGTACGGAAGGCCCTGGAGCGGGAGCTGTACCACGTCATCTCCTTCGACGGCTCCT   487
              * ** ** ***************************************** ** *******

Hs POLR2A     ATGTCAATTACCGACACTTGGCTCTCTTGTGTGATACCATGACCTGTCGTGGCCACTTGA   4620
Oa EST        ACGTCAATTACCGGCACTTGGCTCTCCTGTGTGATACCA--------------------   526
              * *********** ************ ************
```

>>>>>>>> Forward primer <<<<<<<< Reverse primer

▼ Exon boundary ⋆ Identical nucleotide

Genbank Accession Numbers: Hs POLR2A: NM_000937, Oa EST: CD288457

Glyceraldehyde-3-phosphate dehydrogenase (GAPDH)

```
Hs GAPDH    GGAGTCAACGGATTTGGTCGTATTGGGCGCCTGGTCACCAGGGCTGCTTTTAACTCTGGT  180
Oa GAPDH    GGAGTGAACGGATTTGGCCGCATCGGGCGCCTGGTCACCAGGGCTGCTTTTAATACTGGC  111
            ***** *********** ** ** ****************************  ****

Hs GAPDH    AAAGTGGATATTGTTGCCATCAATGACCCCTTCATTGACCTCAACTACATGGTTTACATG  240
Oa GAPDH    AAAGTGGACATCGTTGCCATCAATGACCCCTTCATTGACCTTCACTACATGGTCTACATG  171
            ******** ** ***************************  ********** ******

                                                  >>>>>>>>>>>>>>>>>>>>
Hs GAPDH    TTCCAATATGATTCCACCCATGGCAAATTCCATGGCACCGTCAAGGCTGAGAACGGGAAG  300
Oa GAPDH    TTCCAGTATGATTCCACCCATGGCAAGTTCCACGGCACAGTCAAGGCAGAGAACGGGAAG  231
            ***** ******************** ***** ***** ******** ************

Hs GAPDH    CTTGTCATCAATGGAAATCCCATCACCATCTTCCAGGAGCGAGATCCCTCCAAAATCAAG  360
Oa GAPDH    CTCGTCATCAATGGAAAGGCCATCACCATCTTCCAGGAGCGAGATCCTGCCAACATCAAG  291
            ** ***************  ****************************  **** ******

                    <<<<<<<<<<<<<<<<<<<<
Hs GAPDH    TGGGGCGATGCTGGCGCTGAGTACGTCGTGGAGTCCACTGGCGTCTTCACCACCATGGAG  420
Oa GAPDH    TGGGGTGATGCTGGTGCTGAGTACGTGGTGGAGTCCACTGGGGTCTTCACTACCATGGAG  351
            ***** ******** *********** ************** ******** *********

Hs GAPDH    AAGGCTGGGGCTCATTTGCAGGGGGGAGCCAAAAGGGTCATCATCTCTGCCCCCTCTGCT  480
Oa GAPDH    AAGGCTGGGGCTCACCTGAAGGGTGGCGCCAAGAGGGTCATCATCTCTGCACCTTCTGCT  411
            ************** ** **** ** ***** ***************** ** ******

Hs GAPDH    GATGCCCCCATGTTCGTCATGGGTGTGAACCATGAGAAGTATGACAACAGCCTCAAGATC  540
Oa GAPDH    GACGCTCCCATGTTTGTGATGGGCGTGAACCACGAGAAGTATAACAATACCCTCAAGATT  471
            ** ** ******** ** ***** ******** ********* **** * *********

Hs GAPDH    ATCAGCAATGCCTCCTGCACCACCAACTGCTTAGCACCCCTGGCCAAGGTCATCCATGAC  600
Oa GAPDH    GTCAGCAATGCCTCCTGCACCACCAACTGCTTGGCCCCCCTGGCCAAGGTCATCCATGAC  531
             ****************************** ** ************************

Hs GAPDH    AACTTTGGTATCGTGGAAGGACTCATGACCACAGTCCATGCCATCACTGCCACCCAGAAG  660
Oa GAPDH    CACTTTGGCATCGTGGAGGGACTTATGACCACTGTCCACGCCATCACTGCCACCCAGAAG  591
             ******* ******** ***** ******** ***** **********************
```

>>>>>>>> Forward primer <<<<<<<< Reverse primer

▼ Exon boundary ⋆ Identical nucleotide

Genbank Accession Numbers: Hs GAPDH: NM_002046, Oa GAPDH: NM_001190390

References

1. Jennings, R.B. and C. Steenbergen, Jr., *Nucleotide metabolism and cellular damage in myocardial ischemia.* Annu Rev Physiol, 1985. **47**: p. 727-49.
2. Cassavaugh, J. and K.M. Lounsbury, *Hypoxia-mediated biological control.* J Cell Biochem, 2011. **112**(3): p. 735-44.
3. Wang, G.L. and G.L. Semenza, *General involvement of hypoxia-inducible factor 1 in transcriptional response to hypoxia.* Proc Natl Acad Sci U S A, 1993. **90**(9): p. 4304-8.
4. Semenza, G.L., *Regulation of oxygen homeostasis by hypoxia-inducible factor 1.* Physiology (Bethesda), 2009. **24**: p. 97-106.
5. Semenza, G.L., *Targeting HIF-1 for cancer therapy.* Nat Rev Cancer, 2003. **3**(10): p. 721-32.
6. Webb, J.D., M.L. Coleman, and C.W. Pugh, *Hypoxia, hypoxia-inducible factors (HIF), HIF hydroxylases and oxygen sensing.* Cell Mol Life Sci, 2009. **66**(22): p. 3539-54.
7. Wang, G.L., et al., *Hypoxia-inducible factor 1 is a basic-helix-loop-helix-PAS heterodimer regulated by cellular O2 tension.* Proc Natl Acad Sci U S A, 1995. **92**(12): p. 5510-4.
8. Wang, G.L. and G.L. Semenza, *Purification and characterization of hypoxia-inducible factor 1.* J Biol Chem, 1995. **270**(3): p. 1230-7.
9. Jiang, B.H., et al., *Hypoxia-inducible factor 1 levels vary exponentially over a physiologically relevant range of O2 tension.* Am J Physiol, 1996. **271**(4 Pt 1): p. C1172-80.
10. Huang, L.E., et al., *Activation of hypoxia-inducible transcription factor depends primarily upon redox-sensitive stabilization of its alpha subunit.* J Biol Chem, 1996. **271**(50): p. 32253-9.
11. Kewley, R.J., M.L. Whitelaw, and A. Chapman-Smith, *The mammalian basic helix-loop-helix/PAS family of transcriptional regulators.* Int J Biochem Cell Biol, 2004. **36**(2): p. 189-204.
12. Jiang, B.H., et al., *Dimerization, DNA binding, and transactivation properties of hypoxia-inducible factor 1.* J Biol Chem, 1996. **271**(30): p. 17771-8.
13. Salceda, S., I. Beck, and J. Caro, *Absolute requirement of aryl hydrocarbon receptor nuclear translocator protein for gene activation by hypoxia.* Arch Biochem Biophys, 1996. **334**(2): p. 389-94.
14. Kallio, P.J., et al., *Signal transduction in hypoxic cells: inducible nuclear translocation and recruitment of the CBP/p300 coactivator by the hypoxia-inducible factor-1alpha.* EMBO J, 1998. **17**(22): p. 6573-86.
15. Semenza, G.L. and G.L. Wang, *A nuclear factor induced by hypoxia via de novo protein synthesis binds to the human erythropoietin gene enhancer at a site required for transcriptional activation.* Mol Cell Biol, 1992. **12**(12): p. 5447-54.
16. Ebert, B.L. and H.F. Bunn, *Regulation of transcription by hypoxia requires a multiprotein complex that includes hypoxia-inducible factor 1, an adjacent transcription factor, and p300/CREB binding protein.* Mol Cell Biol, 1998. **18**(7): p. 4089-96.
17. Ema, M., et al., *Molecular mechanisms of transcription activation by HLF and HIF1alpha in response to hypoxia: their stabilization and redox signal-induced interaction with CBP/p300.* EMBO J, 1999. **18**(7): p. 1905-14.
18. Carrero, P., et al., *Redox-regulated recruitment of the transcriptional coactivators CREB-binding protein and SRC-1 to hypoxia-inducible factor 1alpha.* Mol Cell Biol, 2000. **20**(1): p. 402-15.

19. Arany, Z., et al., *An essential role for p300/CBP in the cellular response to hypoxia.* Proc Natl Acad Sci U S A, 1996. **93**(23): p. 12969-73.
20. Huang, L.E., et al., *Erythropoietin gene regulation depends on heme-dependent oxygen sensing and assembly of interacting transcription factors.* Kidney Int, 1997. **51**(2): p. 548-52.
21. Hogenesch, J.B., et al., *Characterization of a subset of the basic-helix-loop-helix-PAS superfamily that interacts with components of the dioxin signaling pathway.* J Biol Chem, 1997. **272**(13): p. 8581-93.
22. Ema, M., et al., *A novel bHLH-PAS factor with close sequence similarity to hypoxia-inducible factor 1alpha regulates the VEGF expression and is potentially involved in lung and vascular development.* Proc Natl Acad Sci U S A, 1997. **94**(9): p. 4273-8.
23. Flamme, I., et al., *HRF, a putative basic helix-loop-helix-PAS-domain transcription factor is closely related to hypoxia-inducible factor-1 alpha and developmentally expressed in blood vessels.* Mech Dev, 1997. **63**(1): p. 51-60.
24. Tian, H., S.L. McKnight, and D.W. Russell, *Endothelial PAS domain protein 1 (EPAS1), a transcription factor selectively expressed in endothelial cells.* Genes Dev, 1997. **11**(1): p. 72-82.
25. Gu, Y.Z., et al., *Molecular characterization and chromosomal localization of a third alpha-class hypoxia inducible factor subunit, HIF3alpha.* Gene Expr, 1998. **7**(3): p. 205-13.
26. O'Rourke, J.F., et al., *Oxygen-regulated and transactivating domains in endothelial PAS protein 1: comparison with hypoxia-inducible factor-1alpha.* J Biol Chem, 1999. **274**(4): p. 2060-71.
27. Wiesener, M.S., et al., *Induction of endothelial PAS domain protein-1 by hypoxia: characterization and comparison with hypoxia-inducible factor-1alpha.* Blood, 1998. **92**(7): p. 2260-8.
28. Hu, C.J., et al., *Differential roles of hypoxia-inducible factor 1alpha (HIF-1alpha) and HIF-2alpha in hypoxic gene regulation.* Mol Cell Biol, 2003. **23**(24): p. 9361-74.
29. Raval, R.R., et al., *Contrasting properties of hypoxia-inducible factor 1 (HIF-1) and HIF-2 in von Hippel-Lindau-associated renal cell carcinoma.* Mol Cell Biol, 2005. **25**(13): p. 5675-86.
30. Carmeliet, P., et al., *Role of HIF-1alpha in hypoxia-mediated apoptosis, cell proliferation and tumour angiogenesis.* Nature, 1998. **394**(6692): p. 485-90.
31. Compernolle, V., et al., *Loss of HIF-2alpha and inhibition of VEGF impair fetal lung maturation, whereas treatment with VEGF prevents fatal respiratory distress in premature mice.* Nat Med, 2002. **8**(7): p. 702-10.
32. Iyer, N.V., et al., *Cellular and developmental control of O2 homeostasis by hypoxia-inducible factor 1 alpha.* Genes Dev, 1998. **12**(2): p. 149-62.
33. Ryan, H.E., J. Lo, and R.S. Johnson, *HIF-1 alpha is required for solid tumor formation and embryonic vascularization.* EMBO J, 1998. **17**(11): p. 3005-15.
34. Scortegagna, M., et al., *The HIF family member EPAS1/HIF-2alpha is required for normal hematopoiesis in mice.* Blood, 2003. **102**(5): p. 1634-40.
35. Peng, J., et al., *The transcription factor EPAS-1/hypoxia-inducible factor 2alpha plays an important role in vascular remodeling.* Proc Natl Acad Sci U S A, 2000. **97**(15): p. 8386-91.
36. Hara, S., et al., *Expression and characterization of hypoxia-inducible factor (HIF)-3alpha in human kidney: suppression of HIF-mediated gene expression by HIF-3alpha.* Biochem Biophys Res Commun, 2001. **287**(4): p. 808-13.

37. Makino, Y., et al., *Inhibitory PAS domain protein (IPAS) is a hypoxia-inducible splicing variant of the hypoxia-inducible factor-3alpha locus.* J Biol Chem, 2002. **277**(36): p. 32405-8.
38. Maynard, M.A., et al., *Multiple splice variants of the human HIF-3 alpha locus are targets of the von Hippel-Lindau E3 ubiquitin ligase complex.* J Biol Chem, 2003. **278**(13): p. 11032-40.
39. Heikkila, M., et al., *Roles of the human hypoxia-inducible factor (HIF)-3alpha variants in the hypoxia response.* Cell Mol Life Sci, 2011.
40. Park, S.K., et al., *Hypoxia-induced gene expression occurs solely through the action of hypoxia-inducible factor 1alpha (HIF-1alpha): role of cytoplasmic trapping of HIF-2alpha.* Mol Cell Biol, 2003. **23**(14): p. 4959-71.
41. Sowter, H.M., et al., *Predominant role of hypoxia-inducible transcription factor (Hif)-1alpha versus Hif-2alpha in regulation of the transcriptional response to hypoxia.* Cancer Res, 2003. **63**(19): p. 6130-4.
42. Salceda, S. and J. Caro, *Hypoxia-inducible factor 1alpha (HIF-1alpha) protein is rapidly degraded by the ubiquitin-proteasome system under normoxic conditions. Its stabilization by hypoxia depends on redox-induced changes.* J Biol Chem, 1997. **272**(36): p. 22642-7.
43. Huang, L.E., et al., *Regulation of hypoxia-inducible factor 1alpha is mediated by an O2-dependent degradation domain via the ubiquitin-proteasome pathway.* Proc Natl Acad Sci U S A, 1998. **95**(14): p. 7987-92.
44. Jaakkola, P., et al., *Targeting of HIF-alpha to the von Hippel-Lindau ubiquitylation complex by O2-regulated prolyl hydroxylation.* Science, 2001. **292**(5516): p. 468-72.
45. Ivan, M., et al., *HIFalpha targeted for VHL-mediated destruction by proline hydroxylation: implications for O2 sensing.* Science, 2001. **292**(5516): p. 464-8.
46. Masson, N., et al., *Independent function of two destruction domains in hypoxia-inducible factor-alpha chains activated by prolyl hydroxylation.* EMBO J, 2001. **20**(18): p. 5197-206.
47. Tanimoto, K., et al., *Mechanism of regulation of the hypoxia-inducible factor-1 alpha by the von Hippel-Lindau tumor suppressor protein.* EMBO J, 2000. **19**(16): p. 4298-309.
48. Maxwell, P.H., et al., *The tumour suppressor protein VHL targets hypoxia-inducible factors for oxygen-dependent proteolysis.* Nature, 1999. **399**(6733): p. 271-5.
49. Cockman, M.E., et al., *Hypoxia inducible factor-alpha binding and ubiquitylation by the von Hippel-Lindau tumor suppressor protein.* J Biol Chem, 2000. **275**(33): p. 25733-41.
50. Kamura, T., et al., *Activation of HIF1alpha ubiquitination by a reconstituted von Hippel-Lindau (VHL) tumor suppressor complex.* Proc Natl Acad Sci U S A, 2000. **97**(19): p. 10430-5.
51. Ohh, M., et al., *Ubiquitination of hypoxia-inducible factor requires direct binding to the beta-domain of the von Hippel-Lindau protein.* Nat Cell Biol, 2000. **2**(7): p. 423-7.
52. Epstein, A.C., et al., *C. elegans EGL-9 and mammalian homologs define a family of dioxygenases that regulate HIF by prolyl hydroxylation.* Cell, 2001. **107**(1): p. 43-54.
53. Bruick, R.K. and S.L. McKnight, *A conserved family of prolyl-4-hydroxylases that modify HIF.* Science, 2001. **294**(5545): p. 1337-40.

54. Aprelikova, O., et al., *Regulation of HIF prolyl hydroxylases by hypoxia-inducible factors.* J Cell Biochem, 2004. **92**(3): p. 491-501.
55. Marxsen, J.H., et al., *Hypoxia-inducible factor-1 (HIF-1) promotes its degradation by induction of HIF-alpha-prolyl-4-hydroxylases.* Biochem J, 2004. **381**(Pt 3): p. 761-7.
56. Lando, D., et al., *Asparagine hydroxylation of the HIF transactivation domain a hypoxic switch.* Science, 2002. **295**(5556): p. 858-61.
57. Hewitson, K.S., et al., *Hypoxia-inducible factor (HIF) asparagine hydroxylase is identical to factor inhibiting HIF (FIH) and is related to the cupin structural family.* J Biol Chem, 2002. **277**(29): p. 26351-5.
58. Lando, D., et al., *FIH-1 is an asparaginyl hydroxylase enzyme that regulates the transcriptional activity of hypoxia-inducible factor.* Genes Dev, 2002. **16**(12): p. 1466-71.
59. McNeill, L.A., et al., *Hypoxia-inducible factor asparaginyl hydroxylase (FIH-1) catalyses hydroxylation at the beta-carbon of asparagine-803.* Biochem J, 2002. **367**(Pt 3): p. 571-5.
60. Dames, S.A., et al., *Structural basis for Hif-1 alpha /CBP recognition in the cellular hypoxic response.* Proc Natl Acad Sci U S A, 2002. **99**(8): p. 5271-6.
61. Freedman, S.J., et al., *Structural basis for recruitment of CBP/p300 by hypoxia-inducible factor-1 alpha.* Proc Natl Acad Sci U S A, 2002. **99**(8): p. 5367-72.
62. Loenarz, C. and C.J. Schofield, *Physiological and biochemical aspects of hydroxylations and demethylations catalyzed by human 2-oxoglutarate oxygenases.* Trends Biochem Sci, 2011. **36**(1): p. 7-18.
63. Hewitson, K.S., et al., *Oxidation by 2-oxoglutarate oxygenases: non-haem iron systems in catalysis and signalling.* Philos Transact A Math Phys Eng Sci, 2005. **363**(1829): p. 807-28; discussion 1035-40.
64. Semenza, G.L., *Hypoxia-inducible factor 1: oxygen homeostasis and disease pathophysiology.* Trends Mol Med, 2001. **7**(8): p. 345-50.
65. Ehrismann, D., et al., *Studies on the activity of the hypoxia-inducible-factor hydroxylases using an oxygen consumption assay.* Biochem J, 2007. **401**(1): p. 227-34.
66. Koivunen, P., et al., *Catalytic properties of the asparaginyl hydroxylase (FIH) in the oxygen sensing pathway are distinct from those of its prolyl 4-hydroxylases.* J Biol Chem, 2004. **279**(11): p. 9899-904.
67. Hirsila, M., et al., *Characterization of the human prolyl 4-hydroxylases that modify the hypoxia-inducible factor.* J Biol Chem, 2003. **278**(33): p. 30772-80.
68. Chandel, N.S., et al., *Mitochondrial reactive oxygen species trigger hypoxia-induced transcription.* Proc Natl Acad Sci U S A, 1998. **95**(20): p. 11715-20.
69. Simon, M.C., *Mitochondrial reactive oxygen species are required for hypoxic HIF alpha stabilization.* Adv Exp Med Biol, 2006. **588**: p. 165-70.
70. Bell, E.L., et al., *The Qo site of the mitochondrial complex III is required for the transduction of hypoxic signaling via reactive oxygen species production.* J Cell Biol, 2007. **177**(6): p. 1029-36.
71. Agani, F.H., et al., *The role of mitochondria in the regulation of hypoxia-inducible factor 1 expression during hypoxia.* J Biol Chem, 2000. **275**(46): p. 35863-7.
72. Guzy, R.D. and P.T. Schumacker, *Oxygen sensing by mitochondria at complex III: the paradox of increased reactive oxygen species during hypoxia.* Exp Physiol, 2006. **91**(5): p. 807-19.

73. Enomoto, N., et al., *Hypoxic induction of hypoxia-inducible factor-1alpha and oxygen-regulated gene expression in mitochondrial DNA-depleted HeLa cells.* Biochem Biophys Res Commun, 2002. **297**(2): p. 346-52.
74. Pouyssegur, J. and F. Mechta-Grigoriou, *Redox regulation of the hypoxia-inducible factor.* Biol Chem, 2006. **387**(10-11): p. 1337-46.
75. Vaux, E.C., et al., *Regulation of hypoxia-inducible factor is preserved in the absence of a functioning mitochondrial respiratory chain.* Blood, 2001. **98**(2): p. 296-302.
76. Masson, N., et al., *The FIH hydroxylase is a cellular peroxide sensor that modulates HIF transcriptional activity.* EMBO Rep, 2012. **13**(3): p. 251-7.
77. Gerald, D., et al., *JunD reduces tumor angiogenesis by protecting cells from oxidative stress.* Cell, 2004. **118**(6): p. 781-94.
78. Pan, Y., et al., *Multiple factors affecting cellular redox status and energy metabolism modulate hypoxia-inducible factor prolyl hydroxylase activity in vivo and in vitro.* Mol Cell Biol, 2007. **27**(3): p. 912-25.
79. Diebold, I., et al., *The hypoxia-inducible factor-2alpha is stabilized by oxidative stress involving NOX4.* Antioxid Redox Signal, 2010. **13**(4): p. 425-36.
80. Jiang, B.H., et al., *Transactivation and inhibitory domains of hypoxia-inducible factor 1alpha. Modulation of transcriptional activity by oxygen tension.* J Biol Chem, 1997. **272**(31): p. 19253-60.
81. Pugh, C.W., et al., *Activation of hypoxia-inducible factor-1; definition of regulatory domains within the alpha subunit.* J Biol Chem, 1997. **272**(17): p. 11205-14.
82. Yan, Q., et al., *The hypoxia-inducible factor 2alpha N-terminal and C-terminal transactivation domains cooperate to promote renal tumorigenesis in vivo.* Mol Cell Biol, 2007. **27**(6): p. 2092-102.
83. Dayan, F., et al., *The oxygen sensor factor-inhibiting hypoxia-inducible factor-1 controls expression of distinct genes through the bifunctional transcriptional character of hypoxia-inducible factor-1alpha.* Cancer Res, 2006. **66**(7): p. 3688-98.
84. Stolze, I.P., et al., *Genetic analysis of the role of the asparaginyl hydroxylase factor inhibiting hypoxia-inducible factor (FIH) in regulating hypoxia-inducible factor (HIF) transcriptional target genes [corrected].* J Biol Chem, 2004. **279**(41): p. 42719-25.
85. Zhang, N., et al., *The asparaginyl hydroxylase factor inhibiting HIF-1alpha is an essential regulator of metabolism.* Cell Metab, 2010. **11**(5): p. 364-78.
86. Cockman, M.E., et al., *Posttranslational hydroxylation of ankyrin repeats in IkappaB proteins by the hypoxia-inducible factor (HIF) asparaginyl hydroxylase, factor inhibiting HIF (FIH).* Proc Natl Acad Sci U S A, 2006. **103**(40): p. 14767-72.
87. Schultz, J., et al., *SMART, a simple modular architecture research tool: identification of signaling domains.* Proc Natl Acad Sci U S A, 1998. **95**(11): p. 5857-64.
88. Mosavi, L.K., et al., *The ankyrin repeat as molecular architecture for protein recognition.* Protein Sci, 2004. **13**(6): p. 1435-48.
89. Li, J., A. Mahajan, and M.D. Tsai, *Ankyrin repeat: a unique motif mediating protein-protein interactions.* Biochemistry, 2006. **45**(51): p. 15168-78.
90. Sedgwick, S.G. and S.J. Smerdon, *The ankyrin repeat: a diversity of interactions on a common structural framework.* Trends Biochem Sci, 1999. **24**(8): p. 311-6.
91. Huxford, T., et al., *The crystal structure of the IkappaBalpha/NF-kappaB complex reveals mechanisms of NF-kappaB inactivation.* Cell, 1998. **95**(6): p. 759-70.
92. Pettersen, E.F., et al., *UCSF Chimera--a visualization system for exploratory research and analysis.* J Comput Chem, 2004. **25**(13): p. 1605-12.

93. Mosavi, L.K., D.L. Minor, Jr., and Z.Y. Peng, *Consensus-derived structural determinants of the ankyrin repeat motif.* Proc Natl Acad Sci U S A, 2002. **99**(25): p. 16029-34.
94. Zheng, X., et al., *Interaction with factor inhibiting HIF-1 defines an additional mode of cross-coupling between the Notch and hypoxia signaling pathways.* Proc Natl Acad Sci U S A, 2008. **105**(9): p. 3368-73.
95. Coleman, M.L., et al., *Asparaginyl hydroxylation of the Notch ankyrin repeat domain by factor inhibiting hypoxia-inducible factor.* J Biol Chem, 2007. **282**(33): p. 24027-38.
96. Artavanis-Tsakonas, S., M.D. Rand, and R.J. Lake, *Notch signaling: cell fate control and signal integration in development.* Science, 1999. **284**(5415): p. 770-6.
97. Fleming, R.J., *Structural conservation of Notch receptors and ligands.* Semin Cell Dev Biol, 1998. **9**(6): p. 599-607.
98. Shin, D.H., et al., *Inhibitor of nuclear factor-kappaB alpha derepresses hypoxia-inducible factor-1 during moderate hypoxia by sequestering factor inhibiting hypoxia-inducible factor from hypoxia-inducible factor 1alpha.* FEBS J, 2009. **276**(13): p. 3470-80.
99. Ferguson, J.E., 3rd, et al., *ASB4 is a hydroxylation substrate of FIH and promotes vascular differentiation via an oxygen-dependent mechanism.* Mol Cell Biol, 2007. **27**(18): p. 6407-19.
100. Wilkins, S.E., et al., *Differences in hydroxylation and binding of Notch and HIF-1alpha demonstrate substrate selectivity for factor inhibiting HIF-1 (FIH-1).* Int J Biochem Cell Biol, 2009. **41**(7): p. 1563-71.
101. Cockman, M.E., et al., *Proteomics-based identification of novel factor inhibiting hypoxia-inducible factor (FIH) substrates indicates widespread asparaginyl hydroxylation of ankyrin repeat domain-containing proteins.* Mol Cell Proteomics, 2009. **8**(3): p. 535-46.
102. Cockman, M.E., J.D. Webb, and P.J. Ratcliffe, *FIH-dependent asparaginyl hydroxylation of ankyrin repeat domain-containing proteins.* Ann N Y Acad Sci, 2009. **1177**: p. 9-18.
103. Webb, J.D., et al., *MYPT1, the targeting subunit of smooth-muscle myosin phosphatase, is a substrate for the asparaginyl hydroxylase factor inhibiting hypoxia-inducible factor (FIH).* Biochem J, 2009. **420**(2): p. 327-33.
104. Yang, M., et al., *Asparagine and aspartate hydroxylation of the cytoskeletal ankyrin family is catalyzed by factor-inhibiting hypoxia-inducible factor.* J Biol Chem, 2011. **286**(9): p. 7648-60.
105. Linke, S., R.J. Hampton-Smith, and D.J. Peet, *Characterization of ankyrin repeat-containing proteins as substrates of the asparaginyl hydroxylase factor inhibiting hypoxia-inducible transcription factor.* Methods Enzymol, 2007. **435**: p. 61-85.
106. Kelly, L., et al., *Asparagine beta-hydroxylation stabilizes the ankyrin repeat domain fold.* Mol Biosyst, 2009. **5**(1): p. 52-8.
107. Mumm, J.S. and R. Kopan, *Notch signaling: from the outside in.* Dev Biol, 2000. **228**(2): p. 151-65.
108. Gustafsson, M.V., et al., *Hypoxia requires notch signaling to maintain the undifferentiated cell state.* Dev Cell, 2005. **9**(5): p. 617-28.
109. Swiatek, P.J., et al., *Notch1 is essential for postimplantation development in mice.* Genes Dev, 1994. **8**(6): p. 707-19.

110. Conlon, R.A., A.G. Reaume, and J. Rossant, *Notch1 is required for the coordinate segmentation of somites.* Development, 1995. **121**(5): p. 1533-45.
111. Hamada, Y., et al., *Mutation in ankyrin repeats of the mouse Notch2 gene induces early embryonic lethality.* Development, 1999. **126**(15): p. 3415-24.
112. McCright, B., et al., *Defects in development of the kidney, heart and eye vasculature in mice homozygous for a hypomorphic Notch2 mutation.* Development, 2001. **128**(4): p. 491-502.
113. Hardy, A.P., et al., *Asparaginyl beta-hydroxylation of proteins containing ankyrin repeat domains influences their stability and function.* J Mol Biol, 2009. **392**(4): p. 994-1006.
114. Devries, I.L., et al., *Consequences of IkappaB alpha hydroxylation by the factor inhibiting HIF (FIH).* FEBS Lett, 2010. **584**(23): p. 4725-30.
115. Dann, C.E., 3rd, R.K. Bruick, and J. Deisenhofer, *Structure of factor-inhibiting hypoxia-inducible factor 1: An asparaginyl hydroxylase involved in the hypoxic response pathway.* Proc Natl Acad Sci U S A, 2002. **99**(24): p. 15351-6.
116. Elkins, J.M., et al., *Structure of factor-inhibiting hypoxia-inducible factor (HIF) reveals mechanism of oxidative modification of HIF-1 alpha.* J Biol Chem, 2003. **278**(3): p. 1802-6.
117. Lee, C., et al., *Structure of human FIH-1 reveals a unique active site pocket and interaction sites for HIF-1 and von Hippel-Lindau.* J Biol Chem, 2003. **278**(9): p. 7558-63.
118. Lancaster, D.E., et al., *Disruption of dimerization and substrate phosphorylation inhibit factor inhibiting hypoxia-inducible factor (FIH) activity.* Biochem J, 2004. **383**(Pt. 3): p. 429-37.
119. McDonough, M.A., et al., *Structural studies on human 2-oxoglutarate dependent oxygenases.* Curr Opin Struct Biol, 2010. **20**(6): p. 659-72.
120. Trewick, S.C., P.J. McLaughlin, and R.C. Allshire, *Methylation: lost in hydroxylation?* EMBO Rep, 2005. **6**(4): p. 315-20.
121. Klose, R.J., E.M. Kallin, and Y. Zhang, *JmjC-domain-containing proteins and histone demethylation.* Nat Rev Genet, 2006. **7**(9): p. 715-27.
122. Schofield, C.J. and Z. Zhang, *Structural and mechanistic studies on 2-oxoglutarate-dependent oxygenases and related enzymes.* Curr Opin Struct Biol, 1999. **9**(6): p. 722-31.
123. Myllyla, R., et al., *Ascorbate is consumed stoichiometrically in the uncoupled reactions catalyzed by prolyl 4-hydroxylase and lysyl hydroxylase.* J Biol Chem, 1984. **259**(9): p. 5403-5.
124. Hausinger, R.P., *FeII/alpha-ketoglutarate-dependent hydroxylases and related enzymes.* Crit Rev Biochem Mol Biol, 2004. **39**(1): p. 21-68.
125. Ozer, A. and R.K. Bruick, *Non-heme dioxygenases: cellular sensors and regulators jelly rolled into one?* Nat Chem Biol, 2007. **3**(3): p. 144-53.
126. Bracken, C.P., et al., *Cell-specific regulation of hypoxia-inducible factor (HIF)-1alpha and HIF-2alpha stabilization and transactivation in a graded oxygen environment.* J Biol Chem, 2006. **281**(32): p. 22575-85.
127. Linke, S., et al., *Substrate requirements of the oxygen-sensing asparaginyl hydroxylase factor-inhibiting hypoxia-inducible factor.* J Biol Chem, 2004. **279**(14): p. 14391-7.
128. McKeever, D.J., et al., *Studies of the pathogenesis of orf virus infection in sheep.* J Comp Pathol, 1988. **99**(3): p. 317-28.

129. Schofield, C.J. and P.J. Ratcliffe, *Signalling hypoxia by HIF hydroxylases.* Biochem Biophys Res Commun, 2005. **338**(1): p. 617-26.
130. Coleman, M.L. and P.J. Ratcliffe, *Signalling cross talk of the HIF system: involvement of the FIH protein.* Curr Pharm Des, 2009. **15**(33): p. 3904-7.
131. Sonnberg, S., S.B. Fleming, and A.A. Mercer, *Phylogenetic analysis of the large family of poxvirus ankyrin-repeat proteins reveals orthologue groups within and across chordopoxvirus genera.* J Gen Virol, 2011. **92**(Pt 11): p. 2596-607.
132. Haig, D.M. and A.A. Mercer, *Ovine diseases. Orf.* Vet Res, 1998. **29**(3-4): p. 311-26.
133. Whelan, F., *The Aryl Hydrocarbon Receptor: Structural Analysis and Activation Mechanisms*, in *Biochemistry*. 2008, The University of Adelaide: Adelaide, Australia.
134. Sheffield, P., S. Garrard, and Z. Derewenda, *Overcoming expression and purification problems of RhoGDI using a family of "parallel" expression vectors.* Protein Expr Purif, 1999. **15**(1): p. 34-9.
135. Kholod, N. and T. Mustelin, *Novel vectors for co-expression of two proteins in E. coli.* Biotechniques, 2001. **31**(2): p. 322-3, 326-8.
136. Wilkins, S.E., et al., *Factor inhibiting HIF (FIH) recognises distinct molecular features within hypoxia inducible factor (HIF)-alpha versus ankyrin repeat substrates.* J Biol Chem, 2012.
137. Sonnberg, S., et al., *Poxvirus ankyrin repeat proteins are a unique class of F-box proteins that associate with cellular SCF1 ubiquitin ligase complexes.* Proc Natl Acad Sci U S A, 2008. **105**(31): p. 10955-60.
138. Muller, P.Y., et al., *Processing of gene expression data generated by quantitative real-time RT-PCR.* Biotechniques, 2002. **32**(6): p. 1372-4, 1376, 1378-9.
139. Rozen, S. and H. Skaletsky, *Primer3 on the WWW for general users and for biologist programmers.* Methods Mol Biol, 2000. **132**: p. 365-86.
140. Raussens, V., J.M. Ruysschaert, and E. Goormaghtigh, *Protein concentration is not an absolute prerequisite for the determination of secondary structure from circular dichroism spectra: a new scaling method.* Anal Biochem, 2003. **319**(1): p. 114-21.
141. Whitmore, L. and B.A. Wallace, *DICHROWEB, an online server for protein secondary structure analyses from circular dichroism spectroscopic data.* Nucleic Acids Res, 2004. **32**(Web Server issue): p. W668-73.
142. Johnson, W.C., *Analyzing protein circular dichroism spectra for accurate secondary structures.* Proteins, 1999. **35**(3): p. 307-12.
143. Wilkins, S.E., *Characterising the Notch receptor family as substrates for FIH-1*, in *Biochemistry*. 2006, The University of Adelaide: Adelaide, Australia. p. 112.
144. Nandi, S., U.K. De, and S. Chowdhury, *Current status of contagious ecthyma or orf disease in goat and sheep—A global perspective.* Small Ruminant Research, 2011. **96**(2–3): p. 73-82.
145. Ehebauer, M.T., et al., *High-resolution crystal structure of the human Notch 1 ankyrin domain.* Biochem J, 2005. **392**(Pt 1): p. 13-20.
146. Rhoads, R.E. and S. Udenfriend, *Decarboxylation of alpha-ketoglutarate coupled to collagen proline hydroxylase.* Proc Natl Acad Sci U S A, 1968. **60**(4): p. 1473-8.
147. Stenflo, J., et al., *Hydroxylation of aspartic acid in domains homologous to the epidermal growth factor precursor is catalyzed by a 2-oxoglutarate-dependent dioxygenase.* Proc Natl Acad Sci U S A, 1989. **86**(2): p. 444-7.
148. Wilkins, M.R., et al., *Protein identification and analysis tools in the ExPASy server.* Methods Mol Biol, 1999. **112**: p. 531-52.

149. Koivunen, P., et al., *The length of peptide substrates has a marked effect on hydroxylation by the hypoxia-inducible factor prolyl 4-hydroxylases.* J Biol Chem, 2006. **281**(39): p. 28712-20.
150. McDonough, M.A., et al., *Selective inhibition of factor inhibiting hypoxia-inducible factor.* J Am Chem Soc, 2005. **127**(21): p. 7680-1.
151. Bradley, C.M. and D. Barrick, *The notch ankyrin domain folds via a discrete, centralized pathway.* Structure, 2006. **14**(8): p. 1303-12.
152. Mello, C.C., et al., *Experimental characterization of the folding kinetics of the notch ankyrin domain.* J Mol Biol, 2005. **352**(2): p. 266-81.
153. Truhlar, S.M., J.W. Torpey, and E.A. Komives, *Regions of IkappaBalpha that are critical for its inhibition of NF-kappaB.DNA interaction fold upon binding to NF-kappaB.* Proc Natl Acad Sci U S A, 2006. **103**(50): p. 18951-6.
154. Singleton, R.S., et al., *Quantitative mass spectrometry reveals dynamics of factor-inhibiting hypoxia-inducible factor-catalyzed hydroxylation.* J Biol Chem, 2011. **286**(39): p. 33784-94.
155. Lefkowitz, E.J., C. Wang, and C. Upton, *Poxviruses: past, present and future.* Virus Res, 2006. **117**(1): p. 105-18.
156. Hicke, L., *Protein regulation by monoubiquitin.* Nat Rev Mol Cell Biol, 2001. **2**(3): p. 195-201.
157. Essbauer, S., M. Pfeffer, and H. Meyer, *Zoonotic poxviruses.* Vet Microbiol, 2010. **140**(3-4): p. 229-36.
158. Walsh, S.R. and R. Dolin, *Vaccinia viruses: vaccines against smallpox and vectors against infectious diseases and tumors.* Expert Rev Vaccines, 2011. **10**(8): p. 1221-40.
159. Buttner, M. and H.J. Rziha, *Parapoxviruses: from the lesion to the viral genome.* J Vet Med B Infect Dis Vet Public Health, 2002. **49**(1): p. 7-16.
160. Shelley, W.B. and E.D. Shelley, *Farmyard pox: parapox virus infection in man.* Br J Dermatol, 1983. **108**(6): p. 725-7.
161. McFadden, G., *Poxvirus tropism.* Nat Rev Microbiol, 2005. **3**(3): p. 201-13.
162. Haig, D.M., et al., *Orf virus immuno-modulation and the host immune response.* Vet Immunol Immunopathol, 2002. **87**(3-4): p. 395-9.
163. Counago, R.M., et al., *Crystallization and preliminary X-ray analysis of the chemokine-binding protein from orf virus (Poxviridae).* Acta Crystallogr Sect F Struct Biol Cryst Commun, 2010. **66**(Pt 7): p. 819-23.
164. Fleming, S.B., et al., *Infection with recombinant orf viruses demonstrates that the viral interleukin-10 is a virulence factor.* J Gen Virol, 2007. **88**(Pt 7): p. 1922-7.
165. McInnes, C.J., A.R. Wood, and A.A. Mercer, *Orf virus encodes a homolog of the vaccinia virus interferon-resistance gene E3L.* Virus Genes, 1998. **17**(2): p. 107-15.
166. Deane, D., et al., *Orf virus encodes a novel secreted protein inhibitor of granulocyte-macrophage colony-stimulating factor and interleukin-2.* J Virol, 2000. **74**(3): p. 1313-20.
167. Lateef, Z., et al., *Orf virus-encoded chemokine-binding protein is a potent inhibitor of inflammatory monocyte recruitment in a mouse skin model.* J Gen Virol, 2009. **90**(Pt 6): p. 1477-82.
168. Mo, M., S.B. Fleming, and A.A. Mercer, *Orf virus cell cycle regulator, PACR, competes with subunit 11 of the anaphase promoting complex for incorporation into the complex.* J Gen Virol, 2010. **91**(Pt 12): p. 3010-5.

169. Westphal, D., et al., *The orf virus inhibitor of apoptosis functions in a Bcl-2-like manner, binding and neutralizing a set of BH3-only proteins and active Bax.* Apoptosis, 2009. **14**(11): p. 1317-30.
170. Sonnberg, S., S.B. Fleming, and A.A. Mercer, *A truncated two-alpha-helix F-box present in poxvirus ankyrin-repeat proteins is sufficient for binding the SCF1 ubiquitin ligase complex.* J Gen Virol, 2009. **90**(Pt 5): p. 1224-8.
171. Mercer, A.A., S.B. Fleming, and N. Ueda, *F-box-like domains are present in most poxvirus ankyrin repeat proteins.* Virus Genes, 2005. **31**(2): p. 127-33.
172. Zhang, L., N.Y. Villa, and G. McFadden, *Interplay between poxviruses and the cellular ubiquitin/ubiquitin-like pathways.* FEBS Lett, 2009. **583**(4): p. 607-14.
173. Sato, K. and K. Yoshida, *Augmentation of the ubiquitin-mediated proteolytic system by F-box and additional motif-containing proteins (Review).* Int J Oncol, 2010. **37**(5): p. 1071-6.
174. Nakamura, M., et al., *Hypoxia-specific stabilization of HIF-1alpha by human papillomaviruses.* Virology, 2009. **387**(2): p. 442-8.
175. Moon, E.J., et al., *Hepatitis B virus X protein induces angiogenesis by stabilizing hypoxia-inducible factor-1alpha.* FASEB J, 2004. **18**(2): p. 382-4.
176. Yoo, Y.G., et al., *Hepatitis B virus X protein enhances transcriptional activity of hypoxia-inducible factor-1alpha through activation of mitogen-activated protein kinase pathway.* J Biol Chem, 2003. **278**(40): p. 39076-84.
177. Nasimuzzaman, M., et al., *Hepatitis C virus stabilizes hypoxia-inducible factor 1alpha and stimulates the synthesis of vascular endothelial growth factor.* J Virol, 2007. **81**(19): p. 10249-57.
178. Deshmane, S.L., et al., *Activation of the oxidative stress pathway by HIV-1 Vpr leads to induction of hypoxia-inducible factor 1alpha expression.* J Biol Chem, 2009. **284**(17): p. 11364-73.
179. Korgaonkar, S.N., et al., *HIV-1 upregulates VEGF in podocytes.* J Am Soc Nephrol, 2008. **19**(5): p. 877-83.
180. Lyttle, D.J., et al., *Homologs of vascular endothelial growth factor are encoded by the poxvirus orf virus.* J Virol, 1994. **68**(1): p. 84-92.
181. Meyer, M., et al., *A novel vascular endothelial growth factor encoded by Orf virus, VEGF-E, mediates angiogenesis via signalling through VEGFR-2 (KDR) but not VEGFR-1 (Flt-1) receptor tyrosine kinases.* EMBO J, 1999. **18**(2): p. 363-74.
182. Ogawa, S., et al., *A novel type of vascular endothelial growth factor, VEGF-E (NZ-7 VEGF), preferentially utilizes KDR/Flk-1 receptor and carries a potent mitotic activity without heparin-binding domain.* J Biol Chem, 1998. **273**(47): p. 31273-82.
183. Savory, L.J., et al., *Viral vascular endothelial growth factor plays a critical role in orf virus infection.* J Virol, 2000. **74**(22): p. 10699-706.
184. Wise, L.M., et al., *Vascular endothelial growth factor (VEGF)-like protein from orf virus NZ2 binds to VEGFR2 and neuropilin-1.* Proc Natl Acad Sci U S A, 1999. **96**(6): p. 3071-6.
185. Buchan, D.W., et al., *Protein annotation and modelling servers at University College London.* Nucleic Acids Res, 2010. **38**(Web Server issue): p. W563-8.
186. Hussain, K.A. and D. Burger, *In vivo and in vitro characteristics of contagious ecthyma virus isolates: host response mechanism.* Vet Microbiol, 1989. **19**(1): p. 23-36.

187. Wise, L.M., et al., *Major amino acid sequence variants of viral vascular endothelial growth factor are functionally equivalent during Orf virus infection of sheep skin.* Virus Res, 2007. **128**(1-2): p. 115-25.
188. Mossman, K., et al., *Disruption of M-T5, a novel myxoma virus gene member of poxvirus host range superfamily, results in dramatic attenuation of myxomatosis in infected European rabbits.* J Virol, 1996. **70**(7): p. 4394-410.
189. Metzen, E., et al., *Intracellular localisation of human HIF-1 alpha hydroxylases: implications for oxygen sensing.* J Cell Sci, 2003. **116**(Pt 7): p. 1319-26.
190. Balassu, T.C. and A.J. Robinson, *Orf virus replication in bovine testis cells: kinetics of viral DNA, polypeptide, and infectious virus production and analysis of virion polypeptides.* Arch Virol, 1987. **97**(3-4): p. 267-81.
191. Mo, M., S.B. Fleming, and A.A. Mercer, *Cell cycle deregulation by a poxvirus partial mimic of anaphase-promoting complex subunit 11.* Proc Natl Acad Sci U S A, 2009. **106**(46): p. 19527-32.
192. Yen, H.C. and S.J. Elledge, *Identification of SCF ubiquitin ligase substrates by global protein stability profiling.* Science, 2008. **322**(5903): p. 923-9.
193. Werden, S.J., et al., *The myxoma virus m-t5 ankyrin repeat host range protein is a novel adaptor that coordinately links the cellular signaling pathways mediated by Akt and Skp1 in virus-infected cells.* J Virol, 2009. **83**(23): p. 12068-83.
194. Chang, S.J., et al., *Poxvirus host range protein CP77 contains an F-box-like domain that is necessary to suppress NF-kappaB activation by tumor necrosis factor alpha but is independent of its host range function.* J Virol, 2009. **83**(9): p. 4140-52.
195. Camus-Bouclainville, C., et al., *A virulence factor of myxoma virus colocalizes with NF-kappaB in the nucleus and interferes with inflammation.* J Virol, 2004. **78**(5): p. 2510-6.
196. Mohamed, M.R., et al., *Proteomic screening of variola virus reveals a unique NF-kappaB inhibitor that is highly conserved among pathogenic orthopoxviruses.* Proc Natl Acad Sci U S A, 2009. **106**(22): p. 9045-50.
197. Nishioka, Y. and S. Silverstein, *Requirement of protein synthesis for the degradation of host mRNA in Friend erythroleukemia cells infected wtih herpes simplex virus type 1.* J Virol, 1978. **27**(3): p. 619-27.
198. Strom, T. and N. Frenkel, *Effects of herpes simplex virus on mRNA stability.* J Virol, 1987. **61**(7): p. 2198-207.
199. Crawford, N., et al., *Inhibition of transcription factor activity by poliovirus.* Cell, 1981. **27**(3 Pt 2): p. 555-61.
200. McGowan, J.J., S.U. Emerson, and R.R. Wagner, *The plus-strand leader RNA of VSV inhibits DNA-dependent transcription of adenovirus and SV40 genes in a soluble whole-cell extract.* Cell, 1982. **28**(2): p. 325-33.
201. Parrish, S. and B. Moss, *Characterization of a vaccinia virus mutant with a deletion of the D10R gene encoding a putative negative regulator of gene expression.* J Virol, 2006. **80**(2): p. 553-61.
202. Parrish, S. and B. Moss, *Characterization of a second vaccinia virus mRNA-decapping enzyme conserved in poxviruses.* J Virol, 2007. **81**(23): p. 12973-8.
203. Parrish, S., W. Resch, and B. Moss, *Vaccinia virus D10 protein has mRNA decapping activity, providing a mechanism for control of host and viral gene expression.* Proc Natl Acad Sci U S A, 2007. **104**(7): p. 2139-44.
204. Shors, T., J.G. Keck, and B. Moss, *Down regulation of gene expression by the vaccinia virus D10 protein.* J Virol, 1999. **73**(1): p. 791-6.

205. Smith, S.A. and G.J. Kotwal, *Immune response to poxvirus infections in various animals.* Crit Rev Microbiol, 2002. **28**(3): p. 149-85.
206. Semenza, G.L., *Defining the role of hypoxia-inducible factor 1 in cancer biology and therapeutics.* Oncogene, 2010. **29**(5): p. 625-34.
207. Brahimi-Horn, M.C. and J. Pouyssegur, *Harnessing the hypoxia-inducible factor in cancer and ischemic disease.* Biochem Pharmacol, 2007. **73**(3): p. 450-7.
208. t Hoen, P.A., et al., *Deep sequencing-based expression analysis shows major advances in robustness, resolution and inter-lab portability over five microarray platforms.* Nucleic Acids Res, 2008. **36**(21): p. e141.
209. Jung, Y., et al., *Hypoxia-inducible factor induction by tumour necrosis factor in normoxic cells requires receptor-interacting protein-dependent nuclear factor kappa B activation.* Biochem J, 2003. **370**(Pt 3): p. 1011-7.
210. Jung, Y.J., et al., *IL-1beta-mediated up-regulation of HIF-1alpha via an NFkappaB/COX-2 pathway identifies HIF-1 as a critical link between inflammation and oncogenesis.* FASEB J, 2003. **17**(14): p. 2115-7.
211. Reddy, S.A., J.H. Huang, and W.S. Liao, *Phosphatidylinositol 3-kinase as a mediator of TNF-induced NF-kappa B activation.* J Immunol, 2000. **164**(3): p. 1355-63.
212. Scheid, A., et al., *Physiologically low oxygen concentrations in fetal skin regulate hypoxia-inducible factor 1 and transforming growth factor-beta3.* FASEB J, 2002. **16**(3): p. 411-3.
213. Chang, C.W., et al., *Increased ATP generation in the host cell is required for efficient vaccinia virus production.* J Biomed Sci, 2009. **16**: p. 80.
214. Schmierer, B., B. Novak, and C.J. Schofield, *Hypoxia-dependent sequestration of an oxygen sensor by a widespread structural motif can shape the hypoxic response--a predictive kinetic model.* BMC Syst Biol, 2010. **4**: p. 139.
215. Yang, M., et al., *Factor-inhibiting hypoxia-inducible factor (FIH) catalyses the post-translational hydroxylation of histidinyl residues within ankyrin repeat domains.* FEBS J, 2011. **278**(7): p. 1086-97.
216. Shimoda, L.A. and J. Polak, *Hypoxia. 4. Hypoxia and ion channel function.* Am J Physiol Cell Physiol, 2011. **300**(5): p. C951-67.
217. Eden, E., et al., *Proteome half-life dynamics in living human cells.* Science, 2011. **331**(6018): p. 764-8.
218. Rupec, R.A. and P.A. Baeuerle, *The genomic response of tumor cells to hypoxia and reoxygenation. Differential activation of transcription factors AP-1 and NF-kappa B.* Eur J Biochem, 1995. **234**(2): p. 632-40.
219. Simon, M.C. and B. Keith, *The role of oxygen availability in embryonic development and stem cell function.* Nat Rev Mol Cell Biol, 2008. **9**(4): p. 285-96.
220. Maher, E.R., H.P. Neumann, and S. Richard, *von Hippel-Lindau disease: a clinical and scientific review.* Eur J Hum Genet, 2011. **19**(6): p. 617-23.
221. Mandriota, S.J., et al., *HIF activation identifies early lesions in VHL kidneys: evidence for site-specific tumor suppressor function in the nephron.* Cancer Cell, 2002. **1**(5): p. 459-68.
222. Rechsteiner, M.P., et al., *VHL gene mutations and their effects on hypoxia inducible factor HIFalpha: identification of potential driver and passenger mutations.* Cancer Res, 2011. **71**(16): p. 5500-11.
223. Zhong, H., et al., *Modulation of hypoxia-inducible factor 1alpha expression by the epidermal growth factor/phosphatidylinositol 3-kinase/PTEN/AKT/FRAP pathway*

in human prostate cancer cells: implications for tumor angiogenesis and therapeutics. Cancer Res, 2000. **60**(6): p. 1541-5.
224. Thornton, R.D., et al., *Interleukin 1 induces hypoxia-inducible factor 1 in human gingival and synovial fibroblasts.* Biochem J, 2000. **350 Pt 1**: p. 307-12.
225. Treins, C., et al., *Insulin stimulates hypoxia-inducible factor 1 through a phosphatidylinositol 3-kinase/target of rapamycin-dependent signaling pathway.* J Biol Chem, 2002. **277**(31): p. 27975-81.
226. Sachdev, S., A. Hoffmann, and M. Hannink, *Nuclear localization of IkappaB alpha is mediated by the second ankyrin repeat: the IkappaB alpha ankyrin repeats define a novel class of cis-acting nuclear import sequences.* Mol Cell Biol, 1998. **18**(5): p. 2524-34.
227. Yan, M., et al., *BRCA1 tumours correlate with a HIF-1alpha phenotype and have a poor prognosis through modulation of hydroxylase enzyme profile expression.* Br J Cancer, 2009. **101**(7): p. 1168-74.
228. Tan, E.Y., et al., *Cytoplasmic location of factor-inhibiting hypoxia-inducible factor is associated with an enhanced hypoxic response and a shorter survival in invasive breast cancer.* Breast Cancer Res, 2007. **9**(6): p. R89.
229. Couvelard, A., et al., *Overexpression of the oxygen sensors PHD-1, PHD-2, PHD-3, and FIH Is associated with tumor aggressiveness in pancreatic endocrine tumors.* Clin Cancer Res, 2008. **14**(20): p. 6634-9.
230. Kroeze, S.G., et al., *Expression of nuclear FIH independently predicts overall survival of clear cell renal cell carcinoma patients.* Eur J Cancer, 2010. **46**(18): p. 3375-82.
231. Hampton-Smith, R.J. and D.J. Peet, *From polyps to people: a highly familiar response to hypoxia.* Ann N Y Acad Sci, 2009. **1177**: p. 19-29.
232. Loenarz, C., et al., *The hypoxia-inducible transcription factor pathway regulates oxygen sensing in the simplest animal, Trichoplax adhaerens.* EMBO Rep, 2011. **12**(1): p. 63-70.
233. Hakuno, F., et al., *53BP2S, interacting with insulin receptor substrates, modulates insulin signaling.* J Biol Chem, 2007. **282**(52): p. 37747-58.
234. Healy, J.A., et al., *Cholinergic augmentation of insulin release requires ankyrin-B.* Sci Signal, 2010. **3**(113): p. ra19.
235. Her, G.M., et al., *Overexpression of gankyrin induces liver steatosis in zebrafish (Danio rerio).* Biochim Biophys Acta, 2011. **1811**(9): p. 536-48.
236. Ikeda, K., et al., *Molecular identification and characterization of a novel nuclear protein whose expression is up-regulated in insulin-resistant animals.* J Biol Chem, 2003. **278**(6): p. 3514-20.
237. Raciti, G.A., et al., *Partial inactivation of Ankrd26 causes diabetes with enhanced insulin responsiveness of adipose tissue in mice.* Diabetologia, 2011. **54**(11): p. 2911-22.
238. Wang, X., et al., *Regulation of ANKRD9 expression by lipid metabolic perturbations.* BMB Rep, 2009. **42**(9): p. 568-73.
239. Wilcox, A., et al., *Asb6, an adipocyte-specific ankyrin and SOCS box protein, interacts with APS to enable recruitment of elongins B and C to the insulin receptor signaling complex.* J Biol Chem, 2004. **279**(37): p. 38881-8.
240. Li, J.Y., et al., *Expression of ankyrin repeat and suppressor of cytokine signaling box protein 4 (Asb-4) in proopiomelanocortin neurons of the arcuate nucleus of mice produces a hyperphagic, lean phenotype.* Endocrinology, 2010. **151**(1): p. 134-42.

241. Nagel, S., et al., *Therapeutic manipulation of the HIF hydroxylases.* Antioxid Redox Signal, 2010. **12**(4): p. 481-501.
242. Yan, L., V.J. Colandrea, and J.J. Hale, *Prolyl hydroxylase domain-containing protein inhibitors as stabilizers of hypoxia-inducible factor: small molecule-based therapeutics for anemia.* Expert Opin Ther Pat, 2010. **20**(9): p. 1219-45.
243. Qing, G. and M.C. Simon, *Hypoxia inducible factor-2alpha: a critical mediator of aggressive tumor phenotypes.* Curr Opin Genet Dev, 2009. **19**(1): p. 60-6.
244. Vaupel, P. and A. Mayer, *Hypoxia in cancer: significance and impact on clinical outcome.* Cancer Metastasis Rev, 2007. **26**(2): p. 225-39.
245. Poon, E., A.L. Harris, and M. Ashcroft, *Targeting the hypoxia-inducible factor (HIF) pathway in cancer.* Expert Rev Mol Med, 2009. **11**: p. e26.
246. Moerke, N.J., *Fluorescence Polarization (FP) Assays for Monitoring Peptide-Protein or Nucleic Acid-Protein Binding*, in *Current Protocols in Chemical Biology*. 2009, John Wiley & Sons, Inc.
247. Jameson, D.M. and S.E. Seifried, *Quantification of protein-protein interactions using fluorescence polarization.* Methods, 1999. **19**(2): p. 222-33.
248. Sutton, E., et al., *Identification of SOX3 as an XX male sex reversal gene in mice and humans.* J Clin Invest, 2011. **121**(1): p. 328-41.

ADDENDUM

Chapter 1: Introduction

- p. 20, last sentence: “multiple surfaces” should read “multiple binding sites”
- p. 21, Fig 1.2A: “90°C” should read “90°”
- p. 25, final paragraph: “Data from my Honours research” should read “Data from *in vitro* hydroxylation assays performed during my Honours research”
- p.34, paragraph 2: “enable FIH” should read “allows FIH”
- p.34, bottom of page: “Cockman *et al.*” should read “Coleman *et al.* (2007)” and should reference citation [96] at the end of the sentence.
- p. 39, second sentence of first paragraph should read “Although this residue engages in a backbone hydrogen bond with FIH, there is little evidence to suggest that the identity of the side-chain is important for either binding or hydroxylation. The side-chain carboxylate does not form any salt bridges, and is not in close proximity (<4Å) to any basic patches on the surface of FIH."
- p. 39, second sentence of second paragraph: “…such as stability” should read “…such as the conformational stability of the folded domain”
- p. 40: the last sentence of the first paragraph should read, “The specific aims are listed below, with the rational for each aim detailed in the subsequent sections.”

Chapter 2: Materials and Methods

- p. 51, WCEB: “0.42 mM NaCl” should read “0.42 M NaCl”
- p. 51, CD Buffer: should read “5 mM Sodium Phosphate, pH 8.0 (prepared using 5 mM stock solutions of NaH_2PO_4 and Na_2HPO_4 in a 1:18 v/v ratio at 4°C)
- p. 53: the third paragraph (pMBP) should state that there is a recognition site for TEV protease in the linker between the MBP-tag and FIH.

Chapter 3: Differences in hydroxylation and binding of HIF and ARD substrates by FIH

- p. 88, “Figure 3.6” should read “Figure 3.5”
- p. 89, bottom paragraph should read:

“Previous studies have demonstrated that FIH forms homodimers in solution, and that its ability to do so is essential for hydroxylation of HIF [115, 118]. Conservative mutation of Leu340 in FIH (L340R) was found to disrupt its hydrophobic dimer interface, resulting in a form of FIH that is structurally similar to the wildtype enzyme, but predominantly monomeric [118]. The L340R mutant can bind, but is unable to hydroxylate a peptide from the HIF-1α CAD. To determine whether dimerisation is also required for hydroxylation of Notch, an L340R point mutation was generated in FIH by site-directed mutagenesis….”

Chapter 4: Structural determinants of FIH substrate recognition and hydroxylation

- p. 101, second sentence of the second paragraph should read “Although the majority of the experimental data presented in this paper was produced by myself, an equivalent body of data was generated by Sarah Karttunen (nee Linke), who is co-first author on the paper. Sarah’s work characterises a conserved RLL motif in the HIF CAD, and is presented in Figures 6 and 7.”
- p. 103, author contribution table: “Sarah Karttunen” should read “Sarah Karttunen (nee Linke)”

Chapter 5: Characterisation of Orf virus ARD proteins as substrates for FIH

- p. 127, third sentence of first paragraph should be followed by "The search was performed using the NCBI BLAST tool (http://blast.ncbi.nlm.nih.gov/Blast.cgi) with the blastp algorithm, using the FIH substrate motif 'LXXXXπ(D/E)ϕN' to interrogate the non-redundant protein sequence database, as well as the refseq collection."
- p. 130, final paragraph: third sentence should read "However, this was deduced to be a gel artefact."
- p. 138: the following sentence should be added at the end of the final paragraph "HIF-1α was unable to be detected by western blot in LT lysates, although this is not unexpected given the low levels of HIF present under normoxic conditions [10, 42]. Nevertheless, both HIF-1α and HIF-2α have previously been shown to be expressed in sheep skin tissue under hypoxic conditions [249,250].
- p. 151: "...levels of Glut1 are not altered in cells lacking endogenous FIH" should cite reference 85 (Zhang *et al*., 2011), and not reference 27.
- p. 153: "...but found no evidence for stabilisation of HIF-1α protein in response to ORFV infection" should refer to Figure 5.5 instead of Figure 5.4.

Chapter 6: Final Discussion

- p. 156: The following statement: "FIH has recently been reported to engage in high-affinity interactions with two other proteins, Mint3 and matrix metalloproteinase-14 (MMP14), neither of which contains an ARD or any sequence resembling a hydroxylation motif." should cite the following references:

  Sakamoto, T. And Seiki, M., *Mint3 enhances the activity of hypoxia-inducible factor-1 (HIF-1) in macrophages by suppressing the activity of factor inhibiting HIF-1.* J Biol Chem, 2009. 284(44): p. 30350-9.

  Sakamoto, T. And Seiki, M., *A membrane protease regulates energy production in macrophages by activating hypoxia-inducible factor-1 via a non-proteolytic mechanism.* J Biol Chem, 2010. 285(39): p. 29951-64.

- p. 157, the following paragraph and Figure should be inserted at the top of the page, under the heading *Structural Preference for FIH Substrates*:

Until recently, our knowledge of FIH substrate recognition was limited by the fact that the HIF-α proteins were the only published substrates for FIH. The identification of ankyrin repeat proteins as novel substrates led to the definition of a consensus hydroxylation motif, LXXXXX(D/E)VN, based on similarities between the hydroxylation sites in HIF-α, IκBα, p105 and Notch1. However, the continued identification of new ARD substrates over the last 5 years has enabled this consensus to evolve from the originally defined motif.

Figure 6.1 presents an alignment of the sequences of all sites of FIH-catalysed asparaginyl hydroxylation verified to date, including those identified in this thesis. The residues defined in the original substrate motif are still fairly well conserved; the majority of hydroxylation sites contain a -8 leucine, -2 aspartic/glutamic acid and -1 valine. Other conserved features include a hydrophobic residue (usually alanine) at the +1 position and a cysteine or alanine at the -3 position. Several other sites (e.g. -7 L/V/I, -4 G, +3 D/E) appear to be biased toward certain residues amongst ankyrin repeat but not HIF-α substrates. Given that these residues are highly conserved in all ankyrin repeats irrespective of hydroxylation, their conservation likely reflects a requirement for maintenance of the ankyrin fold, as

opposed to hydroxylation by FIH. Thus, as highlighted in Figure 6.1, the FIH substrate consensus is perhaps better defined as LXXXX(C/A)(D/E)VNA.

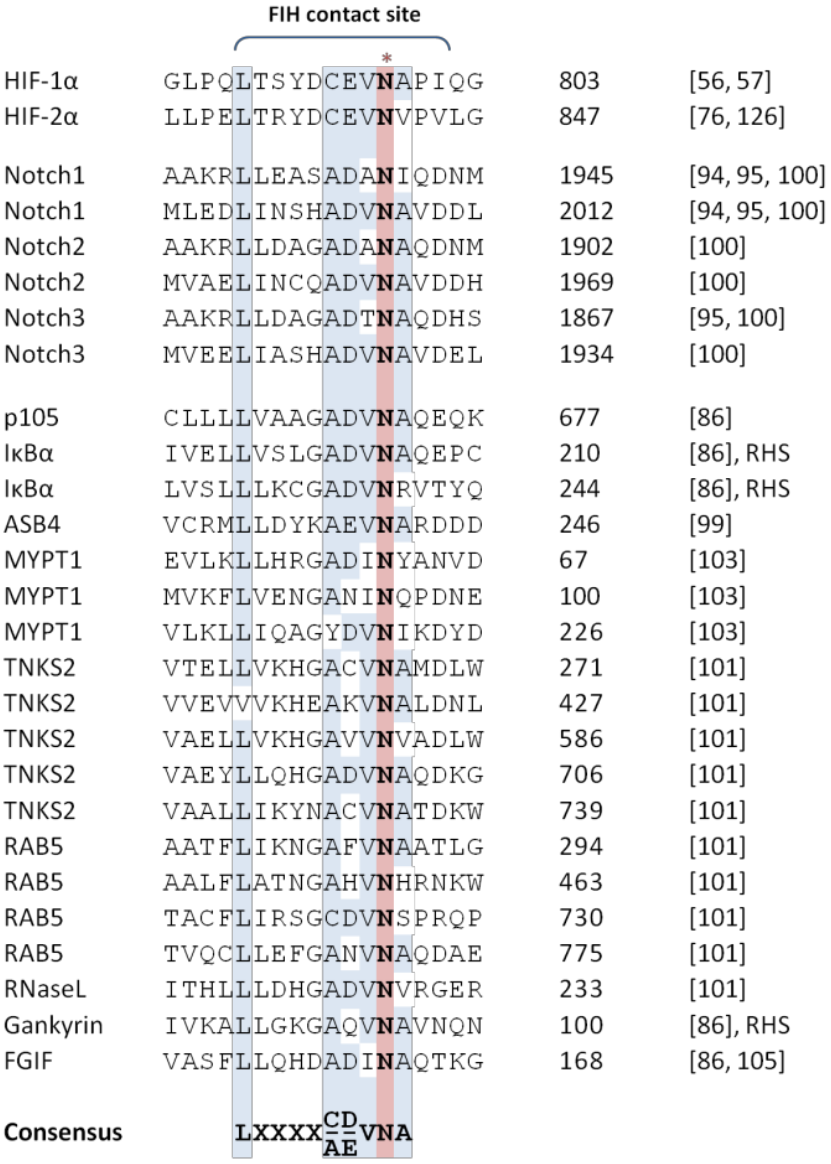

Figure 6.1 – Consensus hydroxylation motif for FIH substrates

Sequence alignment of hydroxylation sites from FIH substrates. The numbers to the right specify the target asparagine residue, which is highlighted in pink in the sequence. Conserved residues that form the consensus sequence for hydroxylation by FIH are highlighted. RHS = Rachel Hampton-Smith.

Appendix 2: Development of a FP-based binding assay

- p. 186, Figure A2.3, the upper and lower panels should be labeled 'A(ii)' and 'B,' respectively, and the following Figure included as panel A(i):

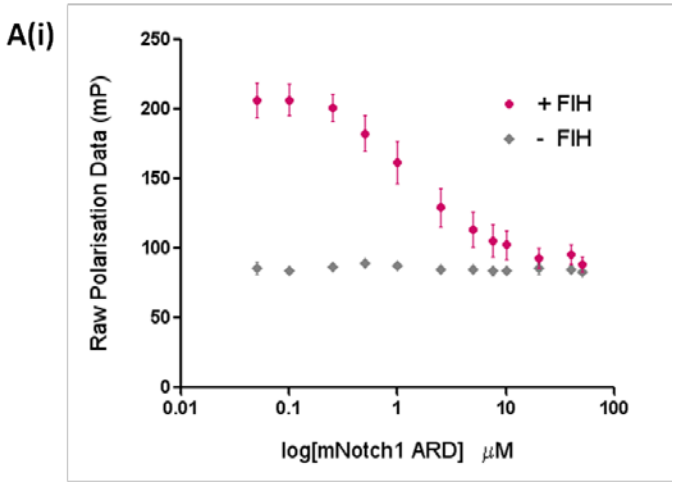

The legend should read "Affinity-purified Trx-6H-tagged Notch1 ARD (A) and Trx-6His alone (B) were assayed for their ability to compete with a fluorescently labelled Notch peptide in FP competition binding assays. A constant amount of tracer (400 nM) and MBP-hFIH (5 μM) were titrated with increasing concentrations of Trx-6H-tagged Notch1 ARD. Data in panel A(i) are the mean raw polarisation values from 3 independent experiments ± SD. Raw data were background corrected by subtraction of polarisation measured in the absence of FIH, then expressed as a percentage of the initial polarisation (measured in the presence of FIH but absence of any competing protein). Normalised data were fit to a one-site competitive binding curve using Graphpad PRISM software. Data in A(ii) and B are the mean of triplicate reactions ± SD and are representative of three independent experiments."

Throughout the thesis

- "Coomassie" is misspelt as "coomassie" on pages 51, 67, 71, 76, 78, 80, 83, 90, 130, 133-135 & 137. Likewise, "Western blot" should be spelt "western blot" on pages 49, 67-68, 136, 138 & 189, "co-immunoprecipation" should be "co-immunoprecipitation" on page 150, and "Dh5α" should be "DH5α" on page 63.

References

249. Scheid, A. *et al. Physiologically low oxygen concentrations determined in fetal skin regulate hypoxia-inducible factor 1 and transforming growth factor-β 3. FASEB J,* 2002. Mar;16(3):411-3.

250. Grover, T. *et al. Hypoxia-inducible factors HIF-1α and HIF-2α are decreased in an experimental model of severe respiratory disease syndrome in preterm lambs. Am J Physiol Lung Cell Mol Physiol.* 2007. Jun;292(6):L1345-51.